Titre: Title:	Processing and characterization of conductive carbon nanotube nanocomposite nanofibers and microfibers
Auteur: Author:	Saeedeh Mazinani
Date:	2009
Type:	Mémoire ou thèse / Dissertation or Thesis
Référence: Citation:	Mazinani, S. (2009). Processing and characterization of conductive carbon nanotube nanocomposite nanofibers and microfibers [Thèse de doctorat, École Polytechnique de Montréal]. PolyPublie. https://publications.polymtl.ca/8456/

UNIVERSITÉ DE MONTRÉAL

PROCESSING AND CHARACTERIZATION OF CONDUCTIVE CARBON NANOTUBE NANOCOMPOSITE NANOFIBERS AND MICROFIBERS

SAEEDEH MAZINANI
DÉPARTEMENT DE GÉNIE CHIMIQUE
ÉCOLE POLYTECHNIQUE DE MONTRÉAL

THÈSE PRÉSENTÉE EN VUE DE L'OBTENTION
DU DIPLÔME DE PHILOSOPHIAE DOCTOR (Ph.D.)
(GÉNIE CHIMIQUE)
JUIN 2009

Your file Votre référence
ISBN: 978-0-494-53801-2
Our file Notre référence
ISBN: 978-0-494-53801-2

UNIVERSITÉ DE MONTRÉAL

ÉCOLE POLYTECHNIQUE DE MONTRÉAL

Cette thèse intitulée:

PROCESSING AND CHARACTERIZATION OF CONDUCTIVE CARBON NANOTUBE NANOCOMPOSITE NANOFIBERS AND MICROFIBERS

présentée par : MAZINANI Saeedeh

en vue de l'obtention de diplôme de : Philosophiae Doctor

a été dûment acceptée par le jury d'examen constitué de:

M. LEGROS Robert, Ph.D., Président

M. DUBOIS Charles, Ph.D., membre et directeur de recherche

M. AJJI Abdellah, Ph.D., membre et codirecteur de recherche

M. CARREAU Pierre J., Ph.D., membre

M. KO Frank, Ph.D., membre

To :

My Parents;

"My lovely mother" and "My father"

ACKNOWLEDGEMENTS

I do appreciate the precious support and help of my supervisors *Prof. Charles Dubois* and *Prof. Abdellah Ajji*. I do really believe that without their great help, it was impossible to do this project. I should also thank all my ex-teachers and supervisors from the first year of primary school up to now.

I do thank the great help of my colleagues and friends during this work. My especial thanks are dedicated to the best and closest friends of mine who never left me alone. The spiritual support of my intimate friends has always been a great motivation during all the difficult steps of this project; some of them never stopped supporting me even from far distances; and they patiently stayed with me during passing the most difficult steps of this thesis.

I thank all the staff and technicians of Industrial Material Institute (IMI). They are the reason of some fundamental improvements in this project, especially the valuable helps of *Mr. Jacques.Dufour* is appreciated. I also appreciate all the technicians and staff of école polytechnique de montréal; chemical engineering department for their valuable support. Specifically, I thank the patience of Ms. *Weawkamol Leelapornpisit* during the difficult work of morphological study in this thesis.

And finally, my special thanks to *my parents* and *my brother*; all the achievements of this work really belong to my mother and my father.

RÉSUMÉ

Il y a moins de deux décennies que les nanotubes de carbone (CNTs) ont été inventés et mis au point. Les CNTs ont été largement utilisés pour améliorer les propriétés électriques ou mécaniques de différents matériaux et, en particulier, les polymères et les fibres polymères. Le facteur de forme important et l'orientation des CNTs dans la direction principale des fibres polymères se traduit par une amélioration considérable de la conductivité électrique. L'électrofilage est la méthode la plus fréquemment utilisée pour la production des nanofibers. Ce processus, d'abord connu sous le nom de pulvérisation électrostatique (avant 1993), n'a fait l'objet que de quelques publications. Toutefois, il a été récemment largement utilisé dans différents domaines d'applications. Les fibres nanocomposites surtout les fibres fabriquées par l'électrofilage ont fait l'objet de plusieurs investigation ont été largement dans l'industrie textile. Mais l'utilisation des CNTs pour la fabrication des fibres et nanofibres conductrices, reste encore à développer.

Dans ce travail, nous avons principalement étudié les nanofibres nanocomposites/CNTs produites par l'électrofilage. Une revue de la littérature pertinente a été effectuée à la fois pour la production par électrofilage et pour le filage à l'état fondu. Du point de vue expérimental, deux types fibres nanocomposites ont été produites :

1. La fabrication et la caractérisation des nanofibers nanocomposites à base de CNT fabriquées par électrofilage. Dans cette section, nous nous sommes concentrés principalement sur la caractérisation finale de la nappe de fibres produite par l'électrofilage en particulier aux fortes concentrations et selon divers types de CNTs. Les systèmes polystyrène (PS)/CNT et polyéthylène téréphtalate (PET)/CNT ont été considérés avec des une seul mur (SWCNT), double mur (DWCNT) ou murs multiples (MWCNT).

2. Le filage à l'état fondu et la caractérisation fondamentale finale des fibres nanocomposites polymères/CNTs. Dans cette partie, nous avons principalement mis l'accent sur la fabrication des fibres nanocomposites PET/CNT, qui est la préoccupation principale de cette étude.

La dispersion des CNTs dans les fibres PS/CNT obtenues par électrofilage a été corrélée à leur morphologie et propriétés physiques. Un copolymère de type SBS styrène-butadiène-styrène (SBS) a été utilisé avec succès comme d'agent interfacial pour améliorer la dispersion des CNTs dans solution de PS. Les mesures de la conductivité électrique sur des nappes nanocomposites ont montré un seuil de percolation électrique au-dessous de 4% MWNT. L'utilisation du SBS a permis d'obtenir des conductivités électriques supérieures. Les résultats obtenus à partir de ce travail ont montré que l'état de la dispersion a été un facteur déterminant de la morphologie finale des nanofibres et des propriétés des nappes produites par électrofilage. À des faibles concentrations de CNTs, une mauvaise dispersion produit des fibres de diamètre plus grand; alors qu'elle génère des fibres en forme de perles pour des hautes concentrations.

Pour les nanofibres PET/CNT, les mesures de la conductivité électrique sur des nappes nanocomposites ont montré un seuil de percolation électrique d'environ 2% en MWNT. Les résultats de cristallographie ont montré que l'augmentation de la concentration en CNTs augmente aussi le taux de cristallinité. Les mesures par spectroscopies infrarouge à transformée de Fourier (IRTF) et Raman ont établi que l'orientation de tous les deux de chaînes de PET aussi que de CNT sont augmentés par la production des nanofibers alignés ci-dessous de la percolation par rapport aux nanofibers produites en mode stationnaire. Les résultats des tests mécaniques sur des nanofibres orientées ont montré une amélioration importante des propriétés mécaniques pour les concentrations sous le seuil de percolation. Cet effet a été moins considérable pour les fortes concentrations en CNTs.

La production et la caractérisation des microfibres nanocomposites PET/CNT produites par le filage à l'état fondue ont été également l'une des préoccupations principales de cette recherche. Nous avons étudié différentes conditions de mises en œuvre afin d'améliorer la qualité des fibres produites. L'augmentation de la concentration des CNTs facilite le procédé de filage par rapport à la fibre PET pure. Nos résultats ont montré qu'il était possible d'obtenir des fibres conductrices avec une concentration de 2% en MWNT. L'utilisation d'un rapport d'étirage élevé a favorisé la dispersion des CNTs et l'obtention d'une meilleure conductivité électrique. L'étude de l'orientation de la phase cristalline dans la fibre PET a prouvé que l'addition des nanoparticules diminue l'orientation des unités cristallines à l'intérieur des fibres. Les propriétés mécaniques en tension mesurées aux fibres nanocomposites ont été jusqu'à trois fois supérieures à celles des fibres pures.

Finalement, un essai de modélisation a été effectué au dernier chapitre de cette thèse et a impliqué deux méthodes distinctes. Dans la première, il était question d'étudier la formation du cône au bout de la seringue et la déformation du jet. L'effet de l'ajout des CNTs sur le changement de forme du cône et l'initiation du jet et son étirage a été étudié en utilisant des méthodes empiriques et la technique d'analyse d'images.

ABSTRACT

Carbon nanotubes (CNTs) were invented and developed in less than two decades ago. CNTs have been widely used to enhance the electrical or mechanical properties of different materials especially polymers and polymer fibers. One-direction orientation of CNTs along fiber axis causes considerable enhancement of the electrical conductivity. Electrospinning is the most frequently used method for nanofiber production. This process was known as electrostatic spraying before 1993, and there were only a few studies employing this technique; however, it is widely used in different areas of applications nowadays. Nanocomposite fibers manufacturing, especially by electrospinning for nanocomposite nanofiber production, has been widely studied in textile industry. However, use of CNT in conductive fibers and nanofiber manufacturing and fundamental characterization of final properties is still in its developing stage.

In this work, we studied mainly CNT nanocomposite nanofibers produced by electrospinning. Therefore, the works available in the field of nanofiber production especially CNT nanocomposite nanofibers will be presented. Thereafter, the previous studies available in CNT nanocomposite melt-spun fibers were reviewed. In the experimental section, CNT nanocomposite nanofibers were produced by electrospinning in addition to melt-spinning. In the process of conductive nanocomposite nanofibers production, two main studies were performed:

1. Processing and characterization of CNT-based nanocomposite nanofibers by electrospinning process. In this section, we concentrated mainly on characterization of final electrospun mat especially at high range of CNT concentrations and various CNT types.
2. Melt-spinning and final fundamental characterization of polymer/CNT nanocomposite fiber. In this part, we mainly focused on polyethylene terephthalate (PET)/CNT nanocomposite fibers manufacturing which is the main concern of this study.

In electrospinning, polystyrene (PS)/CNT and PET/CNT were produced by using different types and concentrations of CNTs including single-wall carbon nanotube

(SWCNT), double-wall carbon nanotube (DWCNT), and multi-wall carbon nanotube (MWCNT). The effect of a wide range of CNT concentrations and types for electrospinning were studied here and combined with these two polymers.

In PS/CNT electrospun nanofibers, dispersion of CNTs was correlated to morphologies and properties of nanocomposite fibers. A copolymer as an interfacial agent (SBS, Styrene-butadiene-styrene type) was used to improve the dispersion of CNTs in PS solution. The results showed that the presence of the copolymer significantly enhances CNT dispersion. Electrical conductivity measurements on nanocomposite mats showed an electrical percolation threshold below 4 wt% MWCNT; while the samples containing SBS included higher values of conductivities below percolation compared to the samples with no compatibilizer. The results obtained from this work showed that dispersion condition was an important controlling factor of final nanofiber morphology and properties of electrospun mat. Poor dispersion caused larger fiber diameter than expected at low CNTs concentrations; moreover poor dispersion caused bead formation at high CNT concentrations which was approved by detecting the localizations of CNTs in bead positions.

In PET/CNT nanofibers, electrical conductivity measurements results on nanocomposite mats showed an electrical percolation threshold around 2 wt% MWCNT. Electrospun nanofiber mats were produced using both static and rotating drum collector. Crystallography test results showed increasing crystalline density by increasing CNT concentration to high CNT concentrations above electrical percolation. The spectroscopy (Fourier transform infra-red (FTIR) and Raman spectroscopy techniques) test results showed both PET chains and CNT orientation increased for aligned nanofiber below percolation compared to randomly oriented nanofibers. Mechanical test results of aligned nanofibers depicted considerable enhancement in mechanical properties especially modulus as much as at least 6 times more than random nanofibers below percolation; while the effect of alignment was less considerable above percolation and at high concentrations of CNTs.

PET/CNT nanocomposite microfiber production and characterization were also one of the main concerns of this research. PET/CNT single microfibers were produce by melt-spinning process. We studied different processing and mixing condition to obtain smooth, well dispersed nanocomposite fibers. Addition of CNTs considerably enhanced the drawability of fiber during spinning compared to pure PET. Our results showed that it was possible to achieve conductive fibers at 2 wt% MWCNT concentration and even more conductive fibers using higher draw ratio (DR) without increasing MWCNT concentration by modified dispersion condition. Study of the orientation of PET crystalline phase in drawn fibers proved that the addition of nanoparticles decreases the orientation of crystalline units inside the fibers. The orientation of MWCNT as well as that of PET chains was studied using Raman spectroscopy at different draw ratios and a high degree of CNT orientation with increasing DR was observed. Mechanical properties results showed interestingly high value of maximum tensile strain at break (ε_{max}) of nanocomposite fibers, up to 3 times more than pure PET fibers after adding MWCNT to nanocomposite fibers. Addition of CNTS caused interestingly enhancement in mechanical properties besides electrical conductivity in both electrospun and melt-spun fibers.

In the last chapter, the empirical modeling of electrospinning process is given. In this chapter, the image analysis technique is used to estimate the jet formation in electrospinning of CNT containing solutions. The results show that EHD theory is not compatible with the system of our study. More over, we used dimensional analysis method to give a relation for estimation of final nanofiber diameter as s function as a function of measurable material and process parameters.

CONDENSÉ EN FRANÇAIS

La nanotechnologie est un champ technologique émergent ayant plusieurs applications dans plusieurs domaines tels que la production et la conception des matériaux nanocomposites. Les nanocomposites polymère sont obtenus par l'incorporation des diverses nanoparticules dans une matrice polymère. Les matériaux polymères ont été utilisés abondamment dans l'industrie textile en raison de leurs propriétés exclusives telles leurs grandes flexibilité et étirabilité. Le concept de la science des nanocomposites polymères dans l'industrie textile et la technologie des fibres permet le développement d'une nouvelle génération de fibres appelées fibres nanocomposites. Particulièrement, l'obtention de fibres polymère conductrices a toujours été un point d'intérêt dans les textiles et l'industrie des fibres. Depuis la découverte des nanotubes de carbones (CNT) par Iijima en 1991, cette nanoparticule a trouvé une gamme d'applications très large dans divers domaines et avec divers matériaux, particulièrement les polymères pour la modification de leur conductivité. L'amélioration de la conductivité des polymères est réalisée par l'addition diverse nanoparticules tels les CNT, reconnus spécifiquement pour cette propriété d'augmentation de la conductivité.

Il y a différentes méthodes de fabrication des fibres selon les propriétés du matériau initial ou le procédé de production. Parmi ceux-ci, les procédé les plus importants sont: le filage à l'état fondu, l'étirage a sec des solutions, l'étirage humide des solutions et impliquent tous un étirage mécanique pour la formation des fibres. L'électrofilage est un nouveau procédé de fabrication de nanofibres qui implique l'étirage par des forces électrostatiques et a été introduit récemment. Les procédés conventionnels de fabrication des fibres incluant l'étirage à l'état fondu, à sec, humide et de gels produisent tous des fibres ayant des diamètres dans les microns. L'électrofilage, aussi

connu comme l'étirage électrostatique, est le principal procédé de production de fibres de dimensions nanométriques. Dans le procédé d'électrofilage, comme pour les autres procédés des fibres, l'incorporation de nanoparticules peut jouer un rôle important dans la modification des propriétés des nanofibres.

Dans ce projet, nous utiliseront les concepts de nanotechnologie dans les nanocomposites en plus de l'électrofilage pour fabriquer des fibres nanocomposites par l'incorporation de nanotubes de carbone. Un polymère devient électriquement conducteur au delà de la concentration de percolation. La plupart des nanofibres polymères et composites ne sont pas encore produites a l'échelle industrielle et la sont encore dans l'étape de la recherche et du développement. Les quatre principaux champs d'application des activités de recherché sur les nanofibres polymère et composite sont dans *les applications biomédicales, la synthèse de nanofils conducteurs, les matériaux composites structuraux et la filtration.*

Dans ce travail, du polystyrène (PS) et du polyéthylène téréphthalate (PET) électrofilés avec différents types et concentrations de CNT ont été produits et caractérisés. La revue des travaux précédents a montré qu'il y avait peu de travaux sur la production et la caractérisation de nanofibres de PS/CNT et PET/CNT. De plus, l'effet de différents types de CNT (une seul mur, double mur ou murs multiples) et leur concentration a été étudié en profondeur pour la première fois. Également, la caractérisation des nanofibres et microfibres conductrices a base de CNT, particulièrement a haute concentration, a été effectué pour la première fois.

À hautes concentrations de CNT, la dispersion est habituellement plus complexe et problématique dans la fabrication des nanofibres conductrices; alors que les CNT sont facilement dispersés a faibles concentrations et la solution requise pour l'électrofilage est habituellement stable pour de longues périodes. Dans le PS/CNT, l'effet de la dispersion sur la morphologie finale des nanofibres, particulièrement à hautes concentrations de

CNTs, a été étudié de manière exhaustive. Ce système a été étudié de divers aspects, tant expérimentalement que théoriquement. Pours les nanofibres électrofilées de PET/CNT, les propriétés finales ont été étudiées par différentes techniques cristallographiques et spectroscopiques. En plus du procédé d'électrofilage, le filage conventionnel à l'état fondu a été employé ici pour produire et étudier la structure et les propriétés finales des microfibres conductrices de PET/CNT. Considérant l'importance du PET dans la technologie des fibres et textiles et les travaux précédents rapportant une gamme acceptable de modification de conductivité avec les CNT, la production des fibres de PET/CNT est le principal point d'attention de ce travail. Les résultats principaux obtenus lors de cette thèse sont résumés comme suit :

1) Des fibres nanocomposite ont été obtenues à travers l'électrofilage de solutions du PS/Di-methyl formamide (DMF) contenant différentes concentrations et types de CNTs. L'état de la dispersion des CNTs a été corrélé aux morphologies et propriétés de fibres nanocomposites. Un copolymère (SBS, type styrène-butadiène-styrène) a été utilisé comme agent interfacial pour modifier la dispersion des CNTs dans la solution de PS avant électrofilage. Les résultats ont montré que la présence du copolymère améliore significativement la dispersion des CNTs. Le diamètre des fibres variait entre 200 nm et 800 nm, dépendamment du type de CNT, de la concentration en polymère et du copolymère. L'étude de la morphologie finale des fibres a montré l'ajout de CNT a causé une diminution dans la formation des fibres perlées avant la concentration de percolation. Cependant, l'ajout de CNT au-delà de la concentration de percolation a augmenté l'occurrence de boules dans les fibres, dépendamment de l'état de la dispersion. La présence du SBS a modifié la dispersion, réduit le diamètre des fibres et l'occurrence de boules dans les fibres. Les mesures de la conductivité électrique sur des mats de nanocomposite ayant des épaisseurs allant de 15 μm à 300 μm ont montré un seuil de

percolation électrique autour de 4% de MWCNT; alors que les échantillons contenant le SBS ont montré des valeurs de conductivité plus élevées au dessous de la percolation en comparaison avec ceux ne contenant pas de copolymère. Une amélioration dans les propriétés mécaniques a été observée avec l'addition de CNT a des concentrations au dessous du seuil de percolation. L'effet du copolymère sur la compatibilité améliorée a été prouvé par la comparaison des propriétés mécaniques obtenues pour le PS/MWCNT et le PS/copolymère/MWCNT.

2) La morphologie, la structure et les propriétés de mats non tissés de fibres conductrices électrofilées de PET/CNT ont été étudiées dans une étape subséquente. Les fibres nanocomposites ont été obtenues par l'électrofilage de solutions de PET dans le mélange acide trifluoro-acetic (TFA)/dichlorométhane (DCM) dans un rapport égal (1:1) et contenant différentes concentrations et types de CNT. Les mats de nanofibres électrofilées ont été produite en utilisant tant le tambour collecteur stationnaire qu'en rotation. Les mesures de conductivité électrique sur les mats nanocomposites a montré seuil de percolation autour de 2% de MWCNT. Les résultats de l'analyse morphologique ont montré des nanofibres plus lisses avec moins de boules lors de l'utilisation du collecteur en rotation, particulièrement a hautes concentration de CNTs. De plus, les nanofibres nanocomposites alignées ont montré des diamètres plus élevés en comparaison à celles produites en mode stationnaire. A partir des tests de cristallographie, un degré de cristallinité plus élevé a été observé avec l'augmentation de la concentration de CNT jusqu'à des niveaux au-delà de ceux du seuil de percolation électrique. Tant la spectroscopie infra rouge a transformé de Fourier que Raman ont montré des comportements similaires pour l'orientation des chaînes de PET et des CNTs dans les nanofibres nanocomposites alignées. L'orientation tant du PET que des CNTs augmente avec l'alignement des nanofibres en dessous du seuil de percolation, alors que cette

orientation était moindre au-delà du seuil de percolation dans les fibres alignées en comparaison avec les mats aléatoires de nanofibres. Les résultats mécaniques ont montré le même comportement au dessous et au dessus du seuil de percolation électrique. Une amélioration considérable dans les propriétés mécaniques, particulièrement le module en tension, a été observée dans les nanofibres alignées; au moins six fois plus élevés que pour les mats aléatoires de nanofibres au dessous du seuil de percolation; alors que l'effet de l'alignement était moins considérable au dessus du seuil de percolation et a hautes concentrations de CNTs.

L'effet de l'ajout de différents types de CNT a été étudié pour la première fois ici dans les échantillons électrofilés. Seules des méthodes de dispersion physique ont été utilisé ; ainsi, nous pouvions faire une comparaison entre tous les types de CNT sans changer leur structure de surface. Les résultats obtenus ont montré qu'en dépit du fait que les SWCNT montrent une amélioration considérable dans la conductivité électrique par sa structure unique ; il est plus difficile à disperser. La faible dispersion des SWCNTs et même des DWCNTs, à cause de leurs plus petites dimensions en comparaison avec les MWCNTs, est un facteur qui a une grande influence, particulièrement a hautes concentrations. Les résultats obtenus à partir du PS/CNT ont montré une valeur plus élevée de la conductivité électrique à 5% de SWCNT en comparaison avec les autres types de CNTs. Ceci étant, une bonne dispersion et compatibilité des MWCNTs avec la matrice PET a causé plus d'amélioration tant dans les propriétés mécaniques qu'électriques. Ainsi, la comparaison des résultats obtenus des SWCNT, DWCNT et MWCNT, particulièrement la caractérisation complète des propriétés finales des nanofibres électrofilées de PET/CNT, ont montré que les MWCNTs sont préférables a hautes concentrations. Même si les SWCNT sont les meilleurs pour la modification de la conductivité, les résultats obtenus ici tant à partir des mesures des propriétés électriques que mécaniques prouvent que les MWCNT est un meilleur choix aux hautes

concentrations de CNT. Ainsi, de manière générale, nous proposons d'utiliser des MWCNT pour les nanofibres nanocomposites à hautes concentrations de CNTs.

3) Des fibres de PET filées à partir de l'état fondu ont été modifiées avec des MWCNT pour obtenir des microfibres conductrices ayant des diamètres plus petits que 90 μm. Les propriétés physiques telle que la cristallinité et l'orientation des fibres telles que filées ont été étudiées par les techniques de diffraction des rayons-X, la spectroscopie Raman et la microscopie pour différent taux d'étirage (DR) et concentration de MWCNT. L'analyse de la morphologie et de l'orientation des MWCNT après le procédé de filage à l'état fondu a montré la formation d'agglomérats et des CNT hautement orientés. L'étude de l'orientation de la phase cristalline du PET dans les fibres étirées a prouvé que l'ajout de nanoparticules diminue l'orientation des unités cristallines à l'intérieur des fibres. L'orientation des MWCNTs aussi bien que celle des chaînes de PET a été étudié en utilisant la spectroscopie Raman à différent DR et un haut degré d'orientation des CNT a été observé à haut DR. Les propriétés mécaniques et électriques des fibres telles que filées ont aussi été étudiées. Nos résultats ont montré qu'il était possible d'obtenir des fibres conductrices à une concentration de 2% de MWCNT et des fibres plus conductrices en utilisant un DR plus élevé ont aussi été obtenues sans augmenter la concentration de MWCNT. Les résultats des propriétés mécaniques ont montré des valeurs élevées de la déformation maximale à la rupture en tension des fibres nanocomposites, jusqu'à trois fois plus que pour le PET seul. Les fibres nanocomposites de PET/CNT ont montré une augmentation phénoménale de l'étirabilité des fibres telles que filées et de l'élongation à la rupture dans les tests mécaniques. Ceci à cause du rôle des MWCNTs dans la réduction de la formation de la phase cristalline et l'augmentation de la dissipation de l'énergie imposée par la phase amorphe. Ceci est obtenu parceque les

chaînes polymère ont adhéré raisonnablement aux nanoparticules de MWCNTs dans la dispersion modifiée.

4) Finalement, un essai de modélisation a été effectué au dernier chapitre de cette thèse et a impliqué deux modélisations distinctes. Dans la première, il était question d'étudier la formation du cône au bout de la seringue et la déformation du jet. L'effet de l'ajout des CNTs sur le changement de forme du cône et l'initiation du jet et son étirage a été étudié en utilisant des méthodes empiriques et la technique d'analyse d'images. Les résultats obtenus ont été comparé avec la théorie Electro-Hydro-Dynamique (EHD). Ensuite, le diamètre final des nanofibres a été étudié en fonction des paramètres mesurables du matériau et du procédé dans la seconde partie. Nous avons utilisé la méthode d'analyse adimensionnelle pour la prédiction du diamètre final des nanofibres à différentes concentrations de MWCNT. À travers cette modélisation empirique, nous avons: 1) analysé le changement dans la formation du jet et du profil de vitesse à différentes concentrations de MWCNT, 2) évalué l'applicabilité de la théorie EHD et des hypothèses faites dans cette théorie ainsi que le rôle des hypothèses simplificatrices et 3) proposé deux équations pour l'estimation du diamètre moyen des nanofibres par l'utilisation de la méthode d'analyse adimensionnelle et comparé aux résultats expérimentaux.

TABLE OF CONTENTS

List of Tables

List of Figures

List of Symbols

α & θ	The angle between dipole moment of particular vibration and chain axis (FTIR)
γ & α	Surface tension
ε	Hencky strain
ε	Tensile strain
ε	Permittivity & Dielectric constant
$\dot{\varepsilon}$	Elongation rate
η & μ	Viscosity
θ	The angle between the unit crystalline cell axes (XRD)
λ	Wave length
ν	Cinematic viscosity
ρ	Density
σ	Tensile stress
σ	Volume conductivity
σ_V	Viscoelastic stress
σ	Surface charge density
τ	Stress
A	Absorbance (FTIR)
D	Dichroic ratio
e	Electrical charge
E	Electrical field
f	Herman orientation function (FTIR, XRD)
f_A	Air drag force
f_C	Columbic force
f_E	Electric field force
f_G	Gravitational force
f_S	Surface tension force

f_V	Viscoelastic force
l	Length
G	Elastic modulus
I	Total constant electrical current
K	Liquid conductivity
m	Total mass
P	Pressure
q	Heat flow (DSC)
Q	Volume flow rate
R , r	Radius
S	Electrical conductivity
t	Time
$\mathbf{t_t^e}$ & $\mathbf{t_n^e}$	Tangentional and Normal traction
T	Temperature
u & v	Velocity
V & $\mathbf{V_0}$	Applied voltage
w	Weight fraction
X	Crystallinity fraction
z	Axial distance

Chapter 1

Introduction

Nanotechnology is an emerging field of technology with many applications in different areas such as production and design of nanocomposite material. Polymer nanocomposites are obtained by embedding various nanoparticles in polymer as the matrix. Polymer materials have found a great deal of interest and applications in textile industry because of their exclusive properties such as high flexibility and high drawability. The concept of polymer nanocomposite science in textile industry and fiber technology developed a new generation of fibers called nanocomposite fibers. Especially, obtaining conductive polymer fibers has always been one of the points of interest in textile and fiber industry. Since the discovery of CNTs by Iijima in 1991, this nanoparticle has found a great range of applications in different areas and with various materials especially polymers for conductivity modification. Enhancing the conductivity of polymer fibers is achieved by adding different types of nanoparticles such as CNT which is the best-known particle for conductivity enhancement.

From another aspect, one of the most recently employed processes for nanofiber production is electrospinning. Conventional fiber processing techniques including wet, dry, melt, and gel spinning, are all related to polymer fibers with diameters down to the micrometer range. Electrospinning, also known as electrostatic spinning, is the main method to produce polymer fibers with nanoscale diameters. The ultra-fine electrospun solid nanofibers are notable for small diameters, large surface area to volume ratio, and small pore size. In electrospinning process, the same as other spinning methods, embedding nanoparticles can play an important role for the modification of properties. Even though there has been much progress in the area of electrospinning by different research groups, this process is still under development in different areas of applications.

In this project, we are to employ the concepts of nanotechnology in nanocomposite polymers besides electrospinning to fabricate nanocomposite fibers by embedding CNT in polymer fibers. Different polymer materials such as polyacrylonitrile (PAN), polyvinyl di-fluoride (PVDF) and polymethyl methacrylate (PMMA) combined with CNT have been deeply studied so far to fabricate conductive nanocomposite nanofibers by electrospinning (Ko, Gogotsi et al. 2003; Seoul, Kim et al. 2003; Chakrabarti, Nambissan et al. 2006; Sundaray, Subramanian et al. 2006).

In this work, we are to produce and characterize electrospun PS and PET with different types and concentrations of carbon nanotubes. Review of the previous works shows that there are only a few works concerning the production and characterization of PS/CNT and PET/CNT nanofibers. Moreover, the effect of different types and concentrations of CNTs is extensively studied here. In addition, thorough characterizations of CNT-based conductive nanofibers and microfibers are not available in previous papers. In PS/CNT, we will mainly concentrate on the effect of dispersion on final morphology of nanofibers, especially at high concentrations of CNTs. In PET/CNT electrospun nanofibers, the final properties are investigated by different crystallography and spectroscopy techniques. In addition to electrospinning technique, conventional melt-spinning is employed here to process and study the structure and final properties of conductive PET/CNT micro-fibers. Considering the importance of PET in fiber and textile technology and previous works reporting the acceptable range of conductivity modification with CNT, PET/CNT fiber production is the main point of attention in this work. This thesis is constituted of the following sections:

1. Literature review which is mainly theoretical and experimental description of electrospinning process and CNT-based nanocomposite nanofibers especially PS and PET nanofibers.

2. First paper: The study of structure and properties of PS/CNT nanofibers at different CNT types and concentrations; moreover, studying the role CNT dispersion condition plays on final structure and properties of nanofibers.

3. Second paper: Processing and thorough characterization of PET/CNT electrospun nanofibers at different CNT concentrations and types by various characterization methods.

4. Third paper: inspecting and in-depth characterization of final structure and properties of PET/CNT melt-spun micros-fiber and the role of CNT on modification of final properties.

5. Chapter 9: Empirical modeling of electrospinning of CNT-based solutions employing two methods of image analysis and dimensional analysis for jet and final nanofiber diameter predictions respectively.

6. Finally, we will give a brief review of the final achievements and the summary of the results obtained in this project followed by conclusions and recommendations.

Chapter 2

Literature Review

2.1. Nanotechnology and Nanocomposites

Nanotechnology is an emerging field of technology with different areas of applications such as material science, mechanics, electronics, optics, medicine, plastics, energy, textile and aerospace. The main unifying theme of this technology is the control of matter on a scale below 100 nm, in addition to the fabrication of devices on the same length scale, at least in one dimension. This value is the representative of this technology at manipulating atoms, molecules, and nanosized particles in a manner to manufacture materials with fundamentally new properties. Unlike traditional technologies which are called "top-down", nanotechnology is called "bottom-up". It means that in nanotechnology, the bulk material can be built precisely in tiny building blocks and in conclusion the nanomaterials have fewer defects and higher quality. The fantastic properties of nanomaterials lie in the fact that by reducing the size to nanometer range, the properties of substance dramatically change. As one or more parts of bulk material is in nanometer range or even smaller ($\leq$100 nm, criterion as the benchmark for the nanotechnology classification), it shows unexpected characteristics (Lei Qian 2004; Burger, Hsiao et al. 2006). Richard Feynman was the first one that articulated the matter of nano in 1959, with the basis of "atomic assembly". The term "nanotechnology" was introduced by K. Eric Drexler in his book "Engines of Creation", and since then the field of nanotechnology has been the hot topic of both the academic and industrial interests (Seeram Ramakrishna 2005).

With the term "nanostructure", we mean any object or structure whereby at least one of its dimensions is within nano-scale. A "nanoparticle" is considered as a zero-dimensional nano-element, which is the simplest form of nanostructures. A "nanotube" or

"nano-rod" is one-dimensional nano-element. Whilst "nano-platelet" or "nano-disk" are two-dimensional nano-elements which are useful to manufacture nano-devices along with one-dimensional nanoparticles (Seeram Ramakrishna 2005). From the industrial point of view, nanotechnology includes various areas of applications as predicted in Fig. 2-1.

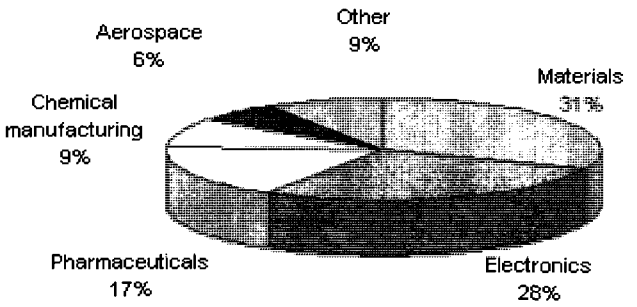

Figure 2-1: Different industrial focuses of nanotechnology by 2010-2015 (www.nanocompositech.com/nanotechnology/nanotechnology-business.htm)

As it is shown, electrical applications and material fields of nanotechnology include a great share of the industrial focus of nanotechnology. Fig. 2-2 shows the change in the trend of nanotechnology applications; this trend also approves that electronic field has been one of the main focus of industrial applications recently.

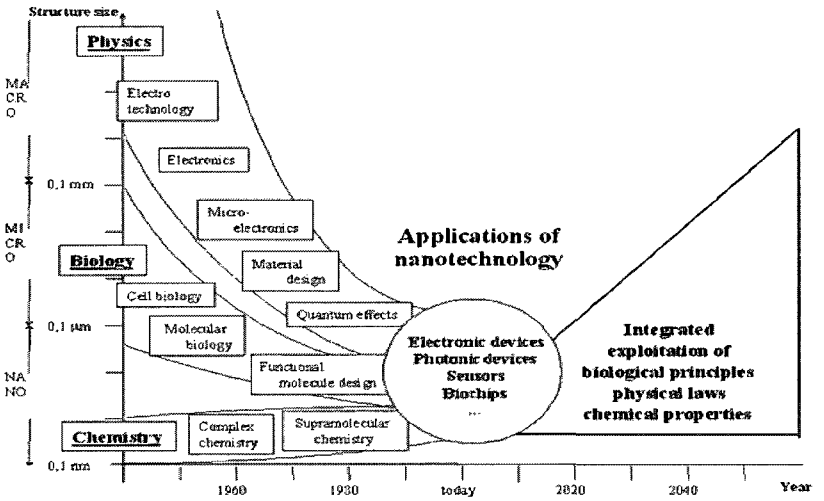

Figure 2-2: The change in trends of nanotechnology applications, past, present and future

2.1.1. Polymer Nanocomposites

Polymers constitute a broad class of materials applicable for manufacturing of composite materials as matrix. Different types of fillers are employed to improve and modify the properties of polymers. The use of nanoscale fillers to enhance the polymer characteristics considering different applications is a well-known way of polymer modification and results in polymer nanocomposites (PNCs) manufacturing. The composition of layered silicates with different types of polyolefins, nylons and thermoset matrices are popular types of PNCs. The researches done in the field of PNCs during the previous 15 years prove the considerable enhancement of mechanical and physical properties of polymers by adding a few amounts of nanoparticles. Moreover, contrary to the conventional composites, nanocomposites are easily processed and properly molded to the finally desired shapes (Richard A. Vaia 2001). There are different types of nanoparticles used to manufacture polymer nanocomposites. Some of the nanoparticles are well known for nanocomposite polymeric fiber manufacturing such as carbon nanofiber and carbon nanoparticles, clay nanoparticles, metal oxide nanoparticles and specifically carbon nanotubes (CNT). In the following parts, some of the properties of nanoparticles employed in manufacturing nanocomposite polymeric fibers will be given.

Carbon nanofiber and Carbon nanoparticle: Carbon nanofibers (CNFs) and carbon black nanoparticles are amongst the most commonly used fillers. CNF can effectively increase the tensile strength especially as they are employed for nanocomposite fibers, while carbon nanoparticles can improve the abrasion resistance and toughness. Both of these particles can enhance the chemical resistance and electrical conductivity (Lei Qian 2004).

Clay nanoparticle: Clay nanoparticles or nanoflakes are manufactured of several types of hydrous aluminosilicates which are different in chemical composition and crystal structure. Clay nanoparticles possess electrical, heat and chemical resistance and also the ability of blocking UV light. (Lei Qian 2004).

Metal oxide nanoparticle: Nanosized particles of TiO_2, Al_2O_3, ZnO, and MgO include the group of metal oxide particles. These nanoparticles possess photocatalytic

ability, electrical conductivity, UV adsorption and photo-oxidizing capacity against chemical and biological species (Lei Qian 2004).

Among different types of nanoparticles, we are working on CNT to develop the electrical conductivity; since carbon nanotubes are one type of the most promising building blocks existing in this field. The properties of different types of CNTs will be described in details in the following part.

2.1.2. CNT/Polymer nanocomposite

Carbon nanotube was first introduced by Iijima in 1991 (Iijima 1991) and among the earliest works on polymer nanocomposite complexion based on CNT was the work reported by Ajayan *et. al.* in 1994 (Ajayan, Stephan et al. 1994). CNTs could easily replace the other nanofillers such as carbon blacks, silicas, clays and carbon nanofiber (CNF). CNTs feature properties such as high flexibility, low mass density and large aspect ratio. Moreover, CNTs include the combined electrical, mechanical and thermal properties. These characteristics of make them suitable candidates to replace the conventional nanofillers and to manufacture multifunctional nanocomposites. CNTs are stronger than steel, lighter than aluminum including considerably high conductivity. Considering these exclusive properties, CNTs and their composites are of great importance in nanocomposite science. CNT production, purification, suspension, filling, functionalization, and application are various fields of study in this regard.

CNTs are long cylinders of covalently bonded carbon atoms (Moniruzzaman and Winey 2006). There are two types of CNTs including single-wall carbon nanotube (SWCNT) and multi-wall nanotube (MWCNT). SWCNT has a shape of single graphene layer rolled up in a cylinder shape, while the graphene layer is a monolayer of sp^2-bonded carbon atoms. The carbon atoms in the cylinder contain the sp^3 character. MWCNT consists of a nested structure the same as SWCNT, but with different layers coaxially around a central hollow core, with the distance between the layers in the range of about 0.34 nm. Double wall carbon nanotube (DWCNT) is a special type of MWCNT consisting of two concentric graphene cylinders. Based on different shapes of nanotubes,

various types of properties are expected from different types of this nanoparticle. For instance, DWCNT is expected to include higher flexural modulus compared to SWCNT, while it has higher toughness compared to MWCNT, because of its smaller size. The structure of different types of CNTs is depicted in Fig. 2-3.

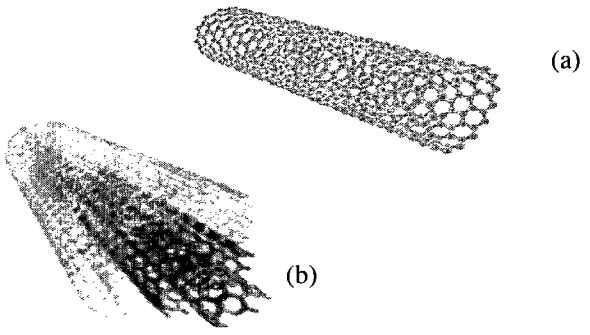

Figure 2-3: Structure of different types of CNTs, (a) SWCNT; (b) MWCNT (http://mavimo.org/chimica/nanotubi)

There are three different ways to produce CNT: Arc discharge, Laser ablation and Chemical vapor decomposition (CVD) (Moniruzzaman and Winey 2006). Recently, electrospinning has been also introduced as a new method of CNT production (Hou and Reneker 2004). All the production methods, mentioned above, result in CNT including a mixture of nanotube chiralities, diameters, and length along with different amount and types of impurities. Since the properties of final CNT/polymer composite are strongly dependent on the diameter and length of the nanotubes, purification is an important stage in CNT production. Moreover, the final characteristics of composite are directly related to the amount of CNT dispersion and its interaction with the matrix; therefore, functionalization and CNT dispersion in matrix are two important stages of CNT/polymer composite manufacturing.

CNT functionalization

There are mainly two methods of CNT dispersion in solution or polymer matrix: covalent and noncovalent methods. The covalent functionalization of the CNT improves the nanotubes dispersion in different solvents and polymers. It basically comes from the

misalignment of the π-orbital of the sp^2-hybridized carbon atoms. In this method, the nanotube surface is prepared to attach covalently to the chemical species. In nanotube/polymer composites, functionalization increases the amount of CNT and polymer interface and therefore it enhances the mechanical properties. For instance, the interfacial adhesion between the covalent or noncovalent functionalized groups of CNT and polymer matrix increases and it results in the improvement of load transfer. However, an important consequence of CNT covalent functionalization is the disruption of the extended π conjugation in nanotubes which has a notable effect on electrical properties. Therefore, noncovalent functionalization is proposed for the mixtures with electrical applications. In this method adsorption of polymer to CNT surface is performed by using an intermediate molecule as coupling agent (Moniruzzaman and Winey 2006).

2.1.2.1. CNT/Polymer nanocomposite fabrication methods

Enhancement of CNT dispersion in matrix causes improvement of final properties of CNT/polymer composite. Three different dispersion or blending methods are mostly used: solutions blending, melt blending and in-situ polymerization. There are other methods such as latex technology, solid-state shear pulverization, and coagulation spinning methods that have also been recently employed for dispersion modification (Moniruzzaman and Winey 2006) as follow:

Solution blending

Solution blending is the most used method to produce polymer nanocomposites. Solution blending involves the dispersion of CNT in a suitable solvent and then addition of the polymer at room temperature or elevated temperature to fabricate the polymer/nanocomposite solution. Manufacturing a metastable composition of CNT in polymers is dependent on employing different methods such as high-power ultrasonication. High-power ultrasonication is an effective method; however it may cause CNT degradation and an adverse effect on final properties. CNT degradation is dependent on the time and power of sonication and also the length of CNT particles. Use

of some additive such as surfactants may improve the dispersion modification, while it might have undesirable effect on some properties (Moniruzzaman and Winey 2006).

There are different methods to modify CNT dispersion in the solution state without functionalization. Ausman and his colleagues proposed the use of DMF as the best solvent for CNT dispersion. They studied different types of solvents and they found DMF as the best solvent (Ausman, Piner et al. 2000). Addition of different types of copolymers has been suggested as a method to stabilize CNT in different polymer solutions. Dror *et al.* proposed using a copolymer of styrene and sodium maleate (PSSty) and Gum Arabic (GA) which is a highly branched natural polysaccharide to improve the dispersion and stability of SWNT in PEO/water solution (Dror, Salalha et al. 2005). In a most recent paper, Sluzarenko *et al.* could modify the amount of CNT-dispersion by adding only a small amount of PS-PI to the solution of PS in DMF (Sluzarenko, Heurtefeu et al. 2006).

Melt blending

In melt blending method, high shear and temperature are applied to disperse the nanotubes in a polymer matrix, and it is the most suitable method for industrial production of CNT nanocomposites. In this method, the matrix is highly viscous; moreover the dispersion of nanotubes is usually limited to low concentrations. This method has been employed so far for different types of polymer/nanoparticles systems including MWNT/nylon-6, SWNT/polypropylene, MWNT/polycarbonate, etc. (Moniruzzaman and Winey 2006).

In-situ polymerization

This method of fabricating polymer nanocomposite is performed by dispersing nanotubes in a monomer followed by polymerization. The same as solution blending, different types of surfactants are employed to improve the initial dispersion of nanotubes in the liquid medium (monomer and solvent). In-situ polymerization causes the covalent bonding between the functionalized nanotube and the polymer matrix using various condensation reactions. One of the most suitable methods in this area is infiltration method in which the reactive agents are embedded into a nanotube structure and then the monomers are subsequently polymerized (Moniruzzaman and Winey 2006).

Other methods

In *pulverization* method, the main focus is to run the mixing process in solid state for high viscous mixing of nanotube/polymer. In the solid-state mechano-chemical pulverization process, CNT is mixed with polymer matrices employing pan milling or twin screw extruder which could be followed by melt mixing. Nanocomposites prepared in this way have the advantages of polymer chains grafting on the nanotube and this method decreases the amount of interfacial tension and tensile modulus (Moniruzzaman and Winey 2006).

In *latex fabrication* method, CNT is dispersed in water and then a suspension of latex nanoparticles is added to polymer. The resulting product is a colloidal mixture which is changed into composites with uniform nanotubes dispersion in a high-viscous matrix. The final nanocomposite is obtained by methods such as freeze-drying and subsequent processing. This method is applicable for the polymers synthesized by emulsion polymerization method or the ones susceptible to change into artificial latexes under high-shear conditions (Moniruzzaman and Winey 2006).

The final method, *coagulation suspension*, is the method to obtain nanotube/polymer composites at very high nanotube loadings. In this case, CNT is dispersed using a surfactant solution, the nanotubes are coagulated into a mesh by wet spinning and then the mesh is converted into solid fiber by slow draw process. This is an exclusive way of fabricating nanocomposites with CNT concentrations of more than 50% (Moniruzzaman and Winey 2006).

2.1.2.2. CNT/Polymer nanocomposite properties

The characteristics of nanotube/polymer composite arise from the polymer and nanotube properties along with the microstructure developed during the processing and manufacturing. Therefore, morphology control has been studied extensively as one of the most effective parameters on final nanocomposite properties. However, the microstructure and morphology control is not necessarily the improvements of all types

of properties; therefore, development in one area might value the loss of the other parameters and characteristics.

CNT alignment

CNTs present high aspect ratios that make them susceptible to orientation by different ways. For instance, methods like mechanical stretching, spin-casting, wet-spinning, melt fiber spinning, and electrospinning are some effective ways of orientation; while the spinning methods are the most effective ones (Moniruzzaman and Winey 2006). In various types of spinning processes, electrospinning is one of the best-known methods of orientation, since it gives the fibers with the least diameters and includes the highest extensional field and tension for CNT alignment.

Electrical conductivity

The capacity of CNT as electrically conducting fillers has been successfully proved. For instance, addition of only a small amount of CNT (0.1 wt% or even less) could increase the electrical properties by some orders of magnitude. This is the case while the other properties such as optical clarity, mechanical properties, or viscosity remains the same. A polymer becomes electrically conductive when it passes the percolation threshold concentration. Percolation threshold is a concentration above which the electrical properties increase considerably. The percolation threshold of CNT/polymer nanocomposite has a small value, because of the structure and high aspect ratio of CNT particles and it strongly depends on the alignment and dispersion of CNT particles in the matrix. Followed by better dispersion and lower alignment of CNT particles and also higher aspect ratio, the percolation threshold of the CNT/polymer nanocomposite will be lower. Increasing the alignment of CNTs in the matrix results in the reduction of nanotube contacts and in this case, the percolation threshold increases (Moniruzzaman and Winey 2006).

The other important point in controlling the electrical properties is the CNT functionalization. It is known that the covalent functionalization by making some changes in the structure of CNTs might decrease the electrical conductivity improvement. However, from another point of view, this reduction in electrical conductivity could be

made up by the dispersion modification occurring in the matrix in the case of functionalization.

Mechanical properties

Some properties of CNTs such as fiber-like structure, low density, high aspect ratio, and extraordinary mechanical properties make them reasonable candidates for composite reinforcement and the mechanical properties modification of polymers. A low concentration of CNTs could result in considerable increase in mechanical properties, while by keeping the concentration of CNT at a low value; it is possible to maintain some polymer properties like toughness in a proper range. In fact, the preferred properties regarding mechanical characteristics could be obtained by making improvement on CNT loading, dispersion and alignment. Imperfection in the amount of load transfer in the matrix causes poor functionality of nanotube/polymer composite regarding the mechanical properties. The load transfer is strongly dependent on the amount of CNT loading and dispersion in the matrix, while agglomeration of the nanoparticles may result in a reduction in the mechanical properties improvement.

Thermal conductivity

The increase in the thermal conductivity is obtained by the atomic vibration. The CNTs show excellent potential for thermal conductivity improvement, and the same trend is expected for the CNT/polymer nanocomposites. While the results achieved for employing CNTs in thermal conductivity improvement does not fulfill the expectations; since the phonons entering the nanotube/polymer system move through the matrix instead of by moving the electrons. The low amount of thermal conductivity transfer in polymer nanocomposites comes from the high thermal resistance existing for heat transfer between the nanotubes in the matrix by the structure of CNTs. The introduction of covalent bonds between the nanotubes resulted in a reduction in the amount of high thermal interfacial resistance of the nanotubes and the thermal conductivity development of nanocomposite (Moniruzzaman and Winey 2006). There are other thermal properties such as decreasing the amount of flammability and increasing the thermal stability obtained by CNT addition. There are some works in the area of CNTs application for

thermal properties modification; however, no considerable results have been obtained in this matter compared to the CNTs use for the electrical properties improvements.

Rheological properties

Addition of nanotubes causes changes in the rheological properties of the nanocomposite system compared to the pure polymer. Rheology has recently been used as a method of studying the microstructure and change in the properties, especially the composite dynamics. The same as the electrical percolation, the rheological properties and percolation are dependent on the amount of CNT loading, dispersion, alignment and aspect ratio. Most of the researchers in this field have proposed that the superposition of the entangled polymer network and the combined nanotube/polymer network is more effective to change the rheological properties rather than the nanotube agglomeration and networking alone. The research results show that the amount of CNT concentration to obtain a reinforced nanotube/polymer network is much lower than the percolation threshold necessary for arranging a conductive network in the matrix (Moniruzzaman and Winey 2006).

Followed by a brief introduction about CNT properties, fiber technology and especially electrospinning and the studies related to this thesis will be reviewed in next parts.

2.2. Fiber Technology

There are different methods of fiber formation in fiber and textile industries depending on type of material and final application; however, most of the methods include the following stages:

1) Preparation of fiber-forming polymer,

2) Preparation of the spinning fluid (polymer melt, solution, emulsion, etc.),

3) Spinning of the prepared fluid mostly by extrusion and deformation of the melt along the spinning line,

4) Drawing;

5) Heat treatment;

6) Textile processing (twisting, oiling, dyeing, etc.) (Ziabicki 1976).

The first stage might be a totally chemical step, while the other ones include several physical structure treatments. There are different methods of fiber manufacturing techniques which are different in initial material properties or the processing method. Among them, the most important processes include: *Melt spinning, Solution dry-spinning, and Solution wet-spinning*. There are other methods which are not as well-known as the ones mentioned above such as: *Phase separation spinning, Emulsion spinning, Gel (semi-diluted) spinning, and reaction spinning*. Moreover, ***electrospinning*** as a new method of nanofiber manufacturing process has been recently introduced and is totally different from the other conventional spinning methods.

2.3. Nanofibers

Nanofiber is a word constituted of two words namely "nano" and "fiber", both of which have been described in previous sections. From different categories of nano-materials point of view, nanofibers would geometrically be placed in one-dimensional region. A nanofiber is a kind of nano-material depending on the size of fiber and might be considered as nanostructured material in the case of being filled with nanoparticles to form the composite nanofibers (Seeram Ramakrishna 2005). There are different ways of manufacturing and processing nanofibers and they will be described below, while electrospinning process seems the most important one, after which nanofiber technology has been developed considerably.

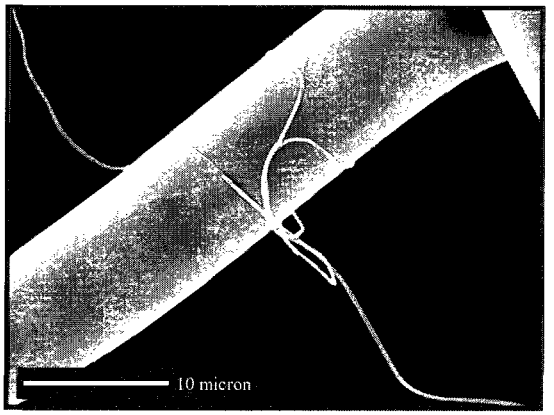

Figure 2-4: Electrospun nanofiber compared to conventional fiber (Burger, Hsiao et al. 2006).

2.3.1. Applications

Four main categories of research activities underway for pure polymer and composite nanofibers are *biomedical applications, semiconductor nanowire synthesis, structural composite materials*, and *filtration* (Sawicka and Gouma 2006).

The biomedical role of nanofibers has extended into various specific applications among which tissue engineering has been most widely studied. Scaffolds and synthetic matrices mimic the structure and biological activities of the natural extra cellular matrix (ECM). Electrospun biocompatible polymer nanofibers can be easily deposited as thin porous mats onto a hard tissue prosthetic device which is used as an implant in human body. Followed by the introduction of composite materials into the electrospun mats, their functionality could be amplified by strategic incorporation of specific species (Sawicka and Gouma 2006).

The next category of electrospun nanofibers especially composite nanofibers and conductive properties improvements has also tremendously expanded possible applications for nanofibers. For instance, one-dimensional metal oxides have been extensively studied due to their modification characteristics on electro-optical, electro-chromic, ferroelectric, catalytic, and gas sensing properties. Versatility of design, and features of electrospinning promise its implementation in multi-functional applications

such as multi-step fiber template technique described previously (Sawicka and Gouma 2006).

Filtration application was the initial purpose of manufacturing nanofiber membranes. Electrospinning is a wise solution for filtering out particles in the submicron range. Polymer nanofibers obtained are electrostatically charged to improve the ability of electrostatic attraction of particles without increasing pressure drop to further improve filtration efficiency (Sawicka and Gouma 2006).

The last topic of nanofiber research is structural–strengthening composite synthesis. Majority of the work presented currently on nanofiber composites is concerned with carbon nanofiber or nanotube reinforcements which are generally manufactured by electrospinning (Sawicka and Gouma 2006).

All the applications of nanofibers are categorized among the above four categories; however, Figure 2-5 shows a more detailed description of polymer and nanocomposite applications of nanofibers.

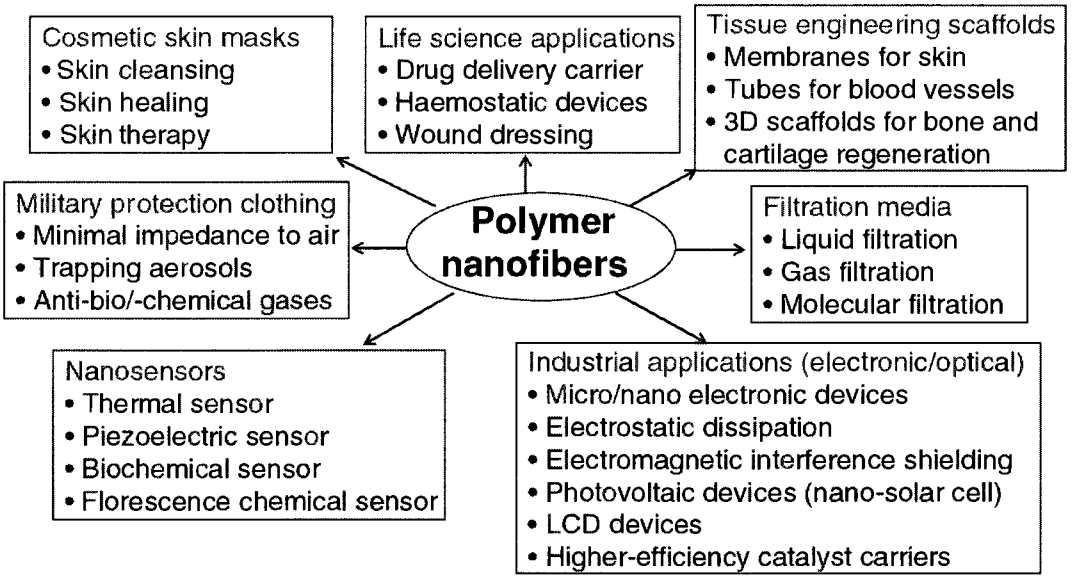

Figure 2-5: Different areas of nanofiber and composite nanofiber applications (Burger, Hsiao et al. 2006)

2.3.2. Production methods

The manufacturing of nanostructured materials could happen in two ways of top-down and bottom-up nano-processing methodologies. The first one is the action of cutting and removal of the bulk materials to change them into desirable sizes; however the second type is based on the idea of employing the building blocks to manufacture the nanostructured materials (Seeram Ramakrishna 2005). There are different methods known as the nanofiber manufacturing techniques including both top-down and bottom-up methods. These methods include drawing, template synthesis, phase separation, self-assembly and electrospinning, which are briefly described as follow:

1. ***Drawing:*** In this method, the nanofiber is produced by using a micropipette and a drop of the liquid that is to be spun to nanofibers. A micropipette with the diameter in the range of micrometers is dipped into the droplet of liquid close to the contact line of the droplet and the surface. The pulling of the micropipette is then occurred with the speed of almost 10^{-4} m/s to obtain the fibre. During this procedure, somehow similar to dry-spinning, the evaporation of the solvent causes solidification and molecular fibre formation (Seeram Ramakrishna 2005).

3. ***Template synthesis:*** In this method, polymer solution is located neighbouring a kind of aluminium mould containing nano-pores, and is forced through the nozzles under water pressure. The solution is entered a water medium after exiting the pores that has the role of non-solvent and causes the fibre to be solidified. In this method, the fibre diameter is determined by the size of pores inserted in the mould (Seeram Ramakrishna 2005).

4. ***Phase separation:*** In this method, the fibres are shaped based on the phase separation mechanism and it is only used for a specific type of systems. A gel of polymer is shaped at the beginning by adding solvent to the polymer system to shape nanofibers. The gel obtained, contains a connecting network of nanofibres shaped in the solvent. The nanofibers are obtained after removing the solvent from the network inside structure (Seeram Ramakrishna 2005).

5. ***Self-assembly:*** In this method, smaller molecules are arranged in a concentric manner to manufacture nanofibers. For this type of nanofibers, molecules can be shaped

among the concentrically arranged shapes to form fibres and upon extension in the plane normal, the fibres are shaped (Seeram Ramakrishna 2005). Intermolecular forces bring the smaller molecules together and determine the final shape of macromolecular nanofiber.

6. ***Electrospinning:*** "Electrostatic spinning" or "Electrospinning" is accounted as a method of spinning; while unlike conventional methods of fibre spinning including wet spinning, gel spinning, dry spinning and melt spinning which are capable of fibre production in micrometer range, electrospinning allows the production of fibres in nanometer range. In this way, it is possible to obtain fibres from several microns down to 100 nm. This is the best commonly known method of nanofiber production by which it is possible to obtain a large number of polymer nanofibers with different properties for various applications. Compared to other methods described above, it is not an exclusive technique for only limited number of polymers. Moreover, it is possible to produce a larger quantity of nanofibers by electrospinning compared to the previous types. In electrospinning, a high voltage electric field is applied on the polymeric fluid stream (solution or melt) exiting through a millimetre- scale nozzle. Followed by the application of this electrical field, the ions produced inside fibre cause splash and nanofibers production (Frenot and Chronakis 2003). This process will be discussed in more details in the next section since it is the main concern of this work.

2.4. Electrospinning

Various types of materials such as polymers, biopolymers and polymer composites can be used in electrospinning to obtain nanofibers. In 1745, Bose could create an aerosol spray by applying a high potential to a liquid shaped at the end of a glass capillary tube. However, electrospinning method was first used by Rayleigh in 1897 (Reneker and Chun 1996), thereafter it was studied in more details by Zeleny in 1917 (Burger, Hsiao et al. 2006). Taylor was the first person who analyzed the electrospinning from physical point

of view and he analyzed more deeply the cone shaping and the other aspects (Reneker and Chun 1996). He investigated the conditions at the point of a droplet deformed by electrical force and described the state of stability. Thereafter, the new method of electrospraying was patented by Formhals in 1934 (Burger, Hsiao et al. 2006). The process has not been employed for large amount of nanofibers production in industrial scale except by the Donaldson Company Inc. mainly for the air filtration applications (Burger, Hsiao et al. 2006).

Contrary to the conventional methods of fiber formation, in which the fibers are shaped under tension and during exiting the die, in electrospinning process, a high voltage is applied on polymer to stretch it and the charge is induced within fluid. Therefore, unlike the conventional methods of fiber-spinning techniques, in the electrospinning process, the fibers are produced in the nanometer range. Electrospinning process is basically similar to electrostatic spraying, both of which involve the use of high voltage to shape the jet. In electrospraying, small droplets of particles are formed because of the break-up of the liquid jet and the process is often applicable for low-viscous solutions; however, in electrospinning, solid fiber is generated as the electrified jet is continuously stretched due to the splashing existing amongst the fibers and solvent evaporation (Li and Xia 2004). Construction of nanoscale composites fibers by electrospinning from a mixture is also possible. The electrospun nanofibers obtained from electrospinning could also be aligned to make a functional structure such as nanotubes and nanowires (Frenot and Chronakis 2003).

2.4.1. Stages and parameters

The electrospinning process is based on imposing the electrical forces on the free charges of the surface and inside the polymeric liquid. In conventional methods of spinning, the fiber is imposed to the tensile, rheological, gravitational, inertial and aerodynamic forces. In the electrospinning process, the tensile force for shaping the fiber is produced by the interaction of the applied electric field with the electric charges carried by the jet in polymer solution. The force is quickly transferred to polymer liquid by

applying the electrical forces on the free charges in polymer. The free charges are generally ions and they could move in response to the electric field (Reneker and Chun 1996). The schematic shape of different stages in electrospinning process is shown below.

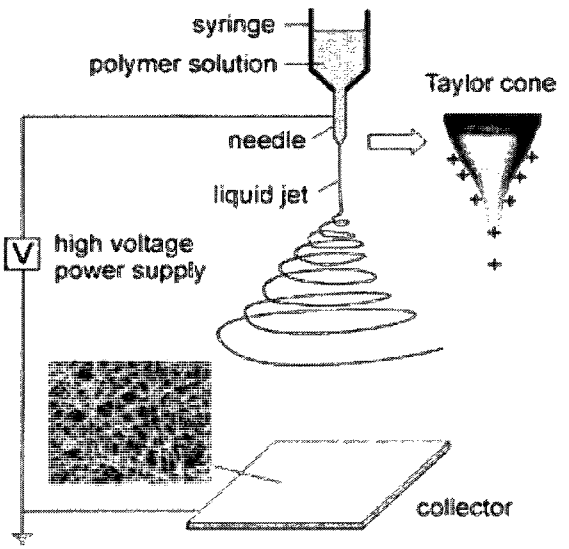

Figure 2-6: The schematic of different electrospinning stages (Li and Xia 2004)

Electrospinning consists of three major parts including a high-voltage power supply, a spinneret (a metallic needle), and a collector (a grounded conductor) (Li and Xia 2004). The power necessary is usually supplied by a direct current (DC). The spinneret is connected to a polymer solution or melt syringe which is supported by a syringe pump. By the use of the syringe pump, the solution is fed through the spinneret at a constant and controllable rate. With applying a high voltage, a pendent drop of polymer solution is shaped at the nozzle and the solution becomes highly electrified and the induced charges are distributed over the surface of the droplet (Li and Xia 2004).

In this way, a jet of liquid is shaped after the exit from the pipette at the beginning, but different regions are known before the final nanofibers production. These stages are four steps including: the jet emerges from the charged surface in the first area of the liquid jet called *base*, then it travels through the *jet region*, and it is divided into many

fibers in the *splaying zone*, and finally the aimed nanofiber is stopped at the *collection region* (Li and Xia 2004). The first region is the base zone, in which a tapered cone is shaped. The axial velocity of the liquid is increased after this area and the polymer is accelerated along the axis of the jet. The base usually has a circular cross section or might have some other shapes if surface tension of the liquid causes the liquid jet to be attracted to the other stationary surface. The second area is the jet zone, in which the electrical forces continue to accelerate the polymer liquid and to stretch the jet. Through this region, the diameter of the jet decreases and the jet is driven by a high electric potential between the solution or melt and the collector. The resisting force in this section in front of filament stretching is the elongation viscosity of the jet. The third zone in which the splaying occurs, the radial forces from the electrical charges carried by the jet are larger than the cohesive energy within the jet, and therefore the single jet is divided into many jets with approximately the same diameter and charge density. The external forces accelerate and stretch the jet, and the stretching followed by the solvent evaporation causes the decrease in the fiber diameter. As the radius of the jet becomes smaller and smaller, the radial force from the charge can be large enough to overcome the cohesive forces and therefore it splits into two or more fibers.

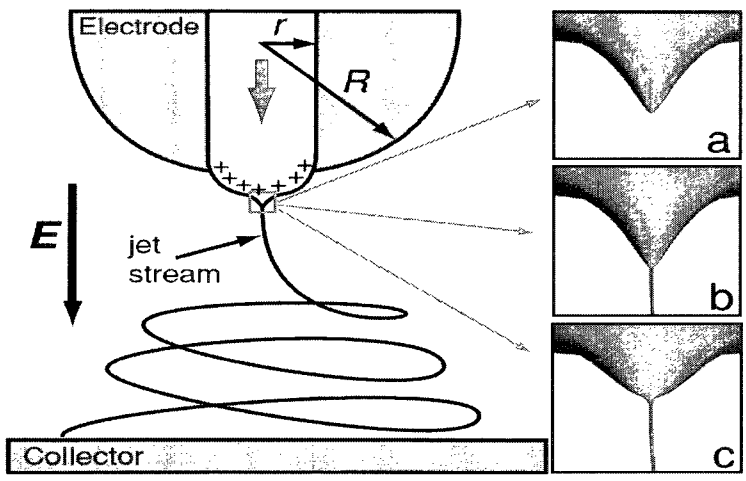

Figure 2-7: The schematic of the jet formation and splashing (Burger, Hsiao et al. 2006)

The collection region is where the jet is stopped and the polymer fiber remaining after solvent evaporation could be collected on the metal surface.

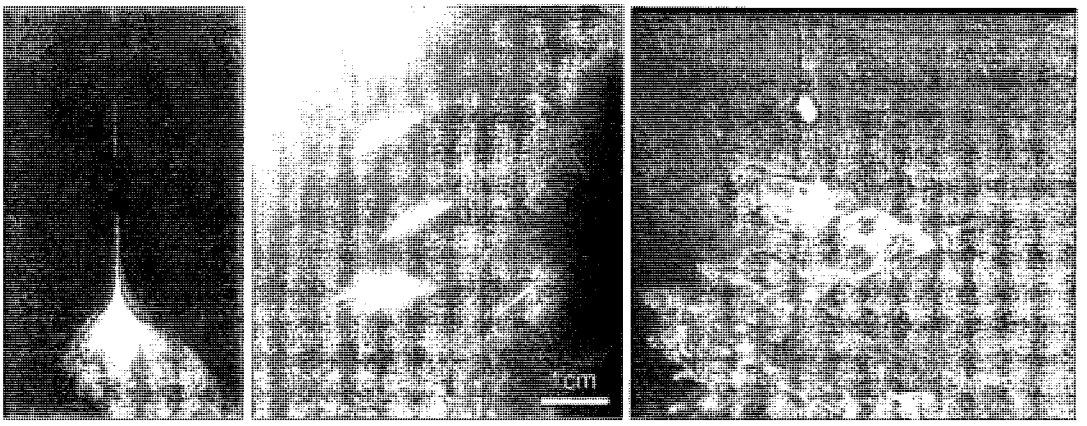

Figure 2-8: Jet formation phenomena in electrospinning process (Burger, Hsiao et al. 2006)

There are different forces controlling the process stages including the jet formation and splashing which are two major electrostatic forces. The first type of the force acting on jet is the electrostatic repulsion between the surface charges; and it carries the charged jet from the spinneret to the target as the main driving force; and the other one is the coulombic force exerted by the external electric field. Coulombic force is imposed on the fiber to separate the adjacent charged carriers along the fiber from the spinneret to target (Wannatong, Sirivat et al. 2004). Under the interaction of these electrostatic forces, the liquid droplet at the tip of the needle is deformed into a commonly cone shape known as Taylor cone which has been described previously (Li and Xia 2004). Once the electric field overcomes a critical value, the electrical forces overcome the surface tension of the polymer solution and they cause the ejection of a liquid jet from the nozzle. The electrified jet then undergoes the stretching process and the long thread is shaped in this way (Li and Xia 2004). The other forces acting on the system include viscoelastic force which is a force in front of charged jet stretching, body or gravitational force and drag force from the friction between the jet and surrounding air (Wannatong, Sirivat et al.

2004). All the above mentioned phenomena and stages are concisely controlled with the following parameters in electrospinning which are the main factors to be studied in this process.

Table 2-1: Different influential parameters of electrospinning process (Tan, Inai et al. 2005)

Properties	Parameters
Solution properties	Viscosity Polymer Concentration Molecular weight of polymer Electrical conductivity Elasticity Surface tension
Processing properties	Applied voltage Distance form needle to collector Volume flow rate Needle diameter
Environmental parameters	Temperature Humidity Atmospheric pressure

2.4.2. Process Background

Although the electrospinning process has been known since 70 years ago, it has only been the topic of interest in the recent few years. Following Formhals` patent in 1934 (Burger, Hsiao et al. 2006), more than 50 other patents in the field of electrospinning were filed (Reneker and Chun 1996). Baumgarten described the electrostatic spinning of acrylic microfibers in 1971 (Reneker and Chun 1996). Reneker and Chun revived this technology in the 1990s and the possibility of employing this

process for different kinds of polymer solutions has been shown in 1996 (Reneker and Chun 1996). At this time and followed by the success of these publications, the name electrospinning was born and widely used in the papers published after Formhal`s work (Li and Xia 2004). In melt state, there are few studies employing this technique (Larrondo and Manley 1981). Chun also used electrospinning for the production of nanoscale fibers of polyethylene, polypropylene and polyester from the melt in vacuum condition (Reneker and Chun 1996). In the three following tables, the papers available in the field of electrospinning and the areas of interests in this process are given concisely.

Table 2-2: Studies that appeared so far about electrospinning set-up innovations (Sawicka and Gouma 2006)

Innovation	**Effect**
Vacuum system	Increased electric field strength (Rangpukan and Reneker (2001))
Multi-jet System	Electrospinning various materials simultaneously including uniform thickness (Gupta and Wilkes (2003), Ding et al. (2004))
Wheel-like bobbin collector	Aligned nanofibers with 1–2 μm gaps between individual threads (Theron et al. (2001))
Two separated electrically conductive substrates	Uniaxially aligned nanofibers stretched across the substrates (Li et al. (2003))
Metal frame collector	Oriented nanofibers (Dersch et al. (2003))
Insulated mandrel collector	Aligned nanofibers (Sundaray et al. (2004))
Copper wire framed drum collector	Nanofibers oriented perpendicularly to the copper wires (Katta et al. (2004))
Spinneret containing two co-axial capillaries	Hollow nanofibers, nanocomposites of 'unspinable' materials (Li and Xia (2004))

Table 2-3: The papers about studying electrospinning process parameters (Sawicka and Gouma 2006)

Parameter under study	**Results obtained**
Needle to collector distance	Exponentially inverse to the volume charge density (Theron et al., 2004) Inversely proportional to bead formation density (Fong et al., 1999; Gupta & Wilkes, 2003) Inverse to the electric field strength (Fong et al., 1999; Theron et al., 2004) Inversely proportional to fiber diameter (Gupta & Wilkes, 2003)
Flow rate	Directly proportional to the electric current (Theron et al., 2004) Directly proportional to the fiber diameter (Sawicka et al., 2005) Inversely related to surface charge density (Theron et al., 2004) Inversely related to volume charge density (Theron et al., 2004)
Voltage	Inversely proportional to surface charge density (Theron et al., 2004) Direct effect on bead formation (Deitzel et al., 2001) AC potential improved fiber uniformity (Kessick et al., 2004) Inversely related to fiber diameter (Gupta & Wilkes, 2003)

Table 2-4: The papers about studying electrospinning solution parameters (Sawicka and Gouma 2006)

Parameter under study	Results obtained
Concentration of polymer	Directly proportional to the fiber diameter (Gupta & Wilkes, 2003) Power law relation to the fiber diameter (Deitzel et al., 2001) Cube of polymer concentration proportional to diameter (Demir et al., 2002) Parabolic – upper and lower limit relation to diameter (Hsu & Shivkumar, 2004)
Ionic strength	Directly proportional to charge density (Zong et al., 2002) Inversely proportional to bead density (Zong et al., 2002)
Solvent	Effects of volume charge density (Theron et al., 2004) Directly related to the evaporation and solidification rate (Theron et al., 2004)
Temperature	Inversely proportional to viscosity (Demir et al., 2002) Uniform fibers with less beading (Demir et al., 2002)
Viscosity	Parabolic relation to diameter, and spinning ability (Hsu & Shivkumar, 2004)

2.4.3. Process Modeling

Similar to all processes, modeling is quite important in studying the electrospinning and there are numerous papers describing the controlling phenomena in electrospinning theoretically for deeply understanding of this process. In electrospinning process, the negative or positive charges of the syringe cause an increase or a decrease in the amount of electrons in polymer solutions. The main source of charge build-up is correlated to the

magnitude of the applied voltage; however, parameters such as the density of free electrons in an aromatic structure have also important effects. In addition, the existence of the ions in the overall neutral polymer helps in the charge build-up. Followed by the charge build-up, the electric force effects the droplet exiting the syringe towards the collector. In addition, a source of similar ions is produced inside the cone and jet which results into build-up the repulsive forces inside jet. Surface tension and other hydrostatic forces are against the jet initiation and splashing. Therefore as the opposing forces such as columbic force and electric field overcome the hydrostatic forces, the second and third regions of the process start to develop. It is possible to describe the process mathematically by employing the concepts of some well known phenomena such as electro-hydrodynamic (EHD) theory and force balance. In most of the modeling works, the fluid is assumed viscoelastic (the importance of elastic forces is clear in polymer materials) and incompressible. Moreover, a cylindrical coordinate structure is assumed to obtain a logical force balance for the system; even though, the first part and the shaped cone structure are well-defined by the spherical coordinate (Seeram Ramakrishna 2005).

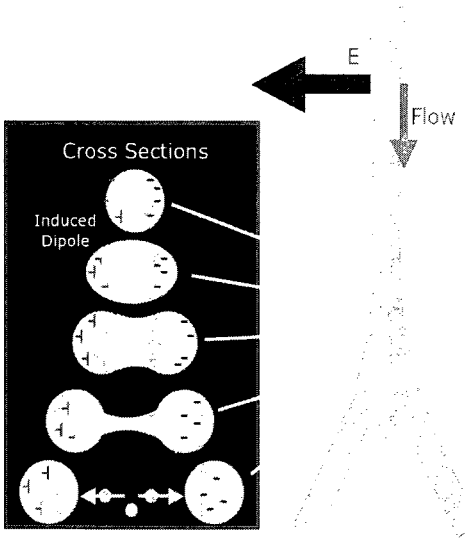

Figure 2-9: Splitting of a liquid jet in electrospinning

In this process, a complex fluid jet is ejected from the end of a syringe and is stretched smoothly by electrostatic forces. In overall, there is a force balance among

various forces existing in the cone, while the gravity and electric polarization stress tend to elongate the droplet by the tangential electric stress on the surface; though viscous drag force slows down the formation of the cone. Moreover, there are two more forces active on the surface of the droplet and in forming cone. These are the surface tension trying to minimize the surface area pulling the surface vertically and an opposing force which is the normal electrical stress. This force tries to maximize the distance between electrical charges on the surface by enlarging the surface area. In the case where the electric field is large enough, the droplet is deformed into the *Taylor cone*. As soon as the electrostatic repulsive forces overcome the surface tension, a fine charged jet develops that is typically 1/100 in diameter of the needle opening. After leaving the cone, this jet then moves toward the counter electrode. While moving to the collector, the jet becomes unstable and in this second stage, there are three possible instabilities. First: where droplets are formed which is referred to as Rayleigh instability; second: where varicose (zig-zag) structures are visible, which is referred to as axisymmetric instability; and third: where a non-axisymmetric bending of the fiber occurs. This last bending instability is the most important one that needs to be achieved, as it is responsible for thinning the fibers from about a micron into the nanometer range.

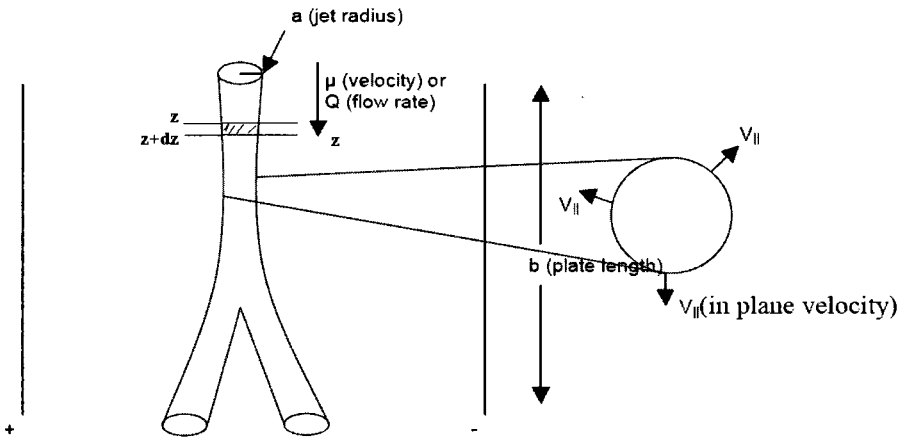

Figure 2-10: The element employed for the modeling

Aside from any additional information such as EHD, first the simplest equations available for the modeling of this process are given here.

- ***Conservation relations***: The basic consideration for the modeling of electrospinning process is the three most important conservation quantities including mass, momentum and the charge density. *For the mass part*, it is possible to write that no mass is produced nor is destroyed, but it is transported from one place to another. Therefore, in a specific control volume between the distances z and $z+dz$, it is possible to write that:

$$m = \rho\pi R^2 dz \tag{2-1}$$

where ρ is the liquid density and R is the jet radius. Over the time interval dt the amount of mass entering and exiting the control volume are:

$$m_{in} = \rho\pi R^2 v dt \Big|_z \tag{2-2}$$

$$m_{out} = \rho\pi R^2 v dt \Big|_{z+dz} \tag{2-3}$$

where v is the liquid velocity.

Considering the mass balance:

$$\Delta_t m = m_{in} - m_{out} \tag{2-4}$$

then we have:

$$\frac{\partial R^2}{\partial t} + \frac{\partial v R^2}{\partial z} = 0 \tag{2-5}$$

For the momentum part, all the processes involving motion should be considered. For the momentum balance of the fluid segment bounded by the sections z and $z+dz$, it is possible to write:

$$M = \rho\pi R^2 v dz \tag{2-6}$$

while:

$$dz = v dt \tag{2-7}$$

The flux of momentum into and out from the bounded volume for the time interval dt can be written as:

$$M_{in} = \rho\pi R^2 v^2 dt \Big|_z \tag{2-8}$$

$$M_{out} = \rho\pi R^2 v^2 dt\Big|_{z+dz} \tag{2-9}$$

The liquid pressures (p) at the boundaries z and $z+dz$ should be considered and therefore:

$$M\Big|_z = p\pi R^2 dt \;\Big|_z \tag{2-10}$$

$$M\Big|_{z+dz} = p\pi R^2 dt \;\Big|_{z+dz} \tag{2-11}$$

Concisely, for the momentum balance, it is possible to write:

$$\Delta_t M = M_{in} - M_{out} + M\Big|_z - M\Big|_{z+dz} \tag{2-12}$$

And then it results into:

$$\frac{\partial}{\partial t}\left(vR^2\right) + \frac{\partial}{\partial z}\left(v^2R^2\right) = -\frac{1}{\rho}\frac{\partial}{\partial z}\left(pR^2\right) \tag{2-13}$$

Combining this equation with conservation of mass gives:

$$\frac{\partial v}{\partial t} + v\frac{\partial v}{\partial z} = -\frac{1}{\rho R^2}\partial pR^2 \Big/ \partial z \tag{2-14}$$

Equation (14) is the simplest form of the momentum balance equation and it has been extended and modified by different authors. For example, Reneker *et al.* could modify the equation by considering an electrical field imposed on a jet of viscoelastic fiber (Reneker, Yarin et al. 2000). In their modification, they proposed the following equation for the momentum balance:

$$m\frac{dv}{dt} = -\frac{e^2}{l^2} - \frac{eV_0}{h} + \pi R^2\sigma_V \tag{2-15}$$

In this Equation, e is the charge, l is the length of ideal rectilinear jet, V_0 applied voltage, h distance from pendant drop to ground collector, σ_V is the viscoelastic stress, and m is the total mass (Reneker, Yarin et al. 2000).

In 2002, Feng considered the stretching of a non-Newtonian electrified jet of a liquid for modeling and simulation of electrospinning (Feng 2002). He divided the electrospinning to two main regions, one at the exit from capillary at the nozzle and during the stretching smoothly from the needle and the other one is the second part which is the bending instability and sufficiently thinning of the liquid. In his model, he focused on the first part which was the main part of the process (Feng 2002). In his modeling

procedure, he could obtain that the jet is elongated by the electrostatic forces while surface tension, viscosity and inertial forces also play an important role. They employed the concept of slender-body theory applicable for various spinning processes ($\left|\frac{dR(z)}{dz}\le 1\right|$) and therefore he could ignore the radial velocity profile. Finally, he could achieve the following model for the momentum balance:

$$\frac{d}{dz}\left(\pi R^2\rho v^2\right)=\pi R^2\rho g+\frac{d}{dz}\left[\pi R^2\left(-p+\tau_{zz}\right)\right]+\frac{\gamma}{R}\cdot 2\pi RR'+2\pi R(t_t^e-t_n^eR') \qquad (2\text{-}16)$$

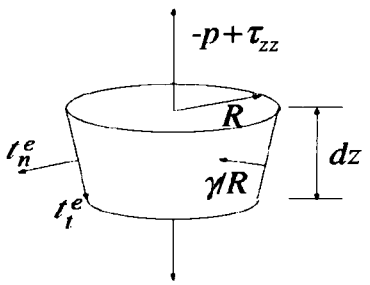

Figure 2-11: Momentum balance element for Feng's model

where τ_{zz} is the axial viscous normal stress, p is the pressure, γ is the surface tension, and t_t^e and t_n^e are the tangential and normal tractions on the surface of the jet due to the electrical field. Compared to the previous models, he could also consider the effect of electrical forces in the force balance equation quite well. The prime indicates derivative with respect to z and R' is the slope of the jet surface. In this model, he employed both the concept of Newtonian and non-Newtonian fluids. In another work, he focused on the determining role of the governing equation of the fluid and the effect of fluid viscoelasticity (Feng 2003). He used the Giesekus viscoelastic model and, employing the previous governing equations, repeated the modeling in this case (Feng 2003).

In the case of *conservation of charge,* the third conservation rule, which is really important in this process and distinguishes electrospinning form the other spinning methods, it is possible to write:

$$I=\pi R^2KE+2\pi Rv\sigma \qquad (2\text{-}17)$$

where: I is the constant total current in the jet, K is the liquid conductivity, E is the vertical component of the electric field and σ is the surface charge density. The second and third terms in this formula refer to the current flow across the jet cross-section and its perimeter respectively along the jet axis (Seeram Ramakrishna 2005).

- ***Force balance equation:*** The forces imposed on the system along with the Newton's second law of motion results in:

$$m\frac{d^2P}{dt^2} = \sum f \tag{2-18}$$

where m is the equivalent mass and the most important forces acting on the system in the simplest forms are:

$$\sum f = f_C + f_E + f_V + f_S + f_A + f_G \tag{2-19}$$

In the above Equation, different forces include: f_C: columbic, f_E: electric field, f_V: viscoelastic, f_S: surface tension, f_A: air drag, and f_G: gravitation respectively. These are the most important controlling forces and we could describe them as follow (Seeram Ramakrishna 2005):

$$f_C = \frac{e^2}{l^2} \tag{2-20}$$

$$f_E = -\frac{eV_0}{h} \tag{2-21}$$

$$\frac{d\sigma_v}{dt} = \frac{G}{l}\frac{dl}{dt} - \frac{G}{\mu}\sigma_v \text{ (To calculate } f_V) \tag{2-22}$$

$$f_S = \frac{\alpha\pi R^2 k}{\sqrt{x_i^2 + y_i^2}}\left[i|x|sign(x) + j|y|sign(y)\right] \tag{2-23}$$

$$f_A = 0.65\pi R\rho_{air}v^2\left(\frac{2vR}{v_{air}}\right)^{-0.81} \tag{2-24}$$

$$f_G = \rho g\pi R^2 \tag{2-25}$$

In the above Equations, the parameters include: e the charge, l is the length of ideal rectilinear jet, V_0 applied voltage, h distance from pendant drop to ground collector, σ_V is the viscoelastic stress, G is the elastic modulus, μ is the viscosity, α is the surface tension,

k is the jet curvature, ρ is the density and v is the cinematic viscosity (Seeram Ramakrishna 2005). The air drag force (f_A) is produced by the movement of the liquid jet in resistance to air and this force along with gravitational force (f_G) could be neglected (Reneker, Yarin et al. 2000). The index i means the i^{th} section of the fiber and $\boldsymbol{i}$ and $\boldsymbol{j}$ are the space unit vectors (Reneker, Yarin et al. 2000).

The equations given above was obtained based on the simplest form of mathematical modeling of the electrospinning process which assumes a rectilinear electrified jet of liquid in an electric field parallel to its axis. In the most applicable and well-known approach for the modeling of electrospinning process, the concept of electrohydrodynamic (EHD) theory is employed. EHD deals with fluid motion induced by electric field. The scientists, who have focused so far on the EHD theory, assume three main parts for the process. These three parts include *cone formation*, the *thinning of fiber* and *drying zone of the fiber* (Sigmund, Yuh et al. 2006). The main portion of the process is the formation of the cone at the nozzle tip and fiber thinning which are the determining factors for the development of nanofibers (Sigmund, Yuh et al. 2006).

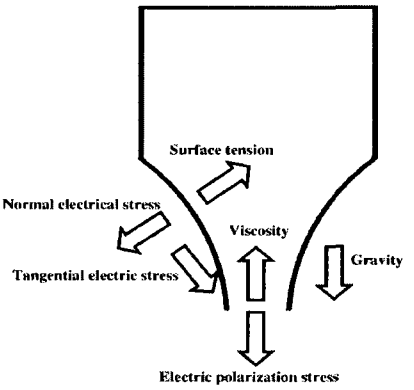

Figure 2-12: Different forces acting on the electrospun liquid jet (Sigmund, Yuh et al. 2006)

EHD description of the phenomena includes the identification of the processes with the presence of the electrical liquids and its movements. Most of the scientists have focused on electrohydrodynamic atomization in the cone-jet mode for many years. Following Zeleny (1914, 1915, 1917), who developed the first solid scientific description

of the process; many people have contributed to understand and model this process. In such a process described by EHD which is quite similar to electrospinning, a liquid is supplied to a nozzle at a low flow rate. Then a droplet is formed at the nozzle, a strong electric field is applied over the droplet and, as a result, the electric field induces free charge on the liquid surface. Consequently, electric stresses occur on the surface and these stresses change the droplet shape into a conical shape. At the cone apex, a liquid jet with a high charge density occurs. In certain circumstances, this jet will break up into highly charged main droplets with a narrow size distribution, and a number of smaller secondary and satellite droplets. The volume ratio of the secondary droplets and the satellites over the main droplets is relatively small, but the number ratio is often larger than one (Hartman, Brunner et al. 1999).

Electrohydrodynamic atomization in the cone-jet mode has to be described by at least three different processes. *The first process is the acceleration of the liquid in the liquid cone.* This acceleration process and the shape of the liquid cone could be described by the force balance of surface tension, gravity, electric stresses in the liquid surface, inertia and viscous stresses. The *second process* in electrohydrodynamic atomization in the cone-jet mode is *the breakup of the jet into droplets.* The third process is *the development of the spray after droplet production.* Electrical interaction between highly charged droplets with different sizes and thus different inertia causes a size segregation select (Hartman, Brunner et al. 1999).

Studying the EHD as the basis phenomena controlling the electrospinning began in 17^{th} century by William Gilbert. He described the formation of a conical shape upon bringing a charged jet above a droplet. Rayleigh in 1882 studied the droplet dynamics and how radially directed forces stemming from interfacial charge offset surface tension. Taylor (1964) was the first who calculated analytically a conical shape, which balanced the surface tension and the electrical normal stress for general material. However, in his assumptions, there was no liquid jet at the cone apex and therefore there was no electrical current and liquid flow through this liquid cone. Joffre (1986) approached the problem numerically, which allowed a more flexible cone shape. Since in Taylor's case, the cone

had to be solved mathematically, only the angle at the cone apex could be used as a parameter. However, also in Joffre's calculations there was no jet and the cone apex was just rounded off (Hartman, Brunner et al. 1999).

Description of the EHD phenomena is obtained by the employment of the liquid motion coupled with the existence of electric field and the modified version of mass and momentum balance equations. In summary, one of the best models presented by Taylor and Melcher include five important equations as follow, and they used Maxwell type constitutive equation for the liquid (Saville 1997):

$$\frac{\tau_\mu}{\tau_p}\frac{\partial \underline{u}}{\partial t} + \mathrm{Re}\,\underline{u}\cdot\nabla\underline{u} = -\nabla p - \frac{1}{2}\underline{E}\cdot\underline{E}\nabla\varepsilon + \nabla\cdot(\varepsilon\underline{E})\underline{E} + \nabla^2\underline{u} \;\&\; \nabla\cdot\underline{u} = 0 \qquad (2\text{-}26)$$

$$\nabla\cdot\sigma\underline{E} = 0 \qquad (2\text{-}27)$$

$$\frac{\tau_c}{\tau_p}\frac{\partial q}{\partial t} + \frac{\tau_c}{\tau_f}\left[\underline{u}\cdot\nabla_s q - q\underline{n}\cdot(\underline{n}\cdot\nabla)\underline{u}\right] = \left\|-\sigma\underline{E}\right\|\cdot\underline{n} \qquad (2\text{-}28)$$

$$\left\|\varepsilon\underline{E}\right\|\cdot\underline{n} = q \qquad (2\text{-}29)$$

$$\begin{aligned}\left[\underline{\underline{\sigma}}^M\cdot\underline{n}\right]\cdot\underline{n} &= \frac{1}{2}\left\|\varepsilon(\underline{E}\cdot\underline{n})^2 - \varepsilon(\underline{E}\cdot\underline{t}_1)^2 - \varepsilon(\underline{E}\cdot\underline{t}_2)^2\right\| \\ \left[\underline{\underline{\sigma}}^M\cdot\underline{n}\right]\cdot\underline{t}_i &= q\underline{E}\cdot\underline{t}_i\end{aligned} \qquad (2\text{-}30)$$

τ_μ is the viscous relaxation time and is equal to $l^2\rho/\mu$, τ_p is the process scale time, $\underline{u}$ is the velocity vector, p is the pressure, $\underline{E}$ is the electric field strength, ε dielectric permittivity, σ is the conductivity, τ_c is the electric characteristic time and is equal to $\varepsilon\varepsilon_0/\sigma$, τ_f is the convective flow rate and it is equal to l/u_f, q is the free charge per unit area, σ^M is the Maxwell stress tensor, $\underline{t}_i$ represents either of two orthogonal tangent vectors embedded in the surface, and $\underline{n}$ is the local outer normal (Saville 1997).

Employing this concept, Fernandez de la Mora (1994) gave the following relations, which estimate the droplet radius and the current through the liquid cone:

$$d_d = b_1(\varepsilon_r)\left(\frac{Q\varepsilon_0\varepsilon_r}{K}\right)^{1/3} + c_1 \qquad (2\text{-}31)$$

$$I = b_2(\varepsilon_r)\left(\frac{\gamma Q K}{\varepsilon_t}\right) + c_2 \qquad (2\text{-}32)$$

where, d_d is the droplet diameter (m), Q is the liquid flow rate ($m^3\ s^{-1}$), K is the conductivity ($S\ m^{-1}$), γ is the surface tension ($N\ m^{-1}$), ε_r is the relative permittivity of the liquid, ε_0 is permittivity of a vacuum ($C\ V^{-1}\ m^{-1}$), I is the current (A), b_1 and b_2 are functions of the liquid permittivity, and c_1 and c_2 are constants, which were equal to zero in the representation of Fernandez de la Mora. These relations are often called the scaling laws for electrohydrodynamic atomization in the cone-jet mode and are only valid for liquid cones with a flat radial profile of the axial liquid velocity in the jet. These relations were modified by Ganan-Calvo (1994, 1997). He gave new relations for b_1 and b_2, and introduced the constants c_1 and c_2. He also presented a new scaling of current and droplet size, where they suggested a new parameter of the characteristics flow rate which is equal to $Q_0=\rho\, K\, \varepsilon_0^{-1}\, \gamma^{-1}$ (Hartman, Brunner et al. 1999).

$$d_d = 3.78\pi^{-2/3}0.6Q^{1/2}\left(\frac{\rho\varepsilon_0}{\gamma K}\right)^{1/6} \qquad (2\text{-}33)$$

$$I = 4.25\left(\frac{(\gamma Q K)}{\ln\left(\left(Q/Q_0\right)^{1/2}\right)}\right)^{1/2} \qquad (2\text{-}34)$$

Following the primer works available in this area and modeling the electrical cone-jet by the use of EHD concept, Hartman *et al.* made a complete analysis on the shaped cone-jet and forces acting on the system as depicted in Figure 2-13.

The droplet size mainly depends on the liquid flow rate and liquid characteristics such as density, viscosity, conductivity, electrical permittivity and surface tension. Moreover, the electrode configuration and the applied potential have some influence on its shape. In the shaped liquid cone, the charge is transported in two ways. The first way is through conduction in the liquid due to the electric fields and the second way is by charge convection. The electric field induces free charge at the liquid surface and this free charge consists of ions. The electric field at the liquid surface accelerates the ions

towards the cone apex and the ions in their turn accelerate the surrounding liquid. It is assumed during the modeling procedure that the ion velocity can not be much larger than the liquid velocity, since the ions loose their velocity due to collisions with the liquid molecules. The liquid velocity and the ion velocity depends then on the local electric field strength, the amount of free charge, and on the flow properties of the liquid (Hartman, Brunner et al. 1999). The final structure of the liquid cone is determined by different forces acting on the system including surface tension, normal electric stress, and the velocity pressure in the cone. Employing the EHD theory, one-dimensional axial momentum equation of the jet may be written as:

$$\frac{2\tau}{r_s} = \frac{\partial\left(\left(\gamma/r_s\right) - \left(\sigma^2/\varepsilon_0\right) + 1/2\rho u_z^2\right)}{\partial z} \qquad (2\text{-}35)$$

In the above equation, r_s is the radius of the liquid cone and jet in the cylindrical coordinate system (z is the axial coordinate along the jet), u_z is the liquid velocity, τ is the tangential stress, and σ is the surface charge density (Hartman, Brunner et al. 1999).

The electric field of a ring of charges could be obtained as:

$$E_z \cong \frac{q}{\varepsilon_0 \Delta z^2} \qquad (2\text{-}36)$$

q is the charge on the ring, E_z is the electrical field strength in axial direction, and therefore, it is possible to write:

$$E_z \cong \frac{2\pi\Delta(r_s\sigma)\Delta z}{\varepsilon_0 \Delta z^2} \cong \frac{\sigma dr_s}{\varepsilon_0 dz} + \frac{r_s d\sigma}{\varepsilon_0 dz} \qquad (2\text{-}37)$$

As the equation shows, since the amount of dr_s/dz is small and negligible, the strength of axial electrical field is strongly dependant on the tangential electrical field strength. From another point of view, the permittivity of the liquid affects only the axial electrical field and not the tangential one, therefore, the amount of electrical field strength is almost independent of the liquid permittivity (Hartman, Brunner et al. 1999). For simplicity, it is possible to assume that axial liquid velocity in the jet is equal to velocity in the jet center, and it is possible to write that:

$$u_z = \frac{Q}{\pi r_s^2} \tag{2-38}$$

Combining the above equations, it is possible to write that:

$$\left(-\frac{\gamma\varepsilon_0}{2r_s\sigma^2} - \frac{2\rho\varepsilon_0 Q^2}{\sigma^2\pi^2 r_s^4}\right)\frac{dr_s}{dz} - \frac{r_s d\sigma}{\sigma dz} \cong \frac{dr_s}{dz} + \frac{r_s d\sigma}{\sigma dz} \tag{2-39}$$

In this equation, two dimensionless numbers can be identified. The first number describes the relation between the surface tension and the normal electric stress. The second dimensionless number identifies the relation between the velocity pressure, and the normal electric stress.

$$\sigma = \left(\frac{\varepsilon_0\gamma}{r_{s*}}\right)\sigma'; r_s = r_{s*} r_s'; z = r_{s*} z' \tag{2-40}$$

where σ' is the dimensionless surface charge, r_s' is the dimensionless radius of the liquid surface, z' is the dimensionless axial coordinate of the jet, and r_{s*} is a characteristic radius. In the cone shape part, the shape is obtained by the surface tension stress and in that of the jet; the shape is determined by the velocity pressure. At the position on the jet, where the first dimensionless number of equation (39) is equal to the value of the second dimensionless number, the velocity pressure becomes dominant over the surface tension, the radius is given by:

$$r_{s,v} \cong \left(\frac{\rho Q^2}{\gamma}\right)^{1/3} \tag{2-41}$$

$r_{s,v}$ is the cone radius, where the jet emerges from the liquid cone (Hartman, Brunner et al. 1999).

The same as the previous approach, the current depends on the charge transport in the liquid cone and the charge in the system is transported in two ways. In the base of the cone, the charge is mainly transported through conduction. On the other hand, in the jet, the charge is mainly transported by charge convection. The current through the cone equals the sum of these two contributions. Therefore:

$$I = \pi r_s^2 E_z K + 2\pi r_s u_z \sigma \tag{2-42}$$

This equation is the same as the one given in the simplest modeling approach. It should be pointed out that the sum of the charges of those in the charge conduction and convention should be equal to zero and consequently,

$$\frac{d\left(r_s^2\left(d(\sigma r_s)/dz\right)\right)}{dz} \cong \frac{Q\varepsilon_0}{K}\frac{d(\sigma/r_s)}{dz} \qquad (2\text{-}43)$$

This equation in the dimensionless form could be written as:

$$r_{s\cdot} = \left(\frac{Q\varepsilon_0}{K}\right)^{1/3} \qquad (2\text{-}44)$$

This is the value representing the radius where the conduction is too low for supplying the current. Therefore, employing the above formula and assumptions and with flat radial profile of the axial velocity, this equation is:

$$I = \frac{Q\left(\gamma\varepsilon_0/r_{s\cdot}\right)^{1/2}}{r_{s\cdot}}\frac{2\sigma'}{r_s'} + Kr_{s\cdot}^{\,2}\left(\frac{\gamma}{\varepsilon_0 r_{s\cdot}}\right)^{1/2}\pi r_s'^{2}E_z' = (\gamma KQ)^{1/2}\left(\frac{2\sigma'}{r_s'} + \pi r_s'^{2}E_z'\right) \cong (\gamma KQ)^{1/2} \qquad (2\text{-}45)$$

In this formula, E'_z is the dimensionless electric field in axial direction (Hartman, Brunner et al. 1999).

Hartman *et al.* modeled the electrospinning process employing the above mentioned EHD concepts. They estimated the amount of charge accumulated during the process and also the shape of the cone in electric field by assuming a Newtonian fluid. They gave a complete physical mathematical model and achieved the forces acting on the system analytically as follow (Hartman, Brunner et al. 1999).

For the part related to the cone shape calculations, they used the Navier-Stokes equation. In their balance, the change in potential energy (pressure p_{liq}, gravity p_g) and the kinetic energy p_{Ekin} (velocity pressure) is in balance with input energy due to the tangential electrical stress τ_{Et} , the change in polarization stress σ_E , and the energy dissipation due to the viscous stresses in the liquid σ_μ , τ_μ and obtained:

$$\frac{\partial\left(p_{Ekin} + p_{liq} - \sigma_\mu - \sigma_\varepsilon - p_g\right)}{\partial z} = \frac{2}{r_s}\left(\tau_\mu + \tau_{Er}\right) \qquad (2\text{-}46)$$

$$p_{liq} = p_{out} + \Delta p_{n,\mu} + \Delta p_{En} + \Delta p_s \qquad (2\text{-}47)$$

where p_{out} is the air pressure, $\Delta p_{n,\mu}$ is the stress in the liquid surface due to viscous stress, Δp_{En} is the normal electric stress in the liquid surface, and Δp_s is the surface tension stress in the liquid surface.

The pressure inside the liquid cone depends on the pressure of the surrounding air and the stresses that occur in the liquid-air surface. The air pressure is independent of the axial coordinate z, and can be neglected. Therefore, only the stresses in the liquid surface are taken into account. The stresses that occur in this surface are *the surface tension* of the liquid, *the normal electric stresses*, and *the viscous surface stress*.

a) $$\Delta p_s = \gamma\left(\frac{1}{r_{s1}} + \frac{1}{r_{s2}}\right) \qquad (2\text{-}48)$$

Δp_s is the pressure difference due to the liquid and air, while r_{s1} and r_{s2} are radii of curvature and for a cylindrical coordinate system, it is possible to write (Hartman, Brunner et al. 1999):

$$\Delta p_s = \gamma\left(\frac{1}{r_s\left(1+\left(dr_s/dz\right)^2\right)^{1/2}} - \frac{d^2 r_s/dz^2}{\left(1+\left(dr_s/dz\right)^2\right)^{3/2}}\right) \qquad (2\text{-}49)$$

b) Normal electric field induces a free electric charge and a polarization charge in the liquid surface and the electric field and these charges create a normal electric stress in the liquid surface.

$$\Delta p_{En} = -1/2\varepsilon_0\left(E_{n,out}^2 - 2\varepsilon_r E_{n.ins}^2 + E_{n,ins}^2\right) \qquad (2\text{-}50)$$

where $E_{\mathrm{n,ins}}$ is the electric field strength normal to the liquid-air surface inside the liquid and $E_{\mathrm{n.out}}$ is the electric field strength normal to the liquid-air surface outside the liquid (Hartman, Brunner et al. 1999).

c) For the third one and viscous surface stress, the balance of normal stresses at the liquid surface as shown in Figure 2-13 results in:

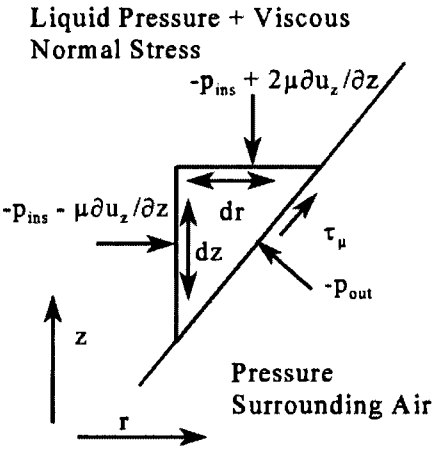

Figure 2-13: The viscous stress and normal stresses balance (Hartman, Brunner et al. 1999)

$$\Delta p_{n,\mu} = \frac{2(dr_s/dz)^2 - 1}{(dr_s/dz)^2 + 1}\mu\frac{\partial u_z}{\partial z} \qquad (2\text{-}51)$$

In this equation μ is the absolute viscosity of the liquid.

The kinetic energy is simply achieved concerning a factor ($C_{profile}$) for the assumption of flat profile. Since the velocity profile is assumed flat, while there is a radial velocity profile in reality.

$$p_{Ekin} = C_{profile} 1/2\rho(\bar{u}_z)^2 \qquad (2\text{-}52)$$

In addition, the tangential viscous surface stresses and also the bulk viscous stresses due to the normal axial stresses should be calculated.

$$\tau_\mu = \frac{3\mu(\partial u_z/\partial z)(dr_s/dz)}{1+(dr_s/dz)^2} \qquad (2\text{-}53)$$

$$\sigma_\mu = 2\mu\frac{\partial u_z}{\partial z} \qquad (2\text{-}54)$$

In the case of using a material capable of being polarized in an electric field during electrospinning process, a kind of normal stress is produced inside the material due to the polarization which could be calculated as:

$$f = \nabla.\varepsilon_0\varepsilon_r E + 1/2(\varepsilon_r - 1)\varepsilon_0\nabla E^2 \qquad (2\text{-}55)$$

where f is the force per unit volume, and E is the electric field strength. It is assumed that all the charges are at the surface of the material and there is no charge at the bulk and therefore:

$$\nabla.\varepsilon_0\varepsilon_r E = 0 \qquad (2\text{-}56)$$

And consequently the polarization stress is:

$$\sigma_E = 1/2(\varepsilon_r - 1)\varepsilon_0(E_{n,ins}^2 + E_t^2) \qquad (2\text{-}57)$$

In this equation, E_t is the tangential electric field strength at the liquid surface.

$p_g = \rho g z$ is the gravitation contribution and tangential electric stress by assuming the accumulation of the charges on the surface is $\tau_{Et} = \sigma E_t$.

As shown in the above equations, there are three important parameters to be calculated including *Electric field*, *Current balance at the liquid interface* and *Axial liquid velocity* at the liquid surface. The electric fields inside and outside the liquid are numerically calculated using Gauss' law:

$$\oint \varepsilon_0\varepsilon_r E \cdot dS = q_c \qquad (2\text{-}58)$$

where S is the surface and q_c is the encapsulated charge.

The current balance is written by assuming two kinds of charge transfer, one of which is the conduction and the other one is the convention as mentioned before and shown in the Fig. 2-14.

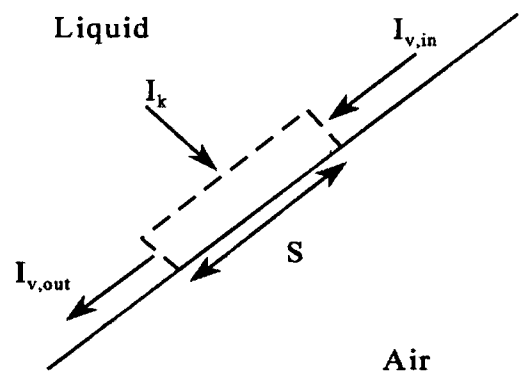

Figure 2-14: Current balance at the liquid-air interface (Hartman, Brunner et al. 1999)

The term related to the conduction part of the current is:

$$I_k = KE_{n,ins}S = KE_{n,ins}2\pi r_s(1+(dr_s/dz)^2)^{1/2}\Delta z \qquad (2\text{-}59)$$

and the conduction term is:

$$I_v = 2\pi r_s u_{z,s}\sigma \qquad (2\text{-}60)$$

where $u_{z,s}$ is the liquid velocity at the liquid-air interface in the axial direction.

The axial liquid velocity at the interface should be calculated for the current balance, either. The following equations should be employed to make the calculations completely:

$$\mu\frac{\partial u_z}{\partial r}+\mu\frac{u_r}{\partial z}=E_t\sigma+\frac{3\mu(\partial u_z/\partial z)(dr_s/dz)}{1+(dr_s/dz)^2} \qquad (2\text{-}61)$$

$$u_r = u_z\frac{dr_s}{dz} \qquad (2\text{-}62)$$

And finally the equation necessary to calculate the velocity at the interface is:

$$\mu\frac{\partial u_{z,s}}{\partial r}=E_t\sigma+\frac{\mu u_z(dr_s/dz)^2}{r_s}\cdot\frac{2(dr_s/dz)^2-4}{1+(dr_s/dz)^2}-\mu u_z\frac{d^2r_s}{dz^2} \qquad (2\text{-}63)$$

By use of the above equations, it is possible to fully analyze the electrospinning process employing the concept of EHD theory. Hartman *et al.* could well predict the cone shapes assuming a Newtonian fluid by these equations besides a complete force balance analysis that they considered in their models (Hartman, Brunner et al. 1999). Spivak and his coworkers presented a model for the steady state jet in electrospinning process in 2000 (Spivak, Dzenis et al. 2000). They considered an electrohydrodynamic model of steady state electrospinning of a single jet in which the liquid was modeled by a power-law rheological model. They could predict some parameters such as final nanofibers radius in a good agreement with the experimental results obtained so far (Spivak, Dzenis et al. 2000). Reneker *et al.* modeled and analyzed the instability of the electrical charged jet by use of the above mentioned equations (Reneker, Yarin et al. 2000). They showed that the longitudinal stress caused by the external electric field acting on the charge

carried by the jet is the main factor to stabilize the straight jet for a part of distance. As a result, a lateral perturbation grew in response to the repulsive forces between adjacent elements of charges carried by the jet. They assumed a Maxwellian type of viscoelastic equation for the liquid part simulation. In their modeling they could show that the effect of gravitational force and aerodynamic forces are negligible (Reneker, Yarin et al. 2000). Yarin and his colleagues, in 2001, modeled the electrospinning process and showed that the stable shape is obtained as a result of balancing between two electrical and surface tension forces as the main controlling parameters (Yarin, Koombhongse et al. 2001). They also concluded that in highly viscoelastic liquids with non-relaxing elastic stresses, that force is also important in determining the final shape of the cone (Yarin, Koombhongse et al. 2001). In 2001, Yarin *et al.* studied the electrospinning of nanofibers and the bending instability of the process (Yarin, Koombhongse et al. 2001). They developed a localized approximation to calculate the bending electric force acting on an electrified polymer jet, which is the most important determining factor in electrospinning process for nanofibers manufacturing. Calculating this force, they obtained an analogy between the electrically driven bending instability and the aerodynamically driven instability. They also calculated the jet paths during the course of nonlinear bending instability leading to the formation of large loops which ends in nanofibers (Yarin, Koombhongse et al. 2001). Hohman and his colleagues studied the same subject and electrospinning jet stability both from the theoretical and experimental points of view (Hohman, Shin et al. 2001; Hohman, Shin et al. 2001). They focused mainly on studying the effect of electric field strength and they showed both theoretically and experimentally that the surface charge density and fiber diameter are the most important determining parameters. They mainly studied the effect of electric field strength on instability of the fiber jet and electrical instabilities. They performed a complete parameter analysis on the electrical instabilities by studying the effect of different parameters on the tangential component of electric field. In their analysis, they mainly aimed to propose a model for correlating the final fiber morphology as a function of different material and process parameters (Hohman, Shin et al. 2001; Hohman, Shin et al. 2001). He *et al.* focused on

modeling of electrospinning process and they could obtain the critical length of straight jet in electrospinning (He, Wu et al. 2005). They used the Chauchy's inequality and could obtain a critical relationship between the radius (r) of jet and axial distance from the nozzle for a stable condition of operation. They used the same concept of previously mentioned formula, and they obtained the critical radius and length of the jet for estimating initiation the instability of the electrospinning system, the same role that Re number plays in conventional spinning method (He, Wu et al. 2005). Kinematics of mechanics of a stable electrospun polymer jet has been recently studied by Helgeson *et al.* (Helgeson, Grammatikos et al. 2008). They used the concept of EHD theory to correlate the influence of mechanics in the straight portion of the jet to final fiber morphology. In their theoretical/empirical analysis, they could predict the final fiber morphology of solutions with a wide range of concentrations and conductivities. The final morphology could be obtained in terms of measurable fluid and process parameters in addition to jet variables. In this way, they could also predict elongation viscosity of liquid jet during electrospinning and its important role on determining the jet kinematics (Helgeson, Grammatikos et al. 2008).

In next part, the main important works in the field of CNT/polymer electrospinning will be reviewed. We will mainly focus on PS/CNT and PET/CNT electrospinning as the main materials of study in this thesis.

2.5. Nanocomposite Nanofibers

Modification of nanofiber properties the same as other polymer materials can be obtained by adding various nanoparticles to achieve the desired properties. For instance, CNT is widely used recently to improve the electrical conductivity of polymer nanofibers. There are two techniques for composite nanofiber manufacturing. In the first method known as polymer template method, electrospun polymer fiber mat is immersed

in composite solution. Followed by soaking procedure, nanoparticles are adsorbed on the surface of polymer fibers. The adsorption procedure is done for a long time followed by the thermal or chemical treatment to improve the final properties of composite nanofibers (Sawicka and Gouma 2006). Another method which is widely applied in nanofiber technology and it is used in this research is the composite nanofibers production by electrospinning of composite solution mixture. This is the method that has been widely used for manufacturing composite nanofibers, since it is possible to control over the composition of the nanoparticles inside nanofibers and also reduce the preparation time. The final composite nanofiber can be treated by thermal or chemical methods to modify the final properties.

2.5.1. CNT/ polymer nanocomposite nanofibers

The use of CNT embedded in nanofibers started by polyacrylonitrile (PAN). This polymer has proper properties to be employed as precursor for manufacturing CNTs, moreover CNTs are easily dispersed and aligned inside PAN nanofibers. In 2003, Ko *et al.* studied co-electrospinning of polylactic acid (PLA) and PAN with SWNT dispersed in DMF which is the best known solvent for CNT dispersion (Ko, Gogotsi et al. 2003). They used CNT in PLA in concentration of 1-5% and with PAN in the range of 1-4%. They employed Raman microspectroscopy, TEM and AFM for characterizing the nanotubes inside fibers. One of the main interests in application of CNTs inside nanofibers is the uniform distribution and alignment of CNTs inside nanofibers which can be detected by TEM, XRD or Raman spectroscopy. In addition, the result of their experiments regarding the mechanical properties proved the important role of CNTs in significantly enhancement of mechanical properties (Ko, Gogotsi et al. 2003). Ye and his colleagues produced nanocomposite nanofibers by using SWCNT and MWCNT embedded in nanofibers (Ye, Lam et al. 2004). In their work, they investigated the mechanical properties and they analyzed two stage rupture behavior of composite fibers under tension and crazing of the polymer matrix. Carbon nanotubes are suitable

reinforcing agents with different mechanisms including hindering crazing extension, reducing stress concentration, and dissipation energy by pull out. The amount of CNTs efficiency in mechanical performance is dependant on particles dispersion and interfacial adhesion between the particles and matrix (Ye, Lam et al. 2004). In 2004, Ge and his colleagues studied the assembly of MWCNT alignment inside PAN nanofibers (Ge, Hou et al. 2004). They could successfully orient the CNT particles inside the fibers by the electrospinning technique and they characterized the orientation by TEM and WAXD methods. They could show that CNT orientation is not dependant only on surface tension and jet elongation but also the particles relaxation inside fibers. The interfacial tension between the oxidized CNT and polymer causes the matrix reinforcement. The production of PAN/CNT sheets by electrospinning has been the point of attention in recent few years because of the exclusive conductive properties of this type of composite material in conductive nanoelectrodes, supercapacitors, and nanosensors (Ge, Hou et al. 2004). Ra *et al.* prepared PAN/MWCNT nanofibers and found that there is an electrical anisotropy in final nanofibers structure. They showed that the amount of electrical conductivity after carbonization along fiber axis is three times larger than that normal to the nanofiber axis direction (Ra, An et al. 2005). This observation proves that CNTs are preferentially aligned along the nanofiber axis. They also found that the amount of nanofiber diameter is dependant on the CNT concentration. The increase in amount of CNT causes the enhanced conductivity of the polymer solution and large electrical current during the electrospinning. The addition of charge accumulation overcomes cohesive force and it intensifies the repulsive forces and smaller fiber diameter is shaped. They used Raman spectroscopy and TEM to justify their results (Ra, An et al. 2005). In 2005, Kedem and his colleagues started studying a new system of PAN nanocomposite of both MWCNT and TiO_2 nanoparticles (Kedem, Schmidt et al. 2005). These particles are applicable as photocatalytic elements with high surface ratio proper for contaminates degradation. The dispersion quality of the nanofibers was studied by cryo-TEM and HRSEM (High Resolution SEM). They found that the desired structure of nanocomposite which is the nanoparticles alignment is achieved at high concentrations (3% MWNT and 6% TiO_2) of

particle loading (Kedem, Schmidt et al. 2005). In the most recent work available in the system of PAN/CNT, Chakrabarti and his colleagues studied the positron annihilation spectroscopy of this composite nanofiber (Chakrabarti, Nambissan et al. 2006). The annihilation parameters detected show the formation of distinct positron trapping sites because of vacancy type defects available in the interface of MWNT and matrix depending on the CNT concentration. By using this trend, they found that addition of CNT causes increasing the vacancy defects as it is expected for higher concentrations (Chakrabarti, Nambissan et al. 2006).

In 2003, CNT composite nanofibers were produced employing PVDF as the matrix by Seoul and his coworkers (Seoul, Kim et al. 2003). They found that different values of percolation threshold were 0.003 wt % CNT for CNT/PVDF/DMF solution, 0.015 wt % for spin coated film of the same material and 0.04 wt% for the electrospun nanofiber mat. They investigated the effect of CNT concentration on viscosity of the solution along with surface tension and conductivity. They showed that the existence of CNTs inside fibers by measuring the electrical conductivity of the final mat at different concentrations of CNTs (Seoul, Kim et al. 2003). Polycarbonate as the basis for the manufacturing of MWCNT composite nanofibers was employed by Kim *et. al* (Kim, Michler et al. 2005). The solution was prepared by dilution of CNT masterbatch followed by solving it in chloroform as the solvent. They investigated in-situ tensile test for the mechanical deformation properties which was performed under TEM. They found that the strain at break of the composite fibers increase due to the slippage of individual nanotubes inside the matrix and therefore the resulting composite is strong and tough. The mechanical properties of the composite fiber are dependant on the alignment and embedding of CNTs inside the fiber and also the porous surface structure of the final nanofiber (Kim, Michler et al. 2005).

PMMA was employed as the matrix for CNT composite nanofiber manufacturing, in 2004, by Sung *et al.* (Sung, Kim et al. 2004). They embedded different concentrations of CNTs from 1 to 5 wt% by the use of in-situ bulk polymerization. Employing this technique, they could obtain well aligned nanocomposite nanofibers but not with

acceptable range of electrical conductivity enhancement compared to the bulk composite film. They proved the existence of CNTs inside fiber by TGA and the chemical structure was analyzed by FTIR; moreover the final fiber structure and CNT alignment was studied by SEM and TEM. They also studied the solution rheological properties at different concentrations of CNT. They found that the existence of pore structures and wrapping of PMMA polymer chains around the CNTs are the main causes of electrical conductivity reduction (Sung, Kim et al. 2004). In 2005, Liu and his colleagues employed SWNT/PMMA and SWNT/PAN for the electrospinning and introduced it as a system of core-shell which is applicable as conductive nanowires (Liu, Wang et al. 2005). In 2006, Sundaray *et al.* studied the electrical conductivity of a single electrospun nanofiber from MWCNT/PMMA (Sundaray, Subramanian et al. 2006). They could produce fibers with enhanced electrical properties to ten times more depending on MWCNT concentrations. They surveyed the system by SEM, TEM and Raman spectroscopy and measured the electrical conductivity at different concentrations of CNTs (Sundaray, Subramanian et al. 2006). In 2006, Kim and his coworkers studied the mechanical properties of various types of nanocomposite nanofibers with different morphologies (Kim, Lach et al. 2006). The system of their study included PC/MWCNT (4 wt%) as one-dimensional nanoparticle, PMMA/Na-MMT (5 wt%) as two-dimensional nanoparticle and PMMA/SiO_2 (10 wt%) as three-dimensional nanoparticle. They observed a kind of brittle to ductile transition by adding nanoparticle which is useful for providing stiffness, strength and toughness in composite materials; however, the final mechanical properties were strongly dependant on the morphology and structure of the nanocomposite nanofibers (Kim, Lach et al. 2006).

In 2003, PEO as the matrix for manufacturing CNT nanocomposite nanofiber was studied by Dror *et al.* (Dror, Salalha et al. 2003). They used highly branched polymer (Gum Arabic) and sodium dodecyl sulfate (SDS) as dispersing agent of MWNT particles in water followed by solution electrospinning. They characterized the degree of orientation and CNT dispersion inside nanofiber by TEM and XRD, and presented a model for the orientation of CNT as rods inside the nanofiber. In nanofibers containing

CNTs, the degree of orientation and crystallization of PEO is reduced while most of the nanotubes are aligned in the fiber direction (Dror, Salalha et al. 2003). Salalha *et al.* studied the same system of PEO/SWNT in 2004. They used copolymer of styrene and sodium maleate as a dispersing agent and showed that the amount of CNT alignment inside the nanofiber is completely dependant on the amount of initial CNT dispersion during sonication. Contrary to previous work about MWCNT, they found that SWNT does not reduce the amount of crystallinity and molecular orientation of the PEO (Salalha, Dror et al. 2004). In 2006, Lim and his colleagues studied CNT alignment embedded in PEO nanofibers (Lim, Lee et al. 2006). They focused on studying the electrical conductivity of the initial solution and final nanofibers and obtained the percolation threshold around 0.5% of MWCNT. They used TEM technique to show the individual CNT alignment inside nanofiber (Lim, Lee et al. 2006).

In 2005, Zhou *et al.* studied the elastic deformation of two systems of MWCNT/PEO and MWCNT/PVA in parallel (Fei, Weiping et al. 2005). Their results showed that the elastic deformation of MWCNT is completely dependant on the elastic modulus of the matrix. Increasing the matrix modulus causes enhancement the amount of composite nanofiber modulus. They achieved elastic modulus of the MWCNT composite nanofibers in range of 100 GPa which is the result of carbon nanoparticles and matrix proper interactions (Fei, Weiping et al. 2005).

In the next two parts, the works available on electrospinning of PS and PS/CNT nanofibers in addition to PET and PET/CNT will be presented.

2.5.2. PS-based electrospun nanofibers

In the earliest works available related to PS based nanofibers production, Megelski *et al.* studied micro and nano-structured surface morphology of nanofibers in 2002 (Megelski, Stephens et al. 2002). They used different kinds of solvents in their research and investigated the final porous pattern of the resulted nanofibers. They showed that both the evaporation rate and the electrical characteristics of the solvent are determining parameters of nanofibers structure (Megelski, Stephens et al. 2002). In 2003, PS solutions

were prepared in different compositions of Tetrahydrofuran (THF) and N,N-Dimethyl Formamide (DMF), and they were electrospun in different electrospinning conditions by Lee *et al.* (Lee, Kim et al. 2003). They showed that the most important properties of final nanofibers such as final fibers morphology are strongly dependant on the solvent type and process parameters. They concluded that surface tension and electrical conductivity of polymer solution were respectively correlated to the critical voltage and throughput (Lee, Kim et al. 2003). The effect of molecular weight and polymer concentration on electrospun polystyrene nanofiber was studied by Pai *et al.* in 2004 (Pai and Gunja 2004). Their results show that the controlling term of jet splitting, splaying and velocity is the amount of $[\eta]c$ which is correlated to both the viscosity and molecular weight. The higher value of $[\eta]c$ shows that the solution has higher viscosity and therefore can travel more easily compared to lower ranges of viscosity. Moreover, in equal values of concentration and molecular weight, the viscosity of the solution in θ solvent is higher and therefore the jet travels less rapidly (Pai and Gunja 2004). Lin *et al.* studied the effect of cationic and non-ionic surfactants on bead morphology of the fibers surface (Lin, Wang et al. 2004). They concluded that the formation of bead structure on the fiber surface is correlated to the insufficient stretching of the fibers that is dependent on the solution properties. The cationic surfactants change the surface tension and solution conductivity while they have no effect on solution viscosity. Lin *et al.* concluded that the addition of cationic surfactant increases the net charge density and therefore the fiber is stretched under stronger charge repulsion and higher speed which results into decrease in final bead concentration (Lin, Wang et al. 2004). In 2005, Shenoy and his colleagues investigated the important effect of chain entanglements on electrospinning of different polymer solutions including polystyrene solutions (Shenoy, Bates et al. 2005). They proved the considerable effect of molecular weight and polymer concentration on electrospun fiber formation. They showed that depending on the concentration and chain entanglements, there are different regions in which the changes in morphology occur. These changes include the beads formation only at low concentrations, and then the bead plus to fiber formation and finally smooth fibers at higher concentrations and entanglements. In addition, they

proposed a semi-empirical model to predict the fiber morphology based on electrospinning parameters (Shenoy, Bates et al. 2005). In 2005, Jarusuwannapoom and his colleagues investigated the effect of eighteen different solvents on the spinnability and final fiber structure (Jarusuwannapoom, Hongrojjanawiwat et al. 2005). They employed solvents with varied properties and depicted that there are different determining parameters for the amount of spinnability. Among the various factors, high enough values of both the dipole moment of the solvent and the conductivity of both solvent and the resulting polymer solutions and high enough boiling point of the solvent are desirable parameters in favor of spinnability. Moreover the values of the viscosity and the surface tension of the solutions should not be so high to reduce the probability of nanofiber spinning (Jarusuwannapoom, Hongrojjanawiwat et al. 2005). In 2006, Pattamaprom *et al.* investigated the effect of solvent on electrospinnability of polystyrene nanofibers in a similar work. They mainly investigated the effect of solvent on the production rate of the nanofibers and they compared various types of solvents (Pattamaprom, Hongrojjanawiwat et al. 2006). They showed that the electromotive force passing in the solution depends on the dipole moments that cause the electrons transfer in the media, while the frictional forces are related to the viscosity. Therefore, the solvents with high dipole moment and low viscosity are the best solvents for electrospinning. The viscosity is the criteria for controlling the amount of production rate and lower viscosity decreases the required value of voltage for nanofiber production (Pattamaprom, Hongrojjanawiwat et al. 2006). In 2006, the change in bead and fiber morphology and also the fiber diameter during the electrospinning of polystyrene was studied by Eda *et al.* (2006). They showed that the transformation in the value of either the molecular weight or polymer concentration can affect final fiber morphology even though the parameter $[\eta]c$ is kept constant (Eda and Shivkumar 2006).

The use of electrospun nanofibers for filtration has been the point of great importance and polystyrene is one of the most suitable materials in this field. In 2006, highly porous fibers of polystyrene were produced by McCann *et al.* They used electrospinning and controlling the phase separation simultaneously for porous structure

formation through the solvent removal. In addition, they could stabilize the final morphology of nano-webs by immersing the electrospun network on the plane collector in liquid nitrogen (McCann, Marquez et al. 2006). Zheng and his colleagues showed that both the surface structure and morphology in addition to the bead on string structure are determining parameters of the functionality of polystyrene nanofibers and their wettability (Zheng, He et al. 2006). The determining factors in their results were the electrospinning condition and solution properties and they showed that it is possible to control the final hydrophobicity by these two factors. They concluded that among the parameters, low surface tension and high viscosity is in favor of smooth fiber formation while low conductivity causes increase in bead structures and fiber sizes (Zheng, He et al. 2006). In one of the latest works available in the field of PS nanofiber production, Wang *et al.* could obtain scaling laws between the final fibers structure and process variables (Wang, Hsu et al. 2006). They concluded that both the diameter of the jet and fiber are scaled with the processing variables such as flow rate, applied voltage and working distance through a power law model. Based on their results, it is possible to conclude about the most important determining parameters and predict the final fiber structure properly. They also showed that for a total scaling relation, a prefactor is required which is related to the material and solution properties such as conductivity, surface tension and viscosity (Wang, Hsu et al. 2006).

PS/CNT nanocomposite nanofiber :

Amongst the first works available for the system of PS/CNT, Sen *et al.* studied the effect of addition of SWCNT to PS besides adding SWCNT to Polyurethane (PU) (Sen, Bin et al. 2004). They could obtain oriented CNTs inside PS nanofiber by TEM method; moreover they studied the effect of functionalization on final mechanical properties of filled PU fibers (Sen, Bin et al. 2004). In 2006, Ji and his colleagues used carboxyl-functionalized MWCNT inside PS and with use of a high speed rotator; they could align the particles along fiber axis (Yuan Ji 2006). They used a three-point bending test to measure the mechanical properties and they also detected increase in the value of Tg by

adding CNT (Yuan Ji 2006). Aussawasathien *et al.* showed that the blend of polyaniline (PANI)/polystyrene (PS) with different chemical composition can be used successfully as sensors (Aussawasathien, Dong et al. 2005). They also demonstrated that CNTs coated with appropriate conducting polymer such as the blends mentioned above can be used for manufacturing a new type of highly sensitive glucose sensors (Aussawasathien, Dong et al. 2005). In 2006, Yuan Ji and his colleagues used carboxyl-functionalized MWCNT inside PS and they showed that the particles arranged quite well and oriented along the fiber axis (Yuan Ji 2006). Pan *et al.* produced polyelectrolyte hollow nanofibers from PS/MWCNT solution mixture (Pan, Ge et al. 2007). In this work, PS/MWCNT electrospun nanofibers were used as templates for self-assembly of polyelectrolytes (Pan, Ge et al. 2007). In one of the most recent works in the field of electrospinning and CNT nanocomposite fiber manufacturing, Sundaray and his coworkers studied the properties of a single nanofiber of PS/MWCNT (Sundaray, Subramanian et al. 2007). They studied the morphology and electrical conductivity of a single nanofiber containing low amount of MWCNT. They obtained a low percolation threshold (0.05% w/w) for only a single electrospun fiber. In their work, they could improve conductivity to 10^{-6} S/cm after percolation (Sundaray, Subramanian et al. 2007).

2.5.3. PET-based nanofibers

Nowadays, polyester fibers are used in different areas of applications from textiles to automobiles industry. Polyester fibers are known for their high resiliency, resistance to wrinkling, high durability, dimensional stability, and resistance to chemical and environmental attack. In this work, we focus on PET/CNT electrospinning and fiber spinning to study their structure and properties from different points of view. Therefore, in this part a brief literature review of the papers available in electrospinning is given which will be followed by the works available in the field of PET/CNT fiber spinning (Part 2.6).

In 2000, in the earliest papers available concerning the subject of PET electrospinning, Kim and LEE studied the thermal properties of PET, PEN (Polyethylene Naphthalate), and blend of PET/PEN (Kim and Lee 2000). They managed the electrospinning process in the melt state for these materials and investigated the results before and after electrospinning. They used DSC and TGA for their analyses and concluded that electrospinning causes increase in crystallinity and decrease in T_g and T_c. Moreover, they showed that high temperature of electrospinning causes thermal degradation and therefore molecular weight reduction (Kim and Lee 2000). In their research, they did not consider the microstructures and fiber final properties and they only studied the thermal bulk properties of the final nanofibers. Kim and his colleagues continued to work on the electrospinning of PET in 2004 by studying the effect of molecular weight and linear velocity of the drum surface (Kim, Lee et al. 2004). They investigated the effect of viscosity regardless of molecular weight and they could obtain nanofibers of different diameters. They studied the effect of drum velocity and its effect on the fiber orientation and the resulting crystallinity by WAXD method (Kim, Lee et al. 2004). They also prepared the electrospun poly(trimethylene terephthalate) (PTT) which is similar to PET in structure with different diameters in range of 200 to 600 nm. They found that the final structure is strongly dependant on the concentration and the circular smooth fibers are obtained by increasing the amount of concentration and viscosity (Myung Seob, Hak Yong et al. 2004). Kim and his colleagues studied the effect of blend ratio of two types of amorphous and crystalline PET and also the heat treatment on final fiber properties (Kim, Lee et al. 2005). They prepared different concentrations of these two types of PET and studied the effect of three parameters including solution viscosity, surface tension and electrical conductivity. Applying different ratios of PET influences on final parameters including morphology, pore size and gas permeability. They also studied the effect of heat treatment and they showed that the parameters such as morphology and pore sizes change before and after heat treatment that considerably affect the amount of gas permeability (Kim, Lee et al. 2005).

Frenot and Chronakis presented some results regarding the electrospinning of PET in 2003. They reviewed the electrospinning process and its features; however, they did not describe about the material and processing conditions in detailed (Frenot and Chronakis 2003). The result of this group for electrospinning of PET in solution state has been published in one of the most recent related papers (Chronakis, Milosevic et al. 2006). They could develop a method for generation of molecular recognition sites in electrospun PET nanofibers. They obtained fibers binding sites capable of selectively binding the target molecules by removing the template by the use of a proper solvent (Frenot and Chronakis 2003). Considering the importance of polyester in textile and fiber industry, Baker and his colleagues started a series of papers concerning the reactive modification of electrospun PET fibers in 2003 (Baker and Brown 2003). They added appropriate acids to the solution and they crosslinked and modified the nanofiber structure under enough UV energy. They could also prove their experimental results by studying the changes in the T_g and crystallinity and thermal properties of the resulted crosslinked PET (Baker and Brown 2003). In 2005, they generally studied the properties of the fibers before and after treatment. They prepared a kind of electrospun web of PET with high surface to volume ratio and susceptible for biocompatibility modification (Baker and Brown 2005). In 2003, McKee and his colleagues started studying a series of papers regarding the subject of electrospinning of branched polyesters (McKee, Long et al. 2003). They synthesized a random copolymer of poly(ethylene terephthalate-co-ethylene isophthalate) polyester combined with a kind of branching agent to study the effect of chain branches on PET final structure and performance. They achieved a defect free nanofiber from this new branched copolymer with the diameter ranging from 1 to 10 μm (McKee, Long et al. 2003). In 2004, they completely studied the rheological properties and final structure of electrospun linear and branched polyesters (McKee, Wilkes et al. 2004). They used the same copolymer of PET-co-PEI with different molecular weights and three regimes of semi-diluted entangled, semi-diluted unengaged and concentrated with both linear and branched structures. They found that the minimum concentration of two times more than the concentration required for chain entanglements

is necessary to obtain a bead-free structure for nanofibers. Followed by studying the effect of chain entanglements on viscosity, they could correlate the electrospun morphology (polymer droplets, beaded structure or nanofibers) to zero shear rate viscosity (McKee, Wilkes et al. 2004). In 2005, Ma *et al.* employed electrospinning process for the production of PET nanofiber mat besides surface modification and they produced a new kind of artificial blood vessel. They improved the protein compatibility; therefore, they introduced a new kind of material completely suitable for blood vessel applications because of the small diameter of fibers mat in the range of 200-600 nm (Ma, Kotaki et al. 2005). In 2006, Hong and Kang studied the hydraulic permeabilities of electrospun nanofiber webs of combined PET and nylon 6 (Hong and Kang 2006). They concluded that the amount of water vapor transport through the electrospun PET and nylon 6 was higher than the spunbonds composed of the same material. They concluded that because of small pore diameter of the electrospun web compared to the spunbond PET/nylon6, there are some deviations in the conventional permeability rules for the nanofibers obtained by electrospinning (Hong and Kang 2006). In one of the most recent works available in study and characterization of PET nanofiber solution electrospinning, Veleirinho and his colleagues studied the effect of initial solution concentration and solvent on final properties of PET electrospun nanofibers (Beatriz Veleirinho 2008; Veleirinho and Lopes-da-Silva 2009). They showed that, at least 10 wt% of PET is in initial solution is required to prepare nanofibers, while higher concentration favors beadless structure nanofibers (Beatriz Veleirinho 2008). They also showed that TFA/DCM volume ratio could be an important determining factor on final nanofibers morphologies and properties (Beatriz Veleirinho 2008).

PET/CNT nanocomposite nanofiber:

Preparation and study the structure and properties of PET/CNT fibers are somehow a new field and there are only a few recent works available in this area. Xushan and his coworker applied MWCNTs in PET and PA 6 nanofibers in 2005 employing melt electrospinning technique (Gao, Tong et al. 2005). They functionalized CNTs by

dispersant and surfactant in ethanol and mixed the particles with PET and PA6 in twin mill extruder. They could obtain considerable change in electrical properties by the reduction of electrical resistance about eight orders of magnitude by only adding 0.1% MWCNT to the fibers (Gao, Tong et al. 2005). This is a point of interest for manufacturing conductive nanofibers out of PET/CNT composite, since a great consequence is achieved by adding only a small amount of CNT. In another work available PBT (Poly (butylene terephthalate)); a kind of polyester similar to PET; has been modified and electrospun combined with CNT (Nah, Mathew et al. 2005). They used electrospinning for production of 5% MWCNT in solution of PBT in hexafluoroisopropanol solvent and they could make considerable enhancement in thermal stability and mechanical modulus (Nah, Mathew et al. 2005). In 2008, Ahn *et al.* investigated the properties and characterizations of PET/MWCNT nanocomposite nanofibers for the first time (Ahn, Chi et al. 2008; Beatriz Veleirinho 2008). They modified the dispersion by MWCNT functionalization up to 3 wt% MWCNT concentration. In this work, different morphological, physical and mechanical properties of nanofibers were studied; however, they could not obtain considerable modification on conductivity because of destruction of CNTs surface after functionalization (Ahn, Chi et al. 2008). In the most recent work available on PET/MWCNT nanocomposite nanofibers, the molecular properties and chain orientation of PET in nanocomposite nanofibers has been studied by Chen and his coworkers (Chen, Liu et al. 2009). They investigated the effect of MWCNT addition on chain confinement of PET at different MWCNT concentrations up to 2 wt% MWCNT concentration by differential scanning calorimetery (DSC) and FTIR methods. They mainly studied the crystalline behavior and PET chains morphologies after electrospinning with and without MWCNT in their work (Chen, Liu et al. 2009). However, their work did not give any additional data about the final electrical and mechanical properties of nanocomposite electrospun nanofibers. There are some interests on electrospinning of PET/CNT nanofiber; however, there is not still a deep characterization of electrospun PET/CNT nanofibers especially at different range of CNT types and concentrations.

2.6. Melt spinning

Melt spinning is the most preferred method to produce different polymer fibers. In this technique, the polymer is melted and pumped through a spinneret (die) with numerous holes (one to thousands). Thereafter, the molten fibers are cooled, solidified, and collected on a take-up wheel. Stretching of the fibers in both the molten and solid states provides enough orientation of polymer chains along the fiber axis. A simple schematic of melt spinning is shown in Figure 2-15.

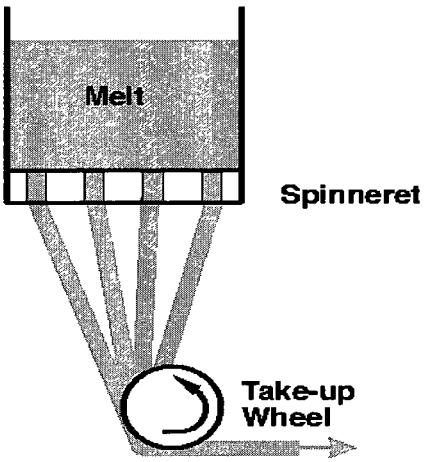

Figure 2-15: Simplified schematic of melt spinning process
(www.polymerprocessing.com/operations/mspin/index.html)

There are numerous papers regarding the use of melt spinning process for production of microfibers as the most important method of fiber fabrication in textile industry. In this project, we use this technique for production of nanocomposite polymer microfibers modified with CNT; therefore, the papers available related to this subject and application of this technique in nanocomposite fiber production will be reviewed in the next parts.

2.6.1. Polymer fibers

The basic types of mass production of polymer fibers include polyolefin (mainly polypropylene), acrylic, polyvinyl alcohol, aliphatic polyamide (such as PA-6, PA-66, and PA-11), polyester (poly(ethylene terephthalate)), hydrated cellulose, triacetate and acetate fibers, during the 1960s-1980s (Perepelkin 2005). The production of these fibers was done based on final demanded properties, availability of the stock, technology and equipment and they constituted the *traditional or first generation of polymer fibers.* Manufacturing these fibers is increasing and they have considerable demand of household and industrial marketing. Nevertheless, saturation of the world market with the traditional type of first generation of polymer fibers and competition between the manufacturers to fulfill the market demand resulted in production of *modified or the second generation of polymer fibers* in the period of 1970s-1980s (Perepelkin 2005). The new generation of modified fibers could totally meet all the requirements for market demand with well-developed new functional properties. There are four different methods of fiber modification to make the fibers prepared for the required final goals including: *Physical methods of modification, Methods of composite modification, Methods of chemical modification* and moreover *Methods of surface modification* which will be described briefly as follow (Perepelkin 2005).

- *Physical methods of modification:* During this type of modification, the supermolecular structure, cross section shape, or outer surface structure of the fiber is modified for the desirable application with no change in chemical structure of the fibers. Controlling the amount of shrinkage, degree of crystallinity, fiber orientation and porosity by process parameters are amongst these methods of modification (Perepelkin 2005).
- *Methods of composite modification:* This method includes addition of different types of particles to the base polymer to improve the fiber properties or blending of polymers. The addition of particles is done at the first stages of polymer preparation or before spinning and it is widely used to process the second generation of polymer fibers

(Perepelkin 2005). Since it is the method due to be employed in this project, it will be described in more detailed in next parts.

- *Methods of chemical modification:* In this method, the chemical structure of the fiber is modified by addition of chemical groups to the fiber before spinning or by copolymerization. The chemical structure of the final fiber is totally changed by this procedure, and the final characteristics are controlled by the modified chemical structure (Perepelkin 2005).
- *Methods of surface modification:* This method is only related to the final surface treatment by either physical or chemical methods followed by fiber manufacturing. This is a less expensive and less difficult method of modification for some types of applications in which surfaces with special characteristics are required (Perepelkin 2005).

2.6.2. Nanocomposite fibers

In previous sections, polymer nanocomposite structures and also fiber technology were basically described; in addition, considering the importance of CNT nanoparticle in this research, some of its exclusive properties were discussed. One of the most important applications of nanotechnology concept is the manufacturing nanocomposite fibers which has a bright view of future applications. So far, particles such as clay, metal oxides and carbon black, graphite nanofibers (GNF), and carbon nanotube (CNT) have been used (Lei Qian 2004). Besides, the method of foam-forming process can be employed in manufacturing nanocomposite fibers. The same as conventional polymer nanocomposites, the main role of nano-sized fillers is the improvement in mechanical strength of final fiber or enhancement of physical properties such as conductivity or antistatic behavior. Additional physical and chemical performances obtained using different methods for manufacturing nanocomposite fibers are achieved by different nanoparticles and they are dependant on the properties of nanoparticle type. Even though particles such as graphite, clay and metal oxides have been employed before, the reduction of their sizes to nanometer range has resulted into their higher performances and new marketing interests. One of the most important points to be considered in

improving the properties would be the distribution of nanoparticles and the amount of nanoparticles dispersion and interaction with the matrix (Lei Qian 2004). As mentioned before, the addition of nanoparticles to the polymer is a method of composite modification; however, the composite polymer should be well-prepared for the special application. Obtaining a stable and homogenous mixture depends on the type of base polymer (Solution or Melt) and also the type of particle. There are various types of particles added to the polymer to modify the final properties of fiber and are given briefly in Table 2-5 (Perepelkin 2005).

Nanocomposite fibers of CNTs along with different polymers especially PMMA and PAN have been produced and studied in different papers (Lei Qian 2004). Carbon nanoparticles and nanofiber with polyester matrices in different concentrations have been also studied.

In this work we focus on PET as the polymer matrix with CNT as filler. In the earliest works available in the application of polyester/Carbon nanoparticle system, Ma *et al.* surveyed polyester/CNF nanocomposite fiber produced by melt spinning. They completely studied processing, structure and properties of the system compared to pure PET (Ma, Zeng et al. 2003). They showed that the amount of tensile strength in good dispersion condition is considerably increased comparing to the pure PET. In recently published paper for the system of PET/CNT, Li *et al.* investigated the microstructure of CNT/PET conductive composite nanocomposite fibers in detailed (Li, Luo et al. 2006). They added 4 wt% of CNT to PET and they could detect considerable changes in the amount of electrical properties. They also investigated some other properties of PET/CNT system such as viscosity, crystallinity and CNT dispersion homogeneity along fiber axis by the use of techniques such as SEM and optical microscopy (Li, Luo et al. 2006). This paper is one of the most related papers and maybe the only one in studying the structure of PET/CNT nanocomposite microfibers. Nevertheless, this system has not been fully investigated in this work. Poor CNT dispersion has resulted in employing high concentrations of CNTs, or it might be the effect of improper processing condition for fiber production. However, no thorough morphological study has been performed in the

previous studies on nanocomposite MWCNT/PET microfibers. Detailed morphological analysis and the effect of dispersion condition have not been deeply studied. Moreover, the effect of processing condition on final mechanical and electrical properties of the fibers has not been paid attention to. These parameters will be studied here through melt spinning of PET/MWCNT fibers. The results of experiments obtained in this study will be given in next chapters.

Table 2-5: Fibers achieved by composite modification method (Perepelkin 2005)

Method and type of particle added	***Final obtained properties***
Addition of TiO_2 to spinning melt (solution)	Mat fibers
Addition of dyes or pigments to spinning melt (solution)	Obtaining stable colors and bright hues in bulk dyeing
Addition of light or thermal stabilizers to melt	Increase in light fastness or thermostability
Addition of fireproofing compounds (phosphorus-,phosphorus-nitrogen-containing) to spinning melt (solution)	Flameproofing
Addition of carbon black, dispersed metal particles or other conducting particles to spinning melt (solution)	Giving stable conductivity
Addition of disperse biologically active substances to spinning melt (solution)	Giving antimicrobial properties
Addition of disperse heavy metal compounds (lead, vanadium, etc.) to melt	Protection from penetrating "soft" radiation
Addition of microencapsulated spirooxazine compounds to melt	Transformation of solar radiation into IR radiation (heat-producing fibers)
Addition of microencapsulated spirooxazine compounds to melt	Change in color as a function of intensity of solar radiation (photochromic fibers)
Addition of microencapsulated thermotropic cholesteric liquid crystals or thermotropic dyes to melt	Change in color as a function of temperature (Thermochromic fibers)
Addition of microencapsulated essential oils to melt	Stable smell of scent, flowers, etc. (aromatic fibers)

2.7. Originality of the work

The literature review showed that there were only a few works concerning the processing and characterization of PS/CNT and PET/CNT electrospun nanofibers the same as PET/CNT microfibers. Two polymers including PS as an amorphous polymer and PET as a semi-crystalline one were mixed with CNTs in electrospinning. We studied the effect of different types of CNTs and in a wide range of concentrations in electrospinning process. Through processing and characterization of CNT based nanocomposite nanofibers with different CNT types and concentrations were not available in the previous works and it was investigated for the first time here to show the important role of dispersion condition. In PS/CNT nanofibers, the effect of dispersion quality and dispersion modification through a new method of compatibilization was one of main concerns of this study. Nanocomposite fibers based on PET/CNT in different spinning methods especially electrospinning have been only studied in a few works so far. We have studied the final properties of PET/CNT electrospun and melt-spun conductive fibers from different aspects especially dispersion condition using two fiber spinning processes to the best of our knowledge for the first time here to modify the final electrical and mechanical properties.

2.8. Objective

The object of this project is to study the effect of CNT concentrations and types in various ranges (dispersion condition) in electrospinning process and final properties of PS/CNT and PET/CNT polymeric nanofibers; besides studying the effect of dispersion condition on final characteristics of PET/MWCNT microfibers in melt-spinning to modify the final electrical and mechanical properties.

Chapter 3

Materials, Processing and Characterization

3.1. Methodology

The methodology to achieve the mentioned objectives through this work is briefly presented in the following chart as individual steps:

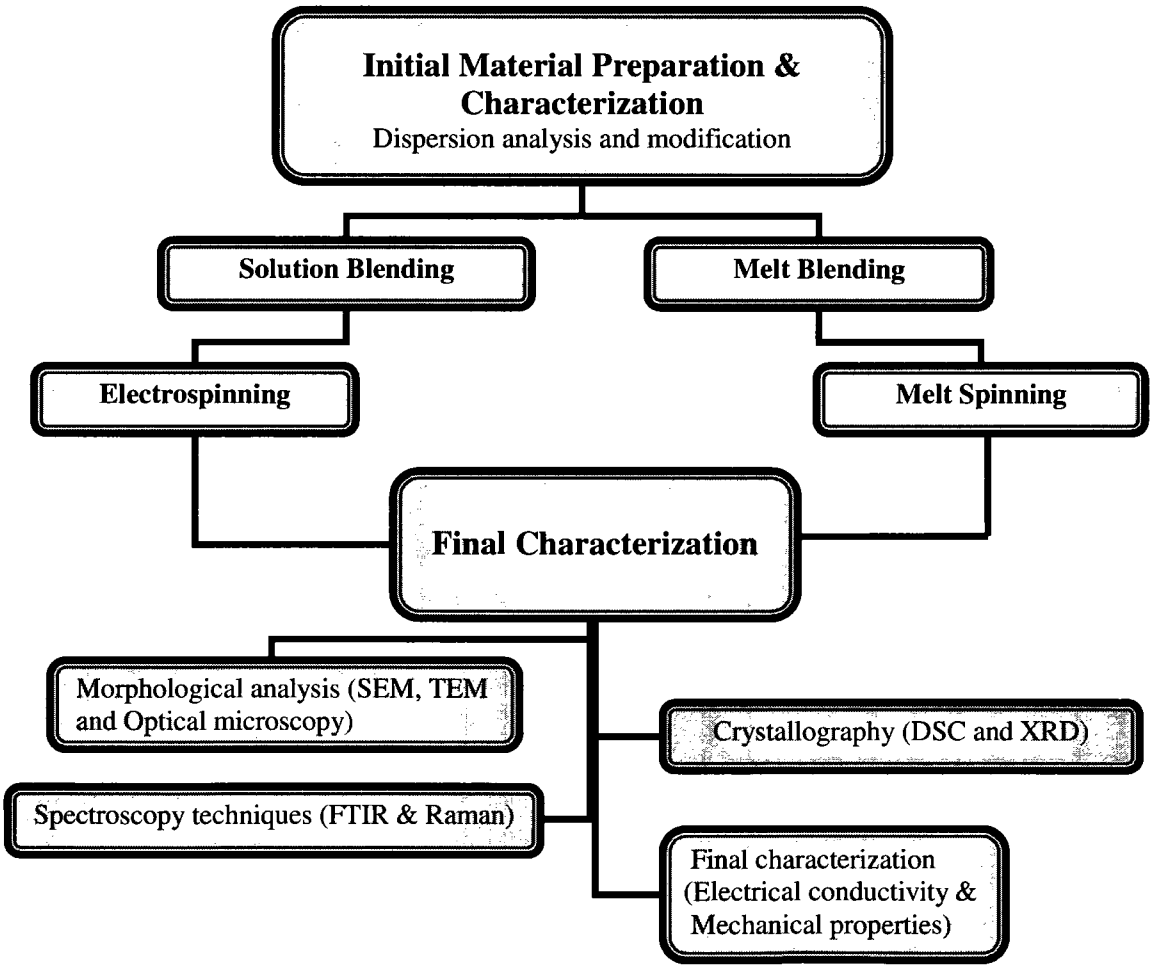

3.2. Materials

In this work, two different processes: electrospinning and melt-spinning are studied independently. Therefore, two groups of materials were used to perform the experiments. In both electrospinning and melt-spinning, the polymers should have proper molecular weight to obtain the fibers. We used extrusion grade of polymers with high enough molecular weight suitable for spinning process.

The materials used to prepare the solution mixtures for electrospinning are:

- Poly(ethylene terephthalate) (PET)- Extrusion grade (Mw≈55000 (Duchesne et al. 2002)); purchased from DuPont Co.; IV=1.
- Polystyrene (PS) – Extrusion grade (168 M); purchased from BASF Co.
- Styrene-Butadiene-Styrene (SBS-Kraton; G-1647), copolymer; purchased from BASF Co. as dispersion modifier for PS/CNT electrospinning.
- Di-Methyl Formamide (DMF) (PS solvent & CNT dispersion media); purchased from Aldrich Co.
- Tri-fluoro acetic acid (TFA) and Di-chloro methane (DCM) (PET solvents); purchased from Aldrich Co.
- Different types of carbon nanotube (CNT) powder; purchased from Helix Co.

Carbon nanotubes used here were produced by chemical vapor deposition process (CVD) as given by Helix Co., USA. Single wall carbon nanotubes (SWCNT) and double wall carbon nanotubes (DWCNT) with purities of 90% and multi wall carbon nanotubes (MWCNT) with purity of 95% were used in electrospinning process as nanoparticles to improve the conductivity. The nominal diameter range of SWCNT, DWCNT and MWCNT were respectively of 1.3 nm, 4 nm and 10-100 nm. All three types of CNT had length in range of 0.5-40 μm. A brief description of two kinds (SWCNT and MWCNT) is given in the following Tables.

Table 3-1: Properties of high-purity SWCNT

Specification	Test Method
External Diameter	~ 1.3 nm
Length	0.5 ~ 40 μm
Purity	> 90%
Amorphous Carbon	< 5%
Ash	< 2 wt%
Specific Surface Area	300 – 600 m^2/g

The materials required to prepare the polymer nanocomposite melt mixture for melt-spinning process include:

- Poly(ethylene terephthalate) (PET)- Fiber grade; purchased from DuPont Co.; IV=1 (Mw≈55000).
- MWCNT masterbatch (15% MWCNT, PET); MB6815-00; purchased from Hyperion Co.

Table 3-2: Properties of standard MWCNT

Specification	Test Method
External Diameter	< 10 nm 10 – 20 nm 10 – 30 nm 20 – 40 nm 40 – 60 nm 60 – 100 nm
Length	Short (1 – 2 mm) Standard (0.5 – 40 mm
Purity	> 95%
Amorphous Carbon	< 2%
Ash	< 0.2 wt%
Specific Surface Area	40 – 300 m^2/g

Final properties characterization is the main concern of this project; therefore, we used MWCNT master-batch in melt state part to improve the dispersion as much as possible and to concentrate totally on final properties characterization rather than initial material preparation.

3.3. Processing and mixing procedure

Two different procedures for mixing and material preparation related to each of the fiber spinning processes (electrospinning and melt-spinning) are presented individually here.

3.3.1. Electrospinning

- ***Mixing procedure:*** Solution mixing was the method employed for initial material preparation containing different concentrations and types of CNTs. The method used for solution preparation in PS solution was different from that in PET solution.

In PS solution, the solution containing polymer or copolymer was prepared using continuous mixing and then CNT was added to the solution. Followed by a short time mixing, the solutions were subjected to continuous sonication for 4 hours using a BRANSON 1510 (80 Watts) sonicator. The sonication was performed in a water bath and the temperature was kept constant all through the sonication by changing the water of bath. The solutions were under mechanical mixing and stirring after sonication; meanwhile, all the solutions containing high concentrations of CNTs were used promptly after sonication and final preparation to prevent from any instability of the solutions containing CNTs.

In PET solution, different methods were used to optimize the initial dispersion condition. Various types of mixing procedure were investigated to obtain solutions as stable as possible and with the least amount of CNT aggregation, especially at high CNT

concentrations. The final procedure employed for solution mixing and at the best condition was as follow: CNT was solved in only TFA part of the solvent excluding DCM. CNT/TFA solutions were subjected to sonication using the instrument and procedure mentioned previously for 2 hours. Thereafter, PET and DCM were added to CNT/TFA solution and were mechanically stirred for complete dissolution of PET in the solvent. Then, the prepared solutions were subjected to sonication condition for more 2 hours to obtain a quite homogenous solution with the least amount of aggregations. The solutions obtained in this method were the most stable CNT containing solutions with the least amount of CNT aggregates.

- ***Electrospinning process:*** In both PS and PET solutions, we used a horizontal type of electrospinning set-up equipped with both static and rotating drum as collector as shown schematically below. The electrospinning set-up employed in this work consisted of a high voltage power supply (Gamma Inc.), a syringe pump to deliver the solution at specific flow rates (PHD 4400, Harvard Apparatus), a syringe connected to a stainless steel needle (22 gauge, Popper & Sons Inc.), and finally a stainless steel collecting drum (15 cm diameter). The amount of flow rate and voltage were dependent on polymer solution system and they will be given in more details in related experimental chapters.

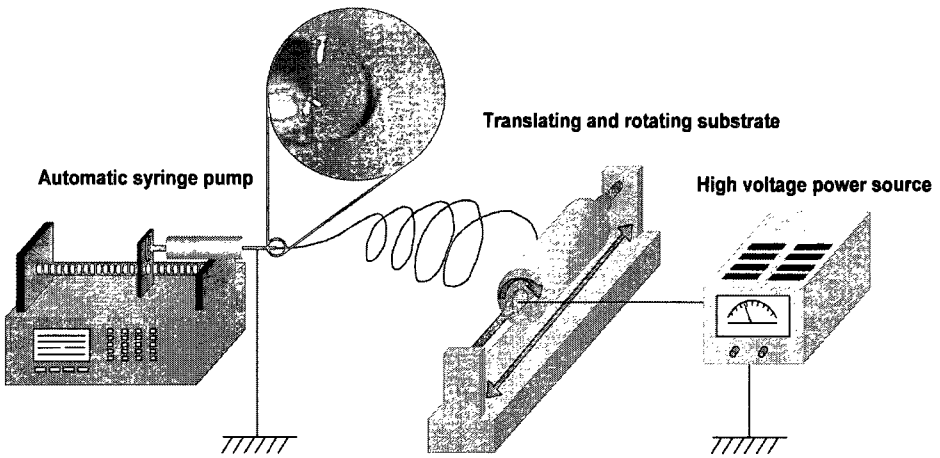

Figure 3-1: Schematic configuration of the horizontal electrospinning set-up used in this project

3.3.2. Melt-spinning

- ***Mixing procedure:*** We used CNT (PET/15% MWCNT) master-batch manufactured nanocomposite. Mixing with pure PET was conducted using a lab-scale twin-screw extruder (Leistritz Group Co.; with 1.78 mm diameter and length of 40D) at controlled temperature and shear rate. The MWCNT master-batch was diluted to the desired CNT concentration by adding various pure PET matrix amounts. Different temperature profiles and rotation speeds were investigated and the final dispersion at different condition was checked to obtain the optimum condition for CNT dispersion. We used this procedure to optimize CNT dispersion in the matrix and to obtain the best dispersion condition at different CNT concentrations. The best condition for CNT dispersion was obtained at 200 rpm screw speed using a reverse temperature profile (common for PET mixing) along extruder screw started from 300 °C (The first zone after hopper) to 270 °C (Die). The twin-screw included 8 thermal zones starting from hopper and ending at the die. The temperature profile used was:
Zone 1 (Hopper): 150 °C; Zone 2: 300 °C; Zone 3: 295°C; Zone 4: 290 °C; Zone 5: 285 °C; Zone 6: 280 °C; Zone 7: 270 °C; Zone 8 (Die): 270 °C.

- ***Melt-spinning process:*** We performed the melt-spinning to obtain single fibers in lab-scale for the aim of final characterization. All the materials were dried before and after mixing and before extruding in oven at the temperature of 120 °C for at least 6 hours. A capillary rheometer (Rosand) combined with a take-up device was used to produce single fibers under controlled pressure and temperature profiles. A schematic of the capillary that we used for fiber spinning is shown in Figure 3-2. The fibers were produced using a barrel temperature of 270 °C and ambient air cooling. All the three zones were set at 270 °C and we used a die of 1 mm diameter. The fibers were produced under constant pressure and with the piston linear velocity of 1 mm/min at ambient temperature.

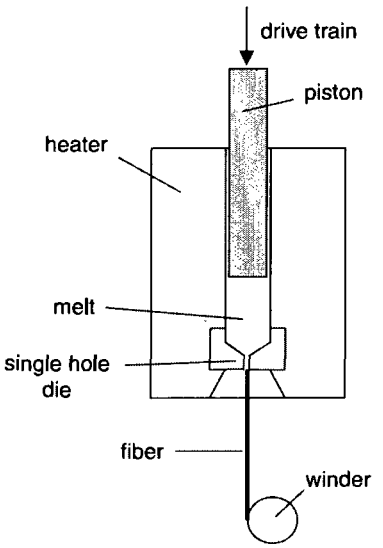

Figure 3-2: Schematic of the capillary extruder for single fiber spinning

3.4. Characterization

Characterization is one of the main important concerns of this work before and after fiber formation. Different characterization methods and their applications and purposes are given in the following chart in more details. The parameters and procedures of each of these experiments are given in the following chapters, including the results related to each of the associated tests. In electrospun nanofibers, the samples were dried under vacuum at room temperature before characterization to evaporate the remaining solvents as much as possible.

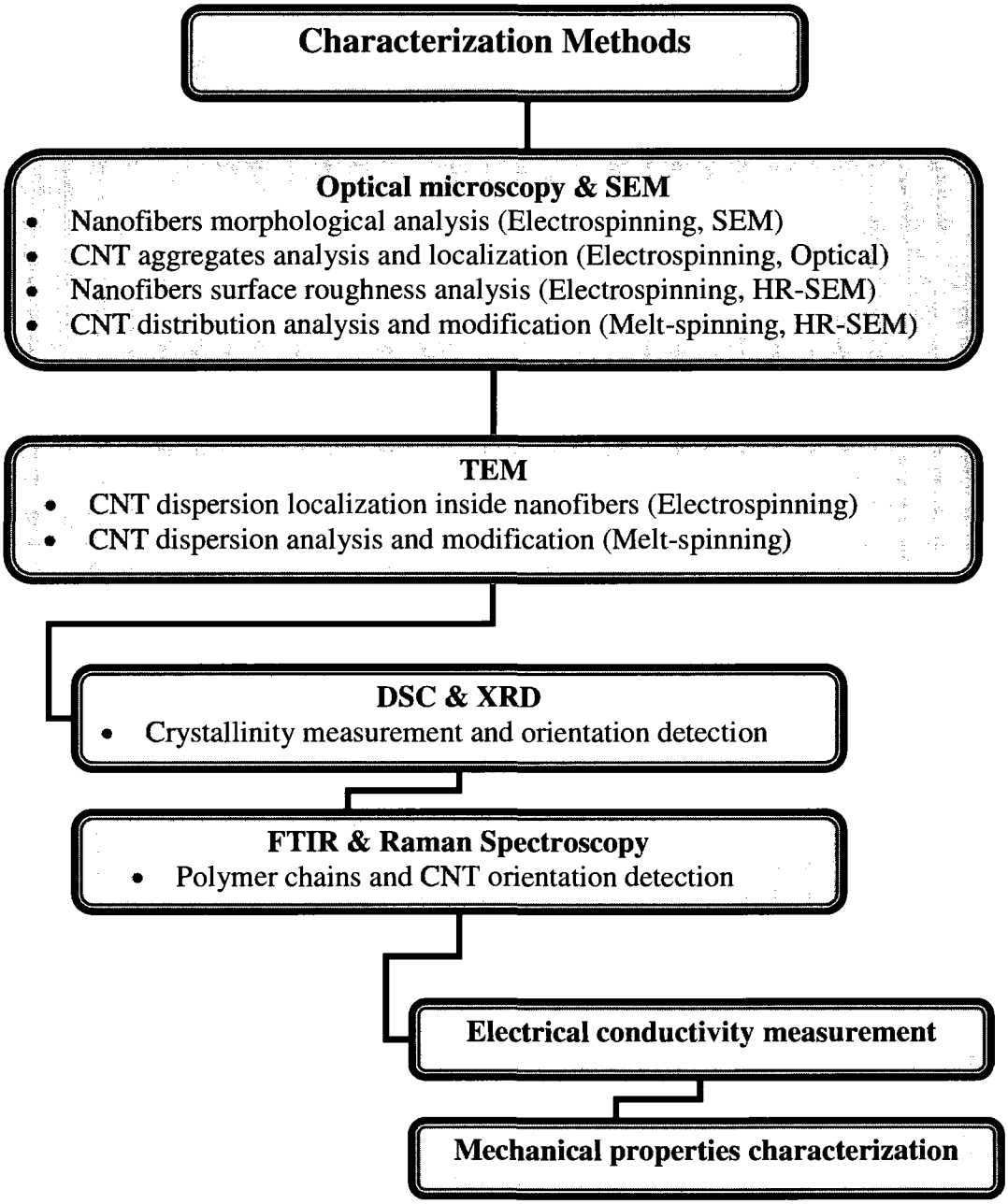
Characterization Methods
Optical microscopy & SEM
• Nanofibers morphological analysis (Electrospinning, SEM)
• CNT aggregates analysis and localization (Electrospinning, Optical)
• Nanofibers surface roughness analysis (Electrospinning, HR-SEM)
• CNT distribution analysis and modification (Melt-spinning, HR-SEM)
TEM
• CNT dispersion localization inside nanofibers (Electrospinning)
• CNT dispersion analysis and modification (Melt-spinning)
DSC & XRD
• Crystallinity measurement and orientation detection
FTIR & Raman Spectroscopy
• Polymer chains and CNT orientation detection
Electrical conductivity measurement
Mechanical properties characterization

Chapter 4

Organization of Articles and Thesis Structure

The main results of this thesis will be given in chapters 5 to 8. Each of these chapters includes the scientific findings in a scientific paper format. The organization of these chapters includes:

- ***Chapter 5*** explains the results obtained by the electrospinning of PS/CNT nanocomposite nanofibers. In this chapter CNT dispersion condition, its effect on final morphology and dispersion modification are mainly studied. This paper was accepted for publication and is in press in Polymer.
- ***Chapter 6*** covers the results of processing and characterization of PET/CNT nanocomposite nanofibers at different CNT types and concentrations. Investigating the final characteristics of nanocomposite non-woven mat is thoroughly given in this chapter. This paper has been submitted to Journal of Polymer Science, Part B; Polymer Physics.
- ***Chapter 7*** studies the final properties of PET/CNT nanocomposite melt-spun fibers in detailed. Dispersion modification and CNT orientation detection and their effect on final properties are given in this paper. This paper has been submitted to Polymer Engineering and Science.
- ***Chapter 8*** includes the empirical modeling results of electrospinning of CNT-based solutions. The applicability of EHD theory in our system and the estimation of final nanofibers based on dimensional analysis are presented in this chapter. This chapter is in preparation as a paper in this group.

Chapter 9 is a general discussion and it covers summary and comparison of the results obtained in this study. Finally, a brief conclusion of this thesis and the recommendations for future works will be given in chapter 10.

Chapter 5

Morphology, Structure and Properties of Conductive PS/CNT Nanocomposite Electrospun Mat*

5.1. Presentation of the article

The objective of the first paper was to study the effect of different types and concentrations of CNTs on final morphology and properties of electrospun nanofibers. We used PS as an amorphous polymer to make the first step as simple as possible. PS is solvable in DMF which is also accounted as one of the best solvents for CNTs solving. Final morphology and properties of electrospun non-woven mat are deeply studied in this article. The results of morphological study show that dispersion condition is an important controlling parameter of final morphology of electrospun nanofibers. A new type of copolymer is introduce and successfully employed as coupling agent in this work for CNT dispersion modification. Final mechanical and electrical properties of electrospun PS/CNT mat with and without copolymer are also given.

---

* ***Polymer*** (2009), **In Press**. doi:10.1016/j.polymer.2009.04.070, 2009.

Morphology, Structure and Properties of Conductive PS/CNT Nanocomposite Electrospun Mat

Saeedeh Mazinani [1], *Abdellah Ajji* [2], *Charles Dubois* [1]

1) CREPEC, Department of Chemical Engineering, Ecole Polytechnique of Montreal, P.O. Box 6079, Station Centre-Ville, Montreal, Quebec, Canada H3C 3A7.

2) CREPEC, Industrial Materials Institute, National Research Council Canada, 75, de Mortagne, Boucherville, Quebec, Canada J4B 6Y4.

5.2. Abstract

The morphologies and properties of Polystyrene (PS)/Carbon Nanotube (CNT) conductive electrospun mat were studied in this paper. Nanocomposite fibers were obtained through electrospinning of PS/Di-Methyl Formamide (DMF) solution containing different concentrations and types of CNTs. The dispersion condition of CNTs was correlated to morphologies and properties of nanocomposite fibers. A copolymer as an interfacial agent (SBS, Styrene-butadiene-styrene type) was used to modify the dispersion of CNTs in PS solution before electrospinning. The results showed that the presence of the copolymer significantly enhances CNT dispersion. The fibers diameters varied between 200 nm and 800 nm depending on CNT type, polymer concentration and copolymer. The final morphological study of the fibers showed that CNT addition caused a decrease in beads formation along fiber axis before percolation threshold. However, addition of CNTs above percolation increased the beads formation, depending on the dispersion condition. The presence of SBS modified the dispersion, reduced the fiber diameter and the number of bead structures. Electrical conductivity measurements on nanocomposite mats of 15 μm to 300 μm in thickness showed an electrical percolation threshold around 4 wt% MWCNT; while the samples containing SBS showed higher

values of conductivities below percolation compared to the samples with no compatibilizer. Enhancement in mechanical properties was observed by the addition of CNTs at concentrations below percolation.

5.3. Introduction

The electrospraying process was discovered by Formhal and disclosed in patent literature in 1934. Since then, this process has found a great deal of interests in spite of its simplicity [1]. Electrospinning is the most frequently used method to produce fibers of nanometric size. This process was known as electrostatic spraying before 1993, and there were only a few publications employing this technique [2]. Reneker and Chun revived this technology in the 1990s and they showed the possibility of employing this process for different kinds of polymer solutions in 1996 [3]. In this process, a syringe pump moves the solution out of the spinneret at a constant and controllable rate. Application of a high voltage difference between the syringe tip and a target screen for collection induces electric charges that are distributed over the surface of droplet, which is finally attracted to the other side due to the high electric field and forms drops, fibers or beaded fibers. Various types of nanoparticles dispersed in polymer solutions have been embedded recently in nanofibers through this process to modify the final properties of electrospun fibers. Among them, carbon nanotubes have attracted a great attention. In fact, rapidly after CNT development [4], this nanoparticle has been widely used to enhance electrical or mechanical properties of electrospun polymer fibers to various extents [5-8].

Ra *et al.* electrospun PAN/MWCNT nanofibers and showed that there is an electrical anisotropy in final nanofibers along fiber axis compared to fiber cross section [6]. They showed that nanofibers diameter is strongly dependant on CNT concentration. An increase in the amount of CNT enhances the conductivity of the polymer solution and

produces a larger electrical current during electrospinning. The addition of charge accumulation overcomes cohesive force and intensifies repulsive forces and fibers of smaller diameter are formed [6]. CNT composite nanofibers were produced using PVDF as the matrix by Seoul *et al.* [7]. They found that there were different values of percolation threshold which were 0.003 wt % CNT for CNT/PVDF/DMF solution, 0.015 wt % for spin coated film of the same material and 0.04 wt% for electrospun nanofiber mat. PMMA was employed as the matrix for CNT composite nanofiber manufacturing, in 2004, by Sung *et al.* [8]. They embedded different concentrations of CNTs from 1 to 5 wt% by the use of in-situ bulk polymerization. However, they detected a reduction in electrical conductivity by this method in comparison with a solution dispersion process. They showed that existence of pore structures and wrapping of PMMA polymer chains around the CNTs are the main causes of electrical conductivity reduction compared to solution mixing method [8]. Enhancement of CNT dispersion and its effect on electrospun fiber morphologies and properties is one of the main aims in this work. We intend to use compatibilization methods rather than chemical modification to improve CNT dispersion and maximize electrical properties. There are several papers related to the use of CNTs as fillers along with dispersion modification techniques employed in electrospinning process [9-11]. New types of block copolymers have recently been introduced for CNT-dispersion modification, especially above electrical percolation. The structures, properties and the method of functionalities of these specific copolymers have been proved both theoretically and experimentally [12-14].

Other studies investigated the structure and properties of PS electrospun nanofibers from different points of view. The earliest among them studied the effect of solvent on final fiber morphologies and fiber surface has been studied. In particular, there is a large number of papers about controlling bead morphology along fiber axis and final fiber morphologies [15-22]. Lin *et al.* studied the effect of cationic and non-ionic surfactants [23] on bead morphology and fiber surface. In 2005, Shenoy and his colleagues investigated the effect of chain entanglements on various polymer solutions for electrospinning, including polystyrene solutions [24]. They proved the considerable

effect of molecular weight and polymer concentration on electrospun fiber formation. They showed that, depending on polymer concentration and chain entanglements, there are different regions in which changes in morphology from beaded to smooth fiber occur [24]. In 2006, the change in bead and fiber morphology and also the fiber diameter during electrospinning of polystyrene was studied by Eda *et al.* [25, 26]. They showed that a change in molecular weight or concentration affects final morphology even though $[\eta]c$ would be kept constant. In another work, they observed that solidification and instability of electrospun fibers could occur at different distances from the capillary, depending on the rheological condition of solution [27]. In one of the most recent works on PS nanofibers production, Wang *et al.* [28] could obtain scaling laws between the fiber final structure and process variables.

There are only few studies focusing on PS/CNT electrospun nanofibers. Sen *et al.* studied the effect of SWCNT addition to PS as well as to polyurethane (PU). They obtained oriented CNT inside PS nanofiber and some other polymeric materials [29], as evidenced from TEM images. In 2006, Ji and his colleagues used carboxyl-functionalized MWCNT inside PS and showed that the particles arranged quite well along the fiber axis [30]. Pan *et al.* produced polyelectrolyte hollow nanofibers out of PS/MWCNT solution mixture [31]. In this work, PS/MWCNT electrospun nanofibers were used as templates for self-assembly of polyelectrolytes [31]. In one of the most recent works in the field of electrospinning and CNT nanocomposite fiber manufacturing, Sundaray and his coworkers studied the properties of a single nanofiber of PS/MWCNT [32]. They investigated the morphology and electrical conductivity of a single nanofiber containing low amount of MWCNT. They obtained a low percolation threshold (0.05% w/w) for only a single electrospun fiber. In their work, they could improve conductivity to 10^{-6} S/cm after percolation [32].

The review of previous work on electrospun CNT filled polymeric fibers shows that several aspects of the materials/process used in their preparation required further study. The final properties of electrospun mat composed of nanocomposite nanofibers including different types of CNTs are one point of interest. In addition, dispersion modification

employing coupling agent and studying its effect on final electrical and mechanical properties is also of considerable interest. Different techniques such as rheometry and viscometry could be employed to perform the effect of adding CNT and studying the effect of dispersion on final morphology and properties. Electrospun polymer/CNT nanofibers and their properties as final conductive non-woven mat were not studied in details so far. Moreover, the properties of PS/CNT at different CNT concentrations are yet to be characterized. The final properties of electrospun PS/CNT as a conductive mat especially at more concentrated levels of CNTs were not shown in any previous works.

In the present study, polystyrene solutions containing different types and concentrations of carbon nanotubes (single-wall, double-wall and multi-wall) are electrospun to produce nanocomposite fibers. The effect of CNT addition on final morphologies of fibers is studied both quantitatively and qualitatively. We mainly focus on final nanofibers and mats characteristics at a wide range of MWCNT concentration and especially at high concentrations of different types of CNTs. Electrical conductivity of electrospun mats composed of PS/CNT nanofibers are evaluated here for the first time. Dispersion of CNT in initial electrospinning solution is studied in detail using rheological and optical techniques. The use of an SBS type copolymer to improve the dispersion of MWCNT in PS solution is, to the best of our knowledge, reported for the first time in this work. In addition, electrical properties and mechanical characteristics of resulting electrospun mats at different CNT contents and types are obtained.

5.4. Experimental

5.4.1. Polymer solution Preparation

The polymer used in this work was an extrusion grade polystyrene (168M, BASF Co.), dissolved at 20% w/w concentration in di-methyl formamide (DMF) (good solvent for PS as well as CNT dispersion); the solvent was purchased from Aldrich Co. Carbon

nanotubes employed in this work were produced by a chemical vapor deposition process (CVD) and purchased from Helix Co., USA. Single wall carbon nanotubes (SWCNT) and double wall carbon nanotubes (DWCNT) with purities of 90% and multi wall carbon nanotubes (MWCNT) with purity of 95% were used in this investigation as nanoparticles to improve the conductivity. The nominal diameter range of SWCNT, DWCNT and MWCNT were respectively of 1.3 nm, 4 nm and 10-100 nm. All three types of CNT had length in range of 0.5-40 μm (Fig. 5-1).

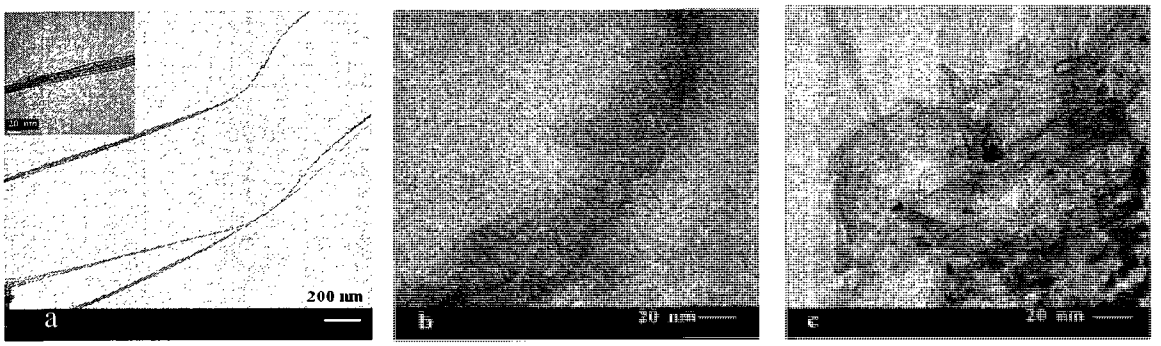

Figure 5-1: Transmission electron Microscopy (TEM) images of CNTs utilized in this work after sonication. a) Multi-wall Carbon Nanotube; b) Double-wall Carbon Nanotube; c) Single-wall Carbon Nanotube; TEM (JEOL, JEM-2100 F).

CNTs at different concentrations were dispersed mechanically in the polymer solution by a 4-hour sonication treatment at room temperature followed by continuous mechanical mixing before electrospinning. No surface modification technique was employed in this work in order to prevent the detrimental effect that these treatments can have on the conductivity of the CNT. TEM results after 4 hours sonication in pure methanol at different positions along CNTs bundles shows no obvious change in CNT length (Fig. 5-1). Styrene-Butadiene-Styrene (SBS-Kraton; G-1647), copolymer was used to improve the dispersion of CNTs in the solutions and electrospun fibers and to study the effect of copolymer addition. Following the proposed method for CNT dispersion modification [14], the copolymer was used in equal amounts of CNT for enhancing their dispersion at different concentrations.

5.4.2. Electrospinning process

The electrospinning set-up employed in this work consisted of a high voltage power supply (Gamma Inc.), a syringe pump to deliver the solution at specific flow rates (PHD 4400, Harvard Apparatus), a syringe connected to a stainless steel needle (22 gauge, Popper & Sons Inc.), and finally a stainless steel collecting drum (15 cm diameter). Fibers mats were collected in both static and rotating drums, based on the requirements of specific samples for different experiments. An average electrical potential difference of 25 kV was employed for all types of materials. The voltage was imposed on the needle, positioned at a 15 cm distance from the collector and a volumetric flow rate of 0.8 mL/hr was imposed. All experiments were conducted at ambient pressure, temperature and average relative humidity of 20%. A summary of different carbon nanotube concentrations and types studied here and the resulting fibers diameter and morphology is given in Table 5-1.

Table 5-1: Summary of nanocomposite nanofibers obtained and the resulting fibers characteristics

Polystyrene Concentration (%w/v)	**CNT Type**	**CNT concentration (%)**	**Resulting Morphology**	**Range of nanofiber diameter (nm)**
20	-	0	High concentration of beads on fibers	400 - 1500
20	MWCNT	0.5 ; 1 ; 2 ; 3 ; 4 ; 5 ; 7	**1 % :** Smooth fibers **Other concentrations** : Bead/Fiber morphology; beads depend on CNT concentrations Less beads compared to pure PS electrospun fibers	300 - 1100
20	MWCNT modified with Copolymer	1 ; 2 ; 3 ; 4 ; 5	**1 % & 2% :** Smooth fibers **Other concentrations** : Bead/Fiber morphology; beads depend on CNT/Copolymer concentrations Less beads compared to the fibers obtained form pure MWCNT/PS nanofibers	200 - 700
20	SWCNT	1 ; 5	Bead/Fiber morphology ; More beads formation at higher concentration (5%)	100 - 1400
20	DWCNT	1 ; 5	Bead/Fiber morphology ; More beads formation at higher concentration (5%)	150 - 1200

5.4.3. Initial material characterization

The effect of CNT on viscosity of the solutions was studied as it represents one of the key properties that may affect the electrospinning process. We used Cannon-Fenske-Routine (CFR) viscometers to characterize the change in viscosity with CNT addition. In addition we used a Bohlin CVO 120 stress-controlled rheometer to evaluate the rheological properties of initial polymer solution.

Optical microscopy observations of initial solutions containing CNTs at the same dispersion condition were used in parallel with viscometry to evaluate the dispersion condition of solutions containing carbon nanotubes at different concentrations.

The conductivity of the solutions at different carbon nanotube concentrations was measured using an accumet AP85 conductivity meter by Fisher Scientific. All the measurements were performed after mixing and before electrospinning.

5.4.4. Morphological characteristics and final properties

Raman spectroscopy technique was used for CNT detection in final non-woven mat. Raman spectra were recorded on a Renishaw spectrometer equipped with an inVia Raman microscope. The samples were tested using a NIR laser (785 nm) with a grating of 1200 g/mm in the regular mode and the microscope magnification used was 20x.

A Hitachi S-4700 scanning electron microscopy (SEM) was used on platinum coated samples to characterize the final morphologies of fibers at different processing conditions. An optical microscope, Dialux 20 (Leitz,WETZLAR), was employed to check and analyze the dispersion condition and position of CNTs inside fibers. This method was used to detect CNTs positions along with dispersion conditions and morphological characteristics.

The electrical conductivity of final electrospun mats was measured to assess the effect of CNT on nanofibers. For this purpose, a two-probe technique was employed, using a combined set-up of KEITHLEY 6620 as a current source and Agilent 34401 A (6 ½ Digit Multimeter) as voltage source.

The mechanical properties of selected samples produced at different processing conditions were obtained from a microtester 5548 (Instron Inc.) All the experiments were conducted on strips of 5 mm in width and 15mm in length cut from electrospun samples. The samples included different ranges of thicknesses from 50 to 300 μm. A load cell of 5 N and stretch speed of 10 mm/min were the best testing conditions for mechanical characterization of the electrospun samples.

5.5. Results and Discussions

5.5.1. Initial material characterization

Various characteristic parameters of the initial solution will determine the final fiber structure and diameter. Among them, surface tension, solution conductivity and viscosity are the most important determining factors. In this work, we mainly focused on the effect of dispersion of CNTs and the suspension viscosity and conductivity on the electrospinning process.

The measurement of viscosity was conducted at different CNT concentrations for samples containing different types of CNTs, with and without copolymer. The results obtained show that the viscosity decreases considerably with addition of CNTs (Table 5-2). The reduction of viscosity is observed in all samples containing CNTs. This could be because of polymer chains break-up during sonication. The reduction in molecular weight causes the viscosity of samples containing CNTs decrease compared to pure PS solution. Addition of MWCNTs, even at 5% concentrations, shows the decreasing viscosity of MWCNT/PS solutions compared to pure PS solution. A comparison of the results at 0.5, 1 and 2% MWCNT shows that addition of MWCNT does not change viscosity with MWCNT concentrations but MWCNTs affect considerably the viscosity of the polystyrene solution above 3%. Below 3% MWCNTs, solutions with MWCNTs are

stable for long period of time, no large agglomerates are found (Table 5-2). Above 3% MWCNT, viscosity of initial solution considerably increases and MWCNTs suspension in solutions are mostly unstable. The results prove that there is a network formation and structure build-up between 2% and 3% for this system. We also studied samples containing a SBS copolymer and MWCNT and a similar result was obtained. In prepared solutions, addition of MWCNT decreases the viscosity of solution (Table 5-2). However, viscosity increases at 3% MWCNT/Co-polymer concentration which shows the region of percolation in this system. The viscosity measured for sample with 2% and 3% MWCNT and copolymer is higher than for samples containing 2% and 3% pure CNT, which could be an evidence of SBS existence along with the dispersed MWCNTs. Copolymer chains interactions with CNTs cause an increase in suspensions viscosity; but they still remain less viscous than original PS solutions. Addition of high molecular weight SBS causes gradual increasing of viscosity. This effect is even more obvious at high concentrations of MWCNT and copolymer (Table 5-2). Therefore, using viscosity as evidence can only be inconsistent with similar systems, since adding copolymer changes the properties of system and viscosity accordingly. The effect of CNT addition on viscosity at 1% concentration of SWCNT, DWCNT and MWCNT is also assessed.

Table 5-2: Relative viscosity of solutions ($\eta/\eta_{solvent}$) at different CNT types and concentrations

CNT Type	**CNT concentration (%)**						
	0	**0.5**	**1**	**2**	**3**	**4**	**5**
MWCNT	160.5 ± 1.0	92±2.7	95.25± 1.7	96.8 ±2.6	121.8± 4.6	129± 4.7	130± 1.4
MWCNT/ Copolymer	160.5 ± 1.0	93.2±1	98±1.4	114.5± 2.4	145.8± 1.7	274.5± 1.7	451.3 ±41.6
SWCNT	160.5 ± 1.0	-	112.2± 4.3	-	-	-	-
DWCNT	160.5 ± 1.0	-	118.5± 0.6	-	-	-	-

MWCNT is much easier to disperse, and therefore, sample containing 1% MWCNT shows the lowest viscosity in spite of larger size of MWCNTs. Therefore, samples with 1% SWCNT and DWCNT show higher viscosities compared to 1% MWCNT and 1% MWCNT/copolymer samples. SWCNT and DWCNT are smaller in size; however, their poor dispersion increases the viscosity of their solutions compared to MWCNT [33, 34]. Viscosity in solutions with MWCNT/copolymer is not different from that with only MWCNT and is lower than that for those containing SWCNT and DWCNT. This could be due to the finer particle size (agglomerates) in solutions with both MWCNT and copolymer and better dispersion quality (Table 5-2). The results obtained show that viscometry could be an indirect mean of evaluating the quality of particles dispersion in the solution. The lower the viscosity, the more the compatibility is between particles and solution and better is the quality of the dispersion. Moreover, it could be used as a criterion for obtaining the system network formation concentration. Below 3% MWCNT, no network structure is formed to cause an increase in the viscosity of the solutions. Even though, despite of high shear rate flow fields in viscosimetry, no network structure could be observed coming from CNT particles, there is still considerable difference in viscosities before and after percolation.

The viscosity of the system was studied at different concentrations of MWCNTs below percolation at low range of shear rate (Fig. 5-2). We used this technique to evaluate the reliability of the results obtained from viscometry technique.

The tests were done at room temperature and constant stress of 20 Pa. The system shows totally Newtonian behavior; however, the reduction of viscosity by molecules break-up is not distinguishable at low frequencies. It shows that in high shear flow field, the difference in viscosities of pure sample with the ones containing CNT is more obvious (Table 5-2 & Fig. 5-2). This could be because of the sliding effect of CNTs in addition to molecular weight reduction in the samples containing CNT. The results in Fig. 5-2 could show that the samples containing 2% MWCNT have no network formation inside as obtained previously by viscometry technique (Table 5-2).

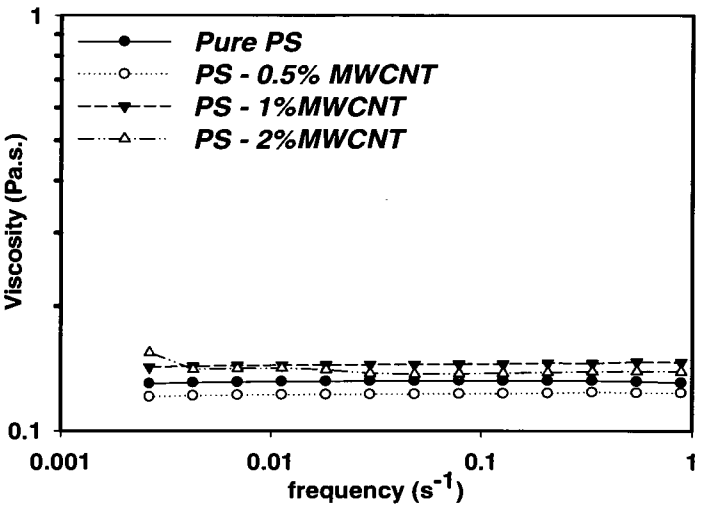

Figure 5-2: Viscosity vs. frequency at different MWCNT concentrations below rheological percolation threshold (CVO 120, Room temperature, at 20 Pa constant stress)

Optical microcopy was also used to evaluate the dispersion condition of CNTs in the initial polymer solution. This technique had the advantage of no limitations in terms of CNT concentration compared to viscosimetry and was very useful in this work. Fig. 5-3 shows the change of particle sizes both below rheological percolation (1% MWCNT) and above percolation (4% MWCNT).

As shown, upon addition of more and more MWCNT, it becomes more difficult to disperse the nanoparticles and large agglomerates are formed. The effect of copolymer addition on the dispersion quality is shown in Fig. 5-3. At 1% concentration (Fig, 5-3a and 3b), addition of copolymer causes a reduction in agglomerated particles size and fewer particles can be observed by optical microscopy. Above percolation and at 4% (Fig. 5-3c and 5-3d), the copolymer presence reduced particles size and allowed formation of an interconnected network structure, and thus MWCNTs are better dispersed with much less agglomerates (Fig. 5-3c and 5-3d).

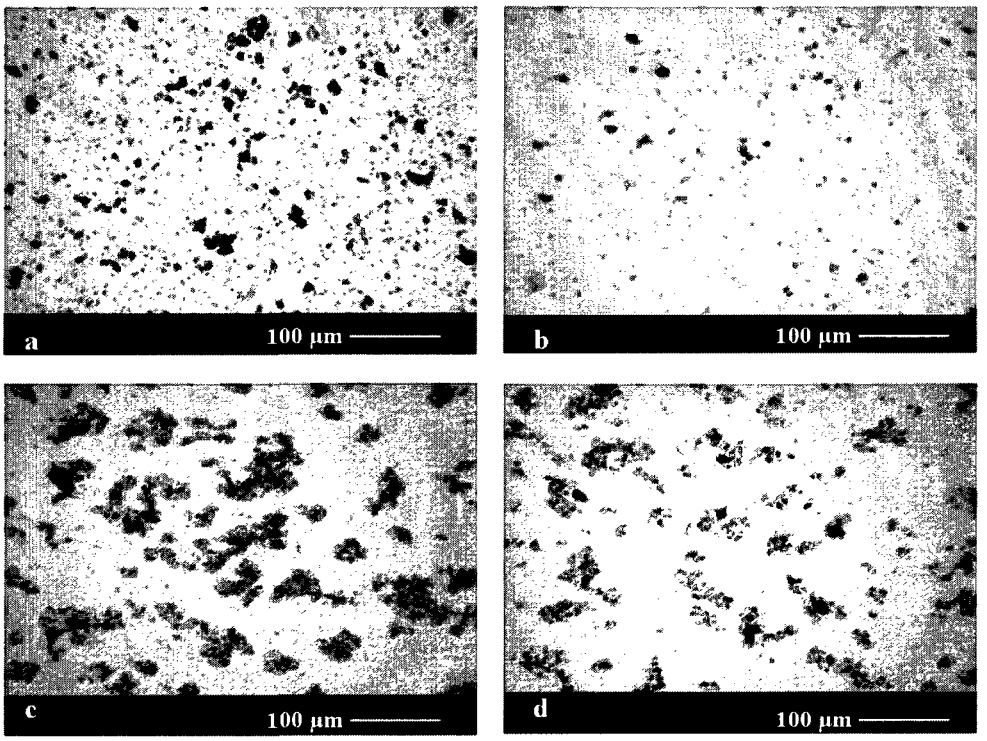

Figure 5-3: Optical microscopy on dispersion condition of initial solution below rheological percolation (1% MWCNT) and above percolation (4% MWCNT) with and without copolymer. a) 1% MWCNT; b) 1% MWCNT & copolymer; c) 4% MWCNT; d) 4% MWCNT & copolymer

The dispersion state of different PS/CNT solutions has been studied by optical microscopy at 5% concentration of different CNTs (Fig. 5-4). The optical images confirm the results from viscometry. SWCNT and DWCNT show the largest sizes of CNT agglomerates and therefore, they induce a higher viscosity below percolation (Fig. 5-4a and 5-4b). In contrast, MWCNT showed smaller and less agglomerates (Fig. 5-4c). Copolymer addition in the latter case even induced particle size reduction compared to MWCNT suspensions without copolymer (Fig. 5-4d).

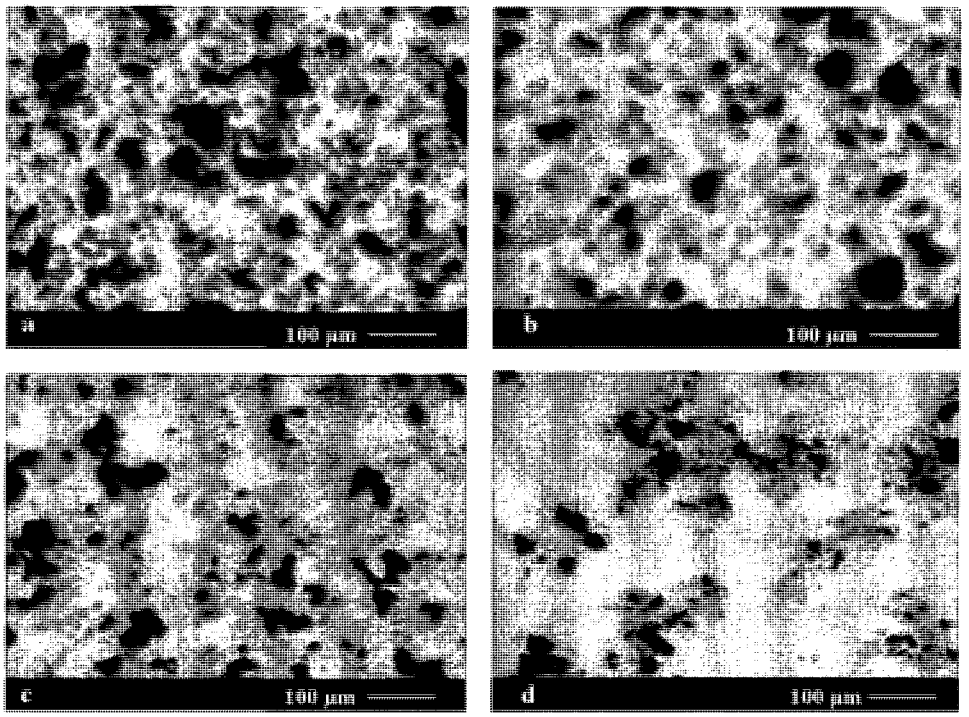

Figure 5-4: Optical microscopy on dispersion condition of initial solution. a) 5% SWCNT; b) 5% DWCNT; c) 5% MWCNT; d) 5% MWCNT & Copolymer

The results obtained from viscosimetry prove that at 1% concentrations of different carbon nanotubes (Table 5-2), the solutions are all below the concentration for network formation. Even though, there is a slight difference of suspension viscosity amongst different carbon nanotube types, it is not significant enough to be an evidence for structure build-up. The increase in the viscosity in the case of SWCNT and DWCNT is because of poor dispersion condition of carbon nanotubes. More over, the results from optical microscopy at 5% (Fig. 5-4) along with viscometry (Table 5-2) could be a proof that the system is above the concentration for network formation at 5% of different carbon nanotubes types. In this study, we mainly compare the results from 1% of different carbon nanotube types which is below network formation as described above (Table 5-2). In addition, 5% concentration of carbon nanotubes is chosen as a concentration above network formation.

The results obtained from electrical conductivity measurements of solutions containing various concentrations of MWCNT are given in Table 5-3. As expected, addition of MWCNT causes an increase of the initial solution conductivity.

Table 5-3: PS/CNT solutions conductivity (μS/cm) at different MWCNT concentrations

Concentration (%)	**0**	**1**	**3**	**5**
MWCNT	1.2	20.3	34.5	88.2

Comparing the results obtained from different types of carbon nanotubes show that SWCNT containing solutions are more conductive; 54 μS/cm at 1% SWCNT concentration compared to 20 μS/cm at 1% MWCNT concentration. Moreover, addition of copolymer causes a decrease in the amount of conductivity; 79 μS/cm at 5% MWCNT/copolymer concentration compared to 88 μS/cm at 5% MWCNT concentration. The reduction in conductivity by adding copolymer might be due to partial coating of the carbon nanotubes by the copolymer coupling agent. The results show that addition of carbon nanotube enhances the conductivity of the system, which could be an important determining factor on final morphology.

5.5.2. Raman spectroscopy

Raman spectra of non-woven mats obtained from different types of carbon nanotubes/PS nanofibers are shown in Fig. 5-5. Among the characteristic peaks of multi-wall carbon nanotubes detected by Raman spectroscopy, three peaks could be distinguished. Two string peaks are located at 1580 cm^{-1} (G), and 1350 cm^{-1} (D) and a weak peak are also detected at around 2700 cm^{-1} (G`) [35, 36].

The intensity and ratio of these peaks (D/G ratio) vary depending on carbon nanotube type and surface structure. The peaks related to SWCNT and DWCNT show more similar structure as expected; however SWCNT and DWCNT are fundamentally different from MWCNT characteristic peaks (D/G ratio).

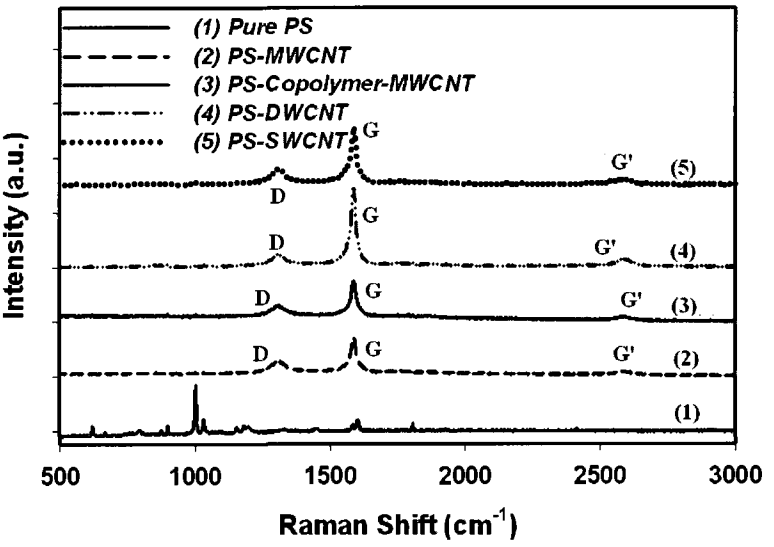

Figure 5-5: Raman spectra of final non-woven mat containing different types of carbon nanotubes

5.5.3. Morphology of electrospun fibers and mats

In this work, two methods were chosen to characterize the final morphologies of fibers. First, the fibers morphologies were analyzed qualitatively through SEM, followed by some quantitative image analysis. Second, optical microscopy was used to detect CNT localizations inside the fibers. Moreover, this technique was also used to evaluate the effect of copolymer addition on final dispersion condition of CNTs inside the fibers.

The final morphologies of the fibers are dependant on several characteristics of the initial solution such as viscosity, surface tension and conductivity in addition to some process and environmental conditions (temperature and humidity). The latter were not changed for this study and only the effect of material parameters was assessed, by changing the types and concentrations of CNTs.

Fig. 5-6 shows the effect of MWCNT addition at different concentrations on final fibers morphologies. As it is depicted in the results, electrospun PS fibers without MWCNTs are mixtures of beads and fibers at 20% PS concentration (Fig. 5-6a). Addition of MWCNTs to the PS solution causes a gradual decrease in the relative number of bead

structures among the fibers. This effect is explained by our previous observation that the addition of MWCNTs increases the solution conductivity and decreases the solution viscosity under high shear rates flow conditions; which are also found in the electrospinning process while solution is moving through syringe before exit. The value of shear rate for the viscometer we have used is in the range of 1-80 s^{-1}. In the electrospinning set-up we can estimate an average shear rate of about 4 s^{-1}, resulting from a 0.8 mL/hr volumetric flow rate through a PS22 gauge. . The best condition for smooth, beadless fiber production is below a 2% concentration of MWCNT (at 1%, beads are even less) (Fig. 5-6c and 5-6d). At 3% and 4% MWCNT and after rheological percolation (Above 3% MWCNT), the amount of bead structures in samples containing different concentrations of MWCNTs is almost the same (Fig. 5-6e and 5-6f). However, at two higher concentrations, 5% and 7% of MWCNT, there is again an increase in the amount of bead structures along fiber axis (Fig. 5-6g and 5-6h). The fibers at higher concentrations had smaller diameters and more beads in their structures compared to lower concentrations of MWCNTs. Followed by the decrease in fiber diameter, the sizes of beads along fiber axis is decreased correspondingly. Therefore, at higher concentrations smaller beads are shaped along fiber axis. The small beads are more obvious in the next optical microscopy test results by dark aggregate formation which will be discussed in more detailed.

The quantitative analysis shows that the fiber diameter reduces as CNT content increases in initial solution up to 4%-5% (Fig. 5-7). At 4%-5% and 7% MWCNT concentration, the value of fiber diameter is optimized and has the least value. The histograms of fiber diameter distribution show that, for all concentrations, a wide distribution of fiber diameters is obtained.

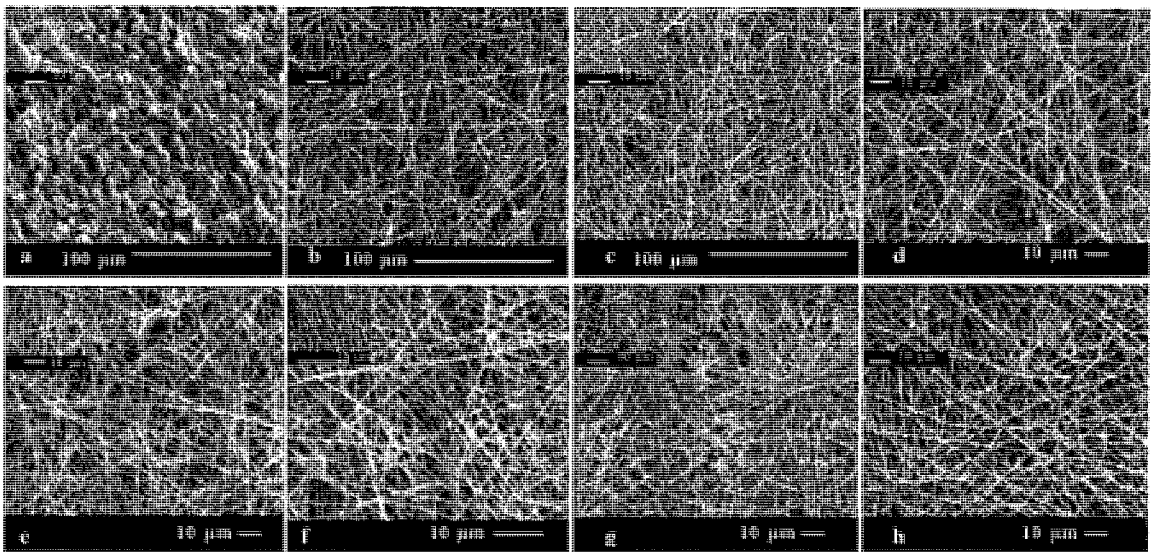

Figure 5-6: SEM photos of PS (20%) / MWCNT at different CNT concentrations. a) Pure PS; b) 0.5% MWCNT; c) 1% MWCNT; d) 2% MWCNT; e) 3% MWCNT; f) 4% MWCNT; g) 5% MWCNT; h) 7% MWCNT.

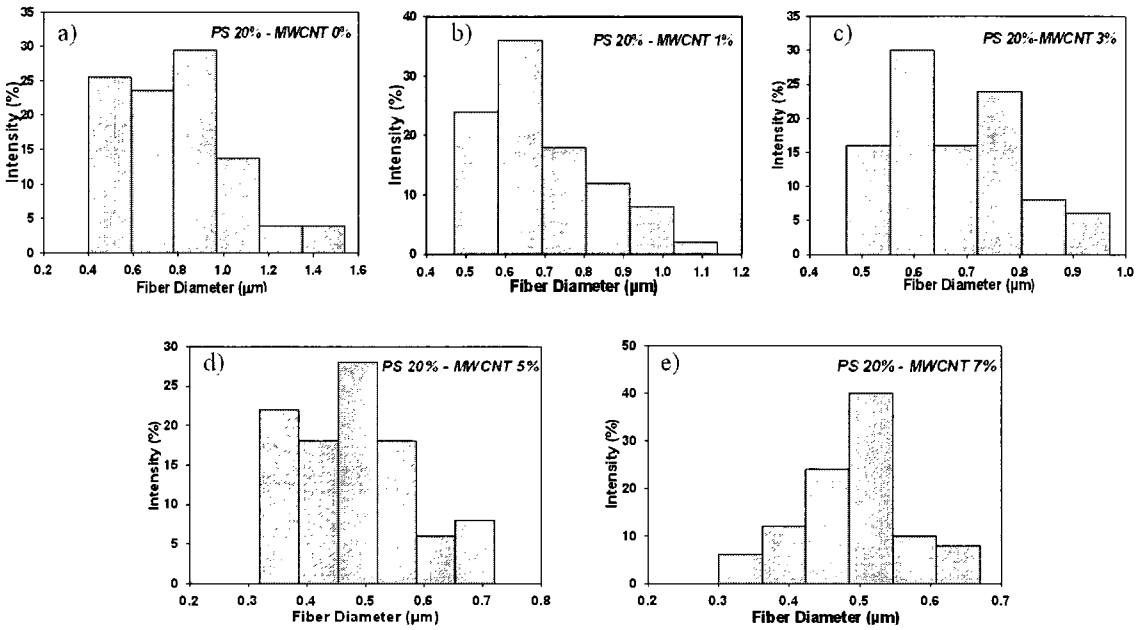

Figure 5-7: Histograms of fiber diameter distribution. a) Pure PS (Average fiber diameter (R_{avg}): 766±288 nm); b) 1% MWCNT (R_{avg}: 676±186 nm); c) 3% MWCNT (R_{avg}: 665±117 nm); d) 5% MWCNT (R_{avg}: 482±83 nm); e) 7% MWCNT (R_{avg}: 518±69 nm).

In the case of MWCNT addition combined with copolymer almost the same morphological trend as discussed above is observed (Fig. 5-8). The smoothest fibers are obtained at 1% and 2% concentrations of MWCNT/copolymer; while bead structures content increases by addition of CNTs to 5% MWCNT/copolymer. A comparison of the morphologies of systems with copolymer and without copolymer shows that addition of copolymer causes a decrease in the amount of bead structures compared to the system with pure MWCNT, for all concentrations.

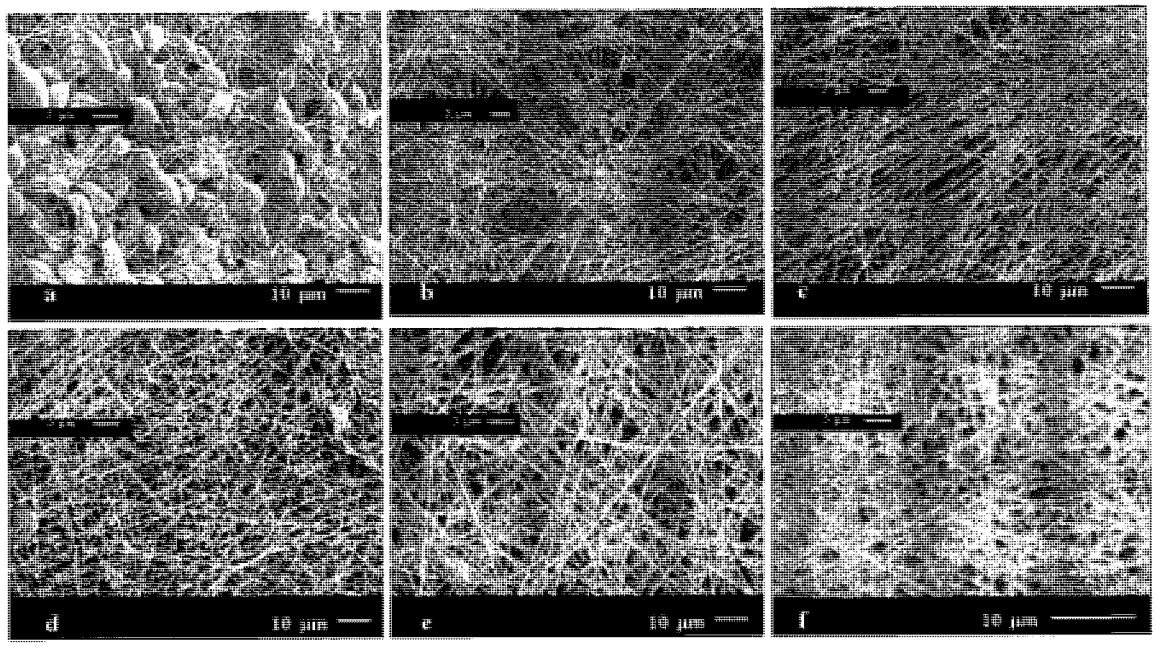

Figure 5-8: SEM photos of PS (20%) / Copolymer / MWCNT at different CNT concentrations. a) Pure PS; b) 1% MWCNT, 1% Copolymer; c) 2% MWCNT, 2% Copolymer; d) 3% MWCNT, 3% Copolymer; e) 4% MWCNT, 4% Copolymer; f) 5% MWCNT, 5% Copolymer.

Histograms of MWCNT/copolymer electrospun fiber show similar trends as samples with pure MWCNT (Fig. 5-9). The addition of MWCNT causes fiber diameter reduction and 4% MWCNT/Copolymer concentration is the optimum value. Fiber diameters decrease considerably by the addition of 1% MWCNT/copolymer. Fibers obtained were more uniformed in fiber diameter in this case and the range of fiber

diameter does not change considerably by adding carbon nanotube concentration. (Fig. 5-9).

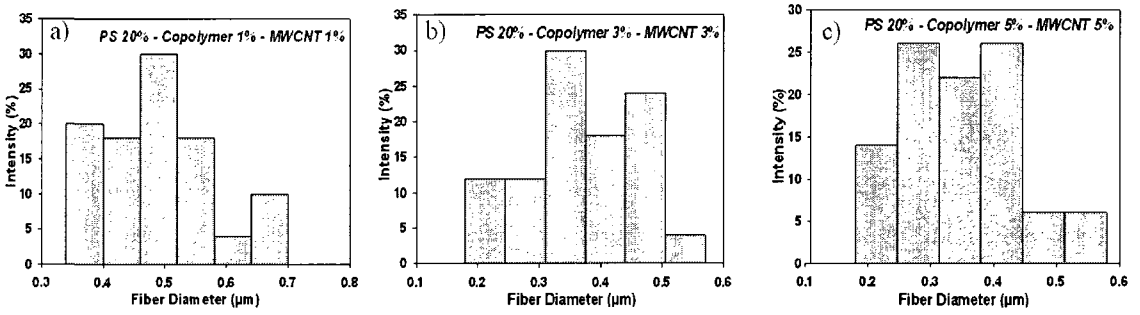

Figure 5-9: Histograms of fiber diameter distribution. a) 1% MWCNT, 1% Copolymer (R_{avg}: 486±108 nm); b) 3% MWCNT, 3% Copolymer (R_{avg}: 324±84 nm); c) 5% MWCNT, 5% Copolymer (R_{avg}: 298±105 nm).

The average diameter of fibers at other concentrations is even lower in samples with copolymer compared to pure MWCNT samples (Fig. 5-7 & Fig. 5-9). This is an additional proof that homogenous dispersion and electrical conduction through fibers results in a larger fiber diameter reduction. At 5% MWCNT/copolymer, the finest fibers are obtained with quite narrow fibers diameter distribution compared to other concentrations.

Optical microscopy was used in parallel with SEM to detect CNT localization inside the fibers. The samples for optical microscopy were electrospun at the processing conditions mentioned above; with the difference that a rotating drum with the speed of 120 rpm was used as collector instead of static drum to produce a thinner electrospun mat in stable electrospinning condition. Fig. 5-10 shows the optical images of electrospun fibers containing different concentrations of MWCNT in suspensions with and without copolymer. The results obtained from this method show that in most cases, beads in MWCNT-containing sections are filled with MWCNT agglomerates (Fig. 5-10). It is also possible to detect some MWCNTs aggregates inside fibers; however, the large ones are located inside the beads along the fibers. At 5%, the number of bead structures increase

and they are filled with MWCNTs. Even though, the fiber diameter and beads sizes decrease, most of those small beads all contain MWCNTs (Fig. 5-10c).

The same results were obtained from optical microscopy of the samples with both MWCNT and copolymer (Fig. 5-10d-f). At 1%, it was difficult to detect MWCNTs by optical microscopy. In samples containing copolymer, it shows that the sizes of MWCNT agglomerates have considerably reduced (Fig. 5-10d). At 3% and 5%, the fibers diameter decreased significantly; however, the bead structures are still MWCNT-aggregate locations. The compatibilizing effect of copolymer has decreased the size of the beads and MWCNT aggregates along fiber axis (Fig. 5-10e and f).

Comparing the results of SEM and optical microscopy shows that there are two main parameters controlling the morphology of fibers for this system during electrospinning: solution conductivity and CNT dispersion condition. Increasing conductivity removes the bead structures, therefore at 1% and 2% (below carbon nanotube network formation), there are less bead structures compared to 0% and 0.5% MWCNT. Above percolation, the morphology of fibers is controlled not only by the conductivity but also by the CNT dispersion condition. At these higher concentration levels, there is no change in solution conductivity and dispersion of CNTs becomes more difficult. The dispersion condition is the controlling parameter of final fiber morphology and of bead formations. Hence, at 5% and 7% MWCNTs, the bead structure greatly increases along fiber axis which could be the result of CNTs poor dispersion. Even though, the solutions at 5% and 7% MWCNTs are in a suitable solution conductivity range to give smooth fibers (The conductivity of solution containing 5% or 7% MWCNT is more than 1% MWCNT concentration which gives quite smooth fibers), the aggregates of CNTs cause bead structures development. The same results were obtained for the samples containing copolymer, and only CNT aggregates and beads dimensions were smaller. Therefore, CNTs are better distributed with finer particles along fiber axis.

The fibers` morphology at 1% of single wall, double wall (below percolation threshold) as well as at 5% (above percolation threshold) are shown on Figure 5-11. The systems containing SWCNT and DWCNT are mixtures of beads and fibers together. At

1% DWCNT or SWCNT (Fig. 5-11a & 5-11b), the amount of beads increased compared to 1% MWCNT but they still have fewer beads compared to pure PS fibers.

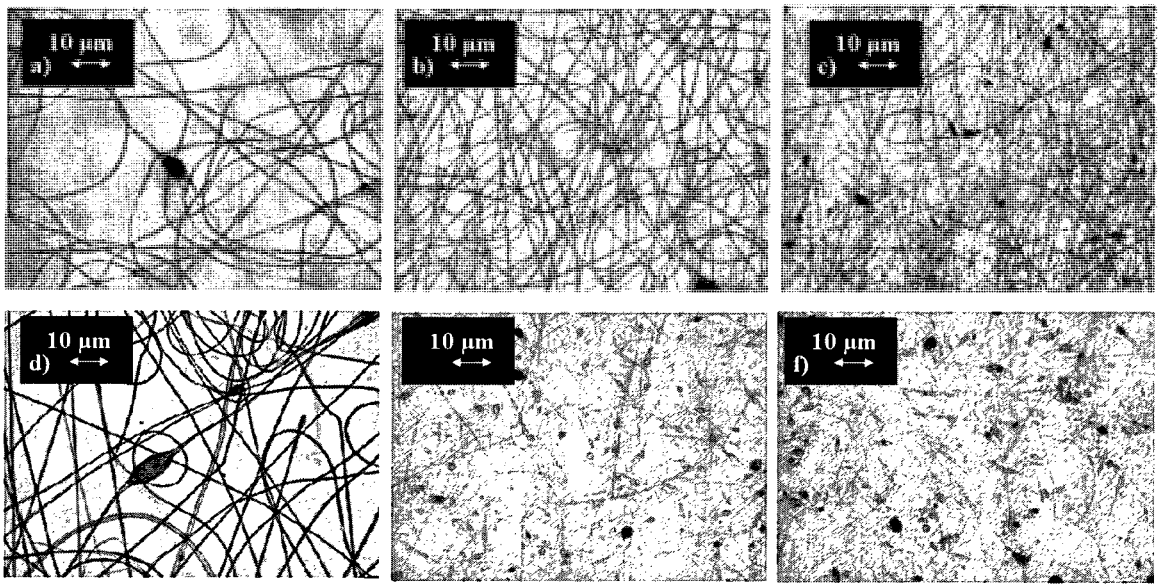

Figure 5-10: Optical microscopy photos of PS/MWCNT electrospun fibers obtained at the same condition, a) 1% MWCNT; b) 3% MWCNT; c) 5% MWCNT; d) 1% MWCNT, 1% Copolymer; e) 3% MWCNT, 3% Copolymer; f) 5% MWCNT, 5% Copolymer.

Quantitative analysis of SWCNT and DWCNT nanocomposite fibers shows that they both have average fiber diameters larger than those obtained for pure PS electrospun system below percolation (Fig. 5-12a & 5-12b). The expectations were to observe smaller diameters because of higher conductivity of SWCNT and DWCNT, but the result is opposite. This may be due to the poor dispersion condition of SWCNT and DWCNT proved by both viscometry and optical microscopy as discussed above. The fibers show a wide diameter distribution and they are mostly located at high range of diameters. Fig. 5-11 also shows the morphologies of fibers at 5% of different CNTs. Fine fibers were obtained at this concentration, with few beads for DWCNT and many beads for SWCNT (Fig. 5-11c & 5-11d). Fibers have low diameters and they obey a normal distribution especially with SWCNT system (Fig. 5-12d). High conductivity of initial solution

decreases the average fiber diameter; however, the fibers are mixed with many beads along axis which is the result of poor dispersion of CNTs (Fig. 5-12d).

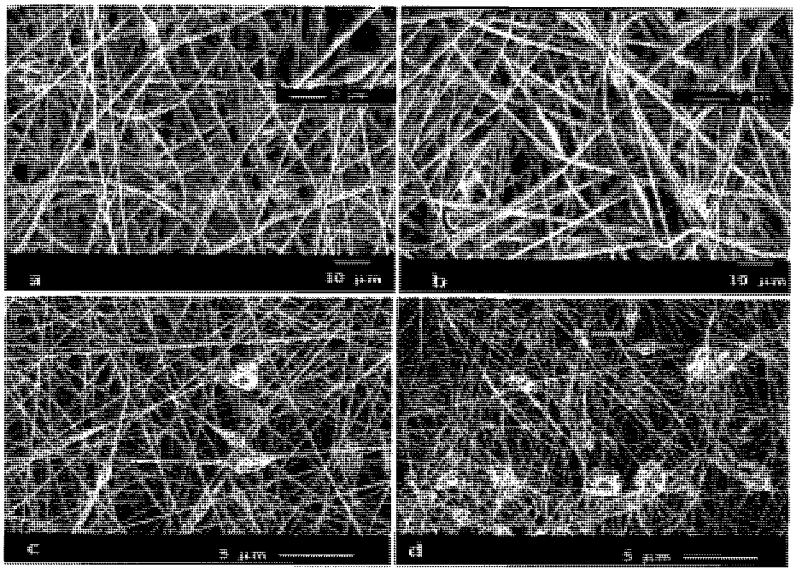

Figure 5-11: SEM photos of 20% PS electrospun fiber containing a) 1% DWCNT; b) 1% SWCNT; c) 5% DWCNT; d) 5% SWCNT

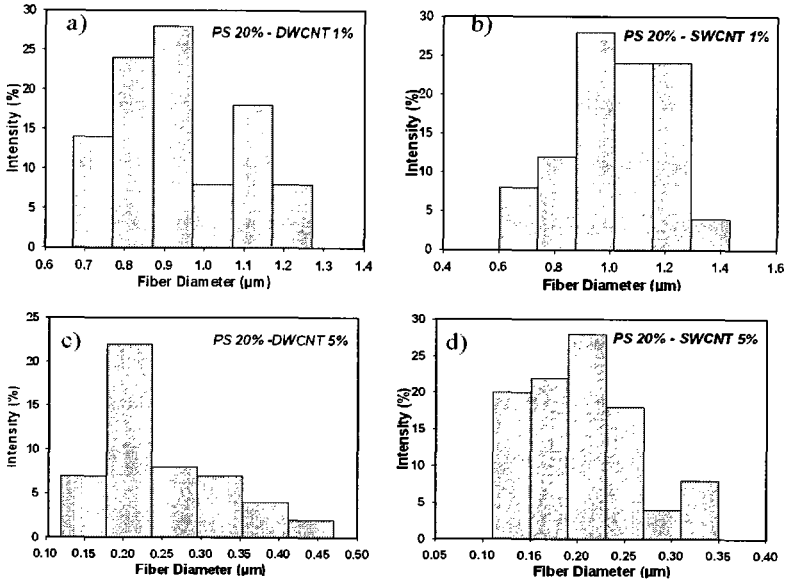

Figure 5-12: Histograms of fiber diameter distribution. a) 1% DWCNT; b) 1% SWCNT; c) 5% DWCNT; d) 5% SWCNT

Fig. 5-13 compares the average fiber diameter of different systems with CNTs at two concentrations. The behavior of the different systems is totally different below percolation (1% CNT) and above percolation (5% CNT). This again emphasizes the effect of the conductivity of the solution and dispersion of CNT as the parameters controlling the fiber diameter as well as morphology of electrospun fibers.

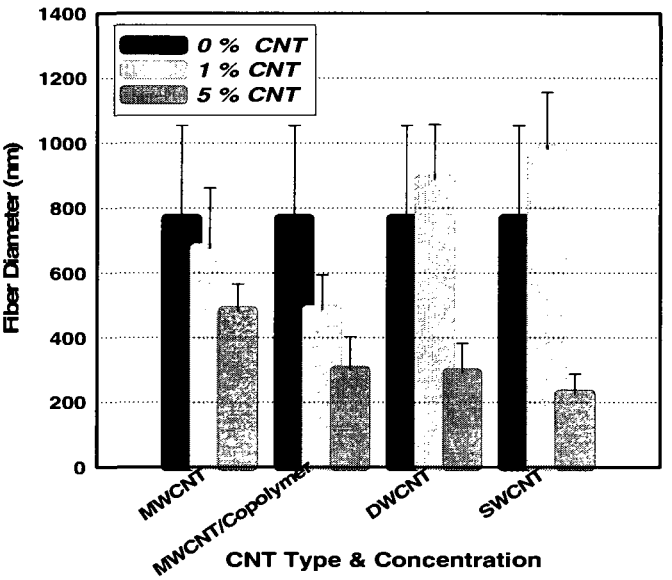

Figure 5-13: Comparison of average fiber diameter at different types of CNTs below percolation (1%) and after percolation (5%)

Figure 5-14 briefly reviews the morphological observations obtained here at different concentrations of CNTs. As it was discussed so far, dispersion condition could be introduced as a controlling factor of final fiber morphology. In the case of good dispersion and very low concentrations of CNTs, finer fibers besides removing bead structure are expected because of increasing conductivity [6, 24]. Therefore, increasing CNT concentrations decreases both bead structures and fiber diameter in all concentrations resulting from high conductivity; however, two different areas are distinguished in the case of poor dispersion based on CNT concentration and percolation threshold (Fig. 5-14).

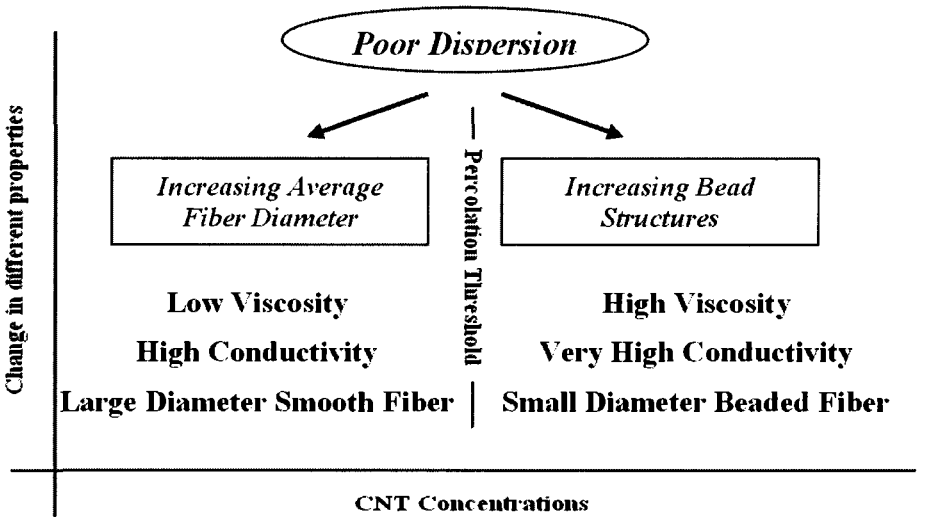

Figure 5-14: The schematic diagram of change in various properties as a function of CNT concentrations and the effect of poor dispersion condition as a controlling factor

The results show that both fiber diameter and smoothness could be controlled by CNT dispersion condition depending on CNT concentration. As it is depicted, at low CNTs concentrations, fibers with larger diameters are the effect of poor dispersion; while the same factor translate by larger fraction of beaded fibers at high concentrations. At low CNT concentrations, an increase in fiber diameter is observed, which is unexpected in solutions with higher conductivity compared to pure PS system due to CNT addition. It is opposite to previous observations with MWCNT dispersions since the increase in conductivity results in fiber diameter reduction [6]. Moreover, the beads disappear from the fibers at low CNT concentrations while the results show the samples have lower viscosities in this range. This results is opposite to previous observations for the effect of viscosity on smooth fibers formation; since the increase in viscosity was accounted as a parameter for smoother fiber formation [24]. Beads removal could be due to the increase of conductivity compared to pure electrospun nanofibers in spite of the lower viscosities of initial solution. Higher conductivity of solution is expected by adding more CNT to the system; however, an increase in fiber diameter is observed here even in highly conductive

solutions especially when there is poor dispersion of CNTs (SWCNT and DWCNT). Therefore, dispersion condition is one of the controlling factors for fiber diameter besides fiber smoothness. Above percolation, the increase in conductivity and viscosity results in significant fiber diameter reduction compared to lower CNT concentrations. At higher CNT concentrations (above electrical percolation), dispersion affects final fiber morphology from another aspect. There are unexpected bead structures along fiber axis which contain CNT aggregated (Fig. 5-10). Poor dispersion above percolation and inhomogeneous electrical conduction along the fiber causes CNT agglomeration and bead formation. The poorer the dispersion, the more the beads are present along the fibers, while the opposite is expected at high values of viscosity and conductivity.

In summary, reduction in molecular weight and viscosity after sonication is not consistent with bead removal from fiber axis [25]; therefore other parameters except of viscosity are controlling the bead morphology and fiber diameter. Here, we believe that CNT dispersion condition and conductivity of initial solution are the main determining factors. As the results of conductivity show, addition of CNT increases the conductivity and the solutions containing SWCNT are more conductive that the solutions with coated MWCNT. Therefore, followed by increasing the initial conductivity we expect two main changes in final morphology: reduction in fiber diameter [6] and bead removal from fiber axis [22] compared to pure electrospun nanofibers. While there is an increase in fiber diameter for the samples below network formation concentration opposite to expectation (SWCNT and DWCNT) and there is increase in bead morphology by increasing the CNT concentration above network formation concentration. Increasing the fiber diameter at 1% CNT concentration in SWCNT and DWCNT which are poorly dispersed prove that dispersion condition is more important than solution conductivity in this case; while this effect is shown as bead formation at high CNT concentration. Comparing the sizes of beads obtained from optical microscopy and SEM in addition to optical microscopy results prove that all the beads are the locations of CNT aggregated and making modification on the dispersion in example by adding copolymer decreases the bead structures to a great extend.

Increasing the conductivity causes larger electric current during electrospinning and will induce large charge accumulations on fiber diameter, and as result, will intensify the electrical force and splashing and finer fibers are formed [37]. In this system, the solvent (DMF) is non-conductive compared to PS/CNT complex and the polymer (PS/CNT) is the charge carrier in these kinds of systems; since the polymer (PS/CNT) is more conductive and the conductivity of solution is dependent on CNT. Therefore, when the CNT is well dispersed, and before network formation, the charge accumulates uniformly on fiber surface and the reduction of fiber diameter along with smooth fiber formation is observed (1% MWCNT and 1% and 2% MWCNT/Copolymer). However, when CNT is not well dispersed, there is localized charge accumulation along fiber axis because of inhomogeneity of polymer solution conductivity. In this case the charge density is not dispersed uniformly along fiber and therefore electric field is not homogenous along fiber. The inhomogeneity of charges and electric field causes bead formation along fiber axis. It means that in some parts, the fiber diameter reduces and in the other parts there are bead structures and increase in fiber diameter (SWCNT and DWCNT solutions in all concentrations and MWCNT solutions above network formation concentration). In 1% SWCNT and 1% DWCNT solutions the quality of dispersion is not satisfactory; therefore beads are formed even at low concentration. However, because of lower conductivity compared to 5% CNT, the charge density and electric field is not strong enough for fiber diameter reduction. As a result, the presence of aggregated CNT causes an increase in the fiber diameter because there is not a strong electric field; moreover, the inhomogeneity of charge density induces the bead formation.

5.5.4. Electrical conductivity results of fiber mats

Electrical conductivity of final electrospun mat was measured as a function of CNT type and concentration. The samples included a wide range of thicknesses from 15 to 300 μm and they were all positioned between two highly conductive layers besides electrodes before starting experiments. The conductivities of all samples were measured in a specific two-probe test fixture. Therefore, all the experiments were run in similar

conditions, constant force and with reliably enough repeatability within 80% of the average conductivity.

Based on electrical percolation theory, the system becomes conductive when a critical concentration is reached which is called percolation threshold. Above electrical percolation, the system is quite conductive. Formation of CNT network causes the electron transport by tunneling or electron hopping which occurs along CNT interconnects [38]. The system studied was the 20% PS and was below percolation for CNTs content up to 2%. No network structure or CNT agglomerate is formed up to 2% MWCNT, which was shown before by viscometry and optical microscopy of initial solution. In MWCNT concentrations above 2%, an internal network structure is formed and the system is getting close to percolation. Below 3% our instrument and set-up was not showing any results which could depict considerable electrical conductivity in the system. At 3% MWCNT and above, sensible modification in conductivity of PS electrospun mat was observed from electrical conductivity measurements. However, 3% MWCNT is not enough to form complete network and to achieve the electrical percolation threshold and the samples are still in the transition region to percolation (1.90×10^{-9} S/cm). Therefore, the conductivity of non-woven mat at 1% and 2% MWCNT concentration is almost zero (Between 10^{-19} and 10^{-9} S/cm (PS/3%MWCNT)). At 3.5% concentration of MWCNT, samples are at electrical percolation threshold (1.02×10^{-5}S/cm) and a considerable increase in electrical conductivity is observed after this concentration (Fig. 5-15). At 5% and 7% CNTs, the conductivity increased; however, the value of conductivity was almost constant after 5% MWCNT (Fig. 5-15). This confirms the results obtained from viscometry which indicates the start of network formation above 2% MWCNT. At 3% the sample is at the beginning of the construction of a complete network, and at 3.5% CNT concentration, the network is complete resulting in a totally conductive mat. Based on percolation theory [39]:

$$\sigma = A(w - w_c)^t \tag{5-1}$$

where σ is the volume conductivity, A and t are constants, and w_c is the critical concentration in which the conductivity is ignorable compared to higher concentration;

the critical concentration for network formation. Considering 3% as w_c, we could obtain $A=8.5\times10^{-5}$ and t=0.795 for this system. We have measured the conductivity through the thickness of non-woven mat. It means that at 3.5 % MWCNT, there are networks for electron transfer between the layers of non-woven mat based on percolation theory. Therefore, the random structures of fibers, which are making different layers of non-woven mat, have enough CNT to make network between layers. As a result, it is possible to predict that the value of conductivity would be more and the percolation threshold would be less even if the conductivity is measured along fiber axis.

For the samples containing both MWCNT and copolymer, a similar concentration effect on the electrical conductivity was found. The electrical percolation threshold (5×10^{-5} S/cm) was observed for 4% CNT concentration. The results obtained show that the electrical conductivity of mats containing compatibilizer is slightly higher than samples containing MWCNT without compatibilizer, below and around percolation threshold (Fig. 5-15). The higher values of conductivity originate probably from the good dispersion condition of MWCNTs in the samples, which reduces agglomeration and helps distribution of MWCNTs along fiber axis. Improving dispersion helps in conductivity modification below percolation. However, after percolation (5%), a decrease in conductivity of sample containing copolymer is observed compared to only MWCNTs containing samples (Fig. 5-15). Moreover, the conductivity reached a constant value more rapidly in samples with copolymer. This might be the result of a reasonable dispersion of CNTs around percolation.

Good dispersion is expected to increase conductivity of mats compared to samples without copolymer. However, coating and compatibilization above percolation may have a reverse effect on conductivity. At 5% w/w concentration, the network of CNTs is organized in the sample with both copolymer and pure MWCNT. Addition of copolymer partially coats the MWCNTs and therefore in spite of forming networks; it could reduce the electrical conduction as has been previously observed [8].

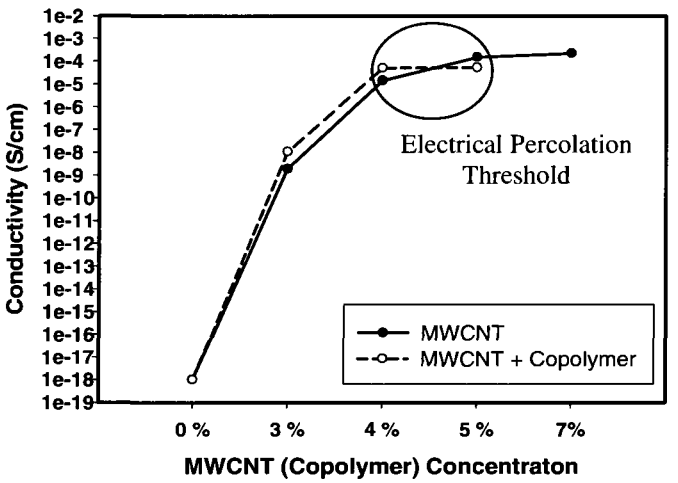

Figure 5-15: Conductivity of samples containing copolymer comparing to samples without copolymer

The conductivities of samples with 5% SWCNT and 5% DWCNT were also measured. At this content, SWCNT shows the highest conductivity as expected (3.7×10^{-4} S/cm). The samples with MWCNT/Copolymer (5.3×10^{-5} S/cm) and DWCNT (5.0×10^{-5} S/cm) show the lowest amount of electrical conductivity. It should be noted that, however, it is quite difficult to disperse the samples with SWCNT and DWCNT, and the fibers obtained show the presence of CNTs aggregates in the fibers in addition to the beads structure. However, the unique structure of SWCNT overcomes the poor dispersion of CNTs and the best conductivity is obtained.

5.5.5. Mechanical characterization of fiber mats

Electrospun PS/MWCNT fiber mats were studied in both cases of with and without compatibilizing copolymer. For the samples without copolymer, addition of MWCNT causes an increase in both modulus and tensile strength before percolation threshold (Fig. 5-16). A gradual increase is observed up to 2% CNT; then a jump in modulus and tensile strength is observed at 3% MWCNT. Above 3% MWCNT, modulus and tensile strength decrease and they are even less than pure PS at 5% MWCNT. At 4%

MWCNT, the internal network of CNT is formed and it is thought to be the main reason for weakening of nanocomposite mats. Since the formation of network is accompanied with weakening of CNT/matrix at high concentrations of CNTs. Increasing MWCNT content and network formation decreases the strength of final PS mat and a reduction in mechanical properties is obtained. The materials obtained above percolation are quite brittle and weak (Fig. 5-16). Almost the same behavior was observed for maximum tensile strain (ε_{max}) in the samples containing MWCNT (Fig. 5-16). The increase of modulus at all concentrations of MWCNT below percolation causes a change into brittle behavior and accordingly, causes a decrease in ε_{max} compared to pure PS. The value of ε_{max} in all concentrations is less than pure PS non-woven mat..

A comparison of the values of modulus and tensile strength with those of the samples containing only MWCNT shows a significant copolymer effect. The modulus and tensile strength are about twice for the samples containing copolymer (Fig. 5-16). Only at 3% MWCNT the value of tensile strength in both samples with and without copolymer are almost the same. Moreover, above percolation, improved mechanical properties for samples containing MWCNT and copolymer are still observed compared to pure PS. Therefore, not only quite conductive systems are obtained above electrical percolation, but also improved mechanical properties are achieved. The behavior of maximum tensile strain (ε_{max}) for the samples with MWCNT and copolymer is totally different from pure MWCNT nanocomposite fibers. ε_{max} increases as a function of MWCNT concentration and it does not decrease even after percolation at 5% MWCNT/Copolymer concentration (Fig. 5-16). It is to be reminded here that any increase in MWCNT is accompanied with the same increase in copolymer concentration for compatibilized nanocomposites. Therefore, copolymer addition brings tough behavior to the electrospun mats even with addition of MWCNT and decreasing modulus after percolation.

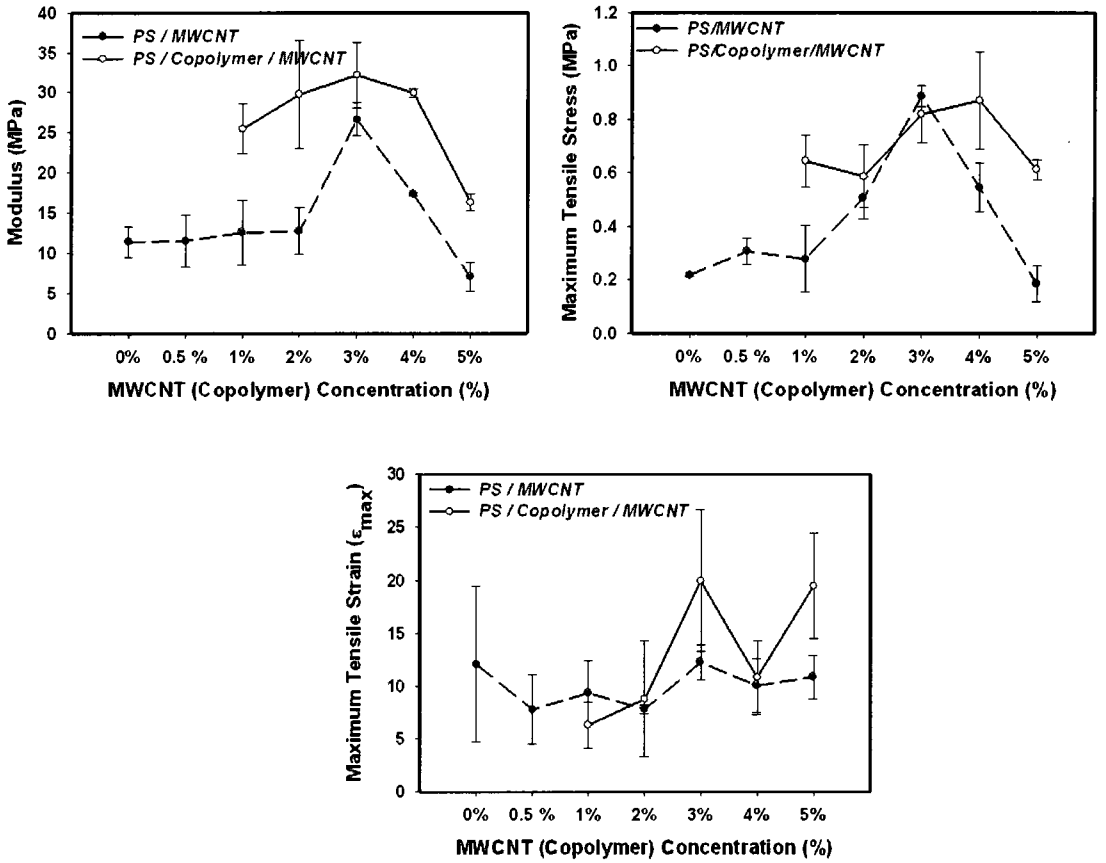

Figure 5-16: Tensile modulus, maximum tensile stress and maximum tensile strain as a function of MWCNT concentrations with and without copolymer.

The localization of the compatibilizer at the interface of CNT and polymer matrix improves the mechanical strength [40]. The results obtained from the mechanical tests and increasing in ε_{max} prove that the added copolymers are improving the interactions at the interface. The improved interface due to copolymer addition results in better mechanical strength of final nanocomposite electrospun mats. From another point of view, addition of copolymer might cause developing a kind of PS/SBS blend as the matrix. The formation of the blend by adding copolymer concentration causes tough behavior of the system and increase in ε_{max}.

The effect of different types of CNTs on final mechanical properties was also studied (Table 5-4). As shown, in contrast with electrical conductivity results, DWCNT

shows the best mechanical properties results. The highest values of modulus, tensile strength and ε_{max} were obtained for the samples with DWCNT. This might originate from the small size of DWCNT compared to MWCNT and more interface and connection with matrix. Compared to SWCNT, DWCNT is easier to disperse and therefore, the mechanical test results improve by adding DWCNT. In the case of SWCNT, in spite of the small sizes of nanotubes, poor dispersion causes the mechanical properties to deteriorate. Similar results have been obtained previously in literature on the effect of DWCNT in mechanical properties modification and obtaining better results compared to MWCNT and SWCNT [34].

Table 5-4: Mechanical properties of different CNT types

CNT Type	**Modulus (MPa)**	**Maximum Tensile Stress (MPa)**	**Maximum Elongation (ε_{max})**
5 % MWCNT	7.0 ± 1.8	0.18 ± 0.07	10.8 ± 2
5 % MWCNT/ Copolymer	16.3 ± 0.1	0.61 ± 0.04	19.4 ± 5
5 % SWCNT	10.4 ± 2.0	0.22 ± 0. 05	8.6 ± 5
5 % DWCNT	23.4 ± 8.6	0.78 ± 0.16	12.3 ± 1

Samples containing both MWCNT and copolymer show best improvement in both mechanical and electrical properties (above percolation). Therefore, the compatibilised MWCNT samples could give the best results from different aspects of view and this is of great interests.

5.6. Conclusions

PS nanocomposite nanofibers combined with different types of CNTs were electrospun in this work for the first time. The final structures and morphologies of electrospun nanocomposite nanofibers were studied along with electrical and mechanical properties of resulting mats. A copolymer was used to improve the dispersion condition of CNT and the resulting suspension was analyzed by means of optical microscopy and viscometry. Comparison of the final morphologies of samples with different dispersion conditions showed that CNT dispersion is an important controlling parameter for final fibers diameter and morphology. Below percolation, poorly dispersed samples showed an unexpected increase in fiber diameter while above percolation threshold, beads formation resulted from poor nanoparticles dispersion. Reasonable electrical conductivity was obtained at the percolation threshold of 4% MWCNT. Electrical conductivity results proved the positive effect of copolymer addition below percolation threshold. However, above percolation, the samples with copolymer showed a lower conductivity which might be because of CNTs coating with copolymer. Moreover, morphologies and final properties of electrospun fibers with different types CNTs (SWCNT, DWCNT, MWCNT, and compatibilised MWCNT) at different concentrations and percolation region were compared in this work. The results show the important effect of dispersion on final fiber morphologies and properties. The best conductivity obtained in SWCNT/PS mixture in spite of poor dispersion. While adding copolymer causes better conductivity results below percolation in MWCNT/PS mixture. The effect of copolymer on improved compatibility was proved through comparison of the mechanical properties test results between PS/MWCNT and PS/Copolymer/MWCNT systems.

5.7. Acknowledgement

The authors would like to acknowledge the financial support of Natural Sciences and Engineering Research Council Canada (NSERC) and from FQRNT (Fonds Québécois de Recherche en Nature et Technologies) for the financial support to carry out this study.

5.8. References

[1] Burger C, Hsiao BS, Chu B. Annual Review of Materials Research 2006; 36:333-368.

[2] Li D, Xia Y. Advanced Materials 2004; 16(14):1151-1170.

[3] Reneker DH, Chun I. Nanotechnology 1996; 7(3):216-223.

[4] Iijima S. Nature 1991; 354(6348):56.

[5] Ge JJ, Hou H, Li Q, Graham MJ, Greiner A, Reneker DH, Harris FW, Cheng SZD. Journal of the American Chemical Society 2004. 126(48):15754-15761.

[6] Ra EJ, An KH, Kim KK, Jeong SY, Lee YH. Chemical Physics Letters 2005; 413(1-3): 188-193.

[7] Seoul C, Kim YT, Baek CK. Journal of Polymer Science, Part B: Polymer Physics 2003; 41(13):1572-1577.

[8] Sung JH, Kim HS, Jin HJ, Choi HJ, Chin IJ. Macromolecules 2004; 37(26): 9899-9902.

[9] Dror Y, Salalha W, Khalfin RL, Cohen Y, Yarin AL, Zussman E. Langmuir 2003; 19(17):7012-7020.

[10] Dror Y, Salalha W, Pyckhout-Hintzen W, Yarin AL, Zussman E, Cohen Y. Progress in Colloid & Polymer Science 2005; 130:64-69.

[11] Salalha W, Dror Y, Khalfin RL, Cohen Y, Yarin AL, Zussman E. Langmuir 2004. 20(22):9852-9855.

[12] Delozier DM, Watson KA, Smith JrJG, Clancy TC, Connell JW. Macromolecules 2006; 39(5):1731-1739.

[13] Nativ-Roth E, Shvartzman-Cohen R, Bounioux C, Florent M, Dongsheng Z, Szleifer I, Yerushalmi-Rozen R. Macromolecules 2007; 40(10):3676-3685.

[14] Sluzarenko N, Heurtefeu B, Maugey M, Zakri C, Poulin P, Lecommandoux S. Carbon 2006; 44(15):3207-3212.

[15] Casper CL, Stephens JS, Chase DB, Rabolt JF. Polymer Preprints (American Chemical Society, Division of Polymer Chemistry) 2003; 44(2):81.

[16] Jarusuwannapoom T, Hongrojjanawiwat W, Jitjaicham S, Wannatong L, Nithitanakul M, Pattamaprom C, Koombhongse P, Rangkupan R, Supaphol P. European Polymer Journal, 2005; 41(3):409-421.

[17] Kang M, Yoon SH, Jin HJ. Polymer Preprints (American Chemical Society, Division of Polymer Chemistry) 2005; 46(2):812-813.

[18] Lee KH, Kim HY, Bang HJ, Jung YH, Lee SG. Polymer 2003; 44(14):4029-4034.

[19] Megelski S, Stephens JS, Rabolt JF, Bruce Chase D. Macromolecules 2002; 35(22): 8456-8466.

[20] Pattamaprom C, Hongrojjanawiwat W, Koombhongse P, Supaphol P, Jarusuwannapoo T, Rangkupan R. Macromolecular Materials and Engineering 2006; 291(7): 840-847.

[21] Wannatong L, Sirivat A, Supaphol P. Polymer International 2004; 53(11):1851-1859.

[22] Uyar T, Besenbacher F. Polymer 2008; 49(24): 5336-5343.

[23]. Lin T, Wang H, Wang H, Wang X. Nanotechnology 2004; 15(9):1375-1381.

[24] Shenoy SL, Bates WD, Frisch HL, Wnek GE. Polymer 2005; 46(10):3372-3384.

[25] Eda G, Shivkumar S. Journal of Materials Science 2006; 41(17):5704-5708.

[26] Eda G, Shivkumar S. Annual Technical Conference - ANTEC, Conference Proceedings 2006. Charlotte, NC, United States: Society of Plastics Engineers, Brookfield, CT 06804-0403, United States.

[27] Shivkumar S, Eda G, James L. Materials Letters 2007; 61(7):1451-5.

[28] Wang C, Hsu CH, Lin JH. Macromolecules 2006; 39(22):7662-7672.

[29] Sen R, Bin Z, Perea D, Itkis ME, Hui H, Love J, Bekyarova E, Haddon RC. Nano Letters 2004; 4(3):459-64.

[30] Yuan Ji SG, Koo J, Li B. MAR06 Meeting of The American Physical Society 2006.

[31] Pan C, Ge LQ, Gu ZZ. Composites Science and Technology 2007; 67(15-16):3271-3277.

[32] Sundaray B, Subramanian V, Natarajan TS. Journal of Nanoscience and Nanotechnology 2007; 7:1793-1795.

[33] Coleman JN, Khan U, Blau WJ, Gun'ko YK. Carbon 2006; 44(9):1624-1652.

[34] Gojny FH, Wichmann MHG, Fiedler B, Schulte K. Composites Science and Technology 2005; 65(15-16):2300-2313.

[35] Antunes EF, Lobo AO, Corat EJ, Trava-Airoldi VJ. Carbon 2007; 45(5):913-921.

[36] Corrias M, Serp P, Kalck P, Dechambre G, Lacout JL, Castiglioni C, Kihn Y. Carbon 2003; 41(12):2361-2367.

[37]. Fridrikh SV, Yu JH, Brenner MP, Rutledge GC. Physical Review Letters 2003; 90(14): 144502.

[38] Kota AK, Cipriano BH, Duesterberg MK, Gershon AL, Powell D, Raghavan SR, Bruck HA. Macromolecules 2007; 40(20):7400-7406.

[39] Wang Q, Dai J, Li W, Wei Z, Jiang J. Composites Science and Technology 2008; 68(7-8):1644-1648.

[40] Ye H, Lam H, Titchenal N, Gogotsi Y, Ko F. Applied Physics Letters 2004; 85(10): 1775-1777.

Chapter 6

Fundamental Study of Crystallization, Orientation and Final Properties of Electrospun PET/Carbon nanotube Nanofibers*

6.1. Presentation of the article

Final morphology and properties of PET/CNT are deeply characterized in this work. Study and characterization of PET/CNT conductive nanofibers are the main aim of this study. Final morphology of PET/CNT electrospun non-woven mat is studied at first step. Moreover, we could produce aligned nanocomposite nanofibers by using a high speed rotating drum. The effect of CNT addition on PET chains crystallization and orientation is studied by different techniques. We could obtain smooth conductive nanofibers with electrical percolation threshold below 2 wt% MWCNT. Crystallography test results show increasing crystalline density by increasing CNT concentration above electrical percolation. This result is opposite to decreasing crystallinity function below percolation by adding CNT. Raman spectroscopy test results show CNT orientation along fiber axis in oriented electrospun nanofibers. Aligned nanofiber production causes considerable enhancement in the amount of modulus even up to 6 times more compared to randomly oriented nanofibers in pure PET non-woven mat in direction of alignment.

---

* ***Polymer Science, Part B; Polymer Physics.*** Submitted May 2009.

Fundamental Study of Crystallization, Orientation and Final Properties of Electrospun PET/Carbon nanotube Nanofibers

Saeedeh Mazinani [1], *Abdellah Ajji* [1,2], *Charles Dubois* [1*]

1) CREPEC, Department of Chemical Engineering, Ecole Polytechnic of Montreal, P.O. Box 6079, Station Centre-Ville, Montreal, Quebec, Canada H3C 3A7.

2) CREPEC, Industrial Materials Institute, National Research Council Canada, 75, de Mortagne, Boucherville, Quebec, Canada J4B 6Y4.

6.2. Abstract

The morphology, structure and properties of Polyethylene terephthalate (PET)/Carbon Nanotube (CNT) conductive electrospun non-woven mat were studied in this paper. Nanocomposite fibers were obtained through electrospinning of PET solutions in trifluoroacetic acid (TFA)/dichloromethane (DCM) with equal volume ratio (1:1) containing different concentrations and types of CNTs. Electrospun nanofiber mats were produced using both static and rotating drum collector. Electrical conductivity measurements on nanocomposite mats showed an electrical percolation threshold around 2 wt% MWCNT. The morphological analysis results showed smoother nanofibers with less bead structures development when using a rotating drum collector especially at high concentrations of CNTs. Moreover, aligned CNT nanocomposite nanofibers depicted larger diameters compared to the nanofibers produced in a static collection mode. From crystallographic measurements, a higher degree of crystallinity was observed with

* Corresponding Author
Tel: +1 (514) – 340 4711 ext. 4893
Fax: +1 (514) – 340 4159
E-mail address: charles.dubois@polymtl.ca

increasing CNT concentrations up to levels above those needed for electrical percolation. Both Fourier transform infra-red (FTIR) and Raman spectroscopy techniques showed similar behaviors of PET chains and CNT orientation in the aligned nanocomposite nanofibers. Both PET and CNT orientation increased along with the alignment of the nanofibers for materials where the nanotube concentration was below the electrical percolation threshold, while the orientation factor was reduced for aligned nanofibers with higher content in CNT. A similar effect of the CNT concentration was observed for the mechanical properties. Considerable enhancement in mechanical properties, especially tensile modulus, was found in aligned nanofibers; at least six times higher than the modulus of random nanofibers at concentrations below percolation; while the effect of alignment was less important above percolation and at high concentrations of CNTs.

6.2. Introduction

The electrospraying process was discovered by Formhal 1934 and since then, this process has received a great deal of interest due to its apparent simplicity [1]. Electrospinning is the most practical technique to produce nanofibers. Until 1993, the electrospinning technology was often referred to as an electrostatic spraying process and only a few publications employing this technique can be found prior to that year [2]. Reneker and Chun revisited this technology in the 1990s and they showed the possibility of employing it for producing fibers from several types of polymer solutions [3]. More recently, various types of nanoparticles were dispersed in the polymer solutions and thus, were embedded in the nanofibers through this process as a means of modifying their final properties. Among them, carbon nanotubes (CNT) have attracted a great attention. In fact, rapidly after CNT development [4], this nanoparticle has been widely used to enhance electrical or mechanical properties of electrospun polymer fibers to various extents [5-8]. An increase in the amount of CNT enhances the conductivity of the

polymer solution and produces a larger electrical current during electrospinning. The addition of charge accumulation overcomes cohesive forces and intensifies repulsive forces among the charges accumulated inside nanofibers and fibers of smaller diameter are formed [6].

Other studies investigated the structures, properties and applications of PET electrospun nanofibers with and without CNT [9-24]. Considering the unique properties of PET, various applications of PET nanofibers have been developed [9-11, 13, 15, 16, 18-23]. These include filtration [9, 16, 19, 20], phase change materials (PCM) [10, 13], charge storage [11], and biomedical applications [15, 18, 21, 22]. However, very few studies addressed with a satisfactorily level of details the structure and properties of PET nanofibers produced by solution electrospinning. The earliest of them was performed by Kim and his colleagues who investigated the electrospinning of PET with an emphasis of the effect of molecular weight and linear velocity of the collecting drum surface [24]. They used X-ray diffraction (XRD) to assess the effect of drum velocity on nanofibers orientation and the resulting crystallinity [24]. McKee *et al.* studied the correlation between solution rheology and final fiber morphologies of branched and linear polyester electrospun nanofibers [23]. They found that the concentration required for bead-free nanofiber production is two times more than c^* (the concentration required for chain entanglement initiation). The effect of chain entanglements on viscosity was also studied and a correlation of the electrospun morphology (polymer droplets, beaded structure or nanofibers) to zero shear rate viscosity was developed [23]. In one of the most recent studies available on PET nanofiber from solution electrospinning, Veleirinho and his colleagues evaluated the effect of initial solution concentration and solvent type on final properties of PET electrospun nanofibers [14]. They showed that at least 10 wt% of PET in initial solution is required to prepare nanofibers, while higher concentration favors beadless structure nanofibers [14]. They also showed that TFA/DCM volume ratio could be an important determining factor on the final morphology and properties of nanofibers [14]. In one of the earliest works available, polybutylene terephthalate (PBT), a polyester similar to PET, was used in electrospinning combined with MWCNT [25]. A suspension

of 5% MWCNT dispersed in a solution of PBT/hexafluoro isopropanol (HIFP) was used for electrospinning and improvements in thermal stability and mechanical modulus were observed [25]. Additional recent studies on structure and properties of PET/CNT nanocomposite nanofibers were also found in literature [26, 27]. In 2008, Ahn *et al.* investigated the properties of PET/MWCNT nanocomposite nanofibers for the first time [26]. They improved the dispersion of 3% w/w or less MWCNT suspensions by an acid treatment on the nanotubes to increase the amount of chemical groups at their surface. Morphology, physical and mechanical properties of the resulting nanofibers were studied; however, the electrical conductivity did not improve significantly [26]. In the most recent work available on PET/MWCNT nanocomposite nanofibers, the molecular conformation structure and chain orientation of PET in nanocomposite nanofibers after electrospinning has been studied by Chen and his coworkers [27]. They investigated the effect of MWCNT addition on PET chain confinement at different concentrations, up to 2 wt% MWCNT, by differential scanning calorimetery (DSC) and FTIR techniques. They mainly studied the crystallinity and morphology after electrospinning PET with and without MWCNT [27]. However, they did not report any data about the final electrical and mechanical properties of their nanocomposite electrospun nanofibers.

In the present study, PET solutions containing different types and concentrations of carbon nanotubes (single-wall, double-wall and multi-wall) are electrospun to produce nanocomposite fibers. The effect of CNT addition on fiber morphology is studied both quantitatively and qualitatively. We mainly focus on final nanofibers and mats characteristics at a wide range of MWCNT concentrations, and especially at high concentrations of different types of CNTs. Moreover, aligned nanofibers are produced by using a rotating drum. DSC, FTIR and Raman spectroscopy are used to characterize the properties of nanocomposite nanofibers obtained with a static collection mode compared with those obtained from a rotating receptor. In addition, electrical conductivity and mechanical properties of the resulting electrospun mats at different CNT contents and types are obtained. PET is an important polymer in fiber and textile industry, and PET/CNT nanofibers have found some points of interests in recent few works available

in this field. However, such extensive characterization of PET/CNT composites nanofibers produced for large variety of CNT concentrations and types and under several processing conditions is, to the best of our knowledge, reported for the first time.

6.3. Experiments

6.3.1. Polymer solution preparation and electrospinning process

The polymer used in this work was a polyethylene terephthalate with IV=1 (Selar 7086, DuPont Co.) with Mw≈55000, dissolved at 10% w/w concentration in an equal volume mixture of trifluoroacetic acid (TFA) and dichloromethane (DCM); both solvents were purchased from Aldrich Co. Carbon nanotubes employed in this work were produced by a chemical vapor deposition process (CVD) and purchased from Helix Co., USA. Single wall carbon nanotubes (SWCNT) and double wall carbon nanotubes (DWCNT) with purities of 90% and multi wall carbon nanotubes (MWCNT) with purity of 95% were obtained. The nominal diameter range of SWCNT, DWCNT and MWCNT were respectively of 1.3 nm, 4 nm and 10-100 nm. All three types of CNT had lengths in the range of 0.5-40 μm. CNTs at different concentrations were dispersed mechanically in the polymer solution by a 2-hours sonication treatment at room temperature in pure TFA solvent followed by continuous mechanical mixing (by a stirrer in a container). The mixture was sonicated an additional two hours after addition of PET and DCM and complete dissolution of PET by continuous stirring. Final solutions were stirred continuously before electrospinning. No surface modification technique was employed in order to prevent its detrimental effect on the electrical conductivity of the CNTs.

6.3.2. Electrospinning process

The electrospinning set-up employed in this work consisted in a high voltage power supply (Gamma Inc.), a syringe pump to deliver the solution at specific flow rates (PHD 4400, Harvard Apparatus), a syringe connected to a stainless steel needle (22 gauge,

Popper & Sons Inc.), and finally a stainless steel collecting drum (15 cm diameter). Fiber mats were collected in both static and rotating drum conditions (to obtain aligned nanofiber by rotating drum). An average electrical potential difference of 10 kV was used on all types of materials. The voltage was imposed on the needle, positioned at a 15 cm distance from the collector and a volumetric flow rate of 0.5 mL/hr was applied. All experiments were conducted at ambient pressure, temperature and average relative humidity of 20%. A summary of the different carbon nanotube concentrations and types studied here and the resulting fibers diameter and morphology is given in Table 6-1. In the case of aligned fiber production, we used a rotating drum (of 150 mm in diameter) speed of 600 rpm and the same electrospinning parameters as mentioned previously.

6.3.3. Morphological analysis and evaluation of CNTs

Two techniques of high-resolution scanning electron microscopy (HR-SEM) and transmission electron microscopy (TEM) were used to study final nanofibers morphologies and surface structure (by HR-SEM) and CNT localization in fibers (by TEM). A Hitachi S-4700 scanning electron microscopy (SEM) was used on platinum coated samples to characterize the final morphologies and surface structures of fibers at different processing conditions and CNT concentrations. Moreover, an optical microscope, Dialux 20 (Leitz,WETZLAR), was employed to assess the dispersion condition and position of CNTs inside fibers.

6.3.4. Crystalline characteristics (DSC and XRD)

Differential scanning calorimetry (DSC, Q1000; TA Instruments) and X-ray diffraction (XRD, Discover, D8, Bruker) were used to study the crystalline behavior of PET/CNT nanocomposite nanofibers. The effect of CNT addition on crystalline structure and behavior of nanofibers was first investigated by DSC. The tests were performed in non-isothermal condition and included a heating/cooling/heating cycle with the rate of 10

°C/min. XRD technique was used besides DSC to characterize the crystalline structure of the system.

Table 6-1: Summary of the produced nanocomposite nanofibers and their resulting characteristics at 10 % w/v concentration of PET

CNT Type and Concentration	Collecting Method	Resulting Morphology	Average Fiber Diameter (nm)
-	Static Drum	Random smooth beadless fibers	1008 ± 137
-	Rotating Drum	Aligned smooth beadless fibers	827 ± 195
1% MWCNT	Static Drum	Random smooth beadless fibers	495 ± 74
1% MWCNT	Rotating Drum	Partially aligned smooth beadless fibers	966 ± 228
2% MWCNT	Static Drum	Random smooth beadless fibers	-
3% MWCNT	Static Drum	Random fibers ; Including small beads	481 ± 78
3% MWCNT	Rotating Drum	Partially aligned smooth beadless fibers	591± 152
4% MWCNT	Static Drum	Random fibers ; Including large beads	-
5% MWCNT	Static Drum	Random fibers ; Including large beads	388 ± 84
5% MWCNT	Rotating Drum	Partially aligned smooth beadless fibers	447 ± 135
1% SWCNT	Static Drum	Random smooth beadless fibers	497 ± 100
5% SWCNT	Static Drum	Random fibers ; Including large beads	445 ± 137
1% DWCNT	Static Drum	Random fibers ; Including small beads	550 ± 137
5% DWCNT	Static Drum	Random fibers ; Including large beads	463 ± 98

In XRD tests, we used an X-Ray goniometer accompanied with a Hi-STAR two-dimensional area detector. The generator voltage and current were 40 kV and 40 mA respectively and the copper Cu Kα radiation (λ = 1.542 Å) was selected by a graphite crystal monochromator. The fibers obtained were examined using wide angle x-ray diffraction (WAXD) method.

6.3.5. Orientation measurements (Raman & FT-IR spectroscopy)

Raman and Fourier transform infrared (FT-IR) spectroscopy techniques were used for CNT and PET/CNT nanofibers orientation measurements. A Nicolet Magna 860 FTIR instrument from Thermo Electron Corp. (DTGS detector, resolution 4 cm^{-1}, accumulation of 128 scans) was employed for a quantitative evaluation of orientation of PET chains in nanofibers at different MWCNT concentrations. Raman was used as the most specific method for CNT quantitative orientation measurements. Raman spectra were recorded on a Renishaw spectrometer equipped with an inVia Raman microscope. The samples were tested using a NIR laser (785 nm) with a grating of 1200 g/mm in a regular mode and use of 50x, short working distance (SWD) microscope. Orientation of MWCNTs was obtained by comparing the spectra in directions parallel and perpendicular to the laser beam in aligned nanofibers.

6.3.6. Electrical conductivity

Electrical conductivity of final non-woven electrospun mats was measured using various instruments. In the case of high resistance materials, a KEITLEY 6517, high resistance meter was used and in the conductive range a combined set-up of KEITHLEY 6620 as a current source and Agilent 34401 A (6 ½ Digit Multimeter) as voltage source were used.

6.3.7. Mechanical properties

The mechanical properties of electrospun non-woven mats produced with different CNT types and concentrations were obtained employing a micro-tester 5548 (Instron Inc.). The tensile test was performed using a 5 N load cell and a speed of 10 mm/min on non-woven mats of various thicknesses from 20 μm to 150 μm; while the average thickness was almost constant for all types of samples.

6.4. Results and Discussions

6.4.1. Morphological analysis and dispersion evaluation

Morphological study of electrospun fibers at different conditions (various CNT types and concentrations) was performed at the first step. PET/CNT nanocomposite fibers at different MWCNT concentrations were produced in a first step and collected as randomly shaped nanofibers on a static drum (Fig. 6-1 & Table 6-1). The results show that all the fibers have almost the same normal distribution of diameters with a narrow range of variation in diameter (Table 6-1). The average fiber diameter of pure electrospun fibers (~1μm) is greatly reduced by adding only 1 wt% MWCNT (Fig. 6-1b). This is attributed to the increase in the conductivity of the solution upon addition of MWCNT [6]. Addition of MWCNT in modified dispersion condition in the initial solution causes a large decrease in average fiber diameter even at 1% MWCNT. The results show that the average fiber diameter decreases gradually to a final diameter of about 400 nm at 5% MWCNT concentration (Table 6-1); this reduction is interpreted as due to the increase in the conductivity of electrospinning solution. Below 3 wt% MWCNT, smooth and beadless fiber structures are obtained. At 3 wt% MWCNT small beads start to develop in spite of the fact that there is still a reduction in final fiber diameter (Fig. 6-1d). The small beads at 3% MWCNT become larger at the higher MWCNT concentration of 4 and 5

wt% (Fig. 6-1e and 6-1f). The bead structures formed along fiber axis will be studied in more detailed using TEM and optical microscopy techniques.

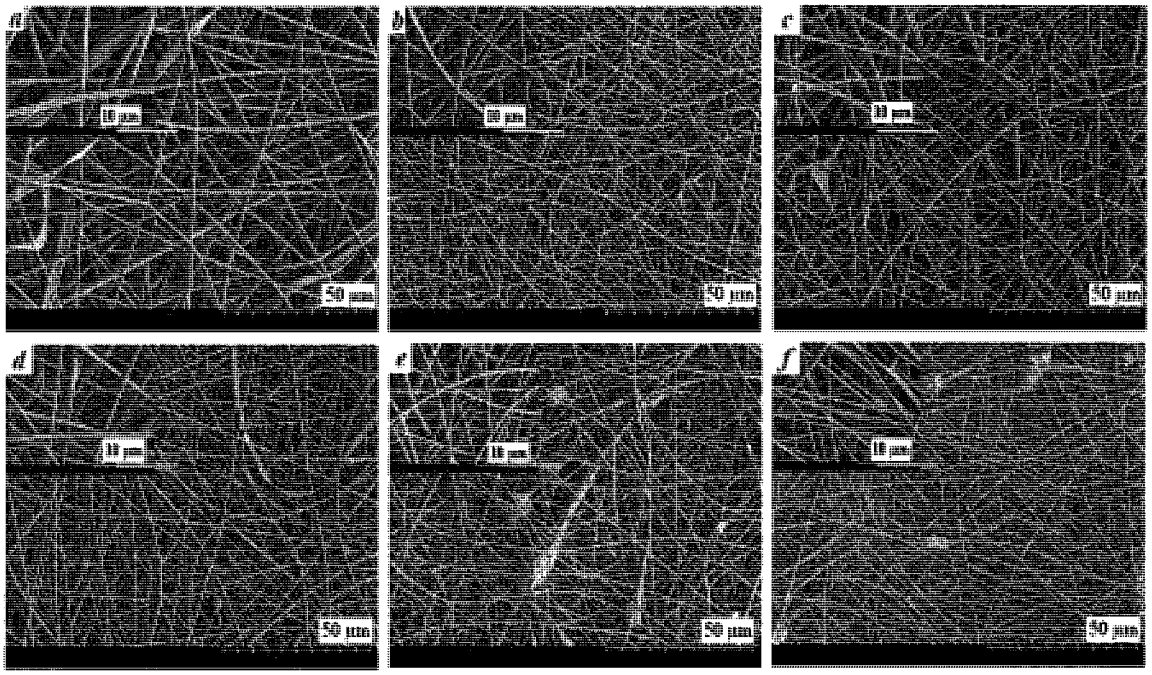

Figure 6-1: SEM photos of PET (10%) / MWCNT at different CNT concentrations. a) Pure PET; b) 1% MWCNT; c) 2% MWCNT; d) 3% MWCNT; e) 4% MWCNT; f) 5% MWCNT.

The effect of two other types of CNTs (SWCNT, DWCNT) at low (1 wt%) and high (5 wt%) concentrations were also studied and compared to the MWCNT. The resulting morphology of the nanocomposite electrospun samples is given in Fig. 6-2.

A Similar nanofiber structure is obtained for all types of CNTs including almost the same range of fiber diameter. Some bead structures develop and the fibers are less smooth at 1 wt% DWCNT (Fig. 6-2b) compared to the other types of CNTs. Moreover, the average final fiber diameter also increased at 1% DWCNT (Table 6-1). At 5% CNT, the same range of fiber diameter is obtained for all types of CNTs (Table 6-1). Moreover, they all include bead structure formation along fiber axis (Fig. 6-2d, 6-2e and 6-2f). All these beads formed along fiber axis showed a rough surface structure. The morphology of

the bead structures formed along fiber axis at high CNT concentration is reported in Fig. 6-3 using optical microscopy (Fig. 6-3a) and high resolution SEM (Fig. 6-3b).

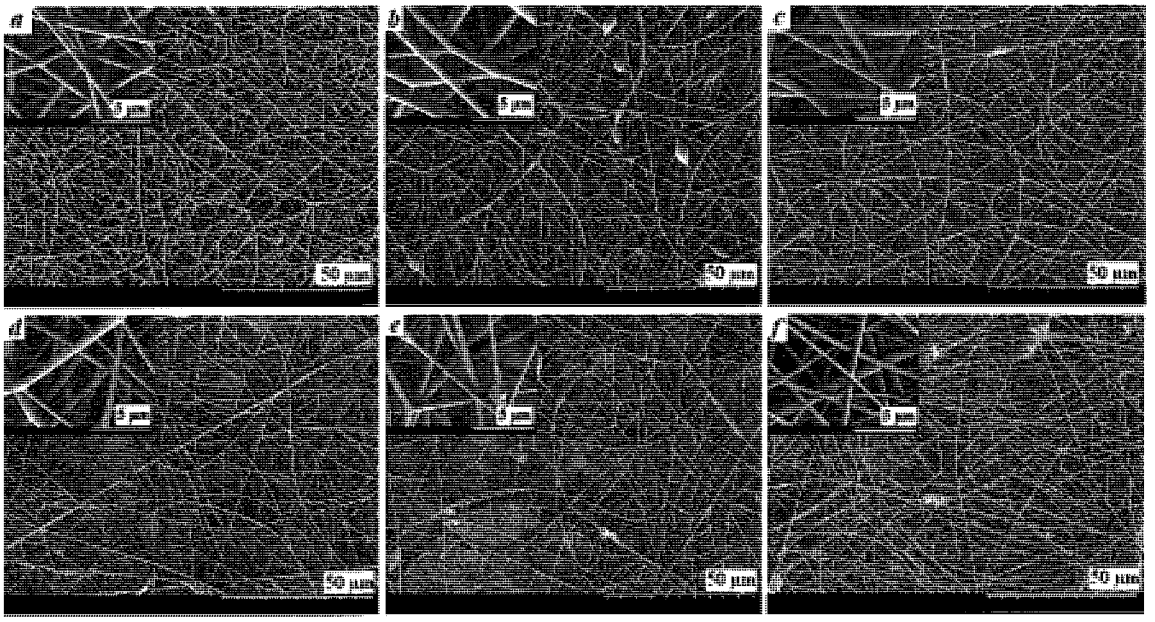

Figure 6-2: SEM photos of PET (10%) electrospun fiber containing a) 1% SWCNT; b) 1% DWCNT; c) 1% MWCNT; d) 5% SWCNT; e) 5% DWCNT; f) 5% MWCNT.

At high concentrations of carbon nanotubes (above 3 wt%), large aggregates are observed along fiber axis and especially at bead positions (Fig. 6-3a). HR-SEM (high resolution SEM) image of the beads and beads surface (Fig. 6-3b) shows the CNT position at bead surface. Therefore, there are aggregates both inside the beads and at bead surfaces of the nanocomposite nanofibers [28].

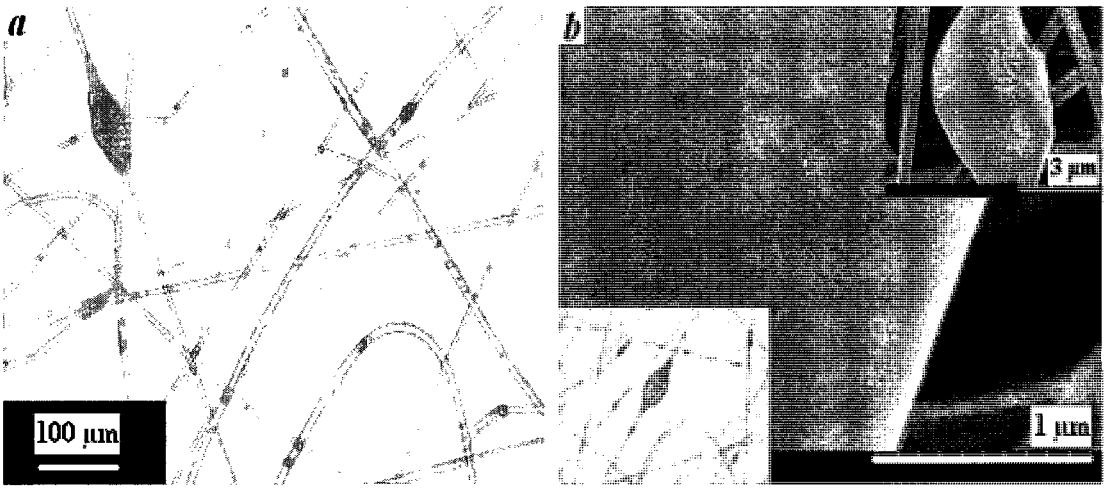

Figure 6-3: CNT localization inside fibers and at fibers surface; PET(10%)/MWCNT(3%); a) Optical microscopy; b) SEM.

Surface structure of the beads along fiber axis at 5% SWCNT and 5% DWCNT was also investigated using HR-SEM technique (Fig. 6-4). As it is shown, aggregates of carbon nanotubes at bead positions and close to the surfaces of the bead structures brings more roughness to the surface of the fibers at bead positions compared to other locations along fiber axis. The roughness at bead positions is probably due to aggregated CNTs close to the surface of the fibers; while the orientation and alignment of carbon nanotubes along fiber axis reduces the aggregates formation. Therefore, aggregate formation at high concentrations of carbon nanotubes changes both fibers morphologies (increasing bead formations, Fig. 6-3) and final surface topologies (increasing roughness, Fig. 6-4) of nanocomposite fibers.

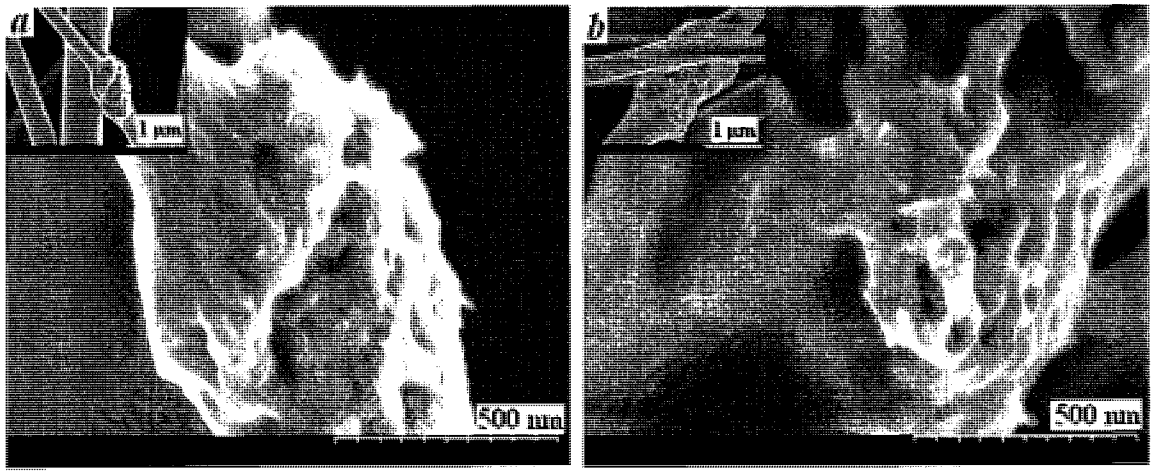

Figure 6-4: HR-SEM photos of surface topology of bead structures at high CNT concentrations. a) PET(10%)/SWCNT(5%); PET(10%)/DWCNT(5%).

TEM method was used to study the relative position of CNTs inside the nanocomposite nanofibers (Fig. 6-5). TEM images of fibers along fiber axis (Fig. 6-5a) and at fiber cross section (Fig. 6-5b) show formation of carbon nanotube small aggregates during fiber formation which confirm the observations mentioned above. In addition, it is possible to detect single oriented carbon nanotube along fiber axis (Fig. 6-5c) after electrospinning.

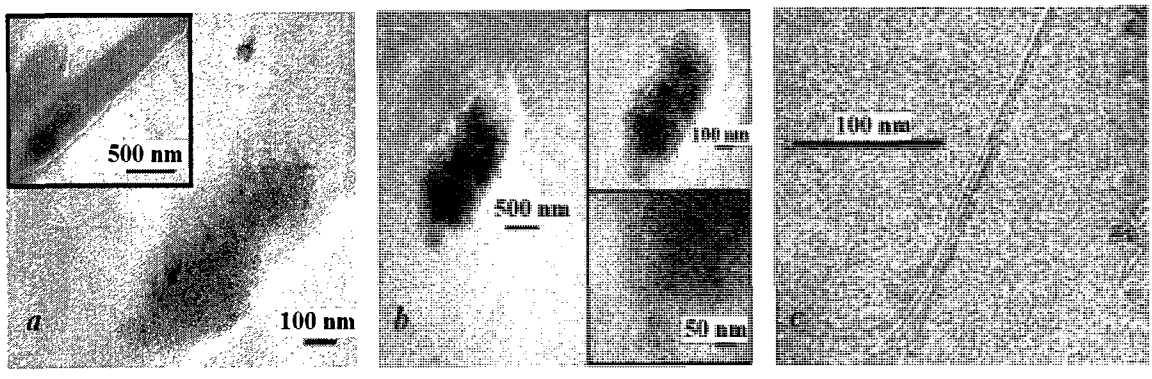

Figure 6-5: TEM photos of CNT localization in PET/MWCNT(3%) electrospun fibers; a) CNT aggregates along fiber axis; a) CNT aggregates across fiber; c) Single CNT along fiber axis.

We used the same processing condition mentioned previously along with a rotating drum to obtain aligned nanofibers and to compare the results with nanofibers collected on static drum. The SEM pictures show that it is possible to obtain an oriented fiber structure in pure PET electrospun fibers (Fig. 6-6a) and partially aligned nanofibers after adding MWCNT (Fig. 6-6b, 6-6c and 6-6d).

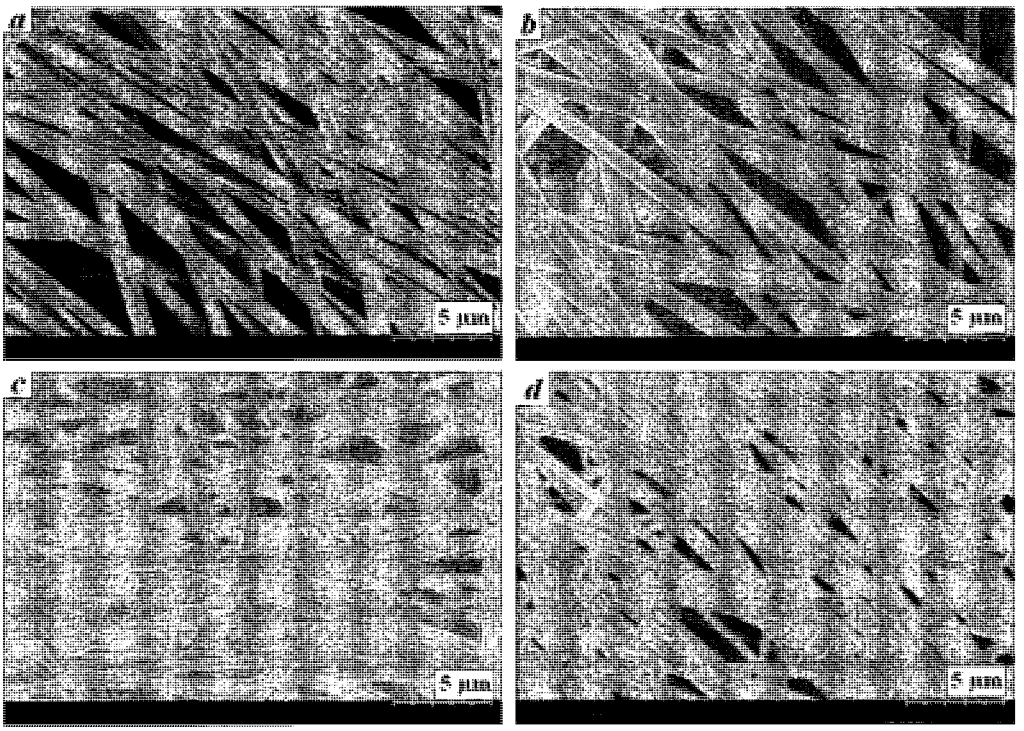

Figure 6-6: SEM photos of aligned PET (10%) / MWCNT at different CNT concentrations. a) Pure PET; b) 1% MWCNT; c) 3% MWCNT; d) 5% MWCNT.

All electrospun samples were quite well aligned macroscopically; however, using SEM observations, it was found that pure PET electrospun nanofibers were more aligned, which is in agreement with the reduction in average fiber diameter of aligned PET nanofibers to about 800 nm (Table 6-1). This reduction in fiber diameter has also been previously reported by Fenessey and Farris [29]. As opposed to what could be expected in light of previously reported data on aligned nanofibers [30], the average fiber diameter is increased by adding carbon nanotubes in aligned nanocomposite nanofibers (see Table

6-1). The increase in average fiber diameter is maximum at 1 wt% MWCNT; however, this effect is also observed at 3% and 5% MWCNT, but to a lesser extent. In addition, the aligned nanocomposite nanofibers present a wider diameter distribution. The result of observation in aligned nanocomposite nanofibers show that there are less large beads along fiber axis after aligned fiber manufacturing compared to random nanofibers of equal amount of CNT concentration. Nanocomposite nanofibers include less bead structure and the sizes of beads are also decreased in aligned nanocomposite nanofibers (these results have not been reported here). We believe that at high concentrations of carbon nanotubes, the electrical forces are more imposed on carbon nanotubes rather that polymer matrix; therefore, more smooth fibers with larger diameters are obtained [6]. The effect of CNT on orientation and after alignment will be discussed in more detailed in the next sections of this paper.

6.4.2. Crystalline characteristics (DSC and XRD)

Final crystalline structure of nanocomposite electrospun fibers and the role of CNT addition are important parameters in controlling the final properties. The effect of CNT addition on PET/CNT electrospun nanocomposite nanofibers was studied in a first step by the DSC technique and then by X-Ray diffraction.

6.4.2.1. DSC Results

The values of ΔH used in different calculations and for DSC analysis reported here have been corrected for nanoparticles content by the following equation to have the data purely related to polymer weight:

$$\Delta H_{i,corrected} = \Delta H_{i,Expriment} / (1 - w_{CNT}) \qquad (6\text{-}1)$$

Then, the degree of crystallinity was calculated by the following equation [31]:

$$X_c = (\Delta H_f - \Delta H_{rc}) / \Delta H_f^0 \qquad (6\text{-}2)$$

where ΔH_f is the enthalpy of fusion, ΔH_{rc} is the enthalpy of re-crystallization occurring during heating cycle and ΔH_f^0 is the enthalpy of fusion of perfectly crystalline structure of PET at equilibrium thermodynamic melt temperature T_m^0 and was taken as 140 J/g [32].

Thermal parameters and the data obtained after a heating/cooling/heating cycle for each sample are given in Table 6-2. The results show first a decrease then an increase in crystallinity as a function of CNT content. MWCNT content below 2 wt% causes a decrease in crystallinity as reported elsewhere [27]. Accordingly, similar trend is also observed for the glass transition temperature T_g. At MWCNT content of 3% or more, an increase in crystallinity and T_g is observed. At 5 wt% MWCNT concentration, maximum crystallinity is obtained. It will be shown thereafter (electrical conductivity) that 2 wt% MWCNT is the critical amount of MWCNT for network formation and electrical percolation threshold; therefore, a change in the trend of crystallinity vs. MWCNT concentration is also observed at 2 wt% MWCNT. Crystallinity is controlled by two factors: nucleation and growth. Addition of CNT increases the nucleation [33]; however, it decreases the rate of growth, and the chains are more inclined to be oriented rather than entering the crystalline cells [27]. Addition of CNT and nucleation accelerates the nucleation and the crystallinity starts earlier; therefore, there is not enough time for the polymer chains to enter the crystalline cells and the overall crystallinity is reduced. Above 2 wt%, the rate of nucleation and crystalline initiation is considerably increased and, as a result, the overall crystallinity is increased by rapid nucleation. The data shown at 1 wt% and 5 wt% SWCNT and DWCNT exhibit the same trend as obtained for MWCNT (Table 6-2). T_g is higher in SWCNT and DWCNT which might be because of the smaller size of SWCNT and DWCNT. The small size of SWCNT and DWCNT causes more interactions of CNT particles with polymer chain. As a result, the overall motion of PET chains is restricted when the sizes of nanoparticles are reduced and an increase in T_g is observed.

The differences in ΔH for the first heating cycle (after electrospinning) and the second heating cycle (from the cooled melt) is a valuable parameter to be studied and is

reported in Table 6-2. The higher value of ΔH obtained after electrospinning is due to the effect of oriented chains in electrospun nanofibers [31]. Oriented chains produced after electrospinning make it easier for crystallization. The oriented chains enter the crystalline cells during cold crystallization and it increases the difference between the ΔH of these two cycles. The higher the oriented chains out of crystalline cells after electrospinning, the higher will be this difference. The confined oriented chain structure below 2 wt% CNT has been reported before [27].

Table 6-2: Thermal parameters of nanocomposite nanofiber mats at different CNT concentrations and types

	T_g (°C)	Crystalline content of electrospun nanofibers (%)	$\Delta H_{first\text{-}heating}$ (J/g)	$\Delta H_{second\text{-}heating}$ (J/g)
Pure PET	76.7	15.6	42.6	41.1
PET/1% MWCNT	75.4	14.3	39.7	38.6
PET/2% MWCNT	75.5	9.4	38.7	38.3
PET/3% MWCNT	76.3	13.6	35.7	33.9
PET/4% MWCNT	77.8	14.4	35.6	33.6
PET/5% MWCNT	79.0	15.1	35.7	33.9
PET/1% SWCNT	81.6	13.2	33.0	28.3
PET/5% SWCNT	81.9	14.1	30.6	28.5
PET/1% DWCNT	79.9	10.8	33.1	30.6
PET/5% DWCNT	81.2	13.0	35.5	29.6

The effect of aligned fiber structure on crystalline behavior is given in Table 6-3. The trend in change of crystallinity is different from that of randomly collected nanofibers. In aligned nanofibers, the crystallinity is less than that for random ones for almost all CNT concentrations. Addition of MWCNT causes gradual increase in the amount of crystallinity. In the case of aligned nanofibers, chain alignment is increased and therefore, the chains are more inclined to be oriented rather than entering crystalline

cells. That is the main reason for the change in ΔH in the first and second heating cycles as mentioned previously. A more precise study of the CNT and PET chain orientations will be discussed in more detailed in the FTIR part.

Table 6-3: Thermal parameters of aligned nanofiber mats at different MWCNT concentrations

	T_g (°C)	Crystalline content of electrospun nanofibers (%)	$\Delta H_{first\text{-}heating}$ (J/g)	$\Delta H_{second\text{-}heating}$ (J/g)
Aligned **Pure PET**	74	11.9	36.4	31.3
Aligned **PET/1% MWCNT**	76.5	13.7	34.8	29.4
Aligned **PET/3% MWCNT**	76.8	14.1	34.3	28.7
Aligned **PET/5% MWCNT**	75.0	14.2	32.6	28.7

6.4.2.2. X-Ray Diffraction Characteristics

XRD diffraction results of electrospun mats at different CNT concentration and type showed an almost amorphous behavior for PET/CNT electrospun nanofibers (Fig. 6-7a and 6-7b). This is in agreement with DSC results, since the crystalline content of nanocomposite electrospun fibers is low and therefore it is not possible to be detected in XRD. However, at 5 wt% MWCNT concentration, a weak crystalline pattern is observed (Fig. 6-7c). This halo observed for 5 wt% MWCNT electrospun fiber is due to the peak positioned at $2\theta=18^{\circ}$ of PET [34]. This shows that at 5 wt%, a crystalline structure begin to form in contrast with other concentrations and CNT types.

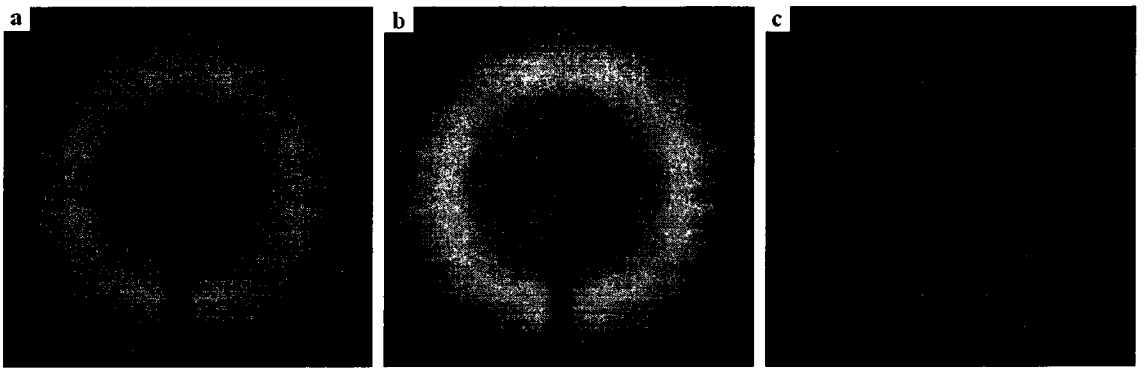

Figure 6-7: XRD pattern of PET/MWCNT electrospun nanofiber mat at different CNT concentrations; a) Pure PET; b) PET/3% MWCNT; c) PET/5% MWCNT.

6.4.3. Orientation detection (FT-IR & Raman spectroscopy)

For a better understanding of the polymer chains and CNT orientations, we used also FTIR and Raman spectroscopy techniques. We investigated samples at different CNT concentrations, types and alignment condition to compare the effect of each of these parameters.

6.4.3.1. FT-IR spectroscopy

Herman orientation equations are used for evaluation of the orientation function. For a uniaxially oriented sample, the dichroic ratio D is defined as:

$$D = \frac{A_{\parallel}}{A_{\perp}} \qquad (6\text{-}3)$$

where A is the absorbance of a specific band parallel or perpendicular to IR polarizer [35]. Then, the Herman orientation function is obtained according to [36, 37]:

$$f = \frac{D-1}{D+2} \cdot \frac{2}{3\cos^2\alpha - 1} \qquad (6\text{-}4)$$

where α is the angle between dipole moment of a particular vibration and chain axis. Based on the vibration selected in IR test, it is possible to use Herman orientation function for the calculation of amorphous or crystalline phase orientations. Here, FTIR

measurements were used to assess the effect of CNT concentration and types, as well as the degree of alignment of the nanofiber structures on chain orientation [38]. There are some effective characteristic peaks related to PET in FTIR. The most important ones are: 973 cm^{-1}: CH_2 vibration of trans conformation with α=32°; 1340 cm^{-1}: CH_2 wagging mode of glycol segment in trans conformation with α=21°; 1370 cm^{-1}: the vibration related to gauche conformation; and 1020 cm^{-1}: absorption band attributed to in-plane vibration of C-H group of benzene with α=20° [35, 39].

In a first step, the ratio of trans to gauche conformers (A_{1340}/A_{1370}) was assessed as a parameter to study the effect of CNT concentration and type on PET chains conformation compared to pure PET electrospun nanofibers [27]. Addition of CNT increased the A_{1340}/A_{1370} ratio because of an increase in trans conformation and decrease in gauche structure (Table 6-4). Addition of CNT causes more trans conformation formation, since nanocomposite nanofiber diameter is significantly decreased even by adding 1 wt% of each type of CNT. Fine nanocomposite nanofibers obtained after CNT addition are the main reason for PET chains orientation, due to the larger draw ratio. The increase in trans conformation content, which is detected here in FTIR test results, might be partially because of the simultaneous increase in crystalline structure formation as obtained from DSC results. This is the case in high MWCNT concentration in which the crystalline content increases; while at lower concentration of MWCNT, chain orientation is the main controlling factor as reported previously [27]. The trans to gauche conformation ratio in SWCNT and DWCNT at two concentrations was measured and almost the same results are obtained (Table 6-4). We believe that, since the final nanocomposite nanofibers include the same range of both crystallinity and diameter, it is expected that they show an almost similar trend in the amount of orientation in random nanofibers.

Table 6-4: Relative FTIR absorbance of trans (1340 cm^{-1}) to gauche (1370 cm^{-1}) conformation (ratio of A_{1340}/A_{1370}) at different CNT concentrations and types of random non-woven mat.

	0%	1 %	2%	3%	4%	5 %
MWCNT	0.41	0.54	0.66	0.57	0.65	0.63
SWCNT	0.41	0.59	-	-	-	0.57
DWCNT	0.41	0.59	-	-	-	0.58

The effect of nanofibers alignment on final physical and mechanical properties compared to random nanofibers was studied here. For that purposes, samples were prepared and cut out of the mat according to Fig 6-8.

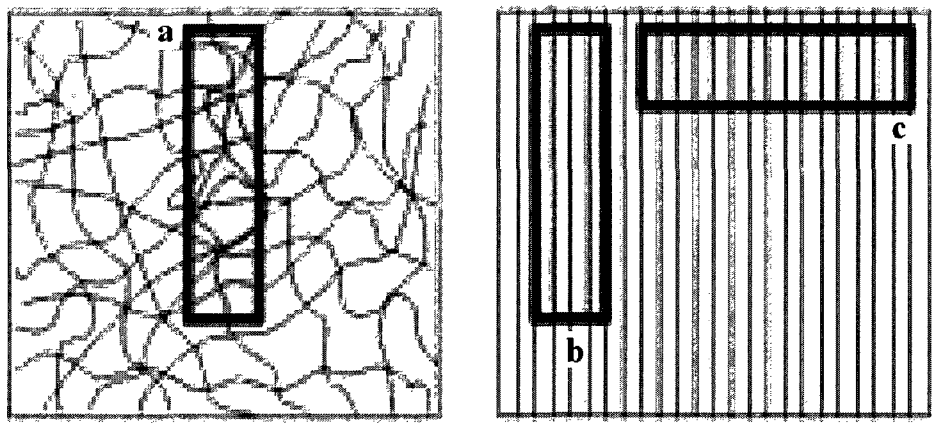

Figure 6-8: Schematic of different samples prepared and used in different experiments; a) Random nanofibers; b) Parallel to aligned nanofibers axis (0°); Perpendicular to aligned nanofiber axis (90°).

A comparison of the values of (A_{1340}/A_{1370}) in randomly oriented nanofibers with those aligned and in parallel to the light (0^{o}) depicts an increase in the amount of trans conformation especially in pure PET nanofibers in aligned nanofibers in spite of lower crystalline density (Table 6-3). The results prove that the maximum difference is obtained at 0% and 1% MWCNT concentration, where they are less crystalline. This could come as a proof for higher amount of PET chains orientation at these concentrations. Quite unexpectedly, at 5 wt% MWCNT, the amount of trans to gauche conformation (A_{1340}/A_{1370}) is even more in randomly oriented nanofibers compared to aligned nanofibers in spite of the fact that the SEM results (Fig. 6-6d) show aligned nanofiber structure formation at 5 wt% MWCNT. Randomly oriented nanofibers containing 5wt% MWCNT have the most amount of crystalline phase and the smallest fiber diameter; therefore, as expected the highest amount of trans conformation mostly because of the higher crystalline content not because of more orientation of the chains. Herman orientation function (f_{1340}) measured for aligned nanofibers shows the same behavior (Fig. 6-9). Since the FTIR experiment is performed over final non-woven mat, it does not cause to obtain as high value of orientation of single nanofibers as expected; therefore, the value of orientation is quite low. Orientation function is reported here only to compare the amount of orientation amongst different aligned nanofibers containing different CNT concentrations. f_{1340} has maximum values at 0% and 1% MWCNT which includes maximum PET chains alignment and orientation compared to the others as reported previously in morphological study.

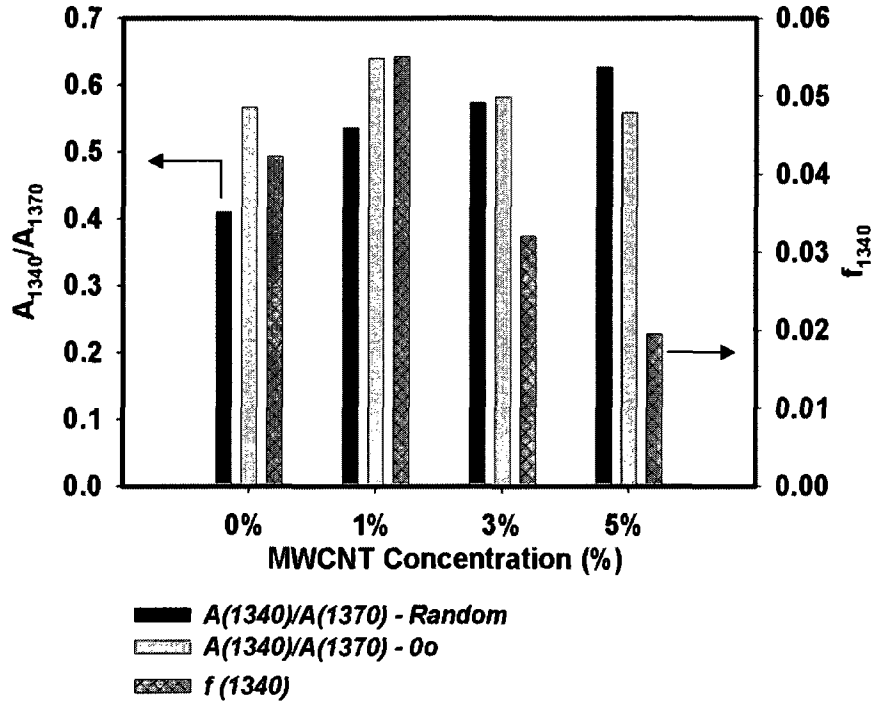

Figure 6-9: Different FTIR characteristic parameters vs. MWCNT concentrations in PET/MWCNT electrospun fibers.

6.4.3.2. Raman spectroscopy

Raman spectra of non-woven mats obtained for different types of carbon nanotubes/PET nanofibers are reported in Fig. 6-10 compared to pure PET electrospun non-woven mat. Among the characteristic peaks of multi-wall carbon nanotubes detected by Raman spectroscopy, three peaks could be distinguished. Two strong peaks are located at 1580 cm^{-1} (G), and 1350 cm^{-1} (D) and a weak peak is detected at around 2700 cm^{-1} (G`) [40, 41]. D/G ratio and different peak positions of these CNTs are different based on various types of CNTs (Fig. 6-10).

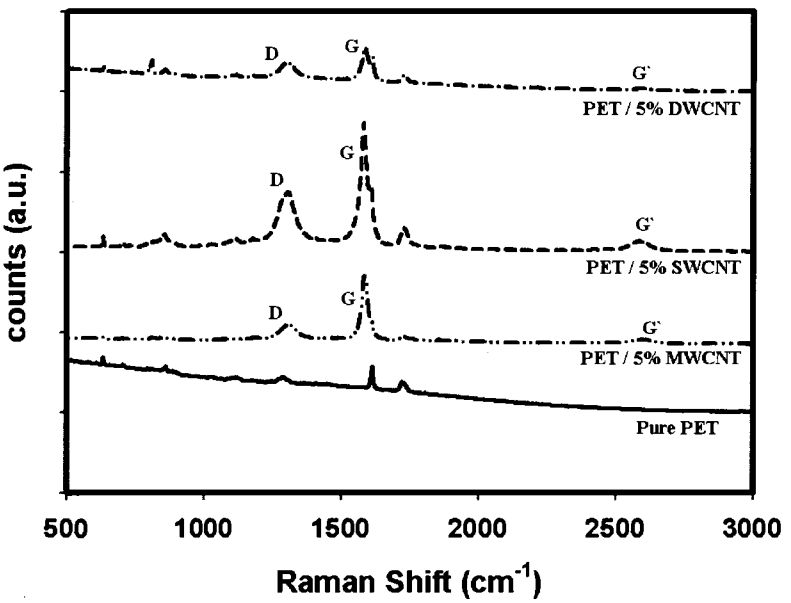

Figure 6-10: Raman spectra of final non-woven mat containing different types of carbon nanotubes

In addition, we used the Raman spectroscopy technique for evaluating CNT orientation in aligned MWCNT/PET nanocomposite nanofibers (Fig. 6-11 & Fig. 6-12). As it is depicted, the spectrum reports quite different intensities in parallel and perpendicular directions (Fig. 6-11). The high intensities of CNT characteristic peaks found in aligned samples parallel to the beam direction proves a high degree of alignment of MWCNT along the nanofiber axis. The results also prove that at 1 wt% MWCNT, quite well aligned CNTs exist inside nanofibers (Fig. 6-11) and the beam intensity is significantly high in the direction parallel to the beam as compared to the perpendicular direction. At a concentration of 5 wt% in MWCNT, there is almost no effect of aligned fiber production on CNT orientation (Fig. 6-12).

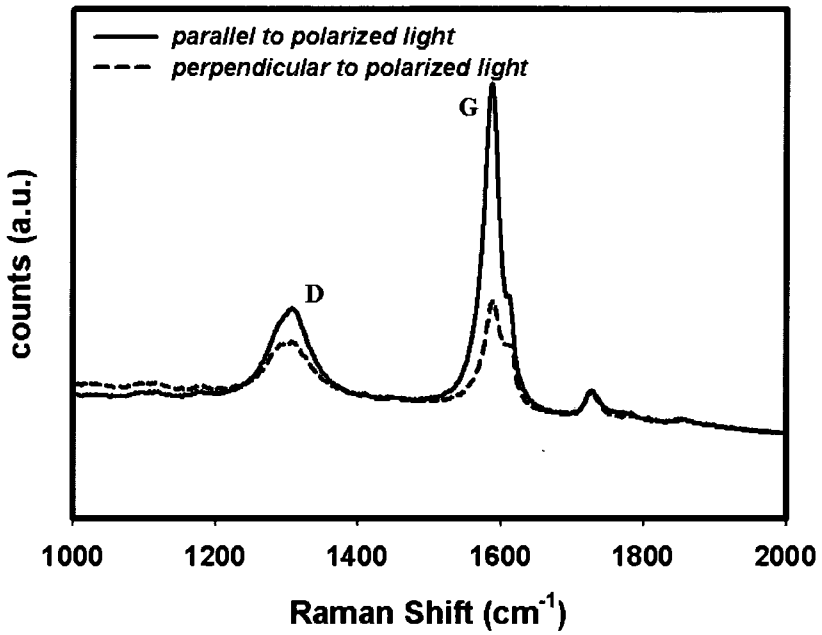

Figure 6-11: Raman spectra of aligned non-woven mat (PET/1%MWCNT) parallel to polarized beam (0°) compared to perpendicular to light (90°).

At 1 wt% MWCNT, the imposed alignment force mainly causes CNT orientation as described previously; and that is the main reason why aligned nanofiber diameter increases as compared to the static collection mode. Since the higher electric force is mainly imposed on CNT orientation, the retardation in splashing and diameter reduction might be expected. Thereafter, the effect of aligned nanofiber production at 1 wt% MWCNT concentration is mainly CNT orientation rather than enhancement in splashing and reduction in final nanofiber diameter. This high range of CNT orientation at 1 wt% MWCNT in aligned nanofiber manufacturing could be of considerable interests in enhancement of single nanofibers conductivity along nanofiber axis. This is also the case in higher CNT concentrations (3% and 5%); alignment might be the main reason for bead removal along fiber axis by using rotating drum. Alignment at high concentration mainly causes CNT bead removal along fiber axis rather CNT orientation and splashing or final nanofiber diameter reduction. In conclusion, aligned nanocomposite nanofibers include larger diameter in all CNT concentrations; however, the nanofibers show more CNT

orientation below percolation (1 wt% CNT) and less bead structure above percolation (3 wt% and 5wt% MWCNT). From another aspect, higher crystallinity and lower diameter and free volume might be a reason for decrease in the amount of CNT orientation at 5 wt% MWCNT concentration. At high concentration of CNTs, large aggregates are formed inside nanofibers as shown previously. The formation of aggregation prevents from high degree of individual CNT orientation and increasing the beam intensity in alignment direction; since it decreases the density of oriented CNTs in aligned direction. Hence, it might be another reason for decrease in the amount of CNT orientation at high CNT concentrations.

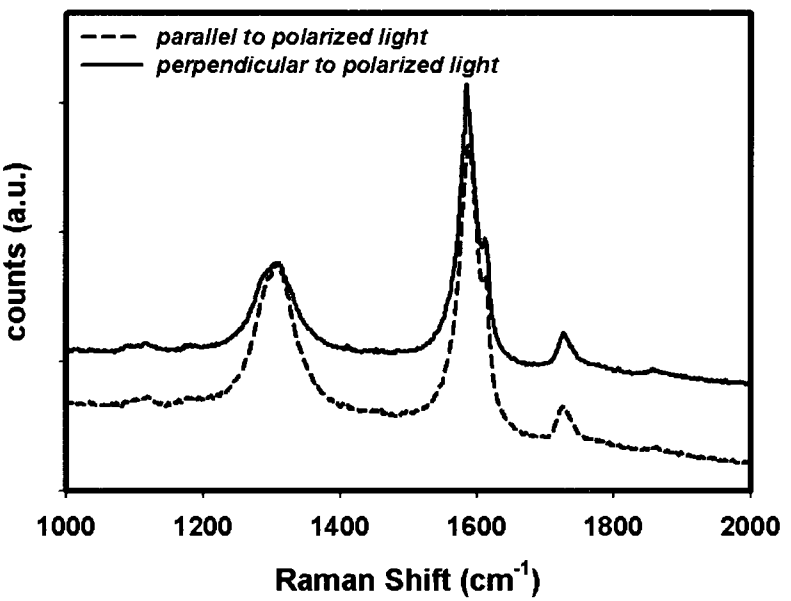

Figure 6-12: Raman spectra of aligned non-woven mat (PET/5% MWCNT) parallel to polarized beam (0^{o}) compared to perpendicular to light (90^{o}).

Raman spectroscopy results are in accordance with previously obtained results in SEM morphological analysis (Fig. 6-6) and FTIR (Fig. 6-7). In aligned pure PET nanofibers and at 1% MWCNT (below percolation), the crystalline content is low and the chains have more freedom and free volume to be oriented and therefore more aligned nanofibers are obtained below percolation based on FTIR results. Nevertheless, increase

in crystallinity above percolation reduces chain movements and free volumes and therefore only a marginal PET chains orientation effect is observed in aligned nanocomposite nanofibers. This is also the case for CNT orientation in aligned nanocomposite nanofibers. At 1% MWCNT, the maximum effect of aligned nanofiber processing is observed. Therefore, aligned nanocomposite nanofibers show more exclusive results in PET chains and CNT orientation below percolation as compared to high concentrations of CNTs.

6.4.4. Electrical conductivity measurement

Electrical conductivity of final electrospun mat was measured as a function of CNT types and concentrations. The samples included a wide range of thicknesses from 40 to 150 μm and they were all positioned between two highly conductive layers besides electrodes before starting experiments. Therefore, all the experiments were run in similar conditions, constant force and with reliably enough repeatability with a deviation less than 15% of the average conductivity.

Based on electrical percolation theory, the system becomes conductive when a critical concentration is reached which is called the electrical percolation threshold. Above the electrical percolation, the system is quite conductive [42]. As the conductivity measurement test results show the nanofibers are quite conductive at 2 wt% concentration of MWCNT and a considerable increase in electrical conductivity is observed above this concentration (Fig. 6-13); based on percolation theory [43]:

$$\sigma = A(w - w_c)^t \qquad (6\text{-}5)$$

where σ is the volume conductivity, A and t are constants, and w_c is the critical concentration in which the conductivity is ignorable compared to higher concentration; the critical concentration for network formation (Fig. 6-13).

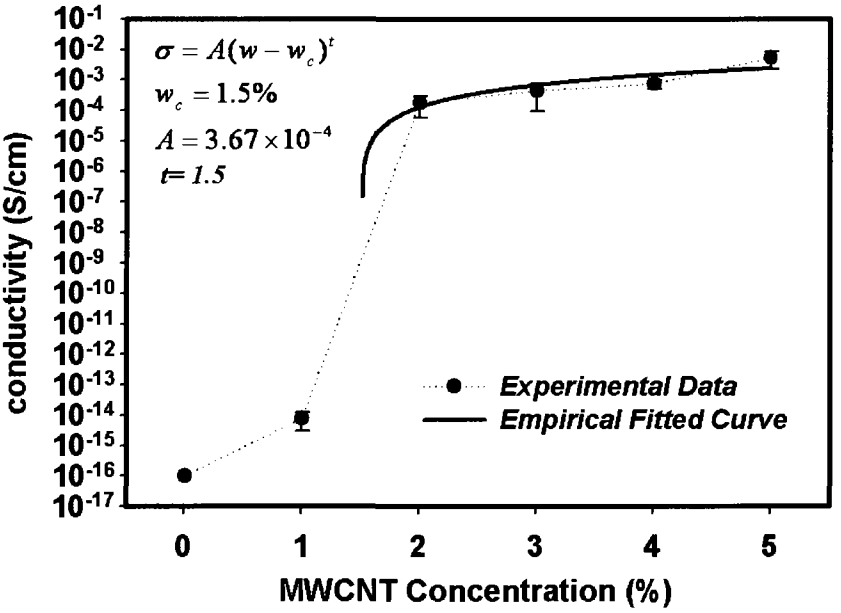

Figure 6-13: Electrical conductivity as a function of MWCNT concentrations.

As the results show, at 2 wt% MWCNT concentration the system is quite conductive and reaches almost a plateau region above 3 wt% MWCNT concentration (Fig. 6-13). The electrical conductivity of different types of CNTs was measured using the same method and at the same condition (Table 6-5). At 1 wt% of different CNTs, all samples including different types of CNTs show the same conductivity. However, at 5 wt% concentration, SWCNT nanofibers include the conductivity almost one order of magnitude lower, compared to DWCNT and MWCNT fibers. This might be because of poor dispersion of SWCNT and DWCNT compared to MWCNT [28]. MWCNTs are easier to disperse; therefore, we obtained better results using this type of CNT. The poor dispersion of SWCNT and DWCNT and aggregates formation as mentioned previously prevent from obtaining desirable conductivity results from these two types of CNTs.

Table 6-5: Electrical conductivity (S/cm) of final electrospun non-woven mat at different CNT concentrations and types

	1 %	5 %
SWCNT	8.2×10^{-15}	7.7×10^{-4}
DWCNT	1.5×10^{-14}	2.6×10^{-3}
MWCNT	7.7×10^{-15}	5.4×10^{-3}

6.4.5. Mechanical properties characteristics

Mechanical properties of electrospun PET/CNT non-woven mats were measured at different CNT concentrations and types [44]. Stress/strain curves obtained from tensile tests at different concentrations of randomly oriented PET/MWCNT non-woven mats are given in Fig. 6-14. Considering the results obtained, the samples containing CNT show more strength and larger elongation at break. At 1 wt% MWCNT, the nanofibers are less crystalline (Table 6-2); however, the chain oriented structure causes a considerable increase in ε_{break}. At 3% and 5%, where the samples are more crystalline (Table 6-2), the behavior is totally ductile in spite of higher CNT concentrations. Crystalline formation in nanocomposite nanofibers and orientation causes an increase in modulus and strength compared to pure PET electrospun mat; while ε_{break} (maximum tensile strain at break) is reduced as compared to nanofibers containing 1 wt% MWCNT (Fig. 6-14).

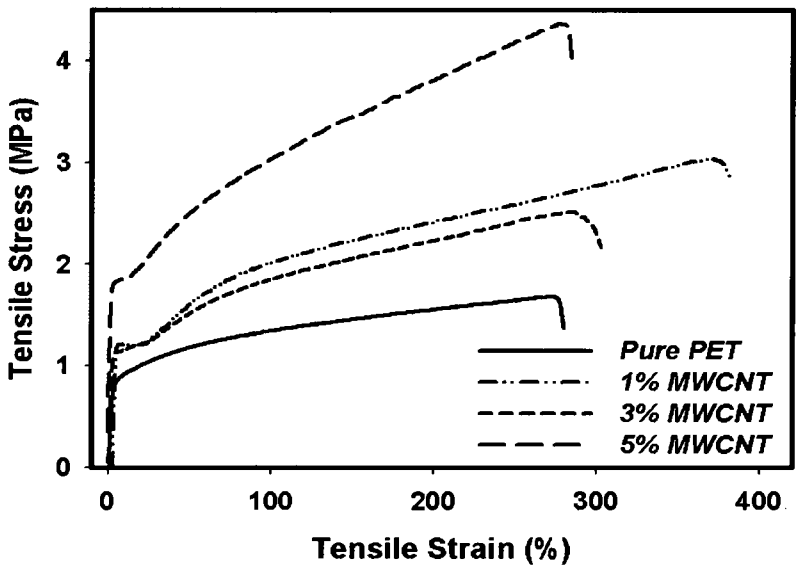

Figure 6-14: Stress/Strain curve of randomly oriented PET/MWCNT electrospun non-woven mat at different MWCNT concentrations.

Mechanical properties of randomly oriented nanofibers (Fig. 6-8a) were compared with aligned nanofibers in both parallel (Fig. 6-8b) and perpendicular (Fig. 6-8c) directions to the alignment and nanofibers orientation (Fig. 6-15). As it is shown, the addition of MWCNT causes an increase in modulus with respect to random PET nanofibers (Fig. 6-15a). However, the effect of MWCNT addition on modulus in aligned nanofibers is totally opposite and it decreases in direction of the alignment (0^{o}). The modulus for aligned mats compared to random ones increases 3 to 6 times depending on MWCNT concentration (Fig. 15a). In random nanofibers, addition of MWCNT causes an increase in chains orientation (below percolation) and crystallinity (above percolation); therefore, adding MWCNT causes increase in modulus. Aligned nanofibers in tensile test cause an increase in modulus in direction of alignment (0^{o}); however, this effect is more important in pure PET nanofibers. By adding MWCNT, the system shifts from aligned nanofibers to partially aligned (Fig. 6-6) and therefore the modulus decreases because of a reduction in nanofibers orientation. The same trend is observed in the values of tensile

strength and pure electrospun samples show the least value in random nanofibers and the highest value in aligned nanofibers in direction of alignment (Fig. 6-15b). The difference in modulus enhancement in aligned nanofibers compared to random mats has the most value at 0% and 1% MWCNT. This result is consistent with FTIR and Raman spectroscopy. It has been shown in FTIR and Raman that the orientation factor of both PET chains and CNTs is maximum at low concentrations of CNTs. At high CNT concentrations, CNT aggregates and poor dispersion could cause stress concentration and week points in mechanical strength.

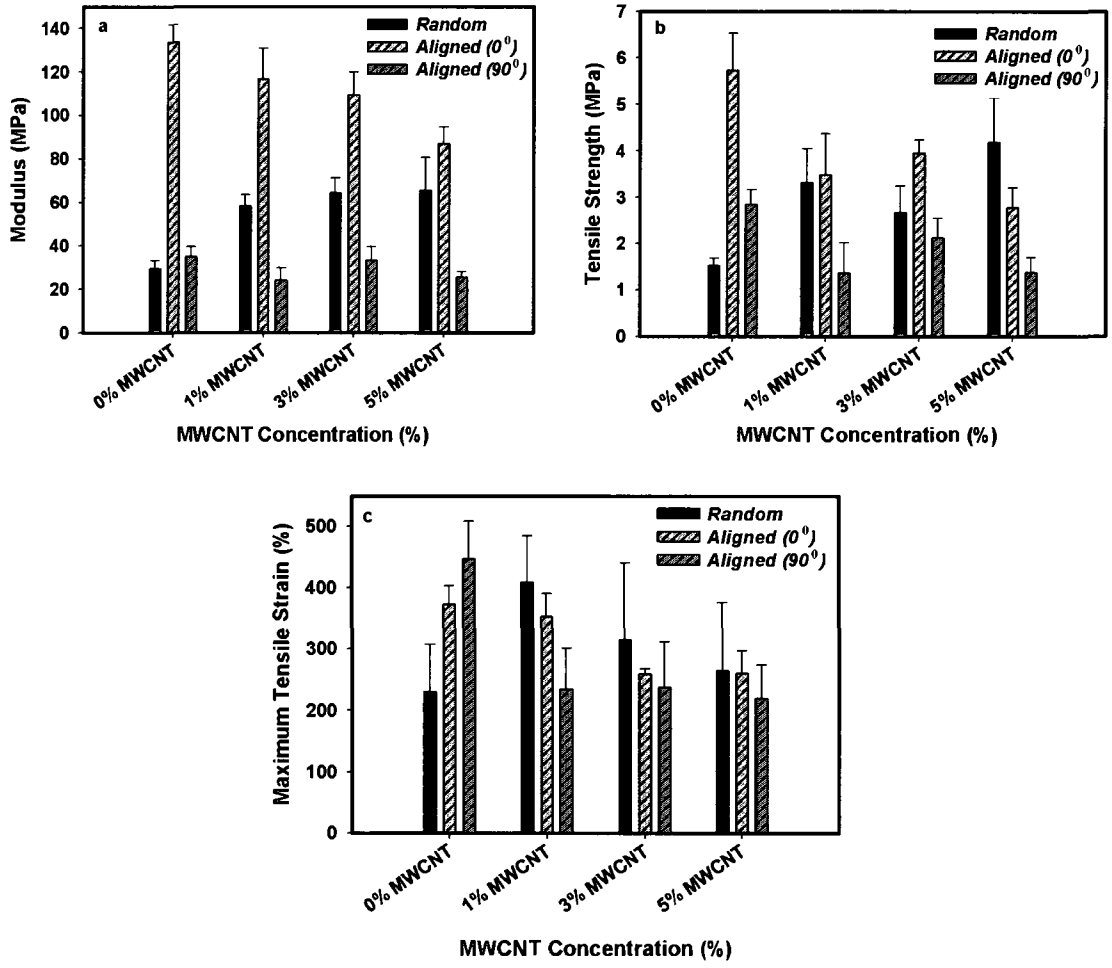

Figure 6-15: Tensile modulus (a), tensile strength (b) and maximum tensile strain (c) as a function of MWCNT concentrations in randomly oriented nanofibers compared to aligned nanofibers in parallel to alignment (0°) and perpendicular to alignment (90°).

In random nanofibers, ε_{break} has a maximum value at 1 wt% MWCNT (Fig. 6-14 and 6-15c). In aligned nanofibers, pure PET shows the highest value of ε_{break} and it decreases by adding MWCNT. The amount of ε_{break} for nanocomposite nanofibers is almost the same as random nanofibers and no considerable effect of alignment are observed in aligned nanocomposite nanofibers. Low modulus and strength in perpendicular direction (90°) causes considerable increase in the amount of ε_{break} especially in pure PET non-woven mats (Fig. 6-15c).

The mechanical properties of the different nanocomposites with varying types of CNT (at 1 wt% and 5 wt%) are compared in Table 6-6. SWCNT and DWCNT are smaller in size and they show more compatibility with PET matrix and therefore they are more effective in mechanical properties enhancement at low concentration as compared to MWCNT. Nevertheless, the mechanical test results show opposite behavior at 5 wt% CNT concentration.

Table 6-6: Mechanical properties of nanocomposite nanofibers non-woven mat at different CNT type and concentrations

CNT Type and Concentration	Modulus (MPa)	Tensile Strength (MPa)	Maximum Tensile Strain (%)
1% SWCNT	69.0 ± 6.8	4.23 ± 0.8	315.6 ± 70.5
5% SWCNT	44.9 ± 7.7	2.1 ± 0.4	148.0 ± 61.0
1% DWCNT	60.0 ± 9.3	3.1 ± 0.9	256.5 ± 137.6
5% DWCNT	46.5 ± 6.6	2.4 ± 0.4	264.8 ± 5.7
1% MWCNT	58.3 ± 5.2	3.3 ± 0.7	408.3 ± 75.9
5% MWCNT	65.4 ± 15.3	4.2 ± 1.0	264.3 ± 110.9

As demonstrated by the results, MWCNT gives better results at high concentration compared to SWCNT and DWCNT. We believe that poor dispersion of SWCNT and DWCNT at high CNT concentrations compared to MWCNT causes poor mechanical properties [28]. Dispersion has an important role on final mechanical properties and it is

quite difficult to disperse smaller sizes of nanotubes at higher concentrations [45, 46]. Therefore, better results are obtained using MWCNT at high CNT concentrations.

6.5. Conclusions

Random and aligned nanocomposite nanofibers of PET with different concentrations and types of CNTs were produced and their morphologies and properties studied by different methods. Electrical conductivity measurements established the percolation threshold at a concentration of 2 wt% in MWCNT. Morphological observations proved that aligned nanofibers containing MWCNT were of larger diameter but with less bead structures along the fiber axis. This proves that aligned nanofiber manufacturing is useful in agglomerate reduction and smooth nanofiber production especially at high CNT concentration. Crystalline content decreased by adding MWCNT below percolation concentration while the trend was opposite at high concentrations of CNTs. In aligned nanocomposite nanofibers, addition of CNTs caused a gradual increase in crystallinity. Therefore, it is possible to obtain nanofibers with higher crystallinity compared to random nanofibers through aligned nanofiber manufacturing at concentrations close to percolation threshold (2 wt%). It could be of considerable importance to produce conductive nanofibers with higher crystallinity through aligned nanofiber production. FTIR results showed that the amount of PET chain orientation in aligned nanofibers is maximum at low MWCNT concentration; while the addition of MWCNT and a higher crystalline content is consistent with a decrease in the PET chains orientation at high CNT concentrations. A similar conclusion on CNT orientation can be drawn from Raman spectroscopy results. The orientation of MWCNT in aligned nanocomposite nanofibers has its highest value at 1 wt% MWCNT. The maximum orientation factor obtained at 1 wt% MWCNT originates of a lesser crystalline content and more free volume available at this concentration as compared to others. Obtaining

higher orientation of CNTs at lower concentration could be an interesting factor to produce more conductive single nanofiber at lower CNT concentration. Considerable effect of alignment on mechanical properties was obtained at low MWCNT concentration; while this effect was less for high concentrations of CNTs which were consistent with FTIR and Raman spectroscopy test results. Significant improvement in mechanical properties especially modulus through adding MWCNT and aligned nanofiber production could be a remarkable factor in final functionality of non-woven mat.

6.6. Acknowledgements

The authors would like to acknowledge the financial support of Natural Sciences and Engineering Research Council Canada (NSERC) for the financial support to carry out this study. We would also like to thank the great help of people at University of Montreal in Raman spectroscopy experiments.

6.7. References

1. Burger, C.; Hsiao, B.S.; Chu, B. Annu Rev Mater Res 2006, 36, 333-368.
2. Li, D.; Xia, Y. Adv Mater 2004, 16, 1151-1170.
3. Reneker, D.H.; Chun, I. Nanotechnology 1996, 7, 216-223.
4. Iijima, S. Nature 1991, 354, 56-58.
5. Ge, J.J; Hou, H.; Li, Q.; Graham M.J.; Greiner, A.; Reneker, D.H.; Harris, F.W.; Cheng S.Z.D. J Am Chem Soc 2004, 126, 15754-15761.
6. Ra, E.J.; An, K.H.; Kim, K.K.; Jeong, S.Y.; Lee, Y.H. Chem Phys Lett 2005, 413, 188-193.

7. Seoul, C.; Kim, Y.T.; Baek, C.K. J Polym Sci, Part B: Polym Phys 2003, 41, 1572-1577.
8. Sung, J.H.; Kim, H.S.; Jin, H.J.; Choi, H.J.; Chin, I.J. Macromolecules 2004, 37, 9899-9902.
9. Veleirinho, B.; Lopes-da-Silva, J.A. Process Biochem 2009, 44, 353-356.
10. Chen, C.; Wang, L.; Huang, Y. Sol Energy Mater Sol Cells 2008, 92, 1382-1387.
11. Ignatova, M.; Yovcheva, T.; Viraneva, A.; Mekishev, G.; Manolova, N.; Rashkov, I. Eur Polym J 2008, 44, 1962-1967.
12. Lin, Y.; Chi, L.; Yao, Y.; Wu, D.C. Iran Polym J (Eng. Ed.) 2008, 17, 373-378.
13. Chen, C.; Wang, L.; Huang, Y. Mater Lett 2008, 62, 3515-3517.
14. Veleirinho, B.; Rei, M.F.; Lopes-da-Silva, J.A. J Polym Sci, Part B: Polym Phys 2008, 46, 460-471.
15. Jung, K.H.; Huh, M.W.; Meng, W.; Yuan, J.; Hyun, S.H.; Bae, J.S.; Hudson, S. M.; Kang, I.K. J Appl Polym Sci 2007, 105, 2816-2823.
16. Dotti, F.; Varesano, A.; Montarsolo, A.; Aluigi, A.; Tonin, C.; Mazzuchetti, G. J Ind Text 2007, 37, 151-162.
17. Ogata, N.; Shimada, S.; Yamaguchi, S.; Nakane, K.; Ogihara, T. J Appl Polym Sci 2007, 105, 1127-1132.
18. Chronakis, I.S.; Jakob, A.; Hagstrom, B.; Ye, L. Langmuir 2006, 22, 8960-8965.
19. Hong, K.H.; Kang, T.J. J Appl Polym Sci 2006, 100, 167-177.
20. Chronakis, I.S.; Milosevic, B.; Frenot, A.; Ye, L. Macromolecules 2006, 39, 357-361.
21. Chen, H. AIChE Annual Meeting, Conference Proceedings, American Institute of Chemical Engineers 3382-3383, New York, U.S.A., 2005, American Institute of Chemical Engineers, New York, United States.
22. Ma, Z.; Kotaki, M.; Yong, T.; He, W.; Ramakrishna, S. Biomaterials 2005, 26, 2527-2536.
23. McKee, M.G.; Wilkes, G.L.; Colby, R.H.; Long, T.E. Macromolecules 2004, 37, 1760-1767.
24. Kim, K.W.; Lee, K.H.; Khil, M.S.; Ho, Y.S.; Kim, H.Y. Fibers Polym 2004, 5, 122-127.
25. Nah, C.; Mathew, G.; Hong, J.P.; Rhee, J.M.; Lee, H.S. Polym. Test. 2005, 24, 712-717.

26. Ahn, B.W.; Chi, Y.S.; Kang, T.J. J Appl Polym Sci 2008, 110, 4055-4063.
27. Chen, H.; Liu, Z.; Cebe, P. Polymer 2009, 50, 872-880.
28. Mazinani, S.; Ajji, A.; Dubois, C. Polymer 2009, In Press, doi:10.1016/j.polymer.2009.04.070.
29. Fennessey, S.F.; Farris, R.J. Polymer 2004, 45, 4217-4225.
30. Jose, M.V.; Steinert, B.W.; Thomas, V.; Dean, D.R.; Abdalla, M.A.; Price, G.; Janowsk, G.M. Polymer 2007, 48, 1096-1104.
31. Litchfield, D.W.; Baird, D.G. Polymer 2008, 49, 5027-5036.
32. Mehta, A.; Gaur, U.; Wundderlich, B. J Polym Sci Polym Phys Ed 1978, 16, 289-296.
33. Anoop Anand, K.; Agarwal, U.S.; Joseph, R. Polymer 2006, 47, 3976-3980.
34. Keum, J.K.; Jeon, H.J.; Song, H.H.; Choi, J.I.; Son, Y.K. Polymer 2008, 49, 4882-4888.
35. Lu, X.F.; Hay, J.N. Polymer 2001, 42, 8055-8067.
36. Cole, K.C.; Ben Daly, H.; Sanschagrin, B.; Nguyen, K.T.; Ajji, A.; Polymer 1999, 40, 3505-3513.
37. Sadeghi, F.; Ajji, A.; Carreau, P.J. J Polym Sci, Part B: Polym Phys 2008, 46, 148-157.
38. Lee, K. H.; Kim, K.W.; Pesapane, A.; Kim, H.Y.; Rabolt, J.F. Macromolecules 2008, 41, 1494-1498.
39. Ajji, A.; Cole, K.C.; Dumoulin, M.M.; Brisson, J. Polymer 1995, 36, 4023-4030.
40. Antunes, E.F.; Lobo, A.O.; Corat, E.J.; Trava-Airoldi, V.J. Carbon 2007, 45, 913-921.
41. Corrias, M. Serp, Ph.; Kalck, Ph.; Dechambre, G.; Lacout, J.L.; Castiglioni, C.; Kihn, Y. Carbon 2003, 41, 2361-2367.
42. Kota, A.K.; Cipriano, B.H.; Duesterberg, M.K.; Gershon, A.L.; Powell, D.; Raghavan, S.R.; Bruck, H.A. Macromolecules 2007, 40, 7400-7406.
43. Wang, W.; Murthy, N.S.; Chae, H.G.; Kumar, S. Polymer 2008, 49, 2133-2145.
44. Inai, R.; Kotaki, M.; Ramakrishna, S. J Polym Sci, Part B: Polym Phys 2005, 43, 3205-3212.
45. Coleman, J.N.; Khan, U.; Blau, W.J.; Gun'ko, Y.K. Carbon 2006, 44, 1624-1652.
46. Sluzarenko, N.; Heurtefeu, B.; Maugey,M.; Zakri, C; Poulin, Ph.; Lecommandoux, S. Carbon 2006, 44, 3207-3212.

Chapter 7

Structure and Properties of Melt-Spun PET/MWCNT Nanocomposite Fibers*

7.1. Presentation of the article

Final properties of PET/CNT melt-spun microfibers are studied in this article. CNT master-batch is diluted to desired CNT concentrations by using a twin-screw melt mixing method. Melt-spun nanofibers are prepared from compounds at different CNT concentrations and they are shaped to microfibers of different ranges of diameters. The samples containing CNTs show high degree of drawability compared to pure melt-spun fibers. We could obtain conductive fibers at 2 wt% MWCNT concentration by modifying the dispersion condition to a great extend. PET chains orientation and crystallization in microfibers was studied by different techniques. The results obtained show that both PET chains orientation and crystallinity is decreases by adding CNT to melt-spun fibers. CNT orientation was also studied at different draw ratios (DR) by Raman spectroscopy technique. Mechanical test results show considerable enhancement in elongation at break of the fibers containing CNTs compared to pure PET fibers.

---

* ***Polymer Engineering and Science.*** Submitted May 2009.

Structure and Properties of Melt-Spun PET/MWCNT Nanocomposite Fibers

Saeedeh Mazinani [1], *Abdellah Ajji* [1,2], *Charles Dubois* [1*]

1) CREPEC, Department of Chemical Engineering, Ecole Polytechnique of Montreal, P.O. Box 6079, Station Centre-Ville, Montreal, Quebec, Canada H3C 3A7.

2) CREPEC, Industrial Materials Institute, National Research Council Canada, 75, de Mortagne Blvd., Boucherville, Quebec, Canada J4B 6Y4.

7.2. Abstract

Polyethylene terephthalate (PET) melt-spun fibers were modified with multi-wall carbon nanotubes (MWCNT) to obtain conductive microfibers smaller than 90 μm in diameter. Physical properties such as crystallinity and orientation of as-spun fibers were studied by X-ray diffraction, Raman spectroscopy and microscopy techniques at different draw ratio (DR) and MWCNT concentrations. Morphological and orientation analysis of MWCNT after melt-spinning process showed agglomerates formation and highly oriented CNTs. Study of the orientation of PET crystalline phase in drawn fibers proved that the addition of nanoparticles decreases the orientation of crystalline units inside the fibers. The orientation of MWCNT as well as that of PET chains was studied using Raman spectroscopy at different draw ratios and a high degree of CNT orientation was

* Corresponding Author
Tel: +1 (514) – 340 4711 ext. 4893
Fax: +1 (514) – 340 4159
E-mail address: charles.dubois@polymtl.ca

observed at high DR conditions. Mechanical and electrical properties of as-spun fibers were also investigated. Our results showed that it was possible to achieve conductive fibers at 2 wt% MWCNT concentration and more conductive fibers using higher DR were also obtained without increasing MWCNT concentration. Mechanical properties results showed interestingly high value of maximum tensile strain at break (ε_{max}) of nanocomposite fibers, up to 3 times more than pure PET fibers.

7.3. Introduction

Specific properties of polyethylene terephthalate (PET) such as high drawability have made this polymer one of the most important polymers in textile industry, as demonstrated by the large body of literature devoted to PET fiber production and properties [1-3]. Among them, one can find reports of different techniques to modify PET fibers properties, and most particularly its electrical conductivity, using carbon nanotubes (CNTs) [4-11]. Maximizing the orientation of carbon nanotubes in CNT nanocomposites fibers is of considerable interest because it considerably enhances mechanical and electrical properties even for low concentration of CNTs. Among the latest studies available, only very few address the issue of improving drawability and conductivity of PET fibers and nanocomposite fibers by using nanoclay and carbon nanotubes respectively [12-14].

Physical and rheological properties of PET/CNT nanocomposites have been studied by different groups [7, 15-20]. Anand *et al.* studied the crystalline structure of single wall carbon nanotube (SWCNT)/PET nanocomposites [15]. Their analysis proved the role of SWCNT as a nucleating agent during crystallization in addition to inducing oriented crystalline formation through pre-orientation of SWCNT in PET matrix [15]. Dispersion of CNT in nanocomposite has been found as one of the main controlling parameters of their final properties [16]. Jin and his colleagues could modify the dispersion through

chemical surface modification of CNT such that they could considerably enhance the mechanical properties [16]. Hu *et al.* studied the rheological and electrical conductivity of PET/MWCNT systems [21]. They showed that dispersion and aspect ratio are the most important determining factors for rheological and electrical percolation. They obtained a low percolation threshold at 0.6 wt% of MWCNT for rheological properties and 0.9 wt% of MWCNT for electrical conductivity [21]. However, no detailed of the structure and morphology of the nanocomposite fibers was performed in terms of dispersion, orientation etc. of the matrix and nanoparticles.

Conductive polymer fibers from polypropylene/carbon nanofiber (CNF) nanocomposites were studied by Kumar *et al.* for the first time [22]. Their results showed an enhancement of the mechanical and electrical properties by the addition of 5% CNF [22]. In the earliest studies available on polyester fibers conductivity modification, Ma *et al.* surveyed polyester/CNF nanocomposite fibers produced by melt spinning [23]. They studied the processing, structure and properties of the composite compared to pure PET [23]. They showed that tensile strength is considerably increased as compared to pure PET only if there is a good dispersion of the nanoparticles. In a recently published paper on PET/CNT, Li *et al.* investigated the microstructure of PET/CNT conductive nanocomposite fibers in more details [13]. They added 4 wt% of CNT to PET and they detected considerable changes in electrical properties above percolation (4 wt%). They also investigated some other properties of PET/CNT system such as viscosity, crystallinity and CNT dispersion homogeneity along fiber axis using techniques such as scanning electron and optical microscopy [13]. However, no precise and thorough morphological study has been performed in previous investigations on nanocomposite MWCNT/PET microfibers. Therefore, the effect of CNTs dispersion and processing conditions on the mechanical and electrical properties of the fibers remained to be assessed.

In this work, we produce melt-spun PET/MWCNT nanocomposite fibers with a precise morphological characterization and control and dispersion modification through mixing procedure. We mainly focus on studying the effect of two important material and

process parameters: MWCNT concentration and draw ratio (DR). The crystalline structure and the effect of MWCNT on final crystallinity are studied by x-ray diffraction (XRD) and differential scanning calorimetry (DSC). Orientation of crystalline phase and polymer chains is also studied in details using XRD, Fourier Transform Infra-Red (FTIR) and Raman spectroscopies. The orientation and morphology of carbon nanotubes are studied by high resolution scanning electron microscopy (HR-SEM) and transmission electron microscopy (TEM) in addition to Raman spectroscopy. Finally, electrical and mechanical properties of the nanocomposite fibers are measured and the role of MWCNT on the drawability of the nanocomposite fibers is evaluated.

7.3. Experiments

7.3.1. Polymer mixing and melt-spinning process

The extrusion grade polyethylene terephthalate (PET) used in this work was Selar 7086 polymer obtained from DuPont Co. A commercial PET/CNT masterbatch, MB-6815-00; composed of PET mixed with 15% Multi-wall Carbon Nanotube (MWCNT); was purchased from Hyperion Catalysis Co. We used a melt mixing method for masterbatch dilution and CNT dispersion. Mixing was conducted using a lab-scale twin-screw extruder (Leistritz Group Co.; with 1.78 mm diameter and length of 40D) at controlled temperature and speed. The MWCNT masterbatch was first diluted to the desired CNT concentration and then dispersed in the PET matrix. We used this procedure to optimize CNT dispersion in the matrix and to obtain optimal dispersion at different CNT concentrations. The best condition for CNT dispersion were obtained at 200 rpm screw speed using a temperature profile along the extruder ranging from 300 °C at the first zone after hopper to 270 °C at the die end.

A capillary rheometer (Rosand) combined with a take-up device was used to produce single fibers under controlled pressure and temperature profiles. The fibers were produced using a barrel temperature of 270 °C and ambient air cooling. Various draw ratios were used. We employed diluted PET/CNT compounds to obtain fibers at different CNT concentrations (containing up to 3 wt% MWCNT) and draw ratios. Above 3 wt% of CNT, the brittle behavior of the nanocomposite decreased the drawability of the fibers. Therefore, only rods were extruded from the nanocomposites with more than 3% MWCNT. The dimensions of the fibers produced in this work at different processing conditions (different draw ratios (DR)) and MWCNT concentrations are given in Table 7-1. The values of DRs are given in proportion to maximum DR (DR_{max}=470) of the nanocomposite fibers (DR_{max} of the fibers with 1% or 3% MWCNT) through the text and in the figures.

Table 7-1: Average diameter of produced fibers at different processing conditions and MWCNT concentrations

	Pure PET	**1% MWCNT**	**3% MWCNT**	**4% MWCNT**	**5% MWCNT**	**7% MWCNT**
DR= 112 ***(20% of DR_{max})***	97 ± 14 (μm)	97 ± 14 (μm)	97 ± 14 (μm)	Only Non-drawn rod-like fibers 200 ~ 800 μm	Only Non-drawn rod-like fibers 200 ~ 800 μm	Only Non-drawn rod-like fibers 200 ~ 800 μm
DR=202 ***(40% of DR_{max})***	66 ± 14 (μm)	66 ± 14 (μm)	66 ± 14 (μm)			
DR=291 ***(60% of DR_{max})***	57 ± 7 (μm)	57 ± 7 (μm)	57 ± 7 (μm)			
DR=380 ***(80% of DR_{max})***	*Impossible to produce*	50 ± 9 (μm)	50 ± 9 (μm)			
DR=470 ***(DR_{max})***	*Impossible to produce*	48 ± 9 (μm)	48 ± 9 (μm)			

7.3.2. Morphological analysis and dispersion evaluation of CNTs

Two microscopy techniques were used here to study and evaluate the distribution and dispersion condition of CNTs in PET matrix: scanning electron microscopy (HR-SEM) and transmission electron microscopy (TEM). A HR-SEM (Hitachi S-4700) on microtomed platinum coated samples was used to investigate the CNTs distribution in PET matrix. TEM (JEOL, JEM-2100 F) was the technique employed after HR-SEM observations to study and optimize the CNTs dispersion in PET matrix. A similar characterization was conducted on the resulting fibers after the processing step.

7.3.3. Crystalline characteristics (DSC and XRD)

Differential scanning calorimetry (DSC, Q1000; TA Instruments) and X-ray diffraction (XRD, Discover, D8, Bruker) were employed to study the crystalline behavior of PET/CNT nanocomposite. The effect of CNT addition on crystalline structure and behavior of drawn fibers compared to molded samples was first studied by DSC. The tests were performed in non-isothermal condition using a heating/cooling/heating cycle with the rate of 10 °C/min. XRD technique was used in addition to DSC to characterize the crystalline structure of the system and to evaluate the orientation in final melt-spun and drawn fibers. We used an X-Ray goniometer which was accompanied with a Hi-STAR two-dimensional area detector. The generator voltage and current were 40 kV and 40 mA respectively and a copper Cu Kα radiation (λ = 1.542 Å) was selected by a graphite crystal monochromator. The fibers obtained were examined using wide angle x-ray diffraction (WAXD) method and the orientation was determined using a pole-figure accessory. The orientation is reported in terms of the Herman orientation function and is given by [24]:

$$f = \frac{\left(3\cos^2\theta - 1\right)}{2} \qquad (7\text{-}1)$$

where θ is the angle between the unit crystalline cell axes (a, b, and c) and the reference axis that is machine direction (MD). Details about the calculations have been given elsewhere [25].

7.3.4. Orientation determination (Raman & FT-IR spectroscopy)

Raman and Fourier transform infrared (FT-IR) spectroscopy techniques were used for CNT and PET orientation determination respectively. A Nicolet Magna 860 FTIR instrument from Thermo Electron Corp. (DTGS detector, resolution 4 cm^{-1}, accumulation of 128 scans) was employed for FTIR experiment. Raman spectra were recorded on a Renishaw spectrometer equipped with an inVia Raman microscope. The samples were tested using a NIR laser (785 nm) with a grating of 1200 g/mm in a regular mode and use of 20x microscope. Orientation of MWCNTs and PET chains was obtained through comparing the spectra in parallel and perpendicular directions to the laser beam of Raman and FTIR spectroscopy respectively.

7.3.5. Electrical conductivity

Electrical conductivity of three types of samples was measured using various conductivity measurement instruments and test fixtures. The electrical conductivity of single rods and fibers at different draw ratios was measured and compared to the electrical conductivity of molded samples. Molded samples were shaped as a disk after compounding and before fiber formation. Below percolation and for materials with low conductivity (insulators), a KEITLEY 6517, high resistance meter was used and in the conductive range and above electrical percolation a combined set-up of KEITHLEY 6620 as a current source and Agilent 34401 A (6 ½ Digit Multimeter) as voltage source were used. We used a two-probe technique with various test fixtures, compatible with the three types of samples below the percolation threshold. Above percolation, the experiments were performed using a four-probe technique.

7.3.6. Mechanical properties

The mechanical properties of samples produced at different processing conditions were obtained employing a micro tester 5548 (Instron Inc.). First, the mechanical properties of single rods were measured at different CNT concentrations to assess the effect of CNT addition on final single rods. For rod-like fibers, the tensile test was performed using a 2 kN load cell and speed of 50 mm/min. The mechanical properties of single fibers up to 3% MWCNT were evaluated at various CNT concentrations and drawing conditions. For the fibers below 100 μm, we used the tensile test load cell of 5N and a speed of 50 mm/min.

7.4. Results and Discussions

7.4.1. Morphological and dispersion analysis

A proper initial dispersion of CNTs in polymer matrix is an important influential parameter on final electrical and mechanical properties. In this work, a CNT masterbatch was diluted to reach the desirable final concentration in the nanocomposite. Screw rotation speed, temperature profile along screw and volumetric flow rates (residence time) were changed during the experiments to obtain the best dispersion condition. The results showed that the screw speed was the most important determining parameter in dispersion modification. Fig. 7-1 shows the resulting dispersion state of the CNT in the diluted masterbatch for a poorly dispersed sample (Fig. 7-1a) produced at 150 rpm screw rotation speed compared to the best dispersion condition (Fig. 7-1b). Comparing these two samples at different magnification allows the conclusion that CNT (3 wt %) is reasonably well distributed in the PET matrix (Fig. 7-1b). Even though, the crystalline structure of PET matrix is the main reason that prevents obtaining the ideal distribution of

CNT the nanocomposite morphology obtained here at best distribution conditions (Fig. 7-1b) indicates a reasonable dispersed CNT morphology.

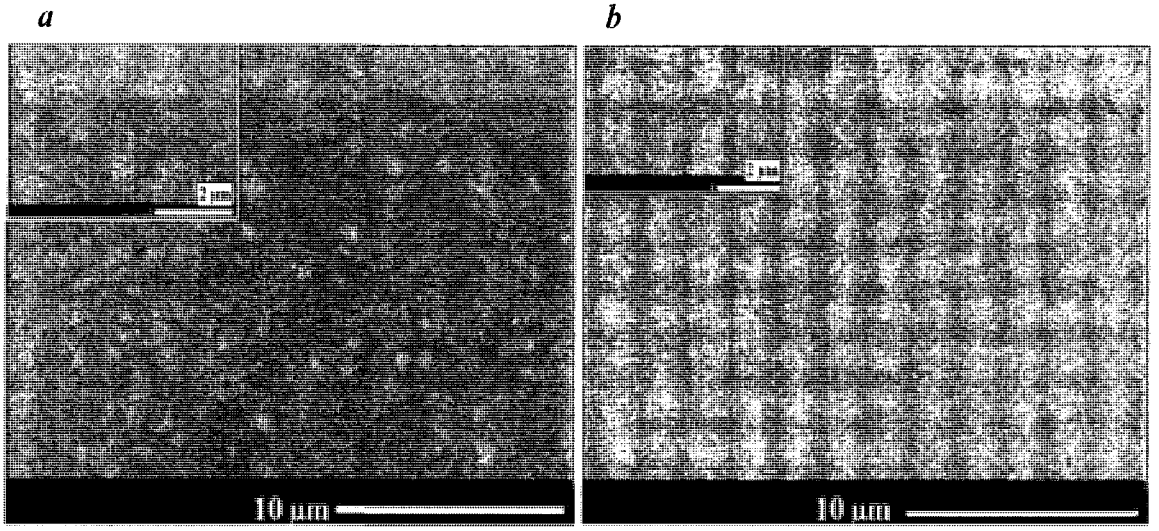

Figure 7-1: HR-SEM images of PET/3%MWCNT at different distribution condition. a) Poor distribution; b) Good distribution; the best distribution condition obtained at 200 rpm using the twin-screw extruder.

A similar dispersion analysis but this time using TEM is reported in Fig. 7-2, again showing a poorly dispersed (Fig 7-2a) at 150 rpm screw rotation speed, and an optimized sample (Fig. 7-2b). As it is shown in these images; in the optimized dispersion condition (Fig. 7-2b); CNTs have been mostly individually dispersed in PET matrix individually with no agglomeration. Therefore, it is expected that interactions of CNTs with PET matrix will help in the improvement of both mechanical properties and electrical conductivity.

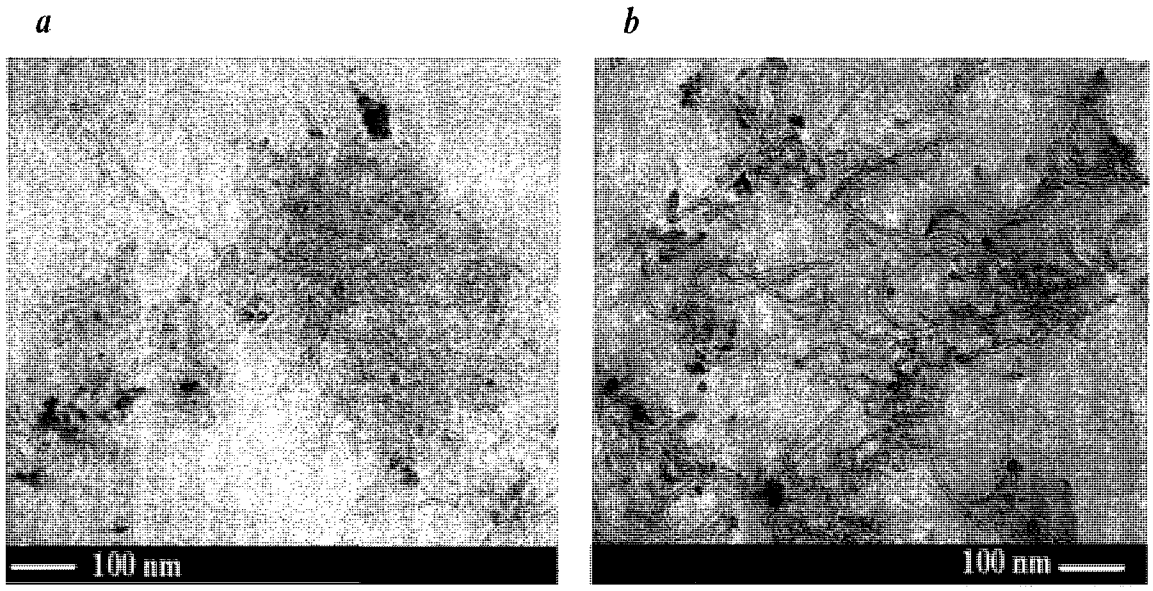

Figure 7-2: TEM images of PET/3%MWCNT at different dispersion condition. a) Poor dispersion; b) good dispersion; the best dispersion condition obtained at 200 rpm using the twin screw.

The best dispersion condition was chosen for CNT masterbatch dilution and PET/CNT composite preparation for fiber formation at different concentrations. TEM images of drawn fibers at 20% of DR_{max} (112) and DR_{max} (470) along fiber axis, and also at cross section of fiber at DR_{max} (Fig. 7-3 & 7-4) are shown at different magnifications. Comparing Fig. 7-3 and Fig. 7-4 shows that more aggregations are observed by increasing DR to DR_{max} during fiber formation. In addition, the TEM results at DR_{max} (Fig. 7-4) show agglomeration formation both along fiber axis and at fiber cross section.

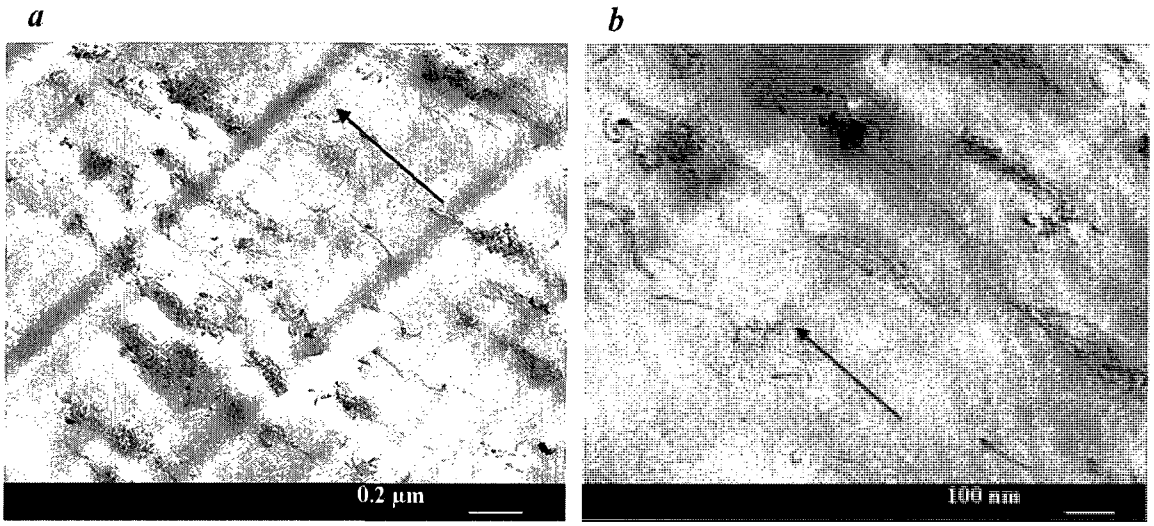

Figure 7-3: TEM images of PET / 3% MWCNT and CNT orientation at 20% of DR_{max} along fiber axis at two different magnifications.

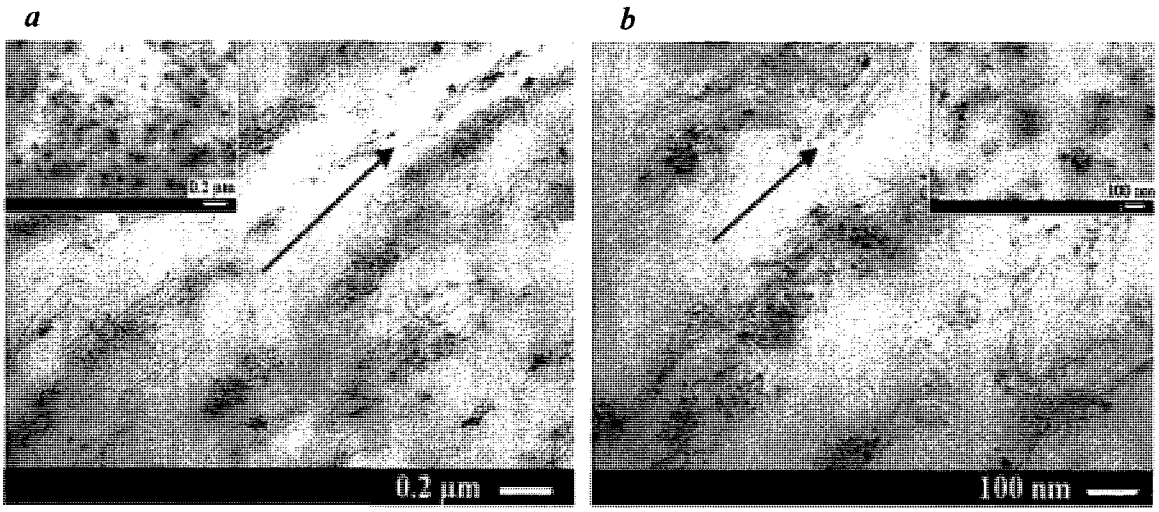

Figure 7-4: TEM images of PET / 3% MWCNT and CNT orientation at DR_{max} along fiber axis and at fiber cross section at two different magnifications.

In the case of maximum draw ratio, the fiber diameter is small (~50 μm). Therefore, the nanotubes are brought closer to each other and they are subjected to a high deformation rate and confined in a small volume. This strongly oriented flow field favors

the formation of clusters. Therefore, as it is shown (Fig. 7-3 and Fig. 7-4), more CNTs aggregates are observed because of less volume and shorter time available for CNTs to be drawn under the high elongation flow rate of fiber spinning at higher values of draw ratio.

7.4.2. Crystalline behavior

Final crystalline structure of nanocomposite melt-spun fibers and the role of CNT addition is an important parameter in controlling the final properties. The effect of CNT addition on X-Ray pattern of PET/MWCNT nanocomposite was studied in a first step, followed by thermal analysis using DSC method.

7.4.2.1. X-Ray Diffraction Characteristics

XRD analysis was performed on compounded nanocomposites that all the samples were prepared under the same molding condition. X-ray pattern of PET/MWCNT at different concentrations after compounding is compared to pure PET in Fig. 7-5 [12].

CNT presence enhances the crystallinity as expected which could be due to the effect of CNT nanoparticles role as nucleating agents. Moreover, a sharp peak around $2\theta=26^0$ (d_{002}) is obtained when CNT is added compared to pure PET. The intensity of this peak increases considerably with increasing CNT concentration as reported previously for polycarbonate and polyethylene carbon nanotube nanocomposite [26, 27]. Addition of CNT causes poor dispersion of nanoparticles in the matrix and agglomerate formation; therefore, XRD is more sensitive to CNT at high concentrations [27]. This peak is located at the same position as that for PET (100) reflection (Fig. 7-5). Therefore, it is difficult to prove if it is only due to CNT addition; however, PET-peak could be enhanced by addition of CNT.

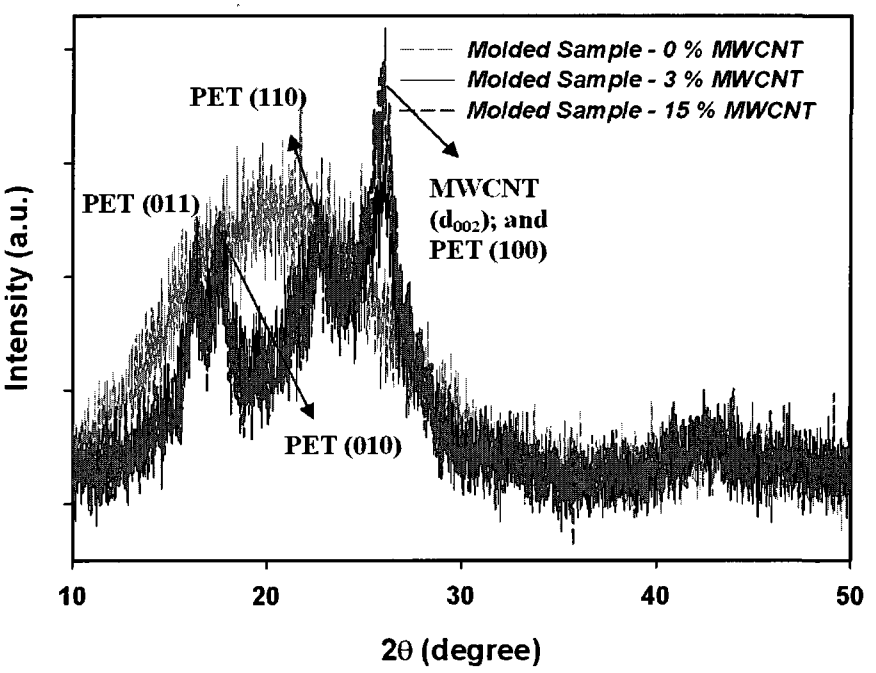

Figure 7-5: X-ray diffraction pattern of PET/MWCNT nanocomposite of molded samples prepared at the same condition at different MWCNT concentrations; pure PET, PET/3% MWCNT, PET/15% MWCNT.

XRD analysis of nanocomposite melt-spun fibers showed totally amorphous structure for nanocomposite fibers at different processing conditions with CNT content up to 3 wt%. We prepared XRD samples of drawn melt-spun nanocomposite fibers by 24 hours annealing at 160 °C. Annealing was mainly used to study the effect of carbon nanotube on crystallinity and orientation. The XRD patterns obtained from melt-spun annealed fibers at different DR and CNT concentrations are shown in Fig. 7-6.

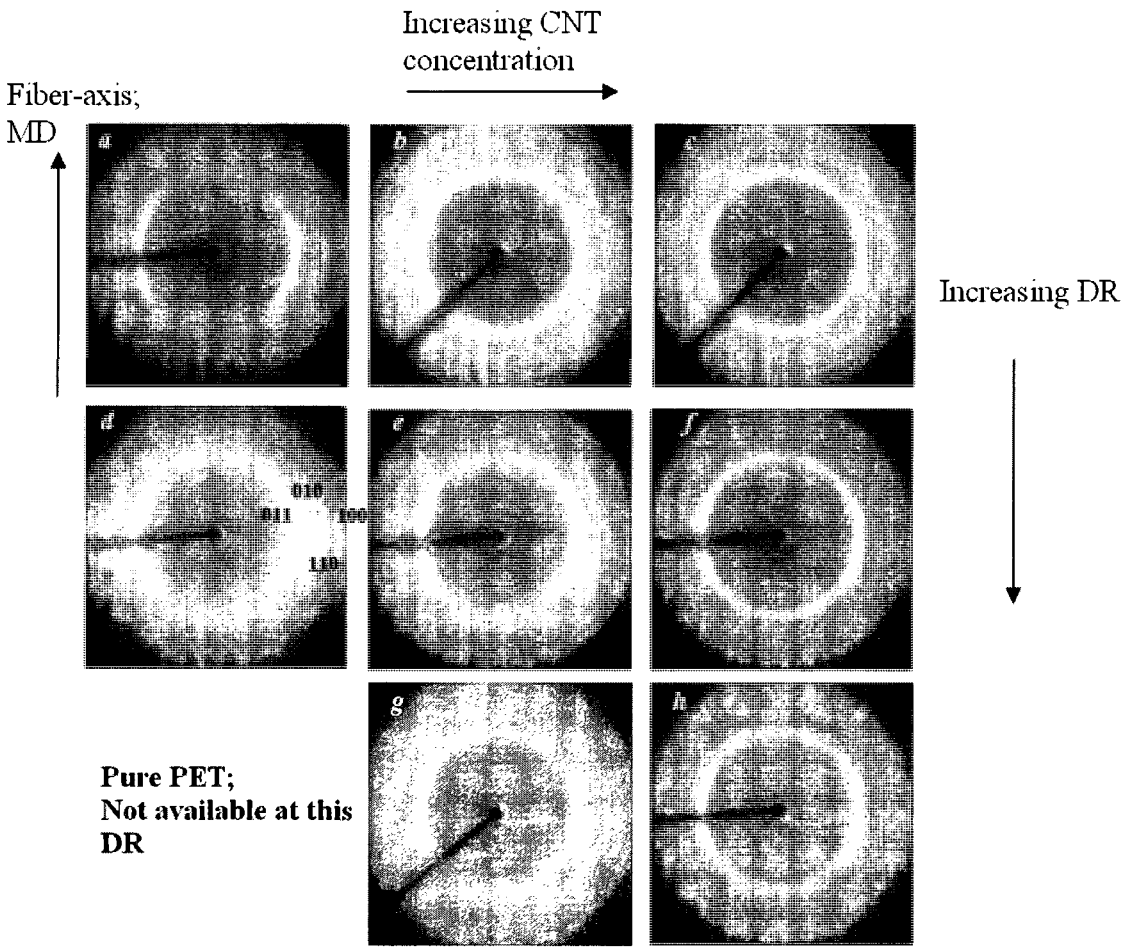

Figure 7-6: XRD pattern of PET/MWCNT melt-spun annealed fiber CNT concentrations and DRs; a) Pure PET, 20% DR_{max}; b) PET/1% MWCNT, 20% DR_{max}; c) PET/3% MWCNT, 20% DR_{max}; d) Pure PET, 60% DR_{max}; e) PET/1% MWCNT, 60% DR_{max}; f) PET/3% MWCNT, 60% DR_{max}; g) PET/1% MWCNT, Max DR_{max}; h) PET/3% MWCNT, DR_{max}.

As the results obtained from WAXD pattern show in Fig. 7-6, it is possible to detect the crystalline planes and their orientation in the melt-spun and annealed fibers [12]. Increasing the CNT concentration at different draw ratios causes a decrease of orientation. We used pole figure accessory to analyze the results obtained from XRD at different conditions after annealing (see Table 7-2). The details of calculations have been

given elsewhere [24]. The a and b axes orientation functions $f_{a,MD}$ and $f_{b,MD}$ were obtained by the pole-figure analysis of the (100) plane ($2\theta = 17^{o}$), and (010) plane ($2\theta = 25^{o}$) respectively. $f_{c,MD}$ was obtained by using the following orthogonality equation [25]:

$$f_{a,MD} + f_{b,MD} + f_{c,MD} = 0 \qquad (7\text{-}2)$$

These measurements and calculations were all performed in GADDS mode. The contribution of CNT peaks here is almost zero contrary to reflection mode of XRD, since the signals related to CNT are quite weak in GADDS mode. Therefore, the analyses are only made over the peaks under the effect of PET crystals and not CNT. It is shown that maximum orientation is obtained in the case of pure PET fibers at different draw ratios. Addition of carbon nanotube decreases the orientation and causes an increased drawability of the fibers.

Table 7-2: Orientation function ($f_{c,MD}$) at different draw ratios and CNT concentrations

	20% DR_{max} (112)	**60% DR_{max} (291)**	**DR_{max} (470)**
Pure PET	0.14	0.12	Not possible to be produced
1% CNT	- 0.08	0.04	0
3% CNT	-0.07	-0.03	-0.03

Carbon nanotubes could act as a nucleating agent and they might accelerate the nucleation [15]. However, nucleation and quiescent crystallization are not the only determining factor. Kinetics of crystallization especially at high speed melt spinning process could be an important determining factor. To prove it, we studied XRD results of as-spun fibers at very low draw ratio and different MWCNT concentrations without post-annealing step (Fig. 7-7). As it is shown, at lower range of DR, the crystalline behavior is just the opposite of previous observation (Fig. 7-6). Addition of CNT at this DR (10% of DR_{max}) enhances the crystallinity and at 3%, clear crystalline fiber is obtained. At low

rate of solidification and fiber formation, the nucleation and quiescent crystallization (and not the crystal growth) are the determining steps of the overall kinetics; therefore, more crystalline structures are obtained by increasing CNT concentrations because of CNTs nucleation effect.

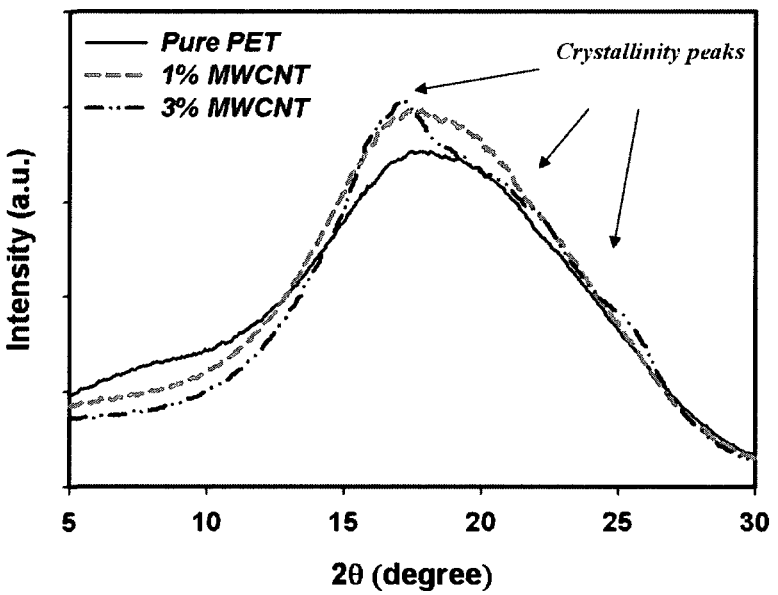

Figure 7-7: WAXD patterns of fibers at 10% DR_{max} and different CNT concentrations.

7.4.2.2. DSC Results

The values of ΔH used in different calculations and for DSC analysis reported here have been corrected for nanoparticles content by the following equation to have the data purely related to polymer weight:

$$\Delta H_{i,corrected} = \Delta H_{i,Expriment} / (1 - w_{CNT}) \qquad (7\text{-}3)$$

Then, the degree of crystallinity was calculated by the following equation [14]:

$$X_c = (\Delta H_f - \Delta H_{rc}) / \Delta H_f^0 \qquad (7\text{-}4)$$

where ΔH_f is the enthalpy of fusion, ΔH_{rc} is the enthalpy of re-crystallization occurring during heating cycle and ΔH_f^0 is the enthalpy of fusion of perfectly crystalline structure

of PET at equilibrium thermodynamic melt temperature T_m^0 and was taken as 140 J/g [28].

The results obtained from heating and cooling cycles of rod-like fibers at different carbon nanotube concentrations are summarized in Table 7-3. As expected, addition of carbon nanotubes causes an increase in the crystallization temperature, T_m and in ΔH_f because of nucleation role of CNTs. In addition, carbon nanotube addition changes the cooling cycle and crystallization behavior of the system. The results show that crystallization starts at higher temperature in the samples containing carbon nanotubes as compared to pure PET rod-like fibers. This proves the role of carbon nanotubes as nucleating agent. Moreover, the overall crystallinity, peak of crystallinity and ΔH_c are all higher in the samples containing carbon nanotubes.

Table 7-3: Thermal parameters of rod-like fibers at different CNT concentrations

	T_m (°C)	ΔH_f	ΔH_{rc}	X_c (%)	T_c (°C)	T_0 (°C)	T_∞ (°C)	ΔH_c
Pure PET	252.7	38.3	26.3	8.6	206.9	218.3	177.5	41.0
1% CNT	252.7	38.0	5.2	23.4	219.8	240.2	188.1	41.5
3% CNT	252.6	40.7	5.2	25.4	222.3	243.9	181.3	43.5
5% CNT	252.7	42.7	2.0	29.1	225.4	248.3	186.9	45.9
7% CNT	252.3	44.5	0	31.8	227.2	247.6	191.5	46.0

Rate and kinetics of crystallization are important factors in final structure of PET and its CNT nanocomposites. The time required to reach 50% relative crystallinity ($t_{1/2}$) is usually reported to compare the rates of crystallization of different samples. It is calculated by using the following equation [14]:

$$X_r = \int_{T_0}^{T} qdT \Big/ \int_{T_0}^{T_\infty} qdT \qquad (7\text{-}5)$$

where X_r is the relative crystallinity; q is the heat flow at temperature T; T_0 and T_∞ are the initiation and termination crystallization temperature respectively. The time related to each temperature is obtained through the heating cycle.

The crystallization curves as a function of time during cooling cycle are reported in Fig. 7-8. As the results show, the samples containing carbon nanotubes have higher values of $t_{1/2}$ (half-time of crystallization) compared to pure samples. This result is brought by the good dispersion of MWCNT in our polymer system, numerous individual small carbon nanotubes acting as nucleating agent. Therefore, the crystalline structure form more rapidly and earlier, but it can not grow fast because of spatial constraints and therefore the kinetics of growth slows down. From another aspect, as the temperature of crystallization increases by adding CNT, the internal entropy of the system increases. High entropy favors more polymer chains movement which is opposite to chains localization in crystal cells. Crystal formation from a thermodynamic stand-point is changed to more stable status with lower entropy. Accordingly, the system with higher entropy at higher temperature requires more time for crystalline cell formation. Initiation at higher temperature due to rapid nucleation causes delay in the system evaluation to stable condition because of higher entropy of the system.

The crystalline content of the as-spun fibers at different carbon nanotube concentrations and DRs up to 3 wt% MWCNT concentrations is given in Table 7-4. The crystalline content is reduced when CNT content is increased. This might be the most important reason for the increase in drawability of the fibers. Addition of carbon nanotubes increases the amorphous phase of the nanocomposite in as-spun fibers. Amorphous phase has the most important role in energy dissipation during stretching. Addition of carbon nanotubes accelerates the initiation of crystallization; therefore the system of nanocomposite fibers is expected to contain many crystals of small sizes that connect the amorphous regions next to each other. This causes enhancement of mechanical properties as well as the drawability of nanocomposite fibers.

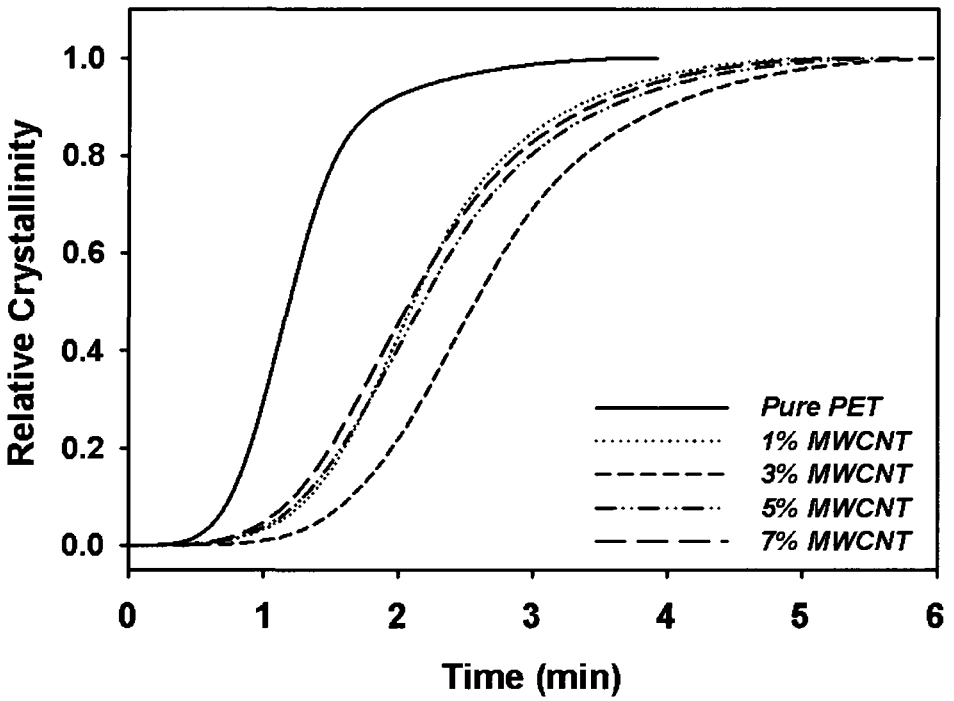

Figure 7-8: Relative crystallinity (%) as a function of time at different carbon nanotube loading during cooling cycle.

Table 7-4: Crystallinity (%) as a function of DR and MWCNT concentration

	20% DR_{max} (112)	60% DR_{max} (291)	DR_{max} (470)
Pure PET	17.2	23.5	Not possible to be produced
1% CNT	16.2	15.8	15.4
3% CNT	16.3	15.4	14.7

7.4.3. CNT and molecular orientation

7.4.3.1. Pure PET fibers orientation (FTIR and Raman Spectroscopy)

Herman orientation equations were used for evaluation of the orientation function. For a uniaxially oriented sample, the dichroic ratio D is defined as:

$$D = \frac{A_{\parallel}}{A_{\perp}} \tag{7-6}$$

where A is the absorbance of a specific band parallel or perpendicular to IR polarizer [29]. Then, the Herman orientation function is obtained according to [25]:

$$f = \frac{D-1}{D+2} \cdot \frac{2}{3\cos^2\alpha - 1} \tag{7-7}$$

where α is the angle between dipole moment of particular vibration and chain axis. Based on the vibration frequency selected in IR test, it is possible to use Herman orientation function for calculation of amorphous or crystalline phase orientation. There are some specific characteristic peaks related to PET in FTIR. The most important ones are: 973 cm^{-1}: CH_2 vibration of trans conformation with α=32°; 1340 cm^{-1}: CH_2 wagging mode of glycol segment in trans conformation with α=21°; 1370 cm^{-1}: the vibration related to gauche conformation; and 1020 cm^{-1}: absorption band attributed to in-plane vibration of C-H group of benzene with α=20° [29, 30].

We selected the 1020 cm^{-1} band for calculations since it is not related to crystalline or amorphous structures [29]; and thus it provides an overall idea about the orientation. All the results were normalized related to the band located at 1410 cm^{-1} [29] (it is not sensitive to anisotropy). The FTIR analysis results show almost the same trend as XRD orientation for crystalline phase orientation (Fig. 7-9). At DR_{max} and 3% MWCNT concentration, a reduction in orientation function is observed. The polymer chains are trapped during crystal initiation at higher CNT concentrations. Therefore, at 3 wt% MWCNT, the chains are trapped by small crystal nuclei and they can not be stretched freely compared to 1% MWCNT. From another aspect, the amorphous chains can not be part of a crystalline cell and thus the amount of total orientation reduces at DR_{max} compared to lower DRs and CNT concentrations only at 3 wt% MWCNT.

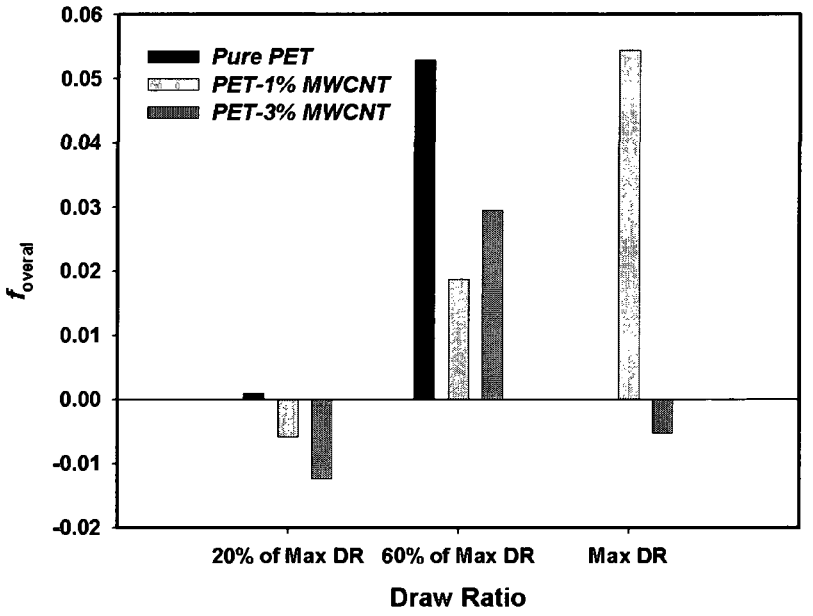

Figure 7-9: Herman orientation function obtained from FTIR analysis at different CNT concentrations and DRs; f_{1020} normalized related to λ=1410 cm^{-1}.

The Raman characteristics peaks of molded PET sample are compared with the ones obtained from oriented fiber structures at different draw ratios both parallel and perpendicular to oriented fibers (Fig. 7-10). As the results show, the peaks parallel (Fig. 7-10 a) to the laser beam are more intense compared to the ones in perpendicular (Fig. 7-10 b) direction which is indicative of orientation.

The change in the intensity of other characteristic peaks at different draw ratios in the samples parallel compared to perpendicular are of great importance. These peaks include: 1310 cm^{-1} related to C-C stretching of the ring in the backbone, 1610 cm^{-1} relative to the stretching of the C_1-C_4 and 1730 cm^{-1} related to stretching of C=O band [14, 31, 32]. All the characteristic peaks of orientation signals are observed here. The most important one is the peak at 998 cm^{-1}, which is related to the crystalline orientation and trans conformational change [32]. This peak is not observed in Raman spectra of molded samples; in addition, there is not such a peak in the Raman spectra of the fibers in perpendicular direction to the beam. This peak is related to the stretching of O-CH_2 and

C-C of the trans conformation of ethylene glycol unit in PET backbone. Existence of this peak in parallel direction shows the orientation of crystalline structures and a part of the amorphous structure close to the crystalline phase since they are related to trans conformation structure [14, 31, 32]. The results of FTIR spectra prove both the existence of molecular orientation and conformational changes during drawing which is correlated to draw ratio.

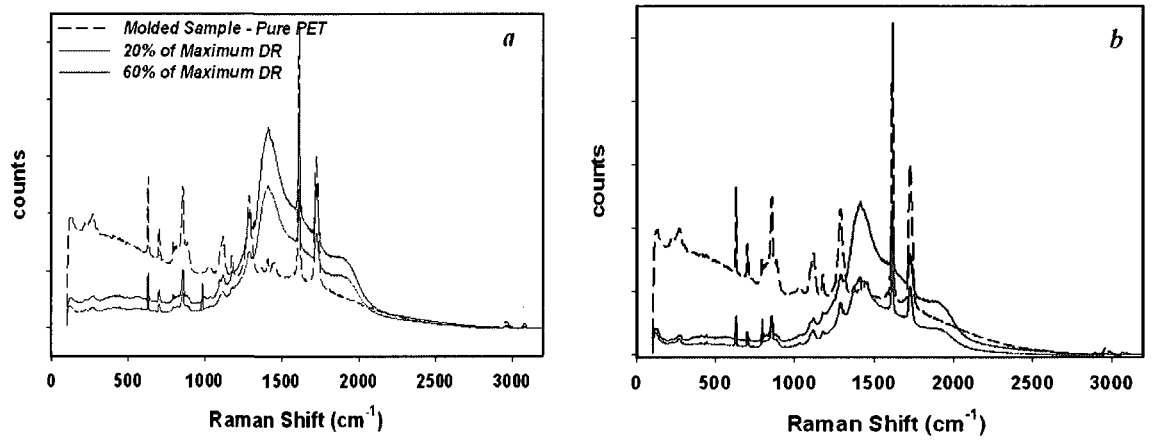

Figure 7-10: Raman spectra of as-spun fibers of pure PET at different draw ratio; a) fibers parallel to polarized light, b) fibers perpendicular to polarized light.

7.4.3.2. CNT orientation study (Raman Spectroscopy)

The same conditions mentioned previously for pure PET fibers for Raman measurements were used for nanocomposite fibers with 1% (Fig. 7-11) and 3% MWCNT (Fig. 7-12) concentrations. The results are given both in parallel (a) and in perpendicular polarization direction (b). In all samples, the Raman spectra are compared to molded samples. Three different characteristic peaks related to carbon nanotubes can be easily observed in the Raman spectra. Two string peaks are located at 1580 cm^{-1} (G), and 1350 cm^{-1} (D) [33-36]. A weak peak is also detected at around 2700 cm^{-1} (G`) which is not sensitive to orientation. G and D peaks are two important peaks related to MWCNT

structure. The intensity of MWCNT in peaks in parallel direction is quite high and they could cover almost all the characteristic peaks of PET, especially in the samples containing 3% MWCNT. The intensity of D and G bands are dependant on draw ratio and the spectra obtained in parallel are quite different from those in perpendicular direction. This could prove the high CNT orientation in the samples as shown previously by morphological study. Especially in the fibers containing 3% MWCNT, the orientation is quite high at maximum draw ratio (Fig. 7-12a).

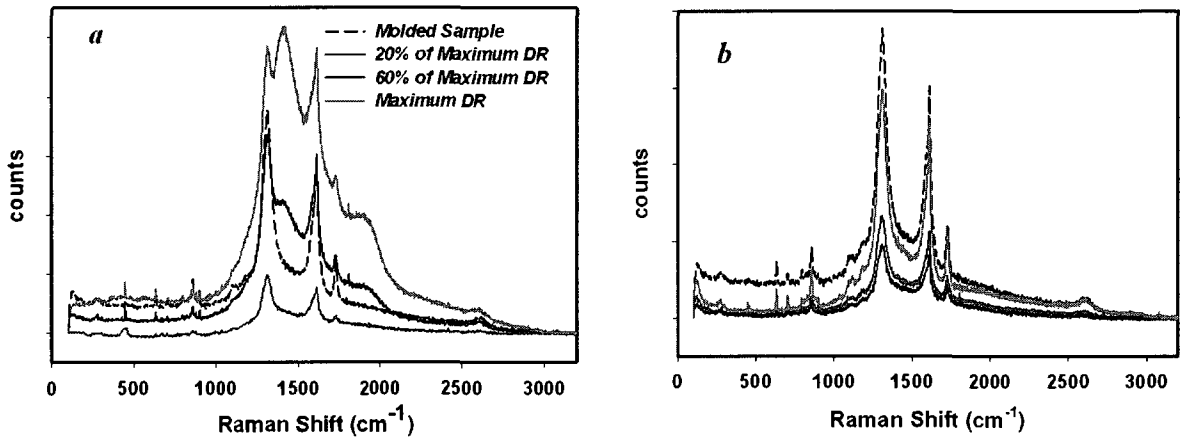

Figure 7-11: Raman spectra of as-spun of PET/1% MWCNT nanocomposite fibers at different draw ratio; a) fibers parallel to polarized light, b) fibers perpendicular to polarized light.

Another interesting point is the change in the orientation characteristic peaks of PET in PET/MWCNT nanocomposite fibers. At high draw ratios of 1% MWCNT nanocomposite fibers, the peaks related to PET orientation appear in parallel direction (Fig. 7-11a). Particularly, the peak located at 1730 cm^{-1} is quite clear; however, no peak could be found in 3% MWCNT nanocomposite fiber (Fig. 7-12a). This could be an evidence of the effect of CNT on orientation and crystallinity. As mentioned previously, the results from Raman spectroscopy prove that addition of carbon nanotube decreases the amount of both orientation and crystallinity of melt-spun fibers.

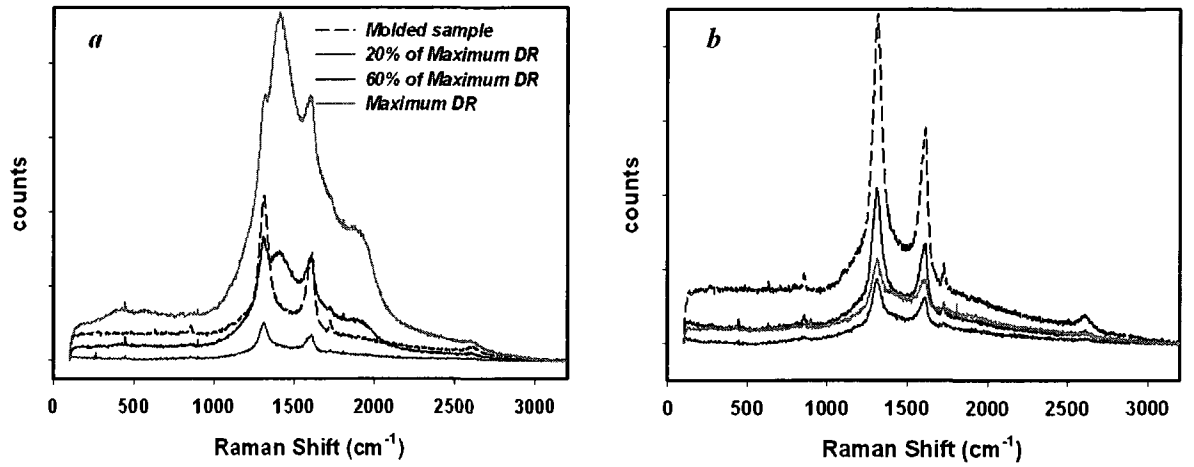

Figure 7-12: Raman spectra of as-spun PET/3% MWCNT nanocomposite fibers at different draw ratio; a) fibers parallel to polarized light, b) fibers perpendicular to polarized light.

Different test methods prove the role of carbon nanotubes in reducing both crystallinity and orientation of PET fibers. For PET/MWCNTs nanocomposite fibers, the morphological analysis test results and Raman spectroscopy techniques show high orientation of CNTs along fiber axis. Similar results and behavior have been repeated in a recent study on PET/clay system [14]. In addition to the reduction in crystallinity and increased drawability by adding carbon nanotube, we could detect a reduction in PET orientation. This has been previously observed in some fibers from polymer blends and PET/clay fibers [14, 37, 38]. When nanoparticles are added, modified shear fields develop around the nanoparticles and therefore the elongation viscosity of the system acting on pure part of fiber is reduced. This in turn will reduce the overall orientation [14, 37, 38]. It is possible to consider the melt spinning system as an iso-strain system. The elongation force is converted into shear at the nanoparticle/polymer interface and therefore applied elongation field on pure polymer phase is reduced [14, 37, 38]. Therefore, followed by stress concentration at interface and nanoparticle phase dispersed in PET matrix, less oriented chains are obtained in nanocomposite fibers compared to pure PET.

7.4.4. Electrical conductivity measurement

The conductivity of different types of samples was measured to study the effect of fiber formation and processing on their final properties. At the beginning, compounded samples were molded into disk-like shapes and their conductivity was measured. The results obtained from their conductivity measurement are compared to rod-like fibers in Fig. 7-13. Both types of samples show percolation threshold at 2 wt% MWCNT concentration. As it can be observed, forming the compound to rod-like fibers causes an increase in conductivity compared to molded sample at the same MWCNT concentration. Rod-like fibers show higher conductivity especially above percolation and after network formation (Fig. 7-13). Higher conductivity of rod-like fibers is the result of partial orientation of MWCNT along fiber axis. Moreover, rod-like fibers reach a plateau region almost at 3 wt% MWCNT concentration. High enough conductivity (0.01 S/cm) is obtained because of good dispersion of carbon nanotubes within PET matrix.

Moreover, we measured the conductivity of fibers of 1% MWCNT (below percolation) and 3% MWCNT (above percolation) in the same way as the other experiments. The conductivity of fibers obtained at different draw ratios is compared to rod-like fibers and molded sample and is presented in Fig. 7-14. As expected, the conductivity of fibers increased by increasing the DR. This effect is clearer in 1% MWCNT and below percolation. The conductivity of fiber at 20% of DR_{max} has increased about one order of magnitude compared to rod-like fibers at the same concentration (1%). At 3%, there is a slight increase in conductivity by increasing DR; however, the effect is not as significant compared to 1% MWCNT concentration. At 3%, the nanocomposite is above percolation and reached a plateau with its ultimate conductivity; therefore, further increasing DR cannot affect considerably the final conductivity.

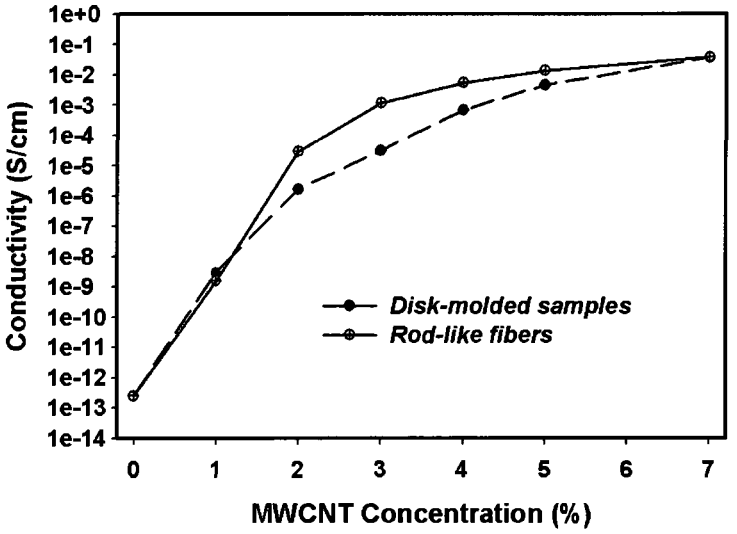

Figure 7-13: Electrical conductivity as a function of MWCNT concentrations.

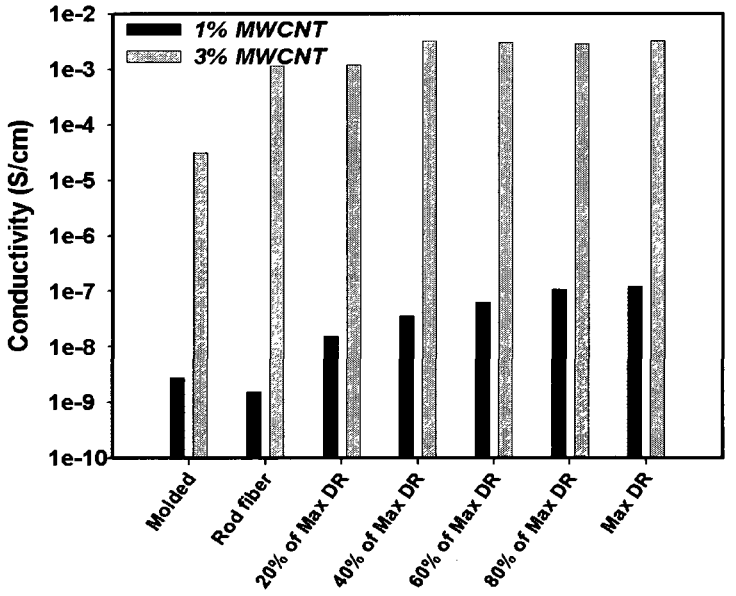

Figure 7-14: Electrical conductivity of fibers at different draw ratio.

The results show that it is possible to decrease the percolation and obtain conductive fibers at lower concentration only by changing processing parameters, particularly by enhancing CNT orientation in the nanocomposite. Finally, our results

show that CNT dispersion and orientation could be the most important determining factor on final conductivities of melt-spun fibers.

7.4.5. Mechanical properties characteristics

At first, mechanical properties of rod-like fibers at different MWCNT concentrations were measured. All the fibers were in the same range of diameter (200-400 μm). Addition of MWCNT decreased the strength, elongation at break and caused a brittle behavior development. In rod-like fibers, there was enough time for the fibers to develop the crystalline structure during their formation. Therefore, addition of MWCNT reduces the amorphous phase concentration. This is probably the reason for the brittle behavior development and reduction in elongation at break from 500% (pure PET) to about 4% (PET/7% MWCNT). The modulus of the fibers at different MWCNT concentrations is given in Table 7-5. As it is shown, addition of MWCNT does not considerably affect the modulus considering experimental uncertainties. A slight increase is observed in the modulus below percolation; while above percolation, modulus decreases. Aggregate formation above percolation and difficulty of MWCNT dispersion in PET matrix above percolation causes a decrease in sample homogeneity. Inhomogeneity could cause stress concentration and weaken the nanocomposite.

Table 7-4: Tensile modulus of rod-like fibers as a function of CNT concentration

	Pure PET	**1% MWCNT**	**2% MWCNT**	**3% MWCNT**	**4% MWCNT**	**5% MWCNT**	**7% MWCNT**
Modulus (MPa)	2327±513	2150±409	2607±186	1859±111	1982±434	2008±567	2084±460

Mechanical properties of as-spun fibers at different MWCNT concentrations were studied for 1 wt% and 3 wt% MWCNT concentrations. The mechanical test results obtained at different DRs are given in Fig. 7-15. As the results show, changing MWCNT concentration and DR does not considerably affect the modulus (Fig. 7-15a) and strength

(Fig. 7-15b). Addition of MWCNT up to 3 wt% slightly increases the modulus of the fibers obtained at different draw ratio, which might be due to the role of MWCNT as reinforcing particle in the melt-spun fibers. Mechanical test results show that addition of MWCNT does not cause a weakening of the mechanical properties at different draw ratios. All the fibers at different MWCNT concentrations and DR show a though behavior and stress hardening was observed in all the samples during the mechanical testing experiments.

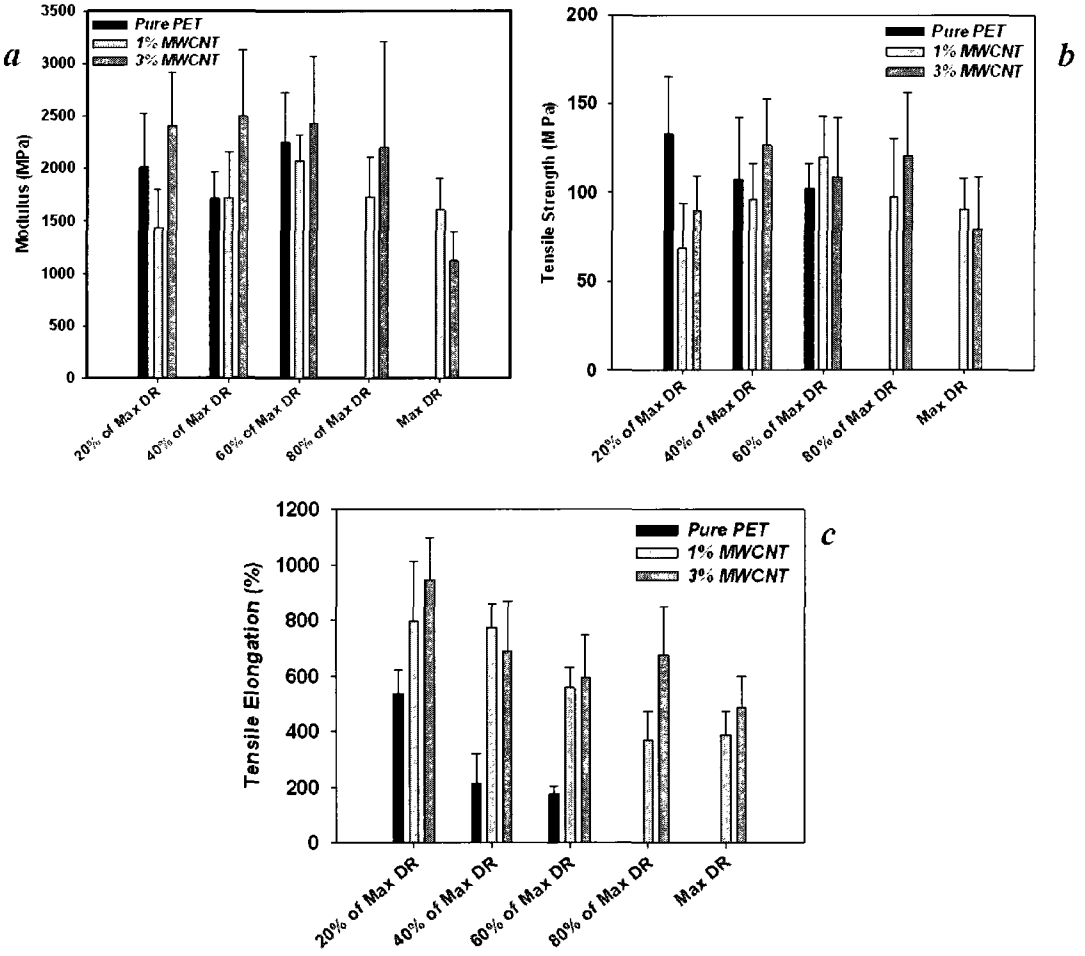

Figure 7-15: Final mechanical properties of fibers at different draw ratios and MWCNT concentrations; a) Modulus; b) Tensile Strength; c) Tensile Elongation.

The results obtained here are in complete agreement with those obtained during fiber spinning. Increasing MWCNT concentration causes an increase in drawability. As the results show, addition of MWCNT to 1% and 3% concentration causes increased drawability up to 3 times compared to pure PET fibers. Fibers containing MWCNT have fewer crystals; however, they have more nucleation for crystal formation initiation. Therefore, the nanocomposite fibers have more amorphous phase. Hence, nanocomposite fiber is composed of polymer chains which are strongly connected to each other in some places; thus, they can better respond to an imposed external stresses. Also, polymer coils in the amorphous phase dissipate more easily the imposed energy. In this way, the fibers produced are in the conductive range; while they have better mechanical properties and significant drawability which is of considerable interest.

7.5. Conclusions

Various morphological and physical properties of PET melt-spun nanocomposite fibers at different MWCNT concentrations and DR were studied in this work. Characterization by microscopy and Raman spectroscopy showed a high degree of MWCNT orientation after fiber spinning. Moreover, it was shown that addition of MWCNT decreases both the crystalline content and polymer chain orientation. DSC results showed that MWCNT slowed crystalline growth which is the main reason for the reduction of crystalline phase formation during melt spinning upon increasing MWCNT concentration. More over, shearing field effect and stress concentration resulting from the MWCNT addition could be the main reason for weakening of the elongation field which caused a decrease in polymer chain orientation after MWCNT addition. Conductivity of single fibers showed that it was possible to reduce the percolation threshold by both dispersion modification and changes in processing conditions. Mechanical test results proved the weakening of properties after percolation because of poor dispersion and

stress concentration. However, addition of MWCNT could incredibly increase the drawability of as-spun fibers and the elongation at break in mechanical test. This was because of the role of MWCNT in the reduction of crystalline formation which favors the dissipation of energy by the amorphous phase; while adhesion of polymer chains to MWCNT nanoparticles is acceptable because of proper dispersion condition of CNT in PET matrix.

7.6. Acknowledgement

The authors would like to acknowledge the financial support of Natural Sciences and Engineering Research Council Canada (NSERC) to this study. We would also like to thank the staff of LCM at University of Montreal for their help in Raman spectroscopy experiments. Finally, we also like to convey an appreciation to Ms. Weawkamol Leelapornpisit for her great help with morphological studies.

7.7. Nomenclature

α	The angle between dipole moment of particular vibration and chain axis (FTIR)
ΔH	Enthalpy (DSC)
θ	The angle between the unit crystalline cell axes (XRD)
A	Absorbance (FTIR)
f	Herman orientation function (FTIR, XRD)
q	Heat flow (DSC)
T	Temperature
w	Weight fraction
X	Crystallinity fraction

7.8. References

1. C.M. Roland, and M.F. Sonnenschein, *Polym. Eng. Sci.* , **31**, 1434 (1991).
2. T.W. Chan, and A.I. Isayev, *Polym. Eng. Sci.* , **34**, 461 (1994).
3. S.P. Rwei, Z.F. Jue, and F.L. Chen, *Polym. Eng. Sci.* , **44**, 331 (2004).
4. S.V. Ahir, Y.Y. Huang, and E.M. Terentjev, *Polymer* , **49**, 3841 (2008).
5. J. Baets, A. Godara, J. Devaux, and I. Verpoest, *Comp. Part A: Appl. Sci. Mfg.* , **39**, 1756 (2008).
6. Z. Hou, K. Wang, P. Zhao, Q. Zhang, C. Yang, D. Chen, R. Du, and Q. Fu, *Polymer* , **49**, 3582 (2008).
7. G. Hu, X. Feng, S. Zhang, and M. Yang, *J. Appl. Polym. Sci.* , **108**, 4080 (2008).
8. S.M. Yuen, and C.C.M. Ma, *J. Appl. Polym. Sci.* , **109**, 2000 (2008).
9. K.P. Ryan, M. Cadek, V. Nicolosi, D. Blond, M. Ruether, G. Armstrong, H. Swan, A. Fonseca, J.B. Nagy, W.K. Maser, W.J. Blau, and J.N. Coleman, *Comp. Sci. Tech.* , **67**, 1640 (2007).
10. D. Wu, L. Wu, G. Yu., B. Xu, and M. Zhang, *Polym. Eng. Sci.* , **48**, 1057 (2008).
11. J.R. Xiao, and J.W. Gillespie Jr., *Polym. Eng. Sci.* , **46**, 1051 (2006).
12. J.K. Keum, H.J. Jeon, H.H. Song, J.I. Choi, and Y.K. Son, *Polymer* , **49**, 4882 (2008).
13. Z. Li, G. Luo, F. Wei, and Y. Huang, *Comp. Sci. Tech.* , **66**, 1022 (2006).
14. D.W. Litchfield, and D.G. Baird, *Polymer* , **49**, 5027 (2008).
15. K. Anoop Anand, U.S. Agarwal, and R. Joseph, *Polymer* , **47**, 3976 (2006).
16. S.H. Jin, Y.B. Park, and K.H. Yoon, *Comp. Sci. Tech.* , **67**, 3434 (2007).
17. H. Kobayashi, M. Shioya, T. Tanaka, and T. Irisawa, *Comp. Sci. Tech.* , **67**, 3209 (2007).
18. S. Tzavalas, D.E. Mouzakis, V. Drakonakis, and V.G. Gregoriou, *J. Polym. Sci. Part B: Polym. Phys.* , **46**, 668 (2008).
19. K.J.Y. Kim, H.S. Park, and S.H. Kim, *J. Appl. Polym. Sci.* , **103**, 1450 (2007).
20. M. Wu, and L. Shaw, *J. Appl. Polym. Sci.* , 477 (2006).

21. G. Hu, C. Zhao, S. Zhang, M. Yang, and Z. Wang, *Polymer* , **47** , 480 (2006).
22. S. Kumar, H. Doshi, M. Srinivasarao, J.O. Park, and D.A. Schiraldi, *Polymer* , **43**, 1701 (2002).
23. H. Ma, J. Zeng, M.L. Realff, S. Kumar, and D.A. Schiraldi, *Comp. Sci. Tech.* , **63**, 1617 (2003).
24. X. Zhang, A. Ajji, and V. Jean-Marie, *Polymer* , **42**, 8179 (2001).
25. K.C. Cole, H. Ben Daly, B. Sanschagrin, K.T. Nguyen, and A. Ajji, *Polymer* , **40**, 3505 (1999).
26. T. D. Fornes, J.W. Baur, Y. Sabba, and E.L. Thomas, *Polymer* , **47**, 1704 (2006).
27. T. McNally, P. Pötschke, P. Halley, M. Murphy, D. Martin, S.E.J. Bell, G.P. Brennan, D. Bein, P. Lemoine, and J.P. Quinn, *Polymer* , **46**, 8222 (2005).
28. A. Mehta, U. Gaur, and B. Wundderlich, *J. Polym. Sci.; Polym. Phys. Ed.* , **16**, 289 (1978).
29. X.F. Lu, and J.N. Hay, *Polymer* , **42**, 8055 (2001).
30. A. Ajji, K.C. Cole, M.M. Dumoulin, and J. Brisson, *Polymer* , **36**, 4023 (1995).
31. J. Purvis, and D.I. Bower, *J. Polym. Sci.; Polym. Phys. Ed.*, **14**, 1461 (1976).
32. S. Yang, and S. Michielsen, *Macromolecules* , **35**, 10108 (2002).
33. E.F. Antunes, A.O. Lobo, E.J. Corat, and V.J. Trava-Airoldi, *Carbon* , **45**, 913 (2007).
34. E.F. Antunes, A.O. Lobo, E.J. Corat, V.J. Trava-Airoldi, A.A. Martin, and C. Veríssimo, *Carbon* , **44**, 2202 (2006).
35. M. Corrias, P. Serp, P. Kalck, G. Dechambre, J.L. Lacout, C. Castiglioni, and Y. Kihn, *Carbon* , **41**, 2361 (2003).
36. W. Chen, X. Tao, and Y. Liu, *Comp. Sci. Tech.* , **66**, 3029 (2006).
37. H. Brody, *J. Appl. Polym. Sci.* , **31**, 2753 (1986).
38. I.S. Miles, *J. Appl. Polym. Sci.* , **34**, 2793 (1987).

Chapter 8

Empirical Modeling of Electrospun CNT-Based Nanocomposite Nanofibers*

8.1. Introduction

The experimental analysis of CNT based electrospun nanocomposite nanofibers could help in fundamental understanding of the effect of CNT addition on final structure and properties of nanofibers. In this part, we study the effect of CNT addition on final nanofibers structure through the preliminary modeling of the electrospinning process. Through this study, it is possible to recognize the effect of CNT on the main controlling parameters and decrease the number of future experiments in this area. The results presented in this section are only primary steps in modeling of polymer/CNT nanocomposite nanofibers. More fundamental study and complementary works are still in progress in our group to finalize and improve the results obtained through this chapter. The modeling procedure includes mainly two different areas. The first part is dealing with studying the cone shaped at the nozzle and deformation to the jet. In this part the effect of CNT addition on changing the shape of the cone and jet initiation and stretching is studied by use of empirical methods and image analysis. The details of various zones characteristics and modeling procedure have been given previously in introduction section. The results obtained in this part are compared with EHD theory to study the applicability of this model for our system. Thereafter, the final nanofiber diameter as a function of measurable material and process parameters is investigated in the second part. We used a dimensional analysis method for the prediction of final nanofiber diameter at different MWCNT concentrations.

---

* ***In preparation***

8.2. Theories and Equations

Similar to previous works in this field, the first modeling part for predicting the final shape of cone and jet is done by employing EHD theory. In this work, the effect of CNT addition is studied by this procedure for the samples containing different concentrations of MWCNTs. All these equations are written for a control volume as shown in Fig. 8-1. In summary, four governing equations of EHD theory for this part of modeling are simplified as follow (Feng 2002):

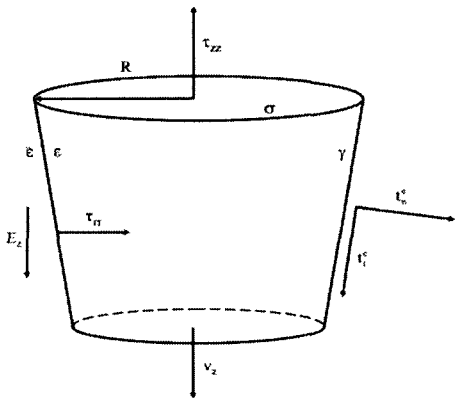

Figure 8-1: Schematic of an element of a jet for EHD theory formulation (Helgeson, Grammatikos et al. 2008)

1) Mass conservation for a fluid of constant density:

$$\pi R^2 v = Q \tag{8-1}$$

where R and v are the radius and velocity respectively and Q is a constant volume flow rate.

2) Charge conservation

$$\pi R^2 KE + 2\pi Rv\sigma = I \tag{8-2}$$

where E is the component of the electric field, K is the electrical conductivity of the liquid, I is the constant total current in the jet and σ is the surface charge density.

3) Momentum equation (details have been given in introduction part)

$$\rho vv' = \rho g + \frac{3}{R^2}\frac{d}{dz}\left(\eta R^2 v'\right) + \frac{\gamma R'}{R^2} + \frac{\sigma\sigma'}{\bar{\varepsilon}} + (\varepsilon - \bar{\varepsilon})EE' + \frac{2\sigma E}{R} \tag{8-3}$$

where ρ is density, γ is surface tension and $\varepsilon, \bar{\varepsilon}$ are the permittivity of the liquid and environment respectively.

4) Internal electrical energy:

$$E(z) = E_\infty(z) - \ln\chi\left(\frac{1}{\bar{\varepsilon}}\frac{d(\sigma R)}{dz} - \frac{\beta}{2}\frac{d^2(ER^2)}{dz^2}\right) \tag{8-4}$$

where $\beta = \frac{\varepsilon}{\bar{\varepsilon}} - 1$ and $\chi = \frac{L}{R_0}$.

These equations in the dimensionless form are changed to (Helgeson, Grammatikos et al. 2008):

$$\pi\tilde{R}^2\tilde{v} = 1 \tag{8-1}`$$

$$\tilde{R}^2\tilde{E}_z + Pe_e\tilde{R}\tilde{v}_z\tilde{\sigma} = 1 \tag{8-2}`$$

$$\tilde{v}\tilde{v}' = \frac{1}{Fr} + \frac{\tilde{T}`}{\mathrm{Re}\tilde{R}^2} + \frac{\tilde{R}'}{We\tilde{R}^2} + \varepsilon\left(\frac{\tilde{\sigma}\tilde{\sigma}'}{\bar{\varepsilon}} + \beta\tilde{E}\tilde{E}' + \frac{2\tilde{\sigma}E}{\tilde{R}}\right) \tag{8-3}`$$

$$\tilde{E}(z) = \tilde{E}_\infty(z) - \ln\chi\left((\tilde{\sigma}\tilde{R})' - \frac{\beta}{2}(\tilde{E}\tilde{R})''\right) \tag{8-4}`$$

where -`- is differentiation along z-direction.

The dimensionless groups and characteristics are defined as (Feng 2002):

Characteristic length: R_0

Characteristic velocity: $v_0 = Q/\pi R_0^2$ (8-5)

Characteristic electric field: $E_0 = I/\pi R_0^2 K$ (8-6)

Characteristic surface charge density: $\sigma_0 = \bar{\varepsilon}E_0$ (8-7)

Aspect ratio: $\chi = \frac{L}{R_0}$

$$\varepsilon = \frac{\bar{\varepsilon}E_0^2}{\rho v_0^2}; \quad \beta = \frac{\varepsilon}{\bar{\varepsilon}} - 1 \tag{8-8}$$

Electrical Peclet number: $Pe_e = \frac{2\bar{\varepsilon}v_0}{KR_0}$ (8-9)

Froude number: $Fr = \frac{v_0^2}{gR_0}$ (8-10)

Reynolds number: $\mathrm{Re} = \frac{\rho v_0 R_0}{\eta_0}$ (8-11)

Weber number: $We = \frac{\rho v_0^2 R_0}{\gamma}$ (8-12)

Most of the modeling procedure is from the point at which jet is developed and stretched. In this work, we are to study the role of CNT addition on jet initiation and stretching. Therefore, we used an empirical method for modeling the first part. A schematic of cone and jet formation is shown in Fig. 8-2. The modeling procedure starts from zone ii, from where the above mentioned governing equations (EHD theory) are valid. The characteristics of zones (ii), (iii) and (iv) have been described previously in Introduction. Zone ii has the largest amount of changes in jet diameter, velocity and strain rate; while these changes are almost zero in zone (iv).

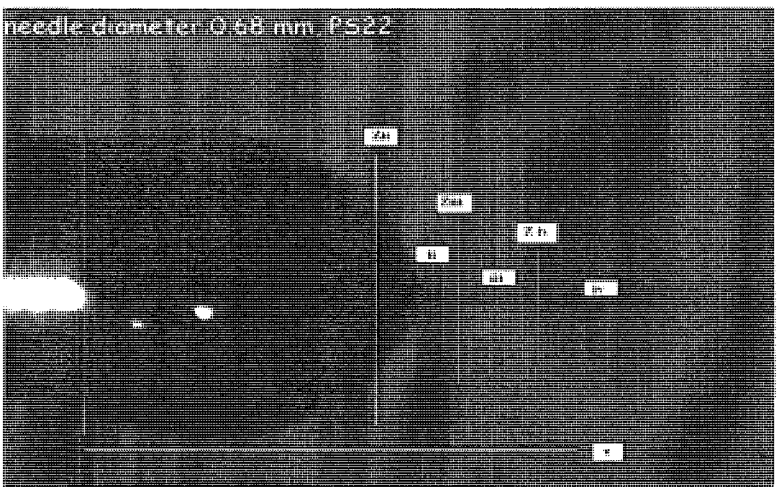

Figure 8-2: Cone and jet obtained by high speed photography for image analysis and different typical zones for modeling.

In the second part of modeling procedure and final nanofiber diameter predictions, we used the newly employed dimensional analysis method. Most of the theories could not give fundamental analysis based on measurable parameters; however, it was possible to obtain the relation between final nanofiber diameter and measurable material and process parameters in this new method. Based on the works available using this theory, it is possible to correlate two important dimensionless numbers: Ohnesorage number (Oh) and electroviscous number (π) as described below (Helgeson and Wagner 2007):

$$Oh = \eta_0 \Big/ \left(\rho \gamma R_f\right)^{1/2} \tag{8-12}$$

$$\pi_1 = \frac{2\bar{\varepsilon}^2 E_0^2}{K\eta_0} \tag{8-13}$$

In this equation, π_1 is a ratio of the electrostatic ($\bar{\varepsilon}E_0^2$) to electroviscous ($\eta K/\bar{\varepsilon}$) stresses experienced by an electrostatically driven fluid jet. This number can be interpreted as a dimensionless stress which is the driving force for jet elongation. As it is shown both of these numbers include material and process parameters, all of which have been described previously. Oh number includes R_f which is final nanofiber wet diameter without considering the solvent evaporation that is correlated to final average fiber diameter through (Helgeson and Wagner 2007):

$$R_f = R_{fiber}(w_p)^{1/2} \tag{8-14}$$

where w_p is polymer mass fraction in electrospinning solution. Based on the theoretical and experimental analysis, it is possible to write down $Oh\alpha(\pi)^n$. The only problem in employing π_1 is that it is a small number of the order of $O(10^{-8})$. Therefore, it is possible to replace it with the following number (Helgeson, Grammatikos et al. 2008):

$$\pi^* = \frac{2(\varepsilon - \bar{\varepsilon})\ E_0^2 R_0^3}{Q\eta_{e,\infty}^+} \tag{8-15}$$

π^* is obtained by similarity to EHD theory equation and permittivity in π_1 is replaced with dielectric constant in π^*. Therefore, this equation is more applicable for final fiber diameter since it includes the rheological data of the solution and it is not a small number like π_1; while π^* includes the extensional rheology of the spinning solution.

E_0 in these equations are defined as electric field strength (voltage/m). We use both of these parameters in this work to give an equation for final diameter of nanofibers with and without MWCNT.

8.3. Experiment

The procedure in this part for sample preparation and the materials is the same as the system described previously in Chapter 5. We used PS with different concentrations of MWCNT to perform the image analysis and measure of voltage and current. The details of sample preparation and electrospinning process have been given in Chapter 5. Electrospinning process was performed at two different flow rates of 0.5 and 0.8 mL/hr to measure current and voltage at different MWCNT concentrations (0%, 1%, 2%, 3%, 4%, and 5%). Material parameters including solution conductivity (K) and viscosity have been reported in Chapter 5. Among the different material parameters three of them, dielectric constant (ε_{DMF}=36.71), liquid surface tension (γ=36.5 mN/m) and density (ρ=1.1 g/cm^3), were assumed constant during calculations. All other parameters were obtained and considered as a function of MWCNT concentrations. The results of a previous study on similar systems show that addition of MWCNT even above percolation only changes γ as much as 30% (Seoul, Kim et al. 2003). Therefore, we have considered this parameter in addition to constant ρ through all the calculations below and above percolation. ε changes with MWCNT concentration and considerably increases above percolation. However, we are only using this parameter for low concentrations of MWCNTs (below 2 wt%). At low range of CNT concentration, it is possible to ignore the small changes of ε by MWCNT addition (Liang and Tjong 2008). The results obtained from final fiber morphological study and estimation of final nanofiber diameter has been given in Chapter 5. We use the results obtained from the experimental section here for our final analysis. In addition to precise measurement of voltage and current during the experiments, we used high speed photography. By this technique, we could obtain final

shape of the cone and jet at equilibrium condition. A typical image obtained during the photography is given in Fig. 8-2.

8.4. Results and Discussion

8.4.1. Image analysis results

In this part, we use the results obtained from high speed photography to calculate the averaged fiber diameter along jet axis. The measurements were performed in three zones: zone (ii): jet initiation; zone (iii): jet stretching and zone (iv): jet thinning. Image analysis was done on ten images (similar to the image shown in Fig. 8-2.) that were selected in stable electrospinning conditions. The calculations were done at different CNT concentrations at 30 points over the entire jet length (Q=0.5 mL/hr).

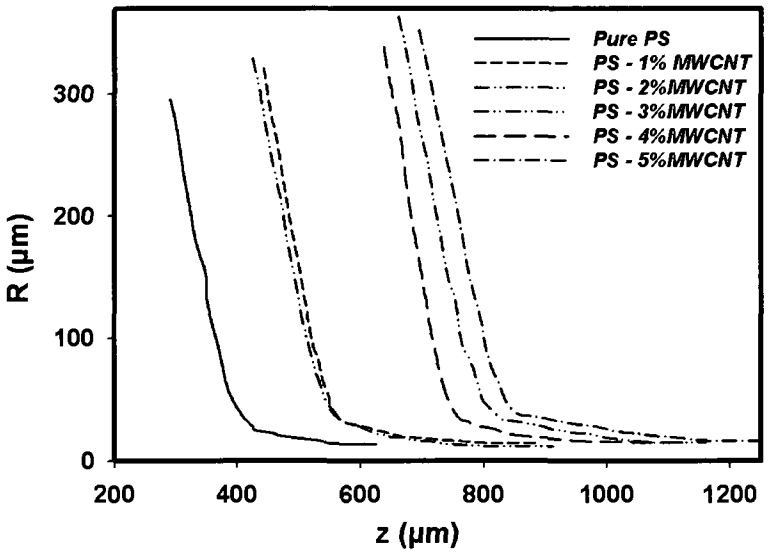

Figure 8-3: Jet radius profile along jet axis at different MWCNT concentrations

As it is shown, CNT concentration influences the shape of the cone. Jet radius decreases sharply at the beginning of jet initiation which is known as zone (ii); however,

these changes are less considerable in zones (iii) and (iv). Addition of CNT causes more conductivity of the solution and therefore the voltages required to obtain the stable condition increases. As a result the size of cones increases. In the system containing MWCNT, jet initiation and zone (ii) is initiated later than in pure PS because of larger size of the cone shaped region during the electrospinning. The radius profile shows that followed by adding MWCNT concentration to 1wt% and 2wt%, there is a shift in jet initiation (z(ii)) and the cone is larger for the first step. However, the cones containing 1wt% and 2wt% MWCNT show quite similar functionality for the radius. As mentioned previously, the system of our study is below percolation for this range of concentration and the addition of MWCNT does not considerably change the stable condition of electrospinning, the shape of cone and the zone of jet initiation. By adding MWCNT to the concentration above percolation, another change occurred and the zone for jet initiation is shifted once more to higher values. It shows that when the system goes above percolation, another change in equilibrium condition of the cone occurs and the cone becomes larger. Therefore, the samples containing 3 wt%, 4wt% and 5wt% show almost similar trend and they include a larger cone size at higher z (ii). The analysis will be performed over pure PS, PS/1%MWCNT (after the first shift in equilibrium condition) and PS/3%; PS/5% MWCNT (after the second shift in radius profile and equilibrium condition).

Table 8-1: Different zones characteristics and process parameter at different MWCNT concentrations (Q=0.5 mL/hr)

	R_0 (μm)	Z(ii) (μm)	Z (iii) (μm)	Z (iv) (μm)	*Voltage (kV)*	*Current (μA)*
Pure PS	678	285	430	550	17.5	2
PS/1%MW	687	430	590	780	22.5	3
PS/2%MW	695	420	595	770	21.5	5
PS/3%MW	698	650	850	1050	21	4
PS/4%MW	683	650	825	1000	23	6
PS/5%MW	700	680	880	1140	23	7

The summary of different regions obtained through image analysis at Q=0.5 mL/hr along with process parameter are given in Table 8-1. These values, in addition to different material parameters are used in the following modeling procedure. The results of studying the radius profile show that jet radius has the following functionality along jet axis (Helgeson, Grammatikos et al. 2008):

$$R = Az^{-n} + Bz^{-1/2} + Cz^{-1/4} \tag{8-16}$$

The results of image analysis obtained here show the same trend and functionality of z for jet radius (Fig. 8-3). The power (n) in zone (ii) is accounted for as one of the system characteristics depending on material and process parameters. The result of n-calculation at different MWCNT concentration is given in Fig. 8-4.

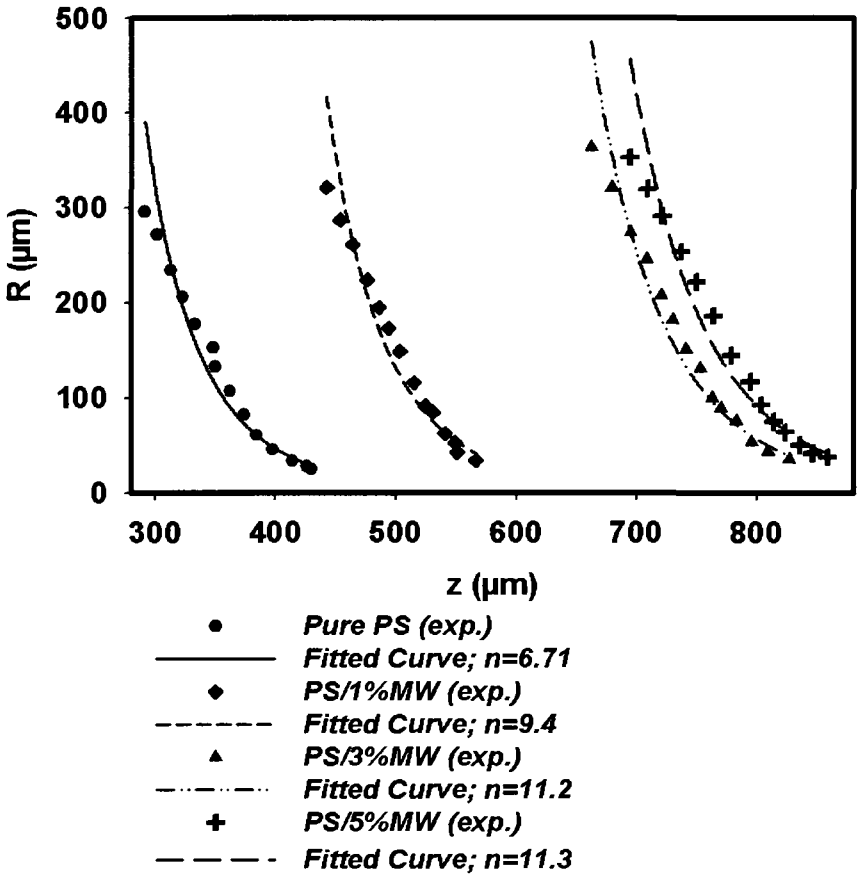

Figure 8-4: Empirical modeling of radius profile along jet axis to calculate the power (n)

As the results show, the power (n) increases by increasing the MWCNT concentration. It shows that in spite of the fact that MWCNT causes a delay in jet initiation; however it causes acceleration in jet radius decrease after jet initiation. This effect might be because of the charge accumulation inside the cone for conductive material. Followed by higher charge accumulation in conductive materials, they are inclined to increase the surface more rapidly to reduce the surface charge density and to obtain more stable condition. Therefore, the value of n is increased by increasing MWCNT concentration and the procedure of reduction in jet radius in zone (ii) is accelerated in more conductive materials.

In addition it is possible to calculate the velocity profile along jet axis by the use of following equation:

$$v(z) = Q / \pi R(z)^2 \qquad (8\text{-}17)$$

We calculated velocity profile at different MWCNT concentration following image analysis results and calculating R(z) and equation 8.17. The velocity profiles along jet axis are shown in Fig. 8-5.

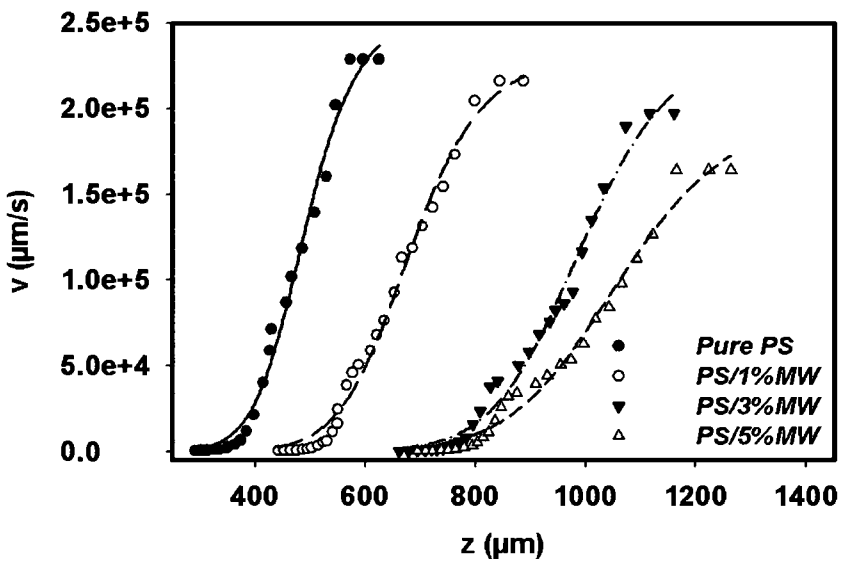

Figure 8-5: Velocity profile along jet axis at different MWCNT concentration

As it was shown previously, jet initiation and acceleration is delayed by adding MWCNT concentration. The velocity shows almost the same value for pure PS and PS/1%MWCNT. However, by increasing MWCNT concentration above percolation the velocity is reduced in jet stretching (z(iii)) and jet thinning (z(iv)) zones. The reduction in jet velocity above percolation could be mainly because of the electrospinning solution viscosity increase due to higher MWCNT content (viscosity is increase by adding CNT to concentrations above percolation as reported previously in Chapter 5). Increasing both MWCNT concentration and the probability of forming the agglomerations at high CNT content is the main reason for the reduction in the value of velocity during the jet formation process compared to the samples below percolation.

From the velocity profiles obtained in the previous part, it is possible to calculate the elongation (extension) rate along jet axis during the electrospinning process at different MWCNT concentrations (Fig. 8-6.).

$$\dot{\varepsilon} = v'(z) \tag{8-18}$$

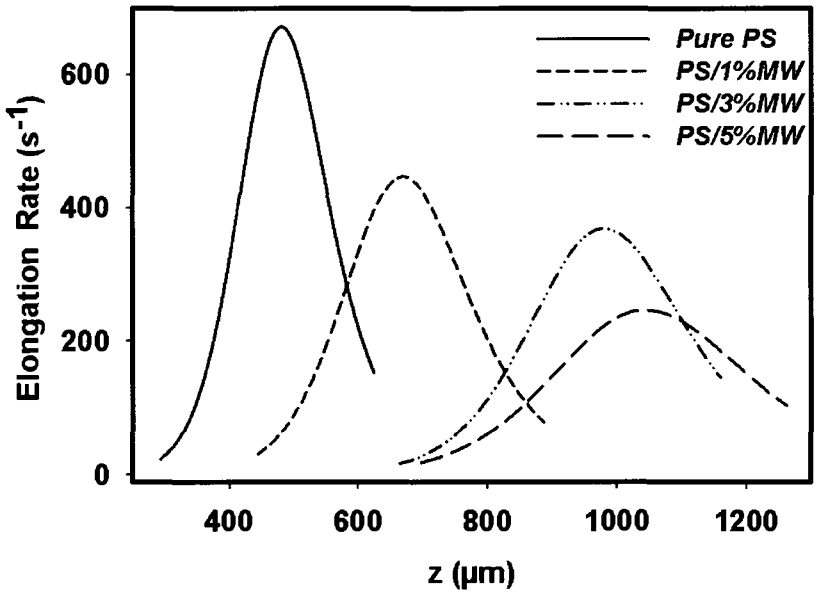

Figure 8-6: Elongation strain rate ($\dot{\varepsilon}$) profile along jet axis at different MWCNT concentrations

The profile of $\dot{\varepsilon}$ was obtained through numerical differentiation of v profile over z-axis. As the results show, $\dot{\varepsilon}$ passes a maximum for all the MWCNT concentrations. A sharp decrease in radius which causes an increase in the velocity is the main reason for the increase in $\dot{\varepsilon}$ in z(ii). The peak is almost located close to the third region initiation (z(iii)). Following by this sharp increase, the change in velocity profile causes $\dot{\varepsilon}$ to slow down and decreases to finally reach a constant value. As it is shown, the value of $\dot{\varepsilon}$ is reduced by increasing MWCNT concentration which might be the effect of viscosity as mentioned previously. The higher viscosity in addition to MWCNT aggregates could cause decrease in the amount of $\dot{\varepsilon}$ in concentrations above percolation where the viscosity increases. Therefore, in the samples containing MWCNT, the solutions are prepared for entering the splashing region a bit later in time compared to pure PS. From another aspect, the delay in jet thinning and reduction in the value of $\dot{\varepsilon}$ in MWCNT containing electrospun fibers causes a broad $\dot{\varepsilon}$ distribution function along jet axis. This might come from the change in electric field during electrospinning and of CNT-containing conductive solutions.

Elongation flow of electrospinning and its characteristics have always been one of the main points of interests in this process. Hencky strain as another important characteristic of electrospinning process is calculated here. The calculation of strain rate could be made with a good approximation by the following equation along jet axis (Fig. 8-7):

$$\varepsilon(z) = Ln(R_0 / R_{(z)}) \qquad (8\text{-}19)$$

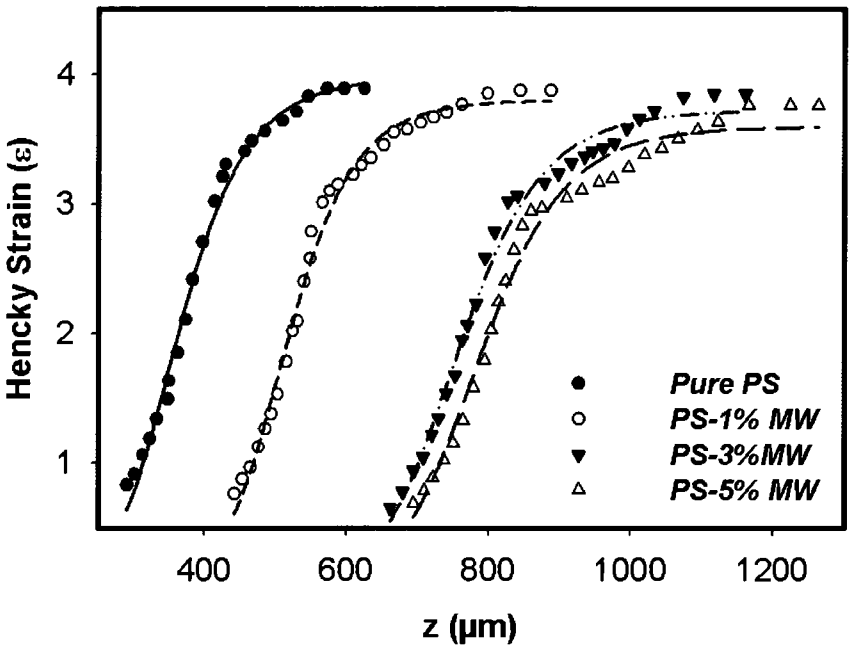

Figure 8-7: Hencky strain profile along jet axis at different MWCNT concentration

All the samples show almost the same trend in changing the amount of ε along jet axis. The only difference among various samples is the delay in the region where the increase in Hencky strain becomes significant and the other trend is the same for all samples. The interesting point here is that the final value of Hencky strain in all samples is almost the same in all liquid solutions as shown above and it is does not depend on MWCNT concentration. The results of image analysis show that the final diameter of the jet in zone (iv) is almost the same and they include equal diameters at different MWCNT concentrations. Therefore, the final strain is almost the same but the initiation of the zones is different.

8.4.2. Comparison with EHD theory

We used the simplified forms of EHD theory equations to compare the obtained results from image analysis with those equations from EHD theory. Regions (ii) and (iii) include the most important changes among the areas studied so far. The equations in these two regions are simplified to the following forms:

$$\tilde{R}\tilde{E}_z = 1 \qquad (8\text{-}2\text{-ii})$$

$$\frac{\tilde{T}'}{\mathrm{Re}_{jet}\tilde{R}^2} + \varepsilon\beta\tilde{E}_z\tilde{E}' = 0 \qquad (8\text{-}3\text{-ii})$$

where:

$$\tilde{T} = \tilde{R}^2(\tilde{\tau}_{rr} - \tilde{\tau}_{zz}) \qquad (8\text{-}20)$$

In these equations, the inertia, gravity and surface tension are neglected, the proof of these assumptions have been given previously. In all these simplifications and modeling, some important assumptions are to be considered: 1) a pseudo-steady elongation flow which results into: $\eta_e^+ = \eta_{e,\infty}$; 2) a pseudo-Newtonian behavior which results into: $Tr_\infty = \frac{\eta_{e,\infty}}{\eta} = \frac{3\eta_0}{\eta_0} = 3$; 3) Existence of stain hardening by the elongation flow field during electrospinning. By considering the above mentioned assumptions, the equations in zone (iii) are simplified as follow:

$$\tilde{T} = Tr_\infty(\tilde{R}^2\tilde{v}') \quad \text{(Newtonian behavior)} \qquad (8\text{-}21)$$

$$\tilde{R}\tilde{E}_z = 1 \qquad (8\text{-}2\text{-iii})$$

$$\frac{(\tilde{R}^2 v_z)'}{\tilde{R}^2} + \pi_\infty\tilde{E}_z\tilde{E}_z{}' = 0 \qquad (8\text{-}3\text{-iii})$$

where $\pi_\infty = \varepsilon\beta\,\mathrm{Re}_{jet}/Tr_\infty = (\varepsilon - \bar{\varepsilon})E_0^2R_0^3/\pi\eta_{e,\infty}Q$; the parameters are the same as the ones described previously in EHD theory equations. Followed by solving equation (8-3-iii) simultaneously with other governing equations and assuming almost the velocity equal to zero at the point of jet initiation and rearranging the equations, it is possible to write:

$$\tilde{R} = [\pi_\infty(\tilde{z} - \tilde{z}(iii))]^{-1/2} \qquad (8\text{-}22)$$

$$\tilde{v} = [\pi_{\infty}(\tilde{z} - \tilde{z}(iii))] \tag{8-23}$$

We are to use these two equations to check the validity of EHD theory for this system. The results of image analysis prove almost the same behavior of R and v functionality along jet axis as described previously in empirical method of solution. However, we could not obtain a proper agreement between the image analysis results and the ones obtained for EHD theory (equations 8-22 and 8-23). For instance equation 8-23 predicts constant value of $\dot{\varepsilon}$ in zone (iii); while the results of experiments show some changes in the value of $\dot{\varepsilon}$ in this region. We tried to use the predictions of EHD theory for pure PS system in a first step, but the predictions of this model with the above mentioned assumptions were far from the empirical results for both R and z. Because of the difference among the values obtained from the theoretical predictions and empirical method results, the results are not reported here. The assumption of Newtonian behavior to solve the above mentioned equations might be the main reason for the incompatibility between the theoretical and experimental data. Therefore, we thought of obtaining an assessment about the elongation viscosity to describe the difference between the empirical and theoretical results. As reported previously, by rearranging equations 8-22 and 8-23, it is possible to define apparent the elongational viscosity in zone (iii) as follows:

$$\eta_{e,app} = \frac{(\varepsilon - \bar{\varepsilon})E_0^2 R_0^2 v_0}{\pi Q \dot{\varepsilon}_{iii}} \tag{8-24}$$

The results obtained from calculating $\eta_{e,app}$ as a function of strain rate and z are given in Fig. 8-8. As the results show the amount of viscosity and strain hardening is much more than expected. The value of η_0 was almost 0.2 Pa.s in pure PS solution. Even though, an increase in the amount of elongation viscosity is expected; however, the values obtained from the modeling are far beyond the expectations.

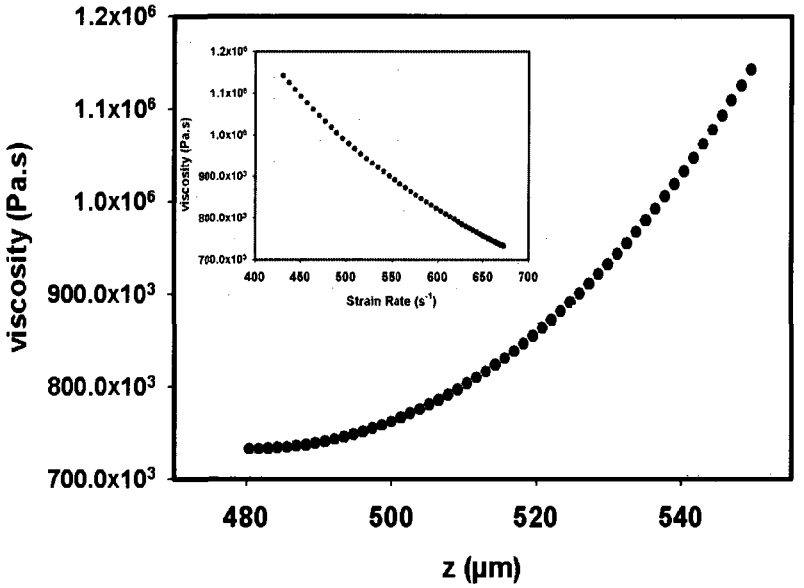

Figure 8-8: Viscosity profile as a function of z and $\dot{\epsilon}$ in pure PS electrospinning liquid

The results of viscosity profile obtained through theoretical modeling shows that assuming Newtonian behavior in this system could be an improper assumption in solving the EHD theory. We are using a high concentration of high molecular weight PS solution (20 wt/v%). Therefore, elastic behavior might be an important determining factor in this case. While the elastic characteristics of polymer solution has been totally ignored during these calculations. Neglecting the term related to viscoelasticity of polymer solutions causes fundamental error in solving the EHD theory, and this might be the main reason the empirical results do not show acceptable compatibility with the results of theoretical solution of EHD theory. It is suggested here that the momentum equation be solved by assuming viscoelastic model for polymer solution and then the results be compared with the results form experiment for pure PS system. While in the case of electrospinning of nanocomposite solutions, more fundamental changes on governing equations of EHD theory are required.

8.4.3. Dimensional Analysis

We used dimensional analysis method here to estimate the final nanofiber diameter. We used both the scaling factors of $Oh\alpha\pi_1^n$ and $Oh\alpha\pi^{*n}$ here. To employ these relations for this system, the electrospinning was performed at different MWCNT concentrations and two different flow rates of 0.5 and 0.8 mL/hr. The final nanofiber diameter was estimated by image analysis on the final diameter of electrospun samples. The morphological analysis and the results obtained have been reported previously in Chapter 5 and the results of morphological analysis are used here.

In first step, we used three types of solutions of 0 wt%, 1 wt% and 2 wt% to study the validity of the relation of $Oh\alpha\pi^{*n}$ for this system. We could not use the solutions of higher MWCNT concentration here. At MWCNT concentration above percolation the assumption of constant dielectric constant mentioned before is not true. Above percolation, dielectric constant increases considerably and therefore the changes as a function of MWCNT concentration cannot be neglected. Therefore, we only use this relation for three low concentrations of MWCNT. Here, we neglect the addition of MWCNT and the role it plays on the characteristics of the solution. Therefore, it is possible to do the curve fitting on nanocomposite samples in a single line with pure PS. Otherwise, straight line only passes through the samples of quite similar materials. We also considered $Tr=3$ during these calculations. The results of our analysis on six different samples are shown in Fig. 8-9. As it is shown, it is possible to obtain a straight line in logarithmic scale with a scaling factor of n= -2/5. The straight line and the scaling factor are in the accepted range for this system. Therefore, it is possible to estimate the changes of nanofiber diameter as a function of measurable material and process parameters as follow:

$$R_{fiber} \alpha \sqrt{w_p} \times \frac{\eta_0^2}{\rho\gamma} \times \left(\frac{(\varepsilon - \bar{\varepsilon}) E_0^2 R_0^3}{\eta_{e,\infty} Q} \right)^{4/5} \tag{8-25}$$

The result of analysis shows that it is possible to predict average nanofiber diameter by equation 8-25. This equation is only applicable for the concentrations below percolation since the change of electrical properties after addition of MWCNT concentration has been neglected in this equation.

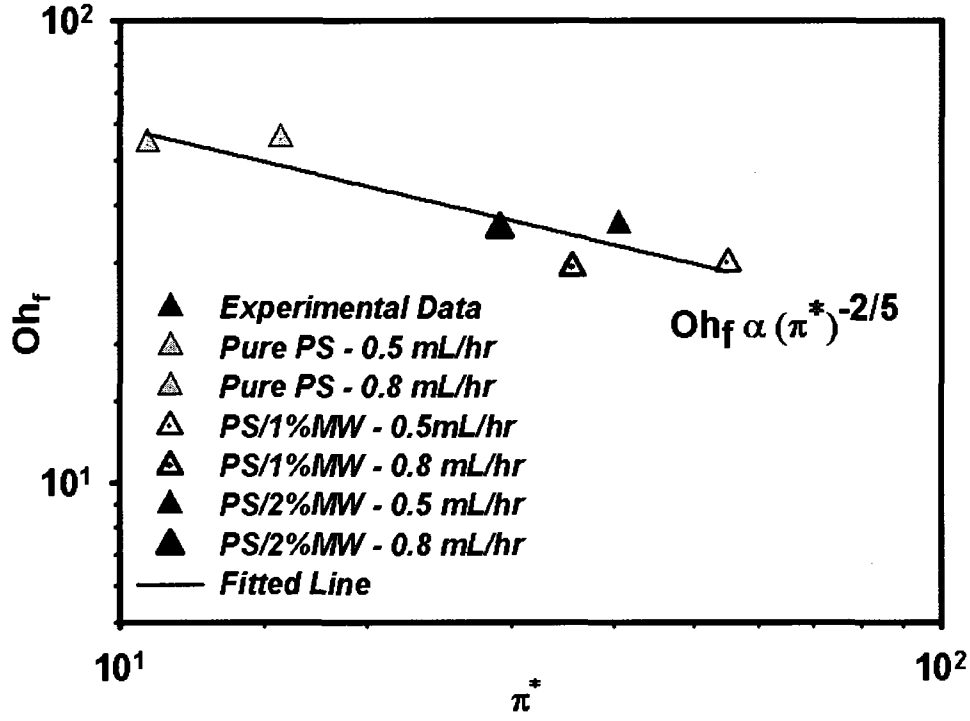

Figure 8-9: Oh_f vs. π^* at different MWCNT concentration and flow rates below percolation

We used the relation between Oh and π_1 in the second step here to predict the final nanofiber diameter for a wide range of MWCNT concentrations $Oh \alpha \pi_1^n$. π_1 includes K and we can consider the change in electrical properties of the solution followed by adding MWCNT concentration. Since the value of K as a function of MWCNT concentration has been obtained previously. In this way, the assumption of constant electrical properties is not considered anymore in the calculations. We employed this relation here only for MWCNT containing solutions. The same as previous step, the solutions were prepared at

different MWCNT concentrations. The voltage and final nanofiber diameter were measured in each concentration and the dimensionless numbers Oh and π_1 were calculated in this way. The results obtained are given in Fig. 8-10. As it is depicted in this figure, it is possible to scale Oh and π_1 in logarithmic scale with a good approximation and therefore it is possible to write:

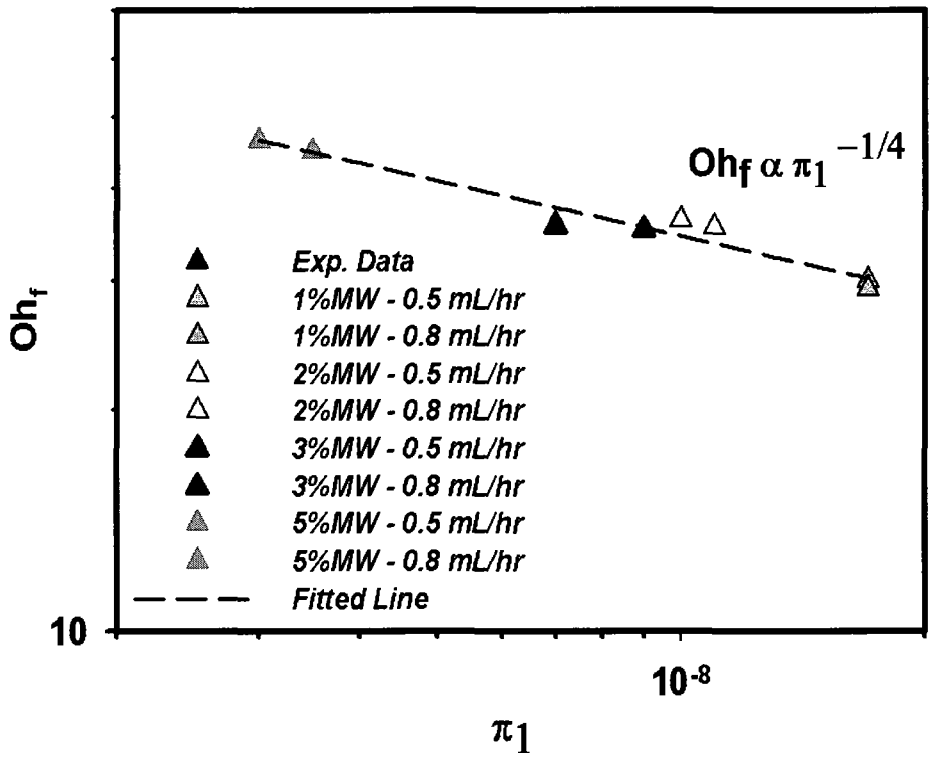

Figure 8-10: Oh_f vs. π_1 at different MWCNT concentration

$$R_{fiber} \alpha \sqrt{w_p} \times \frac{\eta_0^2}{\rho\gamma} \times \left(\frac{\bar{\varepsilon}^2 E_0^2}{K\eta_0} \right)^{1/2} \qquad (8\text{-}26)$$

It is possible to estimate the average nanofiber diameter as a function of different parameters in different MWCNT concentrations by this method.

8.5. Conclusion

In conclusion, through this empirical modeling:

1. The change in jet formation and velocity profile at different MWCNT concentrations were analyzed by the use of image analysis technique and high speed photography.

2. The applicability of EHD theory and the assumptions made in this theory and the role of simplifications were investigated. The results show that with the imposed assumptions, this model is not applicable in our system.

3. Two equations for estimation of final average nanofiber diameter were proposed by using dimensional analysis method. The results obtained were compared with the experimental data available.

As discussed previously, the results obtained here are only the first steps in modeling the electrospinning of polymer/CNT nanocomposite nanofibers. These preliminary results are quite helpful in recognizing the most controlling parameters during the electrospinning of polymer/CNT nanofibers and reduce the number of experiments in future works. Meanwhile, more efforts on the modeling part are in process to complete, improve and clarify the results obtained in this chapter in our group.

Chapter 9

General Discussion

Dispersion of CNT in initial solution before electrospinning is one of the most important controlling factors of processing condition besides the final morphology and properties of nanofibers. Fiber formation causes high degree of CNT orientation along fiber axis and it is known as one of the best methods for CNT orientation. One dimensional structure and high degree of orientation reduces the percolation threshold to lower levels and small amount of CNT. In CNT-based conductive fibers especially nanocomposite nanofibers, high range of conductivity is obtained even at very low concentration of CNT. Therefore, the works concerning the study of a single nanofiber are not dealing with the subject of dispersion problem, since they are mostly dealing with CNT concentrations up to maximum 1 wt%. Studying CNT-containing nanofiber which shape conductive non-woven mat as final electrospinning product has some difficulties in the dispersion field. Investigating the final conductive mat means a non-woven made of nanofiber stacks in which the conductivity along fiber axis is less important than the conductivity between layers. In final non-woven mat, it is required to have high CNT concentrations to obtain conductive mat. Since we investigated final non-woven mat, we were to use high concentrations of CNTs for manufacturing conductive membrane. At this high level of CNT concentrations, dispersion is usually more complicated and more problem making in conductive nanofiber manufacturing.

The effect of dispersion was studied in this work in PS/CNT nanofibers. The results obtained prove that dispersion is accounted as a controlling factor of final morphology and properties. It was shown that poor dispersion can be accounted as one of the most important factors in bead formation along fiber axis besides other instabilities during electrospinning. In addition, it was depicted that it is possible to control final electrical conductivity by modifying the dispersion condition. Well-dispersed CNTs with the aid of copolymer show higher conductivity compared to the fibers containing pure

CNTs. The dispersion condition was also shown as an important controlling factor in both PET/CNT electrospun and melt-spun fibers. Followed by modifying the dispersion condition in PET/CNT nanofibers, more smooth fibers were obtained and less bead structures were detected along fiber axis compared to PS/CNT at equal amount of CNT concentrations. Poor dispersion causes larger fiber diameter at low CNT concentration below percolation threshold of PS/CNT nanofibers; while this effect is not observed in PET/CNT electrospun nanofibers. Comparing the morphological observation results obtained from these two systems approve the important role of dispersion as a significant controlling factor at different CNT concentrations especially at high CNT levels (Figure 9-1). The effect of dispersion was the same in all types of CNTs including SWCNT, DWCNT and MWCNT and similar observation was obtained by comparing these three systems. In PET/CNT melt-spun fibers, it was also found that the dispersion condition is an important determining factor. Comparing the results obtained of conductive fibers with those from the previous works prove that the amount of percolation is reduced to 2 wt% by modifying the dispersion condition of CNTs in PET matrix.

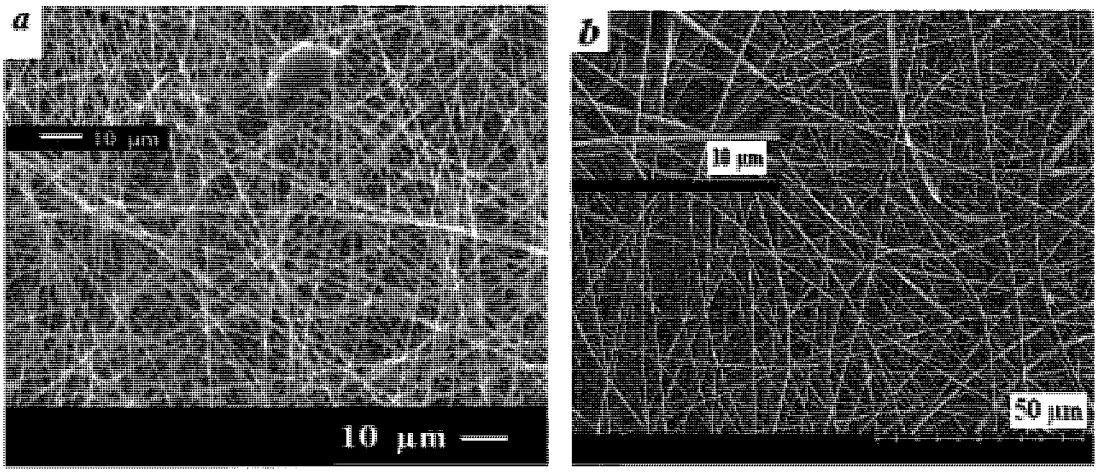

Figure 9-1: PS/CNT electrospun nanofibers (a) compared to PET/CNT (b) at 3 wt% MWCNT concentration

The effect of adding different types of CNTs and sipersion condition was studied for the first time in electrospun samples in this work. We have only used physical method

of dispersion; therefore, we could make an overall comparison over all types of CNTs without changing their surface structure. The results obtained show that in spite of the fact that SWCNT show considerable enhancement in electrical conductivity by its unique structure; it is more difficult to be dispersed. Poor dispersion of SWCNT and even DWCNT because of their smaller sizes compared to MWCNT is an important influencing factor especially at high concentrations of CNTs. The results obtained from PS/CNT showed higher value of electrical conductivity at 5 wt% SWCNT compared to the other types of CNTs. Nevertheless, good dispersion and compatibility of MWCNT with PET matrix causes much more enhancement in both electrical and mechanical properties compared to SWCNT. Therefore, the results obtained from SWCNT, DWCNT and MWCNT and especially full characterization of final properties of PET/CNT electrospun nanofibers prove that MWCNT is more preferred at high CNT concentration. Even though, SWCNT is the best type of CNT for enhancement of conductivity; the results obtained here from both electrical and mechanical properties measurement demonstrate that MWCNT is a better choice at high CNT concentrations. Therefore, from a general view, we would propose MWCNT for high concentrated CNT nanocomposite nanofibers.

PET/CNT electrospun nanofiber was studied in parallel to PET/CNT melt-spun micro-fibers as the main material to be considered in this thesis. Melt-spun fibers were produced at different MWCNT concentrations and draw ratios while nanofibers were produced at different CNT concentrations and types. In electrospun nanofibers, addition of CNTs causes increases in the conductivity and decrease in nanofiber diameter; therefore, increasing CNT concentration acts the same as increasing DR in melt-spinning since it causes decrease in nanofiber diameter. Increasing the draw ratio is obtained by increasing the electrical conductivity and electrical force acting on nanofibers in electrospinning; while it is obtained by increasing collection speed in melt-spun microfibers. Melt-spun fibers were more difficult to be produce because the complicated step of twin-screw dispersion and dispersion modification before spinning; while mixing stage is more straightforward in electrospinning process than melt-mixing. Electrical

conductivity as the main parameter of study shows the same value of around 2 wt% MWNT as electrical percolation threshold for both melt-spun and electrospun fibers.

Similarities obtained from mechanical test results were quite interesting. CNT addition causes changes in the amount of crystallinity and PET chains orientation. The change in crystallinity and orientation do not show similar trends as a function of CNT concentration (The functionality is different below and above percolation as mentioned previously). However, addition of CNT in both electrospun and melt-spun fibers causes considerable increase in the amount of maximum elongation at break. In melt-spun fibers, addition of CNT causes increase in the amount of drawability during melt-spinning process and finer fiber production. This effect is also observed in both types of nanofibers and microfibers after processing and during mechanical experiments. In electrospun nanofibers, drawability is somehow increased by adding CNT; since increasing CNT concentration causes finer fiber production and it acts the same as increasing the draw ratio (Figure 9-2). As mentioned previously, it seems as if the addition of CNTs decreases the crystallinity and PET chains entering the crystalline cells. In molten state, it causes both decrease in crystallinity and orientation; however, in nanofibers, CNT causes the change of formation of crystalline to oriented chains more preferably. This is the main reason for increasing the maximum elongation at break besides drawability of final CNT-based nanocomposite fibers obtained from both of these processes. This effect is not obtained in aligned PET/CNT nanocomposite nanofibers at different CNT concentrations. In aligned nanofibers, the degree of alignment changes by increasing CNT concentration; therefore, the degree of alignment is included as another parameter in calculations and it is not possible to make comparison in this case.

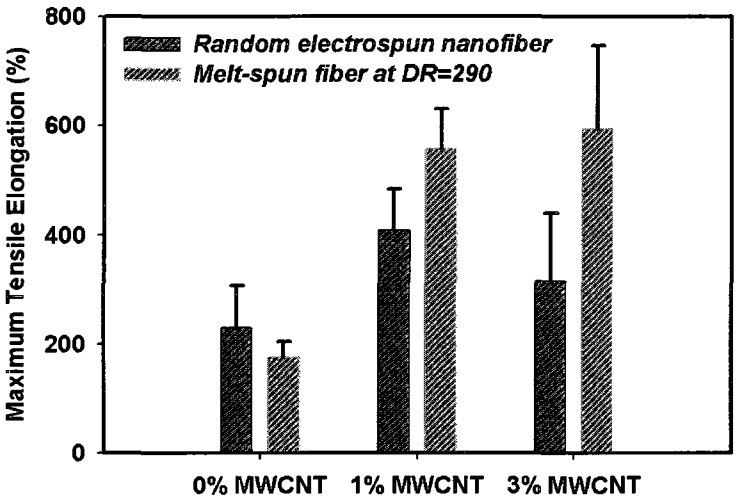

Figure 9-2: Comparison of maximum elongation at break in electrospun and melt-spun fibers at different CNT concentrations

Followed by comparing the effect of CNT on PET chains crystallinity and orientation and comparing the role they play on mechanical properties; we studied CNT orientation in both electrospun and melt-spun fibers. As the results obtained from each observation show it is possible to detect CNT orientation inside fibers by Raman spectroscopy technique. Unfortunately, there is not a direct method to compare the amount of orientation of CNTs in a single fiber in melt spinning and electrospinning. Electrical conductivity can be an indirect judgment method for measuring the degree of CNT orientation. In both systems (Final non-woven electrospun mat and single melt-spun fiber); we obtained similar conductivity and electrical percolation threshold around 2 wt% (Figure 9-3). As described previously, we expect to detect more conductivity along fiber axis of electrospun nanofibers; since we have reported the conductivity of a stack of nanofibers and final non-woven mat here. As a result, we expect to have higher conductivity at lower percolation threshold (less that 2 wt% MWCNT) in electrospun nanofibers. This could prove indirectly that, there is a much higher degree of CNT orientation in electrospun samples compared to melt state. Moreover, comparing the sizes

of fibers in melt-spun and electrospun samples can be an evidence for higher degree of CNT orientation in electrospun nanofibers.

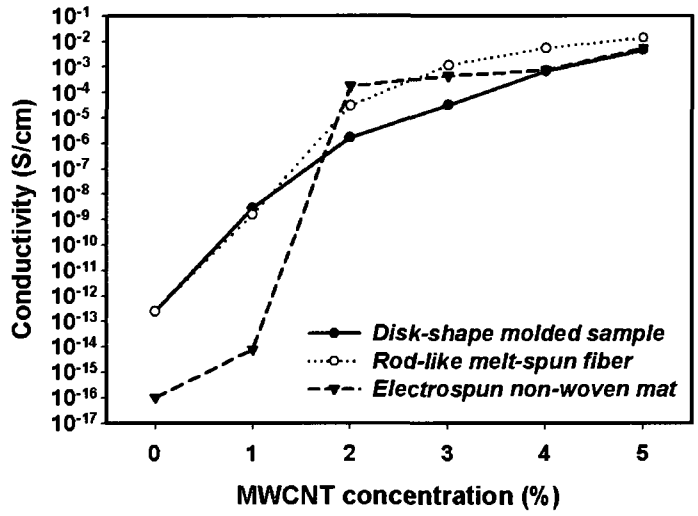

Figure 9-3: Electrical conductivity of different types of samples of PET/CNT composite at different MWCNT concentrations; disk molded, rod-like melt-spun fiber and electrospun non-woven mat

Chapter 10

Conclusions and Recommendations

10.1. Conclusions

In this thesis PS/CNT and PET/CNT were electrospun to nanofibers at different CNT concentrations and types especially at high concentrations of CNTs for the first time to study the effect of dispersion. In addition PET/CNT melt-spun fibers were produced successfully to obtain conductive microfibers. The following conclusions can be drawn from this work:

1. Comparing the final morphologies of nanofibers with different dispersion conditions in PS/CNT electrospun system showed that CNT dispersion is an important controlling parameter for final fiber diameter and morphology.
2. We used a kind of copolymer for dispersion modification of CNT in PS/CNT system. Final electrical conductivity measurement showed the positive effect of copolymer addition below percolation threshold. However, above percolation, nanofibers containing copolymer included a lower conductivity which might be because of CNTs coating with copolymer.
3. The effect of copolymer on enhancement of PS and CNT compatibility was also proved through comparison of the mechanical properties test results.
4. PET/CNT electrospun nanofiber mats were produced using both static and rotating drum (aligned nanofibers) collector. Electrical conductivity measurements on nanocomposite mats showed an electrical percolation threshold of around 2 wt% MWCNT.
5. Crystallography test results proved increasing crystalline density by increasing CNT concentration above electrical percolation opposite to the behavior below percolation. This effect was also observed in mechanical test results.

6. Aligned nanofiber production could considerably enhance the mechanical properties especially modulus. We could obtain aligned nanofibers with the modulus at least 6 times more than random nanofibers below percolation concentration; while the effect of alignment was less considerable above percolation and at high concentrations of CNTs.

7. In this work, we could reduce the percolation of microfibers to 2 wt% MWCNT concentration. Measuring the conductivity of a single melt-spun fiber showed that it was possible to reduce the percolation by both dispersion modification and change in processing condition (DR).

8. DSC analysis results proved that MWCNT slowed down the crystalline growth. This effect is the main reason for the reduction of crystalline phase formation during melt spinning followed by increasing MWCNT concentration.

9. MWCNT addition causes decrease in the amount of PET chain orientation obtained by FTIR measurement. Shearing field after MWCNT addition could be the main reason for weakening of the elongation field which caused a decrease in polymer chain orientation after MWCNT addition.

10. PET/CNT nanocomposite fibers showed incredibly increase in draw ability of as-spun fibers and the elongation at break in mechanical test. This was because of the role of MWCNT in the reduction of crystalline formation and the increased amorphous phase for dissipation of the imposed energy. This is obtained because polymer chains were acceptably adhered to MWCNT nanoparticles by modified dispersion.

11. The change in jet formation and velocity profile at different MWCNT concentrations were analyzed by the use of image analysis technique and high speed photography. In addition, two equations for estimation of final average nanofiber diameter were proposed by using dimensional analysis method. The results obtained were compared with the experimental data available.

10.2. Recommendations

For the future works, the following subjects are recommended:

1. Developing and comparing different methods for CNT dispersion in polymer/CNT nanocomposite electrospun nanofibers at high CNT concentrations. These methods can include chemical modification, in-situ polymerization or other compatibilizing methods. These methods can be used along with different types of CNTs to compare their final properties.
2. Polymer/CNT nanofibers were achieved for the characterization aim and in lab-scale in this thesis. These products can be employed for some applications such as conductive membranes, sensors and biomedical applications followed by some required post-processing modifications.
3. The results obtained here for the melt-spinning of PET/CNT fibers can be scaled up to the industrial scale. Moreover, the effect of some post processing steps such as drawing, annealing and surface modification for specific applications such as biomedical ones can be investigated.
4. Electrohydrodynamic modeling of CNT-filled nanocomposite nanofibers and recognizing the most important controlling forces and phenomena during electrospinning; beside calculation of some parameter such as elongation viscosity and final morphology by modeling.

REFERENCES

Ahn, B. W., Y. S. Chi, et al. (2008). "Preparation and characterization of multi-walled carbon nanotube/poly(ethylene terephthalate) nanoweb." Journal of Applied Polymer Science 110(6): 4055-4063.

Ajayan, P. M., O. Stephan, et al. (1994). "Aligned carbon nanotube arrays formed by cutting a polymer resin-nanotube composite." Science 265(5176): 1212-14.

Ausman, K. D., R. Piner, et al. (2000). "Organic solvent dispersions of single-walled carbon nanotubes: Toward solutions of pristine nanotubes." Journal of Physical Chemistry B 104(38): 8911-8915.

Aussawasathien, D., J. H. Dong, et al. (2005). "Electrospun polymer nanofiber sensors." Synthetic Metals 154(1-3): 37-40.

Baker, D. A. and P. J. Brown (2003). "Reactive routes to making modified nanofiber structures via electrospinning." Polymer Preprints (American Chemical Society, Division of Polymer Chemistry) 44(2): 118-119.

Baker, D. A. and P. J. Brown (2005). "Crosslinked electrospun PET webs." AATCC Review 5(7): 28-33.

Beatriz Veleirinho, M. F. Rei, et al. (2008). "Solvent and concentration effects on the properties of electrospun poly(ethylene terephthalate) nanofiber mats." Journal of Polymer Science Part B: Polymer Physics 46(5): 460-471.

Burger, C., B. S. Hsiao, et al. (2006). "Nanofibrous materials and their applications." Annual Review of Materials Research 36: 333-368.

Chakrabarti, K., P. M. G. Nambissan, et al. (2006). "Positron annihilation spectroscopy of polyacrylonitrile-based carbon fibers embedded with multi-wall carbon nanotubes." Carbon 44(5): 948-953.

Chen, H., Z. Liu, et al. (2009). "Chain confinement in electrospun nanofibers of PET with carbon nanotubes." Polymer 50(3): 872-880.

Chronakis, I. S., B. Milosevic, et al. (2006). "Generation of molecular recognition sites in electrospun polymer nanofibers via molecular imprinting." Macromolecules 39(1): 357-361.

Dror, Y., W. Salalha, et al. (2003). "Carbon nanotubes embedded in oriented polymer nanofibers by electrospinning." Langmuir 19(17): 7012-7020.

Dror, Y., W. Salalha, et al. (2005). "From carbon nanotube dispersion to composite nanofibers." Progress in Colloid & Polymer Science 130: 64-69.

Duchesne, C., X. Kong, et al. (2002). "Molecular orientation and relaxation of poly(ethylene terephthalate) by polarization modulation infrared spectroscopy." Macromolecules 35(23): 8768-8773.

Eda, G. and S. Shivkumar (2006). "Bead and fiber morphologies during electrospinning of polystyrene." Society of Plastics Engineers , Charlotte, NC, United States,.

Fei, W., Z. Weiping, et al. (2005). "Elastic deformation of multiwalled carbon nanotubes in electrospun MWCNTs-PEO and MWCNTs-PVA nanofibers." Polymer 46(26): 12689-95.

Feng, J. J. (2002). "The stretching of an electrified non-Newtonian jet: A model for electrospinning." Physics of Fluids 14(11): 3912-3926.

Feng, J. J. (2003). "Stretching of a straight electrically charged viscoelastic jet." Journal of Non-Newtonian Fluid Mechanics 116(1): 55-70.

Frenot, A. and I. S. Chronakis (2003). "Polymer nanofibers assembled by electrospinning." Current Opinion in Colloid and Interface Science 8(1): 64-75.

Gao, X., Y. Tong, et al. (2005). "Application of multi-wall carbon nanotubes in polymer fibres." Textile Asia 36(7): 35-6.

Ge, J. J., H. Hou, et al. (2004). "Assembly of well-aligned multiwalled carbon nanotubes in confined polyacrylonitrile environments: Electrospun composite nanofiber sheets." Journal of the American Chemical Society 126(48): 15754-15761.

Hartman, R. P. A., D. J. Brunner, et al. (1999). "Electroshydrodynamic atomization in the cone-jet mode physical modeling of the liquid cone and jet" Journal of Aerosol Science 30(7): 823-849.

He, J. H., Y. Wu, et al. (2005). "Critical length of straight jet in electrospinning." Polymer 46(26): 12637-12640.

Helgeson, M. E., K. N. Grammatikos, et al. (2008). "Theory and kinematic measurements of the mechanics of stable electrospun polymer jets." Polymer 49(12): 2924-2936.

Helgeson, M. E. and N. J. Wagner (2007). "A correlation for the diameter of electrospun polymer nanofibers." AIChE Journal 53(1): 51-55.

Hohman, M. M., M. Shin, et al. (2001). "Electrospinning and electrically forced jets. I. Stability theory." Physics of Fluids 13(8): 2201-2220.

Hohman, M. M., M. Shin, et al. (2001). "Electrospinning and electrically forced jets. II. Applications." Physics of Fluids 13(8): 2221-2236.

Hong, K. H. and T. J. Kang (2006). "Hydraulic permeabilities of PET and nylon 6 electrospun fiber webs." Journal of Applied Polymer Science 100(1): 167-177.

Hou, H. and D. H. Reneker (2004). "Carbon nanotubes on carbon nanofibers: A novel structure based on electrospun polymer nanofibers." Advanced Materials 16(1): 69-73.

Iijima, S. (1991). "Helical microtubules of graphitic carbon." Nature 354(6348): 56.

Jarusuwannapoom, T., W. Hongrojjanawiwat, et al. (2005). "Effect of solvents on electro-spinnability of polystyrene solutions and morphological appearance of resulting electrospun polystyrene fibers." European Polymer Journal 41(3): 409-421.

Kedem, S., J. Schmidt, et al. (2005). "Composite polymer nanofibers with carbon nanotubes and titanium dioxide particles." Langmuir 21(12): 5600-5604.

Kim, G. M., R. Lach, et al. (2006). "Relationships between phase morphology and deformation mechanisms in polymer nanocomposite nanofibres prepared by an electrospinning process." Nanotechnology 17(4): 963-972.

Kim, G. M., G. H. Michler, et al. (2005). "Deformation processes of ultrahigh porous multiwalled carbon nanotubes/polycarbonate composite fibers prepared by electrospinning." Polymer 46(18): 7346-7351.

Kim, J. S. and D. S. Lee (2000). "Thermal properties of electrospun polyesters." Polymer Journal (Tokyo) 32(7): 616-618.

Kim, K. W., K. H. Lee, et al. (2004). "The effect of molecular weight and the linear velocity of drum surface on the properties of electrospun poly(ethylene terephthalate) nonwovens." Fibers and Polymers 5(2): 122-127.

Kim, K. W., K. H. Lee, et al. (2005). "Effects of blend ratio and heat treatment on the properties of the electrospun poly(ethylene terephthalate) nonwovens." Fibers and Polymers 6(2): 121-126.

Ko, F., Y. Gogotsi, et al. (2003). "Electrospinning of continuous carbon nanotube-filled nanofiber yarns." Advanced Materials (Weinheim, Germany) 15(14): 1161-1165.

Larrondo, L. and R. S. J. Manley (1981). " Electrostatic fiber formation from polymer melts; 1.Experimental observation on fiber formation and properties." Journal of Polymer Science, Polymer Physics Edition 19(6): 909-920.

Lee, K. H., H. Y. Kim, et al. (2003). "The change of bead morphology formed on electrospun polystyrene fibers." Polymer 44(14): 4029-4034.

Lei Qian, et al. (2004). "Application of nanotechnology for high performance textiles" Journal of textile and apparel, technology and management 4(1): 1-7.

Li, D. and Y. Xia (2004). "Electrospinning of nanofibers: Reinventing the wheel?" Advanced Materials 16(14): 1151-1170.

Li, Z., G. Luo, et al. (2006). "Microstructure of carbon nanotubes/PET conductive composites fibers and their properties." Composites Science and Technology 66(7-8): 1022-1029.

Liang, G. D. and S. C. Tjong (2008). "Electrical properties of percolative polystyrene/carbon nanofiber composites." IEEE Transactions on Dielectrics and Electrical Insulation 15(1): 214-220.

Lim, J. Y., C. K. Lee, et al. (2006). "Controlled nanofiber composed of multi-wall carbon nanotube/poly(ethylene oxide)." Journal of Macromolecular Science - Pure and Applied Chemistry 43(4-5): 785-796.

Lin, T., H. Wang, et al. (2004). "The charge effect of cationic surfactants on the elimination of fibre beads in the electrospinning of polystyrene." Nanotechnology 15(9): 1375-1381.

Liu, J., T. Wang, et al. (2005). "Carbon nanotube core-polymer shell nanofibers." Journal of Applied Polymer Science 96(5): 1992-1995.

Ma, H., J. Zeng, et al. (2003). "Processing, structure, and properties of fibers from polyester/carbon nanofiber composites." Composites Science and Technology 63(11): 1617-1628.

Ma, Z., M. Kotaki, et al. (2005). "Surface engineering of electrospun polyethylene terephthalate (PET) nanofibers towards development of a new material for blood vessel engineering." Biomaterials 26(15): 2527-36.

McCann, J. T., M. Marquez, et al. (2006). "Highly porous fibers by electrospinning into a cryogenic liquid." Journal of the American Chemical Society 128(5): 1436-1437.

McKee, M. G., T. E. Long, et al. (2003). "Synthesis and electrospinning of branched polyesters." Polymer Preprints (American Chemical Society, Division of Polymer Chemistry) 44(1): 792-793.

McKee, M. G., G. L. Wilkes, et al. (2004). "Correlations of Solution Rheology with Electrospun Fiber Formation of Linear and Branched Polyesters." Macromolecules 37(5): 1760-1767.

Megelski, S., J. S. Stephens, et al. (2002). "Micro and nanostructured surface morphology on electrospun polymer fibers." Macromolecules 35(22): 8456-8466.

Moniruzzaman, M. and K. I. Winey (2006). "Polymer nanocomposites containing carbon nanotubes." Macromolecules 39(16): 5194-5205.

Myung Seob, K., K. Hak Yong, et al. (2004). "Nanofibrous mats of poly(trimethylene terephthalate) via electrospinning." Polymer 45(1): 295-301.

Nah, C., G. Mathew, et al. (2005). "Preparation and characterization of properties of electrospun poly(butylene terephthalate) nanofibers filled with carbon nanotubes." Polymer Testing 24(6): 712-17.

Pai, S. and N. J. Gunja (2004). "Effects of the molecular characteristics of polymers on the electrospinning of polystyrene." Society of Plastics Engineers, Chicago, IL, United States.

Pan, C., L. Q. Ge, et al. (2007). "Fabrication of multi-walled carbon nanotube reinforced polyelectrolyte hollow nanofibers by electrospinning." Composites Science and Technology 67(15-16): 3271-3277.

Pattamaprom, C., W. Hongrojjanawiwat, et al. (2006). "The influence of solvent properties and functionality on the electrospinnability of polystyrene nanofibers." Macromolecular Materials and Engineering 291(7): 840-847.

Perepelkin, K. E. (2005). "Principles and Methods of Modification of Fibres and Fibre Materials. A Review." Fibre Chemistry 37(2): 37.

Ra, E. J., K. H. An, et al. (2005). "Anisotropic electrical conductivity of MWCNT/PAN nanofiber paper." Chemical Physics Letters 413(1-3): 188-193.

Reneker, D. H. and I. Chun (1996). "Nanometre diameter fibres of polymer, produced by electrospinning." Nanotechnology 7(3): 216-223.

Reneker, D. H., A. L. Yarin, et al. (2000). "Bending instability of electrically charged liquid jets of polymer solutions in electrospinning." Journal of Applied Physics 87(9): 4531-4547.

Richard A. Vaia, R. K. (2001). "Polymer nanocomposites: synthesis, characterization, and modeling." American Chemical Society, Washington, DC, United States.

Salalha, W., Y. Dror, et al. (2004). "Single-walled carbon nanotubes embedded in oriented polymeric nanofibers by electrospinning." Langmuir 20(22): 9852-9855.

Saville, D. A. (1997). "Electrohydrodynamics: the Taylor-Melcher Leaky dielectric model." Annual Review of Fluid Mechanics 29: 27-64.

Sawicka, K. M. and P. Gouma (2006). "Electrospun composite nanofibers for functional applications." Journal of Nanoparticle Research 8(6): 769-781.

Seeram Ramakrishna, K. F., Wee-Eong Teo, Teik-Cheng Lim, Zuwei Ma (2005). "An introduction to electrospinning and nanofibers." World Scientific Publishing.

Sen, R., Z. Bin, et al. (2004). "Preparation of single-walled carbon nanotube reinforced polystyrene and polyurethane nanofibers and membranes by electrospinning." Nano Letters 4(3): 459-64.

Seoul, C., Y. T. Kim, et al. (2003). "Electrospinning of poly(vinylidene fluoride)/dimethylformamide solutions with carbon nanotubes." Journal of Polymer Science, Part B: Polymer Physics 41(13): 1572-1577.

Shenoy, S. L., W. D. Bates, et al. (2005). "Role of chain entanglements on fiber formation during electrospinning of polymer solutions: Good solvent, non-specific polymer-polymer interaction limit." Polymer 46(10): 3372-3384.

Sigmund, W., J. Yuh, et al. (2006). "Processing and structure relationships in electrospinning of ceramic fiber systems." Journal of the American Ceramic Society 89(2): 395-407.

Sluzarenko, N., B. Heurtefeu, et al. (2006). "Diblock copolymer stabilization of multi-wall carbon nanotubes in organic solvents and their use in composites." Carbon 44(15): 3207-3212.

Spivak, A. F., Y. A. Dzenis, et al. (2000). "A model of steady state jet in the electrospinning process." Mechanics Research Communications 27(1): 37-42.

Sundaray, B., V. Subramanian, et al. (2007). "Preparation and characterization of polystyrene-multiwalled carbon nanotube composite fibers by electrospinning." Journal of Nanoscience and Nanotechnology 7: 1793-1795.

Sundaray, B., V. Subramanian, et al. (2006). "Electrical conductivity of a single electrospun fiber of poly(methyl methacrylate) and multiwalled carbon nanotube nanocomposite." Applied Physics Letters 88(14): 143114.

Sung, J. H., H. S. Kim, et al. (2004). "Nanofibrous membranes prepared by multiwalled carbon nanotube/poly(methyl methacrylate) composites." Macromolecules 37(26): 9899-9902.

Tan, S. H., R. Inai, et al. (2005). "Systematic parameter study for ultra-fine fiber fabrication via electrospinning process." Polymer 46(16): 6128-6134.

Veleirinho, B. and J. A. Lopes-da-Silva (2009). "Application of electrospun poly(ethylene terephthalate) nanofiber mat to apple juice clarification." Process Biochemistry 44(3): 353-356.

Wang, C., C.-H. Hsu, et al. (2006). "Scaling laws in electrospinning of polystyrene solutions." Macromolecules 39(22): 7662-7672.

Wannatong, L., A. Sirivat, et al. (2004). "Effects of solvents on electrospun polymeric fibers: Preliminary study on polystyrene." Polymer International 53(11): 1851-1859.

Yarin, A. L., S. Koombhongse, et al. (2001). "Bending instability in electrospinning of nanofibers." Journal of Applied Physics 89(5): 3018-3026.

Yarin, A. L., S. Koombhongse, et al. (2001). "Taylor cone and jetting from liquid droplets in electrospinning of nanofibers." Journal of Applied Physics 90(9): 4836-4846.

Ye, H., H. Lam, et al. (2004). "Reinforcement and rupture behaviour of carbon nanotubes-polymer nanofibers." Applied Physics Letters 85(10): 1775-1777.

Yuan Ji, S. G., Jaseung Koo, Bingquan Li (2006). "Structure and nanomechanical properties of well-aligned electrospun PS/MWCNT composite nanofibers." The American Physical Society, March 2006 Meeting.

Zheng, J., A. He, et al. (2006). "Studies on the controlled morphology and wettability of polystyrene surfaces by electrospinning or electrospraying." Polymer 47(20): 7095-7102.

Ziabicki, A. (1976). "Fundamentals of Fibre Formation: The Science of Fibre Spinning and Drawing." Wiley.